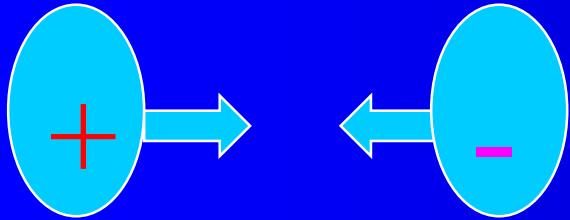# Recombination …

electron –ion recombination

atomic ions

molecular ions

ion –ion recombination

Recombination

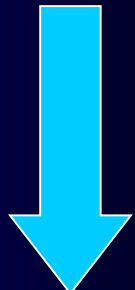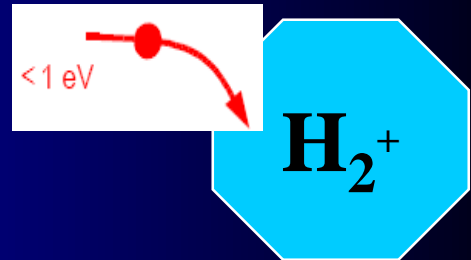**Radiative recombination**

$$Ar^+ + e^- \rightarrow Ar + h\nu$$

Dissociative recombination

$$AB^+ + e \rightarrow A + B$$

$$O_2^+ + e \rightarrow A + B$$

e⁻ + AB⁺

Capture

AB* resonant state(s)

<1 eV

H₂⁺

H₂*

e⁻ + AB⁺
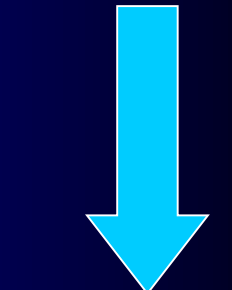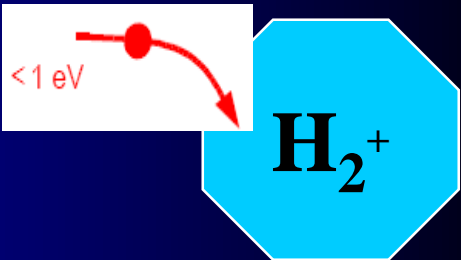
Capture

Auto ionization

AB* resonant state(s)

predissociation

To get high recombination rate, we need
(a) efficient capture
(b) predissociation faster than auto-ionization

Electron –ion recombination

$H^+ + e^- \rightarrow$ products

$H_2^+ + e^- \rightarrow$ products

$H_3^+ + e^- \rightarrow$ products

$H_5^+ + e^- \rightarrow$ products

Processes: at low impact energies

Elastic scattering

$AB + e \longrightarrow AB + e$

- -

Electronic excitation

$AB + e \longrightarrow AB^* + e$

Vibrational excitation

$AB(v''=0) + e \longrightarrow AB(v') + e$

Rotational excitation

$AB(N'') + e \longrightarrow AB(N') + e$

- -
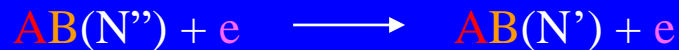
Dissociative attachment /

$AB + e \longrightarrow A^- + B$

$\qquad\qquad \longrightarrow A + B^-$

- -

Impact dissociation

$AB + e \longrightarrow A + B + e$

All go via $(AB^-....)^{**}$.

- -

Dissociative recombination

$AB^+ + e \longrightarrow A + B$

Go via $(AB....)^{**}$.

$H_2^+ + e^- \rightarrow H + H,$

Dissociative Recombination - DR

Electron collisions with H_2^+ - how to describe ????

$H_2^+ + e^- \rightarrow H + H,$

Dissociative Recombination - DR

$H_2^+(1s\sigma) + e(\varepsilon\ell)$

$H_2^{**} [(2p\sigma)^2]$

$H (1s) + H (2\ell)$

< 1 eV

H_2^+

H_2^*

H

H
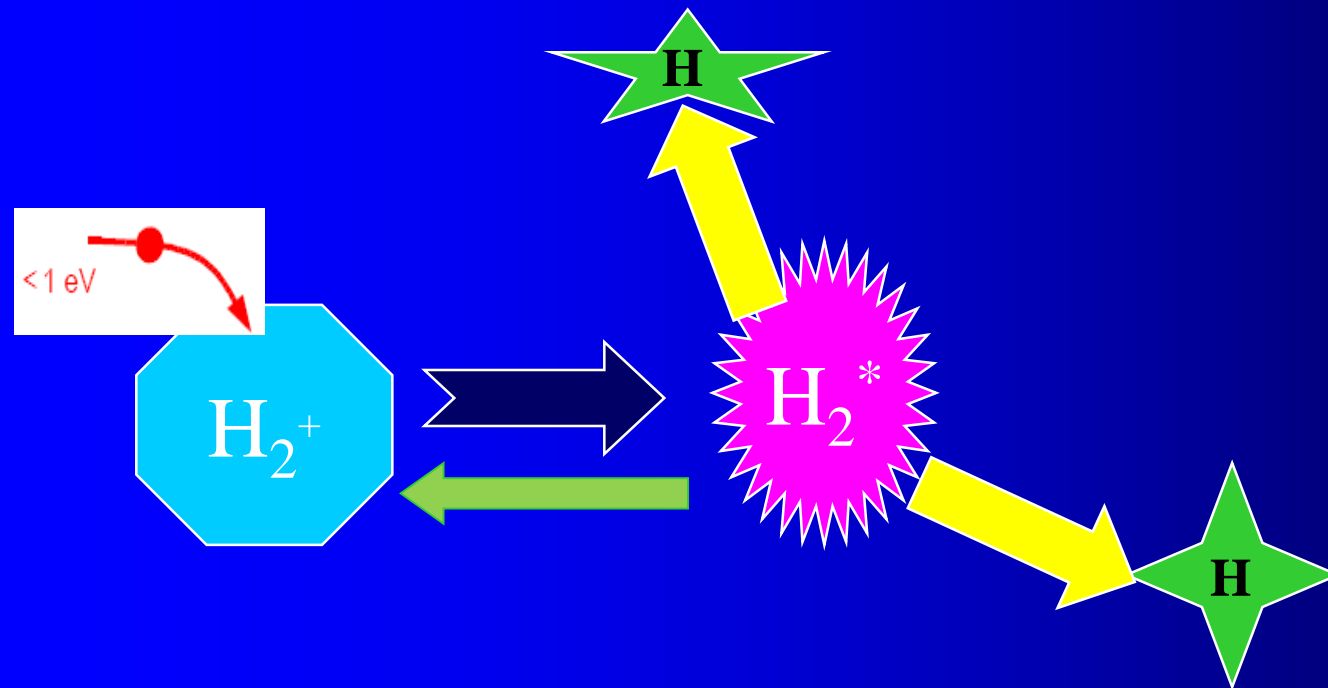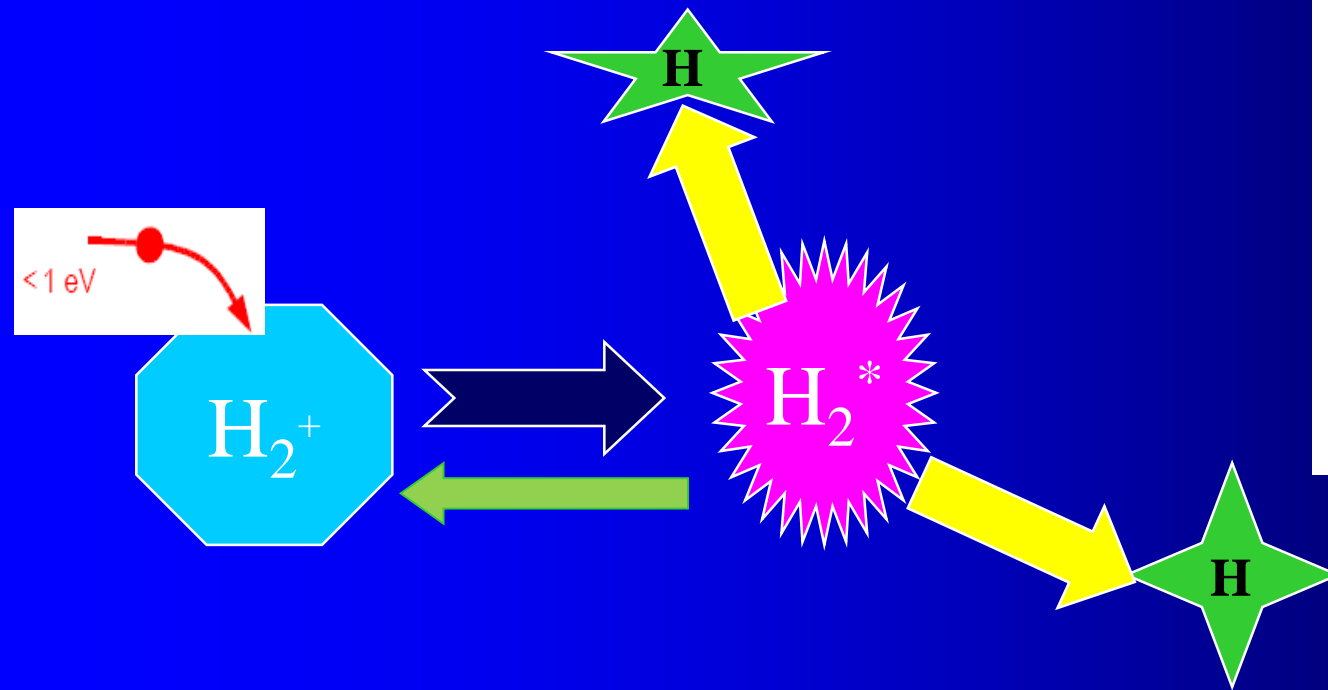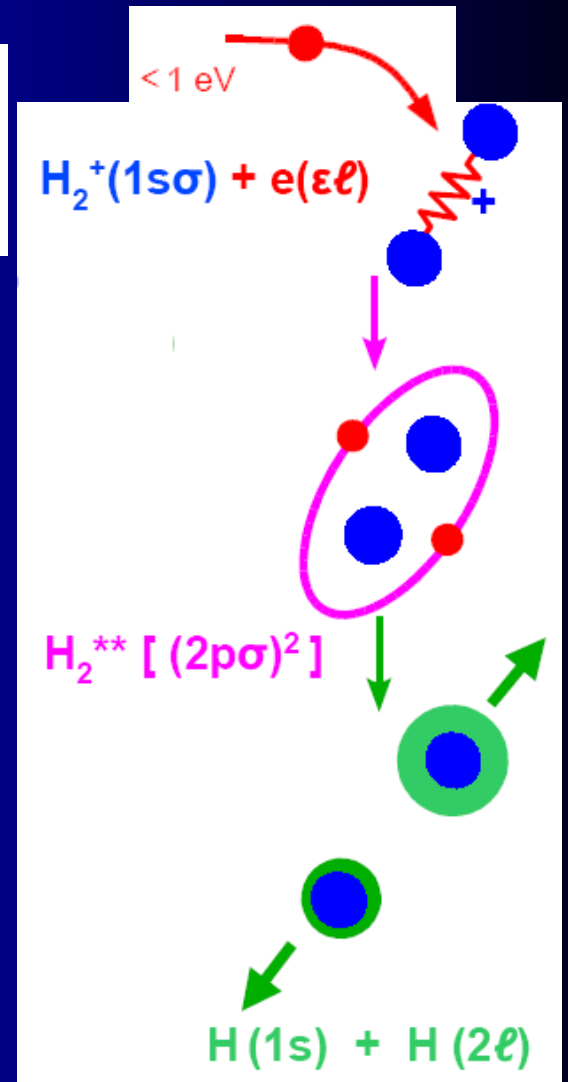
Electron collisions with H_2^+ - how to describe ????

Direct DR process

(a)

Energy (eV) vs Internuclear distance (Å); curves labeled AB^+, AB^{**}, $A+B^+$, $A+B$, with ε

$$AB^+ + e^- \underset{k_{auto}}{\overset{k_c}{\rightleftharpoons}} AB^{**} \xrightarrow{k_{stab}} A + B$$
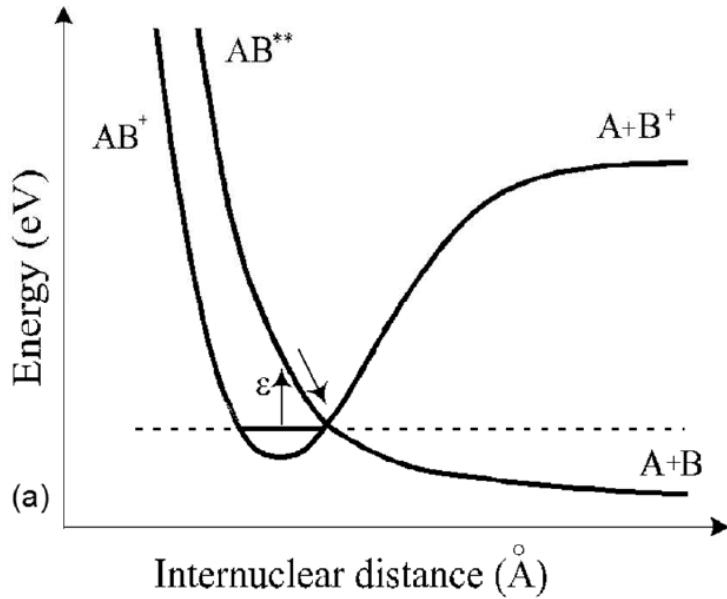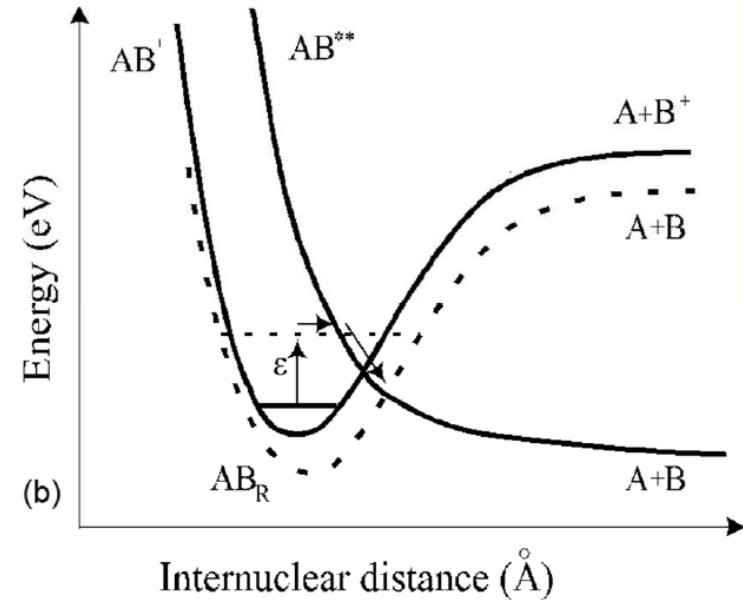
$$\alpha_{dr} \approx T_e^{-0.5}$$

Ions: Ar_2^+, N_2^+, CH_4^+, $NH_4^+(NH_3)_2$ - $\alpha \sim 10^{-7} - 10^{-6}$ cm^3 s^{-1}

Theoretical calculation: H_2^+, HD^+, D_2^+ - $\alpha = 2.3 \times 10^{-8}$, 2.2×10^{-8}, 4×10^{-9} cm^3 s^{-1}, respectively

Direct DR process

Indirect DR process

$$AB^+ + e^- \xrightleftharpoons[k_{auto}]{k_c} AB^{**} \xrightarrow{k_{stab}} A + B$$

$$AB^+ + e^- \rightleftharpoons AB_R^{**} \rightleftharpoons AB^{**} \rightarrow A + B$$
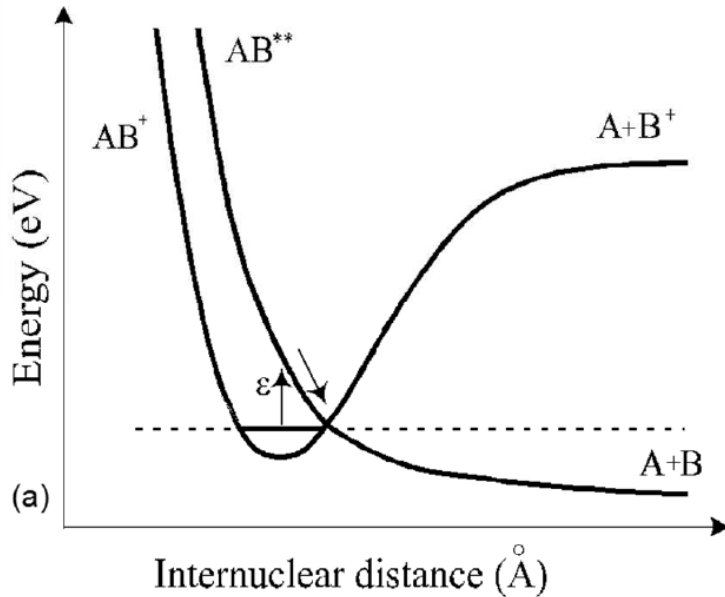
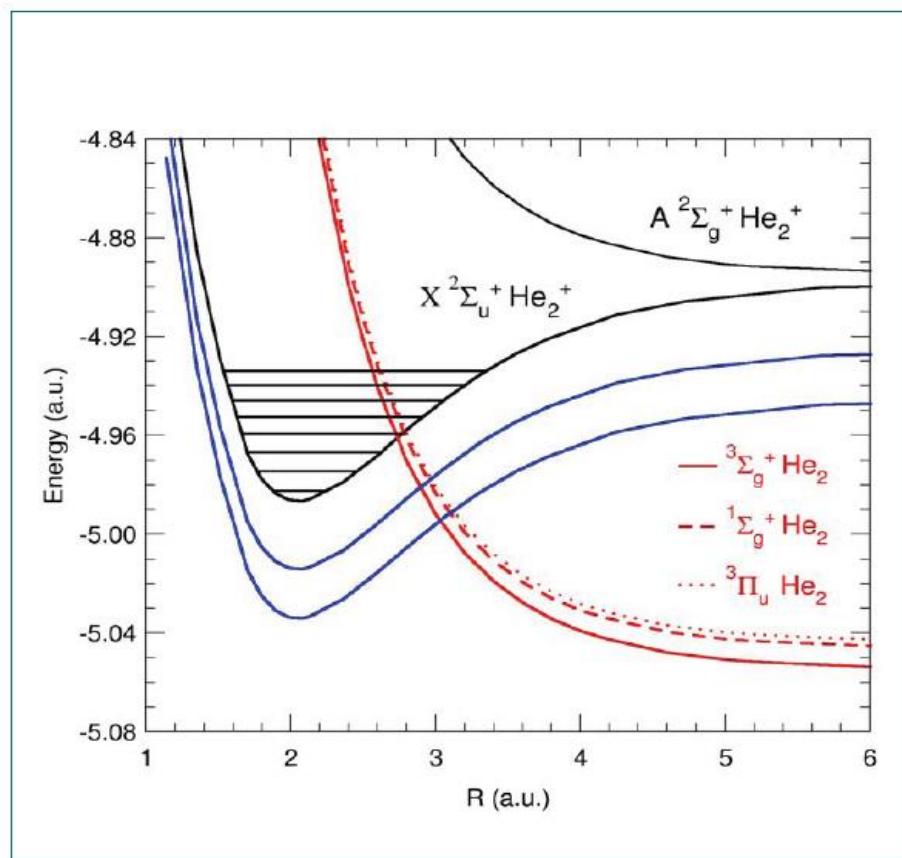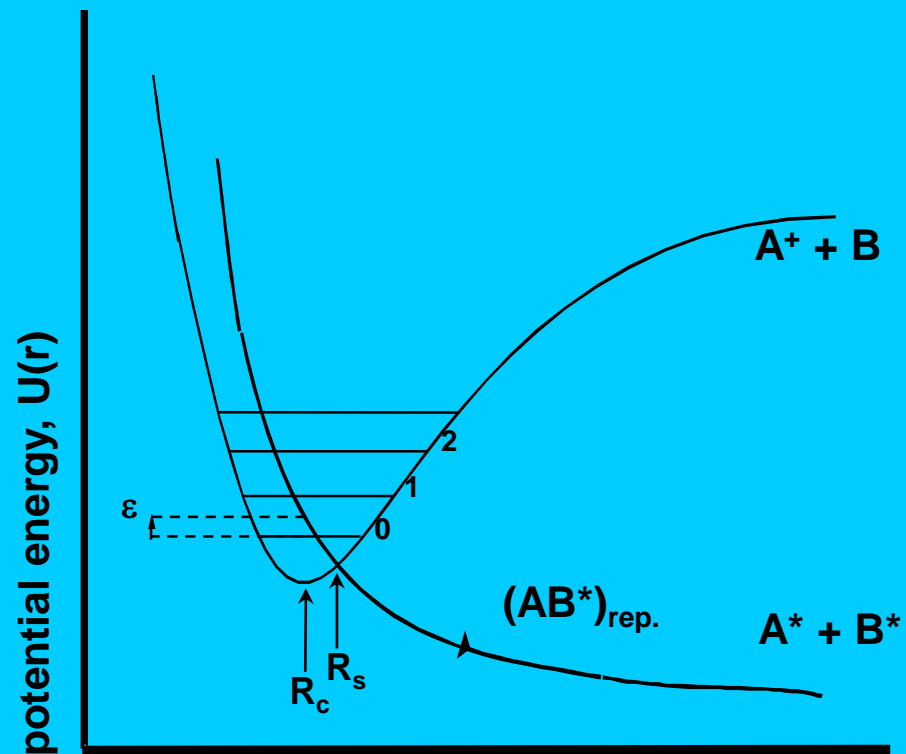$$\alpha_{dr} \approx T_e^{-0.5}$$

$$\alpha_{idr} \approx T_e^{-1.5}$$

$$\alpha(T_e, T_v) \approx T_e^{-0.5} T_v^{-1}$$

Ions: Ar_2^+, N_2^+, CH_4^+, $NH_4^+(NH_3)_2$ - $\alpha \sim 10^{-7} - 10^{-6}$ cm^3 s^{-1}

Theoretical calculation: H_2^+, HD^+, D_2^+ - $\alpha = 2.3 \times 10^{-8}$, 2.2×10^{-8}, 4×10^{-9} cm^3 s^{-1}, respectively

THEORETICAL FRAMEWORK

The states involved: exemple for He$_2^+$/He$_2$ system

2004 DR6 Mosbach

I. Schneider, et al., DR2004 Mosbach

Left figure:

potential energy, U(r)

$A^+ + B$

ε

2

1

0

$(AB^*)_{rep.}$

$A^* + B^*$

R_c R_s

internuclear separation, R

Direct mechanism

Right figure:

potential energy, U(r)

$A^+ + B$

3

ε

0

$(AB^*)_{rep.}$

$A^* + B^*$

AB^* $_{Ryd.}$
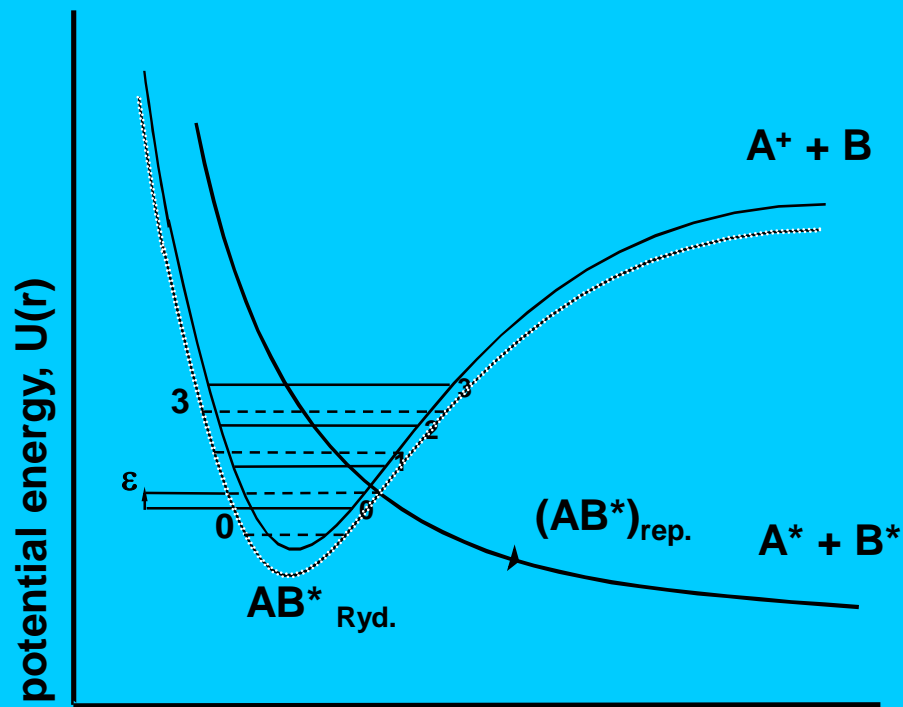
internuclear separation, R

Indirect mechanism

Electron-cold molecular ion reaction: Dissociative Recombination

$AB^+ + e^- \Rightarrow A(n) + B(n') + KER$

Indirect process

Direct process

AB**

Interference

AB$^+$

Rydberg state

e^-

Kinetic Energy Release

A(n)+B(n')

V

R
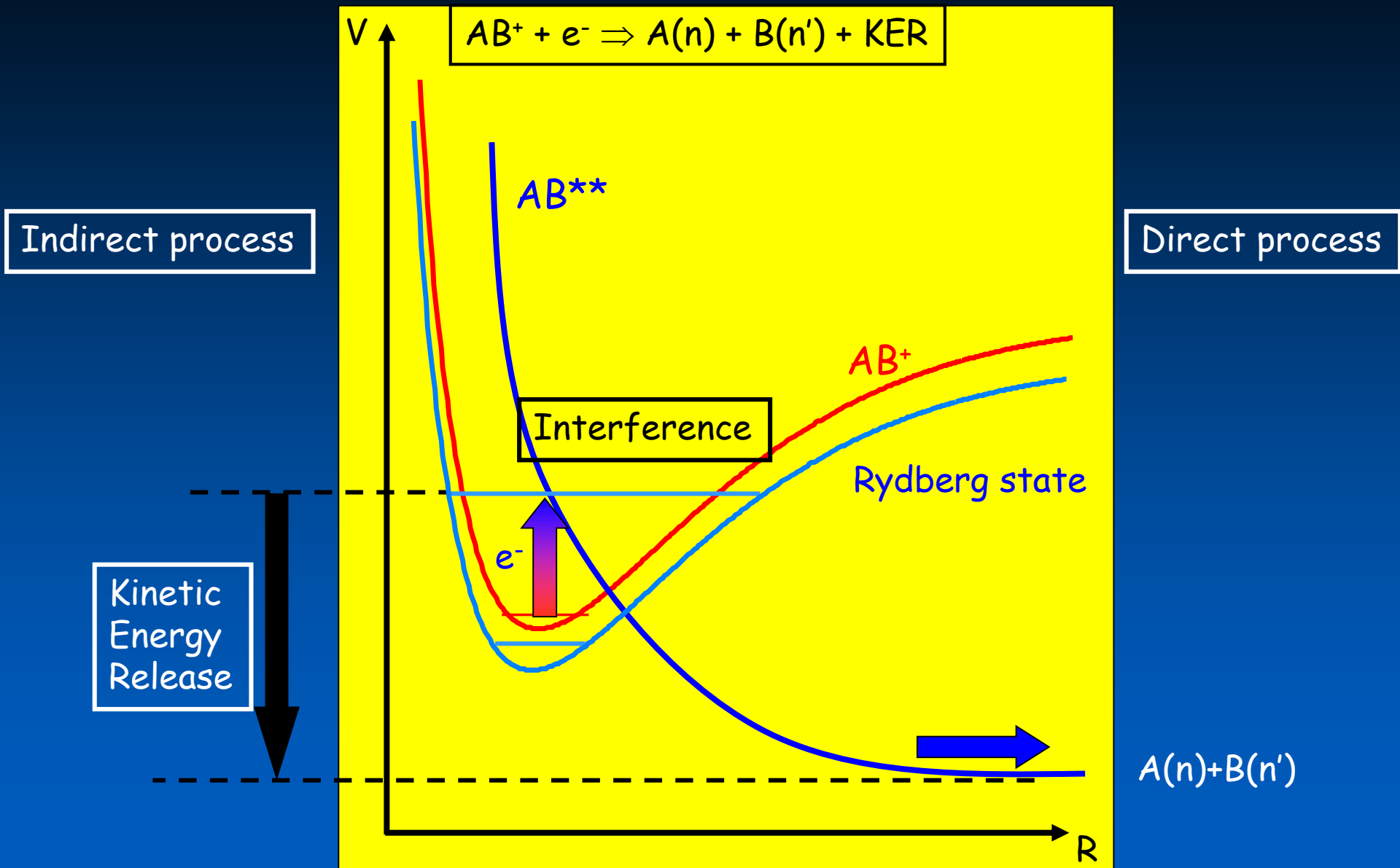
Recombination of H$_3^+$: No ion-neutral crossing
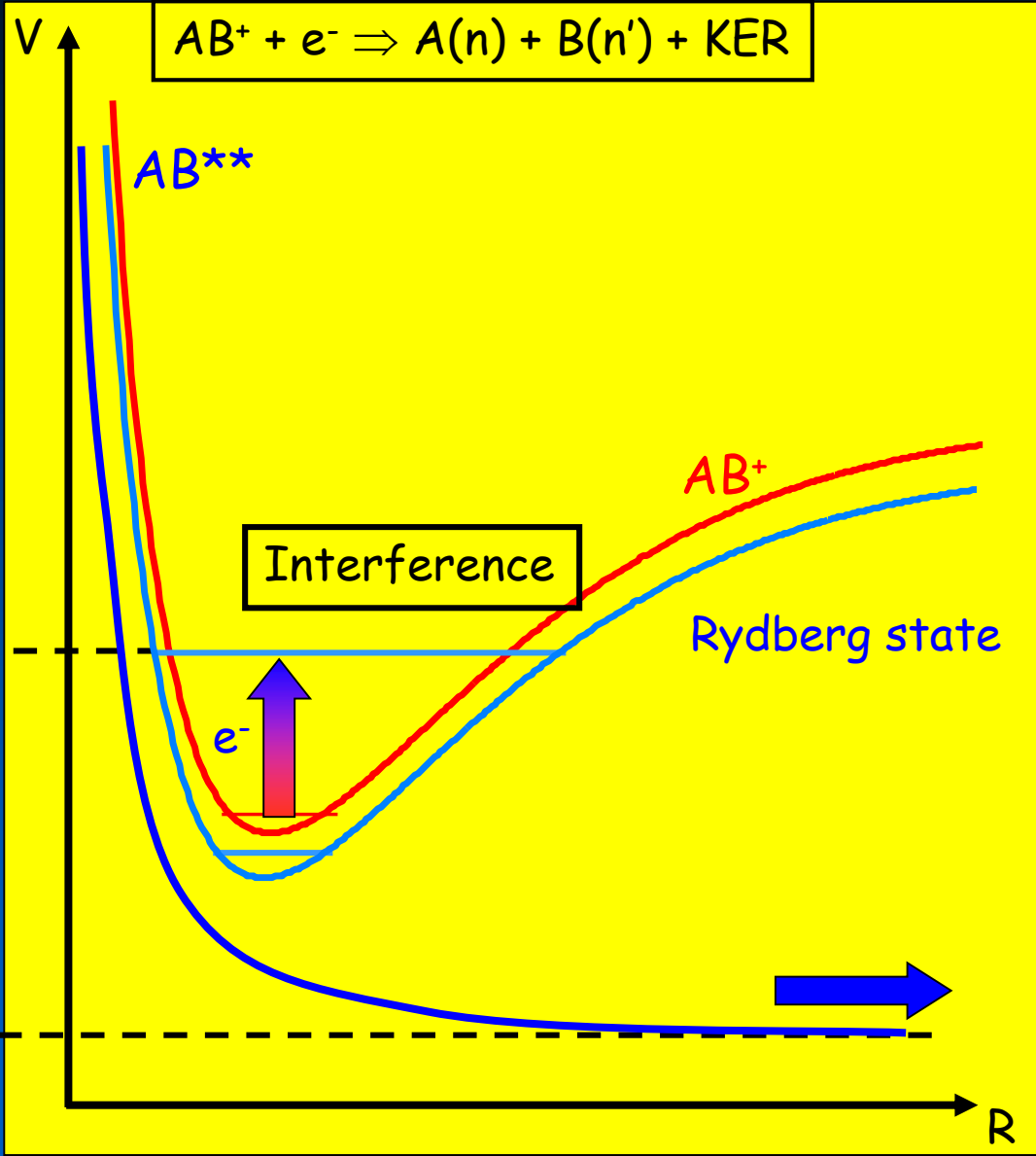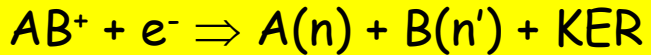
AB$^+$ + e$^-$ $\Rightarrow$ A(n) + B(n') + KER

V

AB**

Indirect process

Direct process

Interference

AB$^+$

Rydberg state

e$^-$

Kinetic Energy Release

A(n)+B(n')

R

$H_3^+ + e^- \rightarrow H + H_2; 3H$

Single collision

v_r

$e^- \ e^- \ e^-$

H_3^+

H

H,

$\sigma(v_r)$ **recombination cross section**

x

I_0 H_3^+ I

I(x)

$I=I_0 \exp(-\sigma n_i x)$

$k(T)=<v\sigma>$

α

Multiple collision

H_3^+

T

e^-
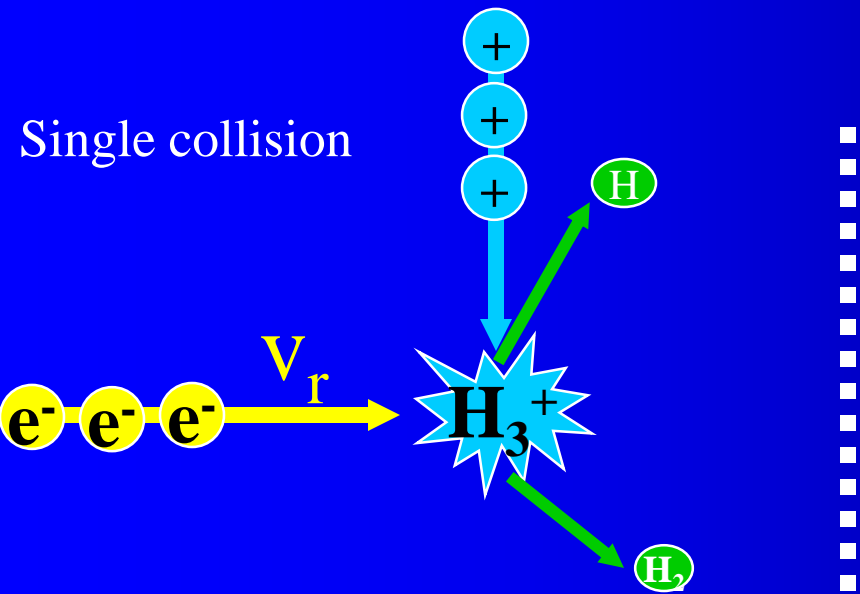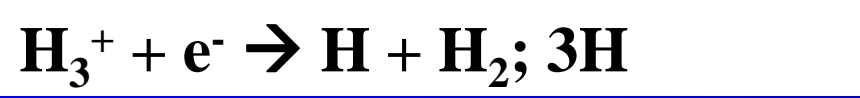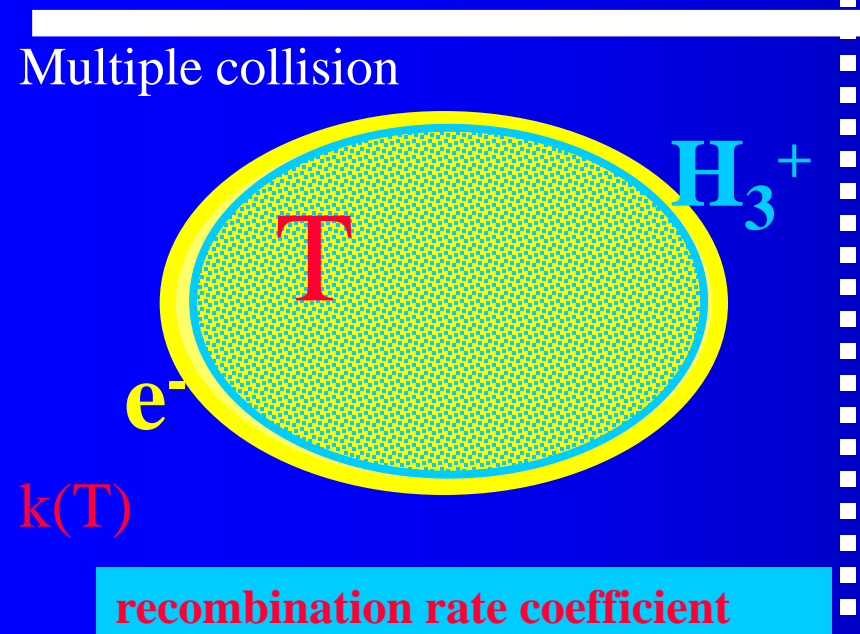
$k(T)$

recombination rate coefficient

$n_e \ [cm^{-3}]$

10^{10}

10^9

10^8

time
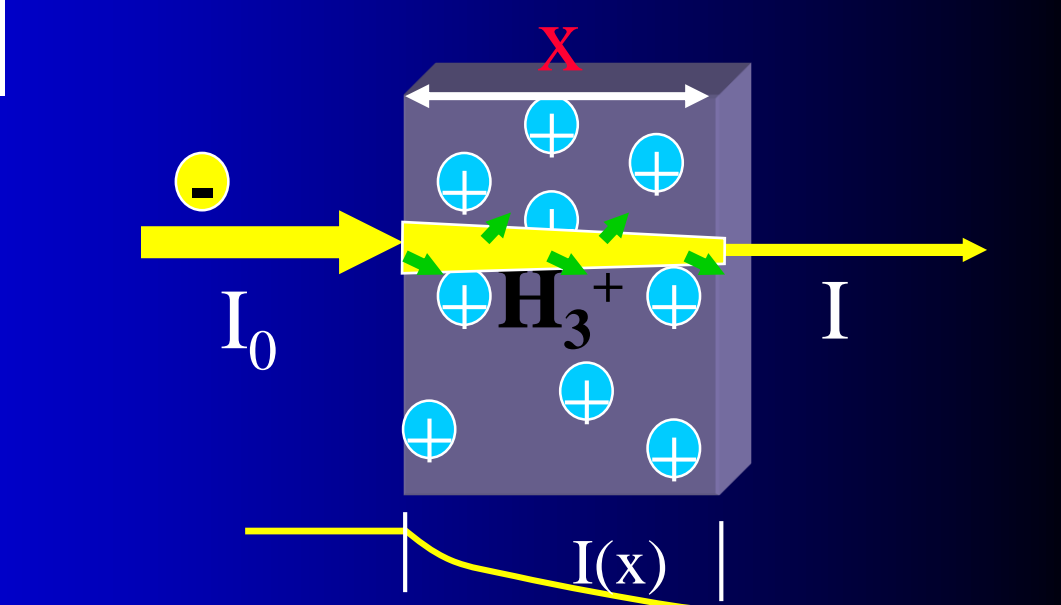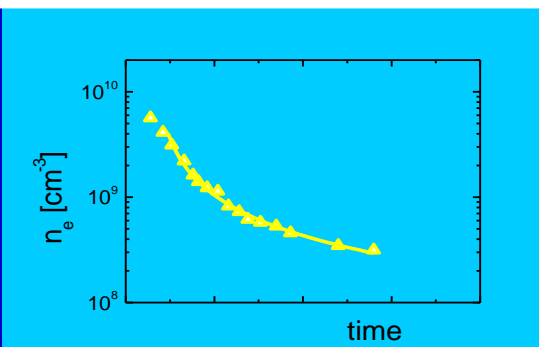
$dn_i/dt=-kn_i n_e$

$dn_e/dt=-kn_e^2$

Concept of recombination rate coefficient (plasma binary reactions)

at T

$e^- + A^+ \rightarrow$ products
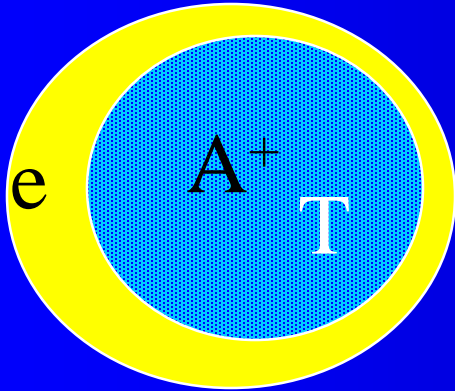
$dN_A/dt = -\alpha n_e N_A$

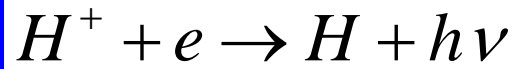**RECOMBINATION RATE COEFFICIENT**

$\alpha = \alpha(T)$

$\sigma = \sigma(v) = \sigma(\varepsilon)$

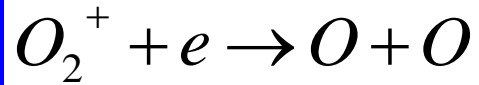**Collision rate coefficient, Recombination rate coefficient**

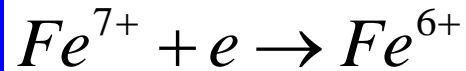$\alpha = \langle \sigma u_r \rangle$

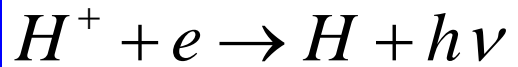# Recombination processes in plasma

Binary Recombination

$$H^+ + e \rightarrow H + h\nu$$

RR

$$O_2^+ + e \rightarrow O + O$$

DR

$$\frac{dn_e}{dt} = \frac{d[O_2^+]}{dt} = -\alpha[O_2^+]n_e = -\alpha n_e^2$$

$$Fe^{7+} + e \rightarrow Fe^{6+}$$

DiR

Recombination processes in plasma

Binary Recombination

$$H^+ + e \rightarrow H + h\nu$$

RR

$$O_2^+ + e \rightarrow O + O$$

DR

$$\frac{dn_e}{dt} = \frac{d[O_2^+]}{dt} = -\alpha[O_2^+]n_e = -\alpha n_e^2$$

$$Fe^{7+} + e \rightarrow Fe^{6+}$$
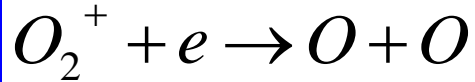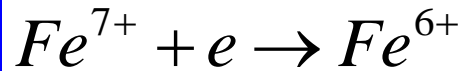
DiR

Ternary electron assisted recombination

$$Ar^+ + e + e \rightarrow Ar + e$$

$$\frac{dn_e}{dt} = \frac{d[Ar^+]}{dt} = -K_e[Ar^+]n_e^2 = -\alpha_{eff}[Ar^+]n_e$$
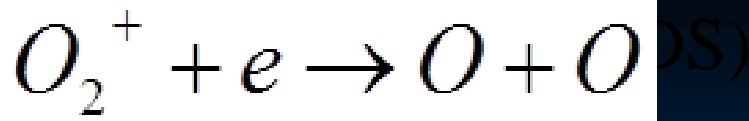
Collisional Radiative Recombination CRR

$$\alpha_{eff} = K_e n_e$$

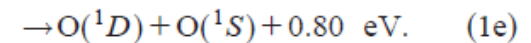## Ternary neutral assisted recombination
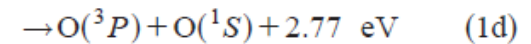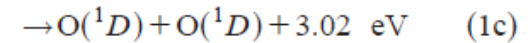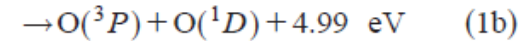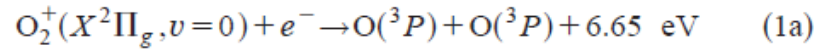
$$Ar^+ + e + He \rightarrow Ar + He$$

$$\frac{dn_e}{dt} = \frac{d[Ar^+]}{dt} = -K_M[Ar^+]n_e[He] = -\alpha_{eff}[Ar^+]n_e$$

$$\alpha_{eff} = K_M[He]$$

$$O_2^+ + e \rightarrow O + O \quad \text{(DS)}$$

Five exothermic channels are available for vibrational ground state O_2^+ ions in zero relative energy collisions with electrons. They are summarized as follows with the associated kinetic energy releases:

$$O_2^+(X^2\Pi_g, v=0) + e^- \rightarrow O(^3P) + O(^3P) + 6.65 \text{ eV} \quad (1a)$$

$$\rightarrow O(^3P) + O(^1D) + 4.99 \text{ eV} \quad (1b)$$

$$\rightarrow O(^1D) + O(^1D) + 3.02 \text{ eV} \quad (1c)$$

$$\rightarrow O(^3P) + O(^1S) + 2.77 \text{ eV} \quad (1d)$$

$$\rightarrow O(^1D) + O(^1S) + 0.80 \text{ eV}. \quad (1e)$$
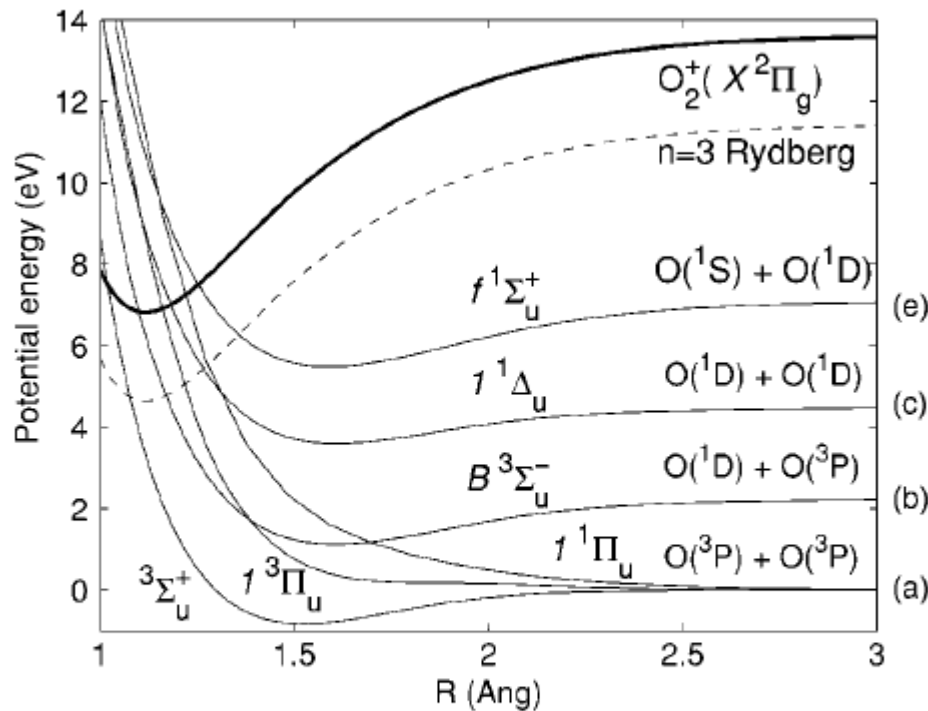

234311-2 Petrignani et al.

FIG. 1. Schematic of the diabatic potential curves relevant for the DR of O_2^+. The dissociation limits connected with each valence capture state are given on the right. The labels (a)–(c), and (e) refer to Eqs. (1a)–(1c) and (1e), respectively.

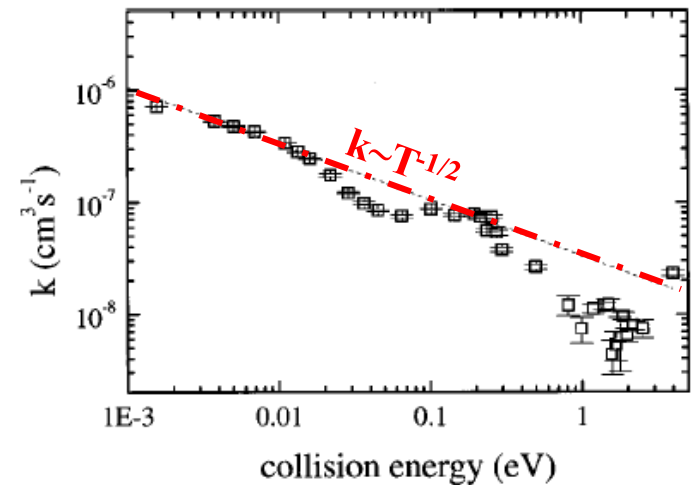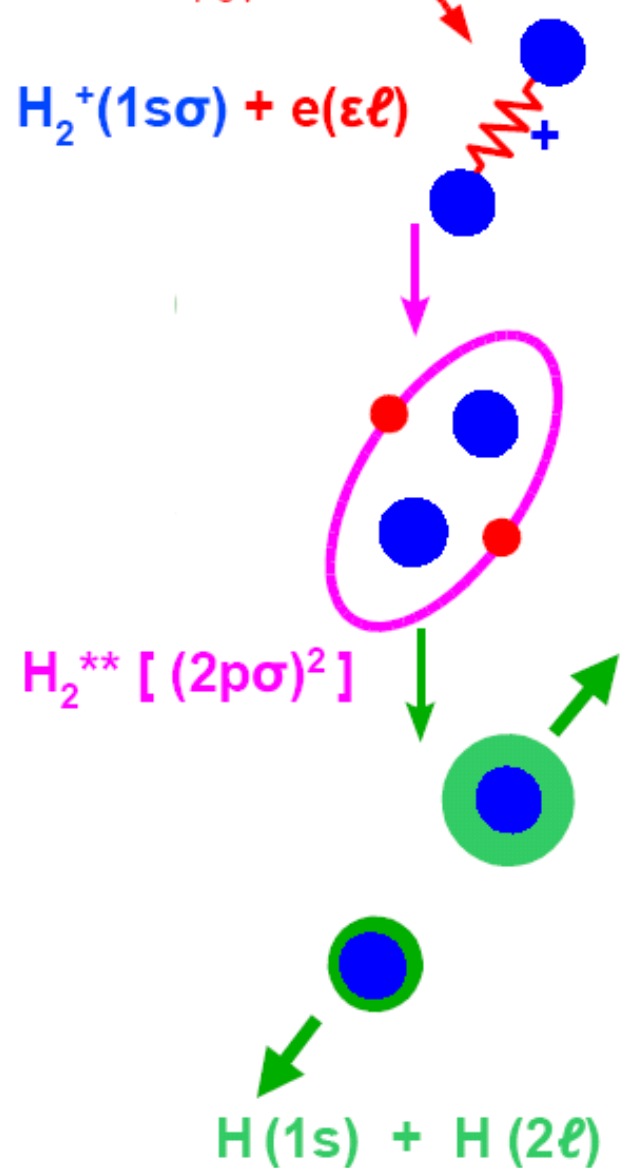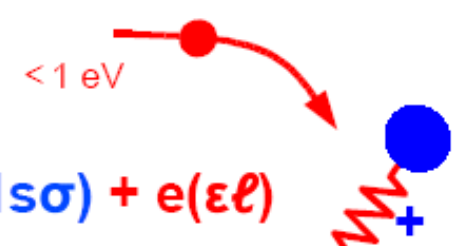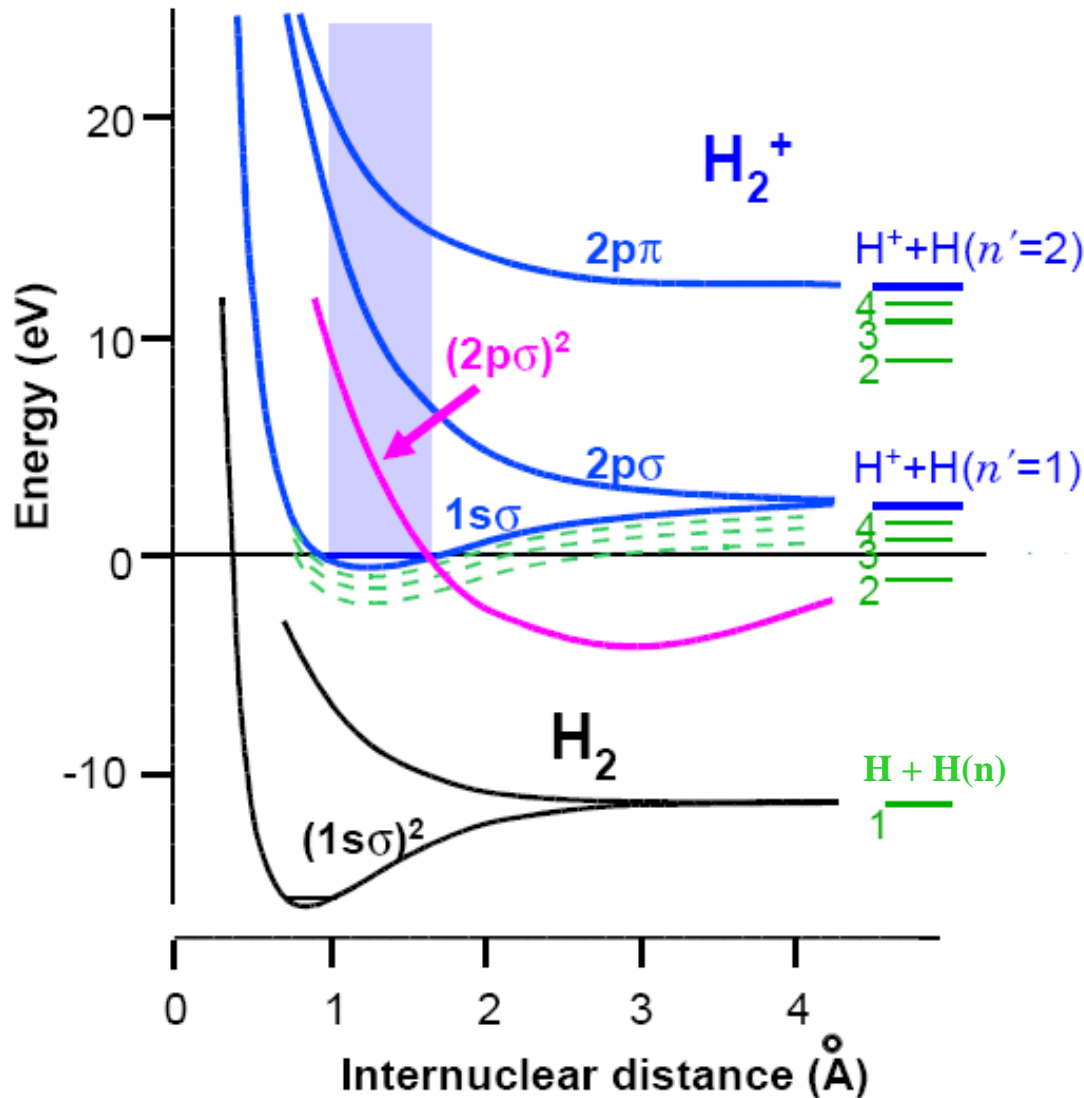6682   J. Chem. Phys., Vol. 114, No. 15, 15 April 2001

$k \sim T^{-1/2}$

FIG. 2. DR rate coefficient k as a function of electron collision energy from 1 meV to 5 eV. Statistical errors are shown at the 1σ level. The dotted line shows the threshold $E^{-1/2}$ behavior. Both the rate coefficient and the energy are shown on a logarithmic scale.
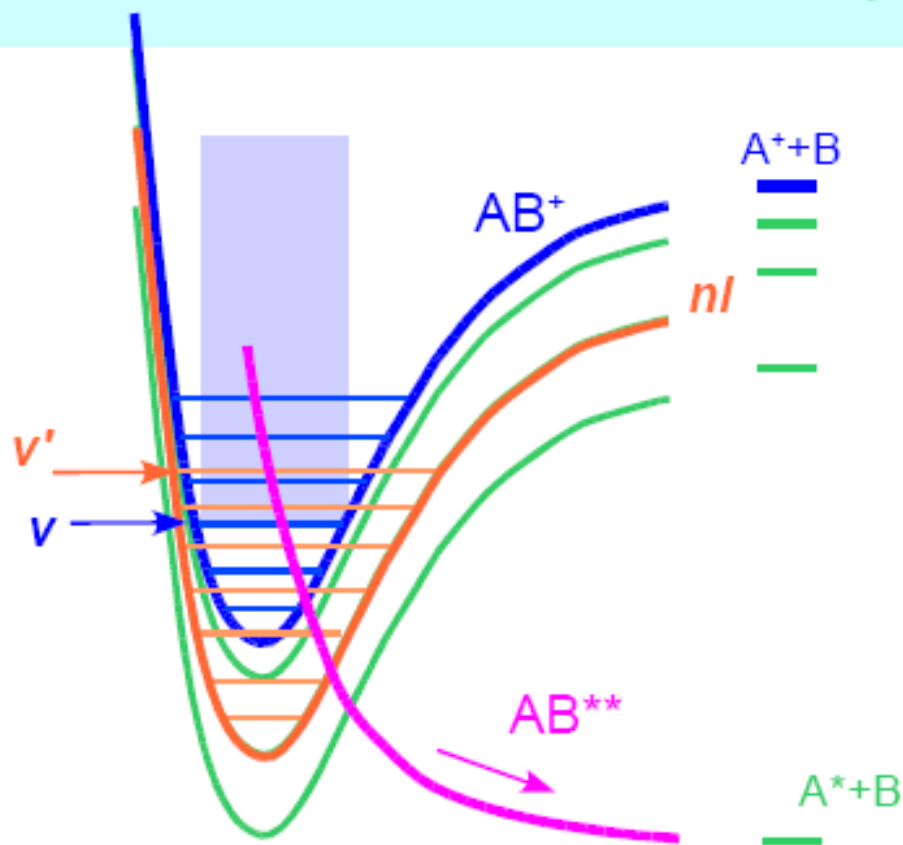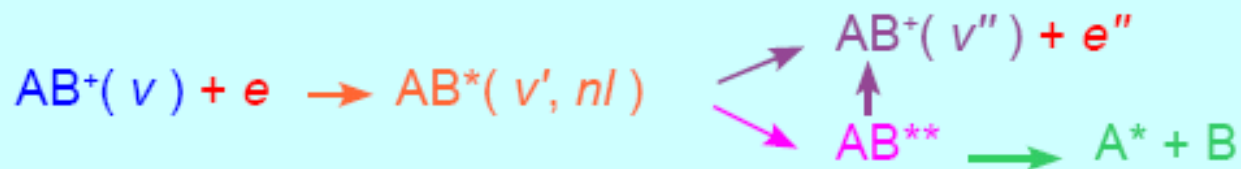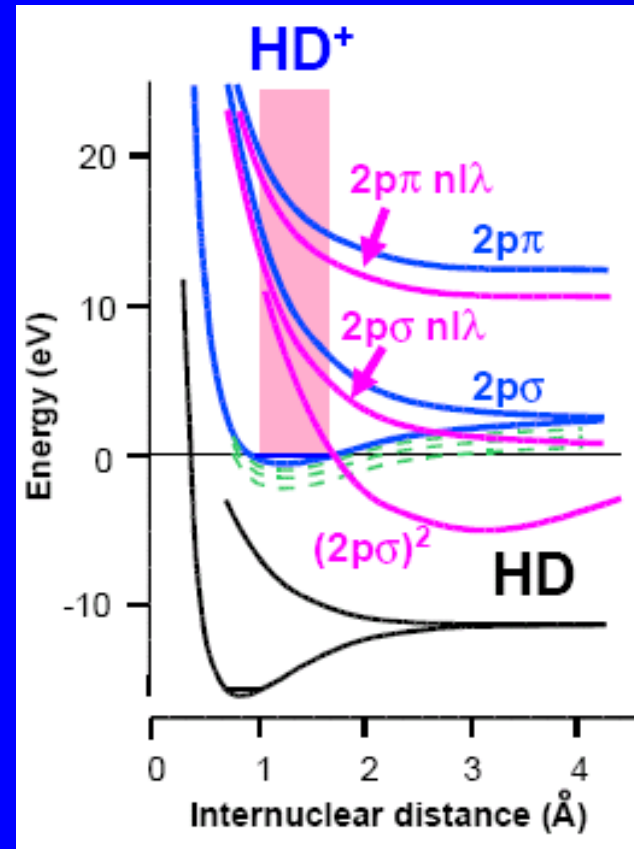
Electron collisions with H_2^+

Resonances

Autoionizing and pre-dissociating Rydberg states

$$AB^+(v) + e \longrightarrow AB^*(v', nl)$$

$$\nearrow AB^+(v'') + e''$$
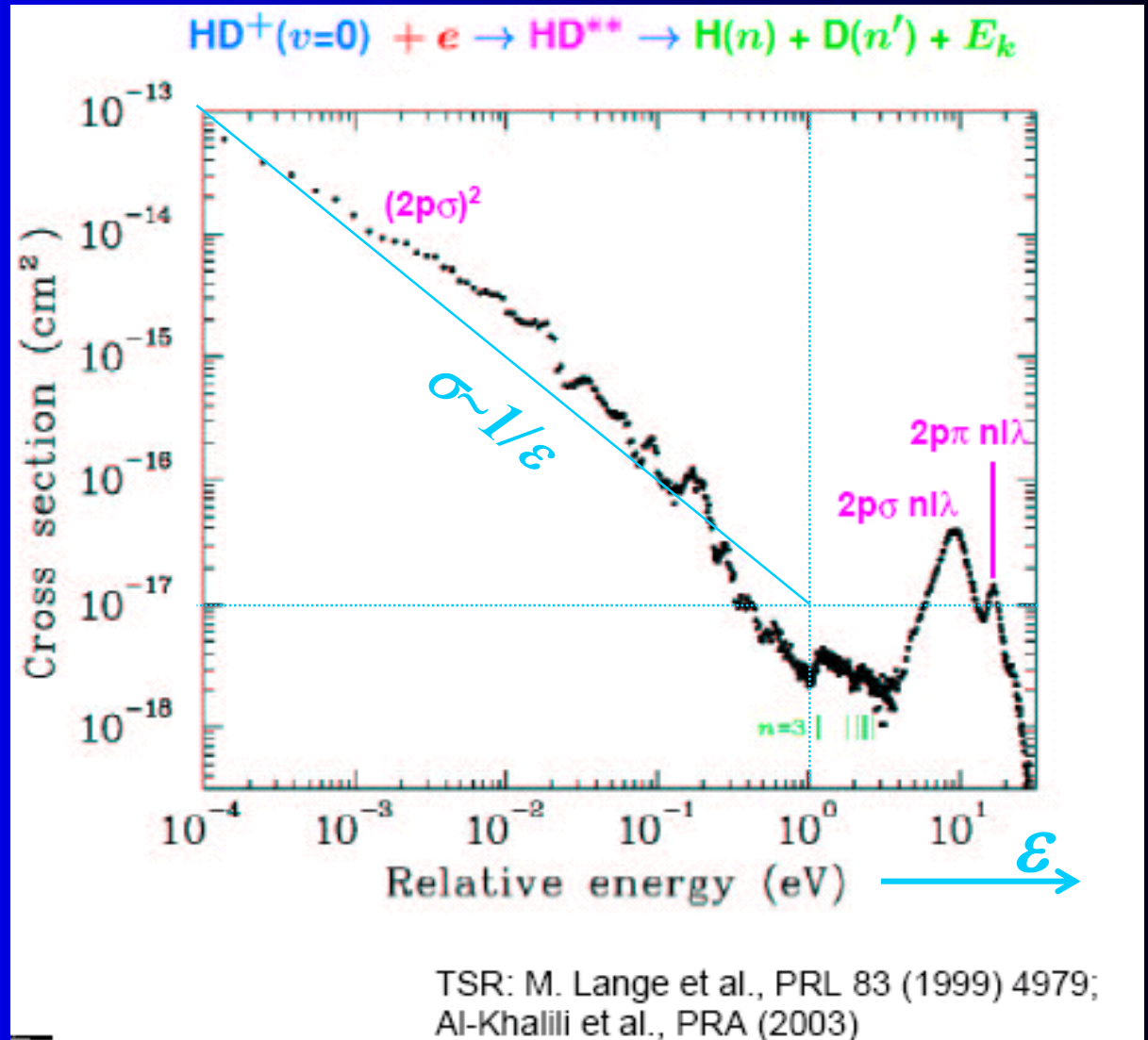$$\searrow AB^{**} \longrightarrow A^* + B$$

$A^+ + B$

AB^+

nl

v'

v

AB^{**}

$A^* + B$

Resonances

Dissociative recombination

HD$^+$

$2p\pi\ nl\lambda$

$2p\pi$

$2p\sigma\ nl\lambda$

$2p\sigma$

$(2p\sigma)^2$

HD

Energy (eV)

Internuclear distance (Å)

$HD^+(v=0) + e \rightarrow HD^{**} \rightarrow H(n) + D(n') + E_k$

$\sigma \sim 1/\varepsilon$

$(2p\sigma)^2$

$2p\pi\ nl\lambda$

$2p\sigma\ nl\lambda$

n=3

Cross section (cm^2)

Relative energy (eV)

ε

TSR: M. Lange et al., PRL 83 (1999) 4979;
Al-Khalili et al., PRA (2003)

Dissociative recombination HD+

HD+

$HD^+(v=0) + e \rightarrow HD^{**} \rightarrow H(n) + D(n') + E_k$
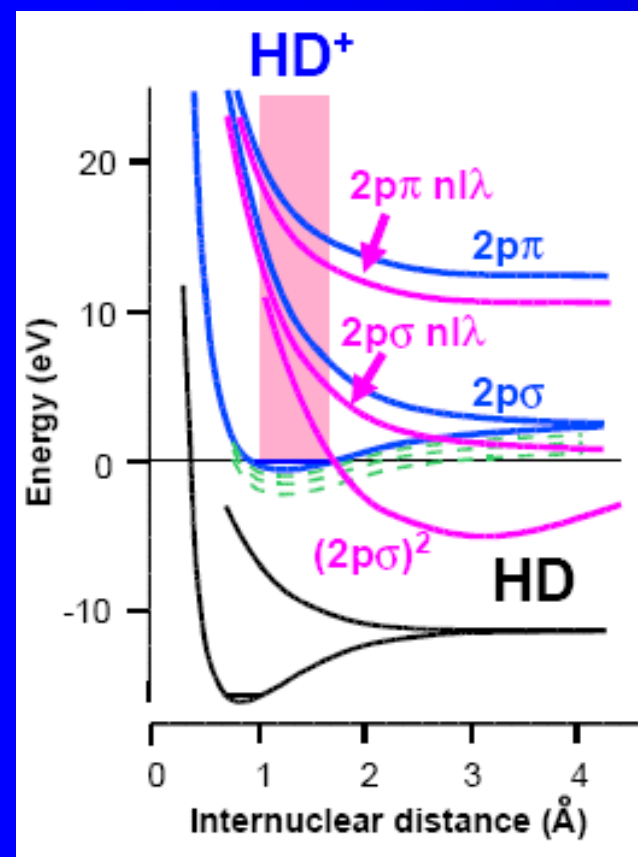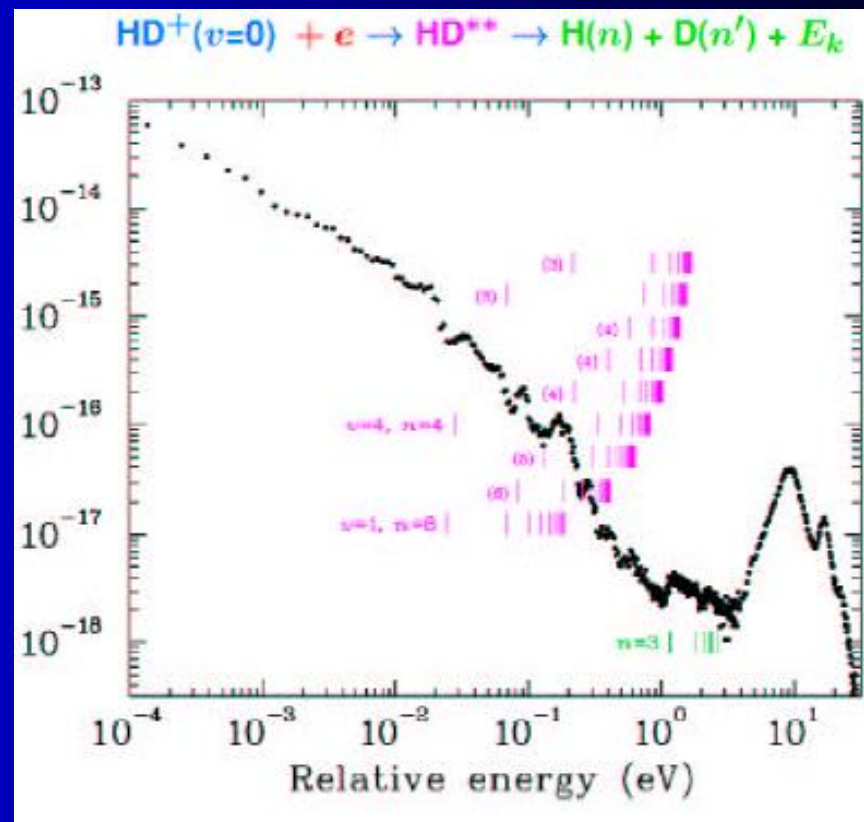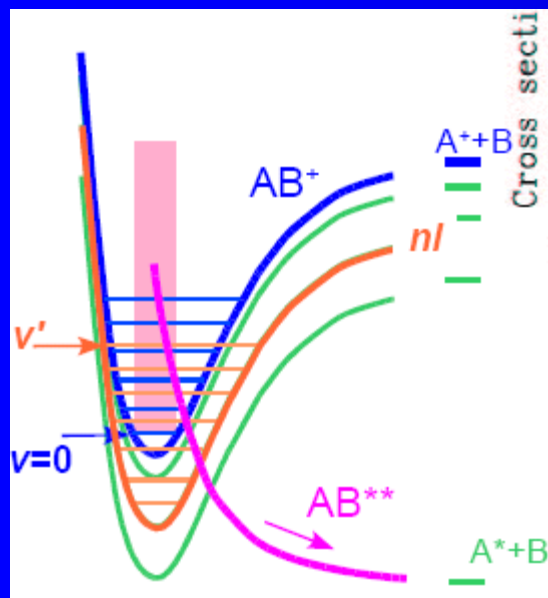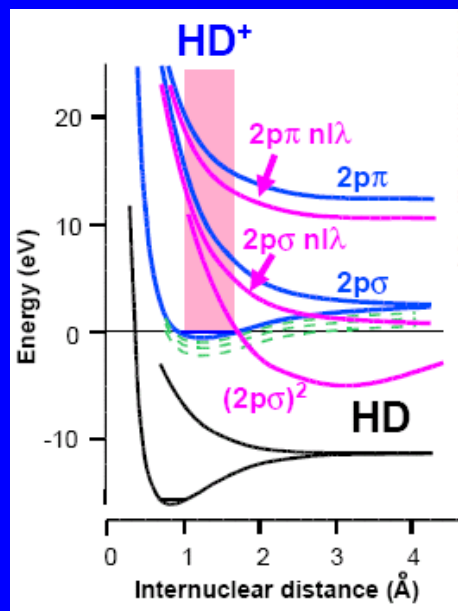
Scan of electron ion relative energy E

Electron temperature $\quad kT_{Per}=4meV$ (30meV for E>0.3eV)

$\qquad\qquad\qquad\qquad kT_{Par}=0.1meV$
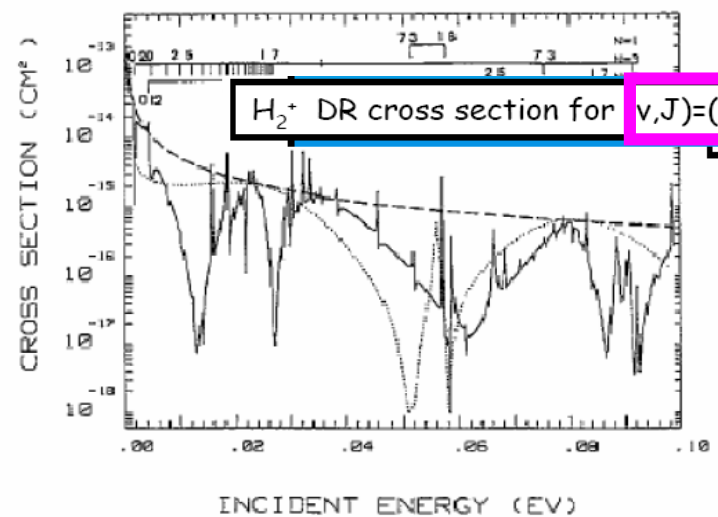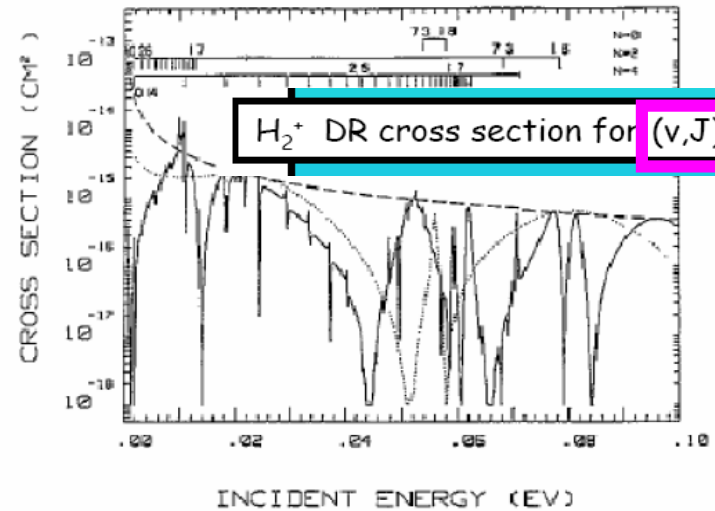
Energy resolution ~4….8 meV (E< 0.08eV)

Absolute accuracy of cross section ca. +- 30%

Recombination H_2^+

Electron collisions with H_2^+

H. Takagi, J. Phys. B, 26, 4815 (1993)

H_2^+ DR cross section for $(v,J)=(0,0)$

H_2^+ DR

H_2^+ DR cross section for $(v,J)=(0,1)$

H_2^+

$2p\pi$

$H^+ + H(n'=2)$

$(2p\sigma)^2$

$2p\sigma$

$1s\sigma$

$H^+ + H(n'=1)$

H_2

$(1s\sigma)^2$

Internuclear distance (Å)

Energy (eV)

CROSS SECTION (CM^2)

INCIDENT ENERGY (EV)
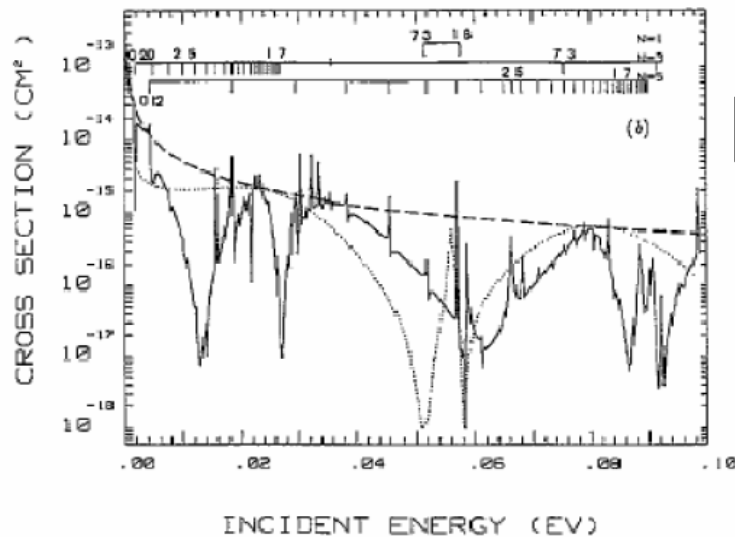
Recombination only one rotational quanta change the whole spectra

H. Takagi, J. Phys. B, 26, 4815 (1993)

Recombination cross section for a single quantum rotational state of H_2^+ (The simplest molecular ion!)
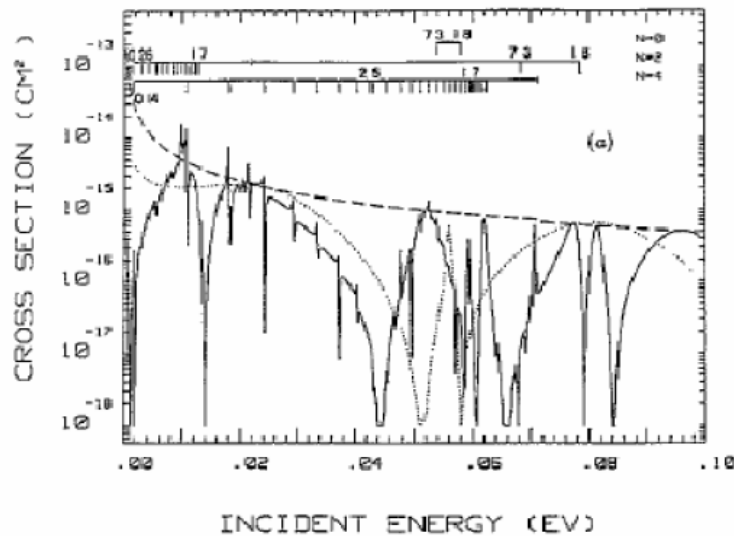
H_2^+ DR cross section for (v,J)=(0,0)

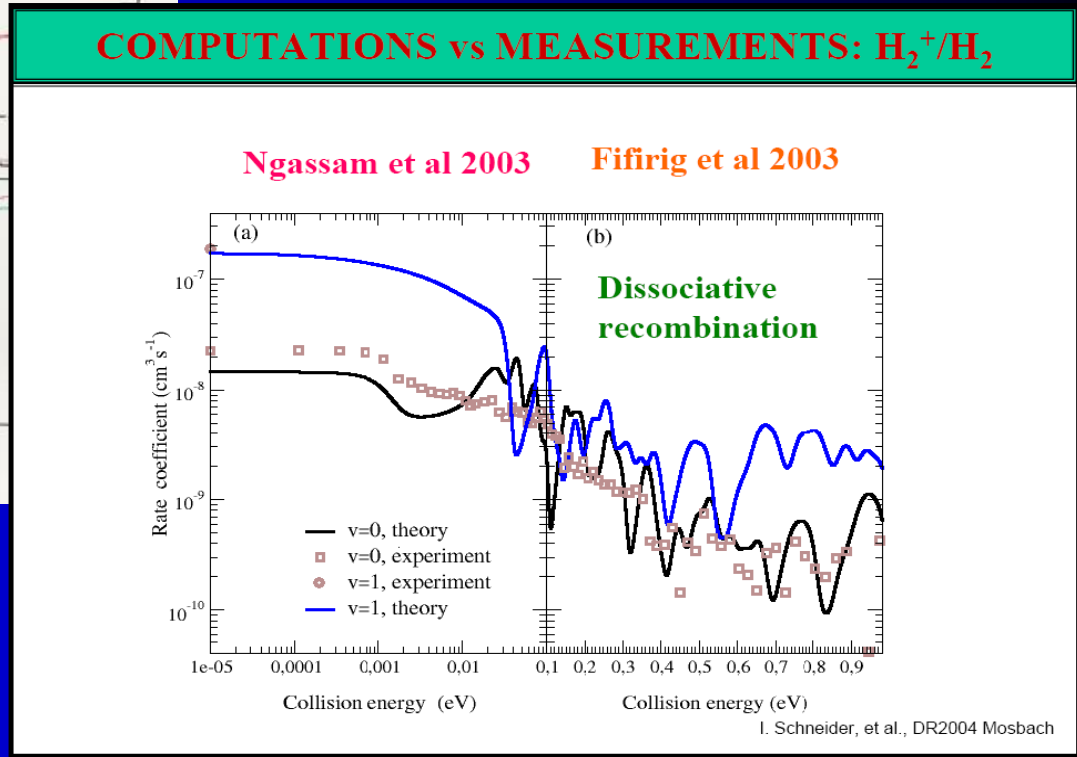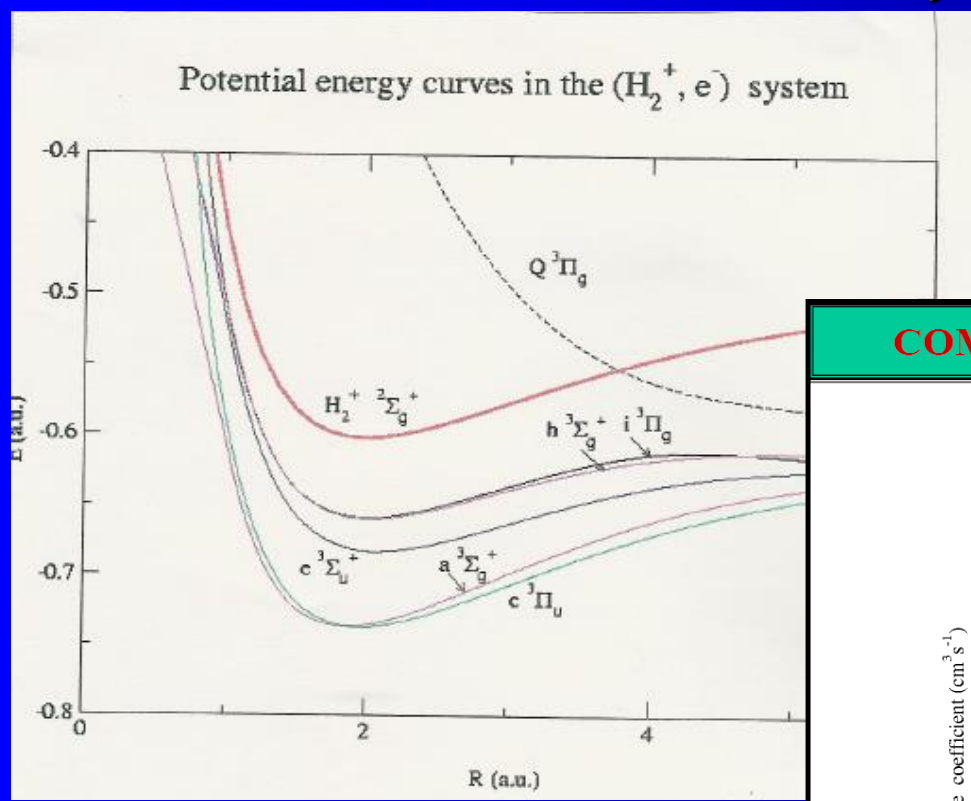Only one rotational quanta of excitation changes the whole spectra!!

H_2^+ DR cross section for (v,J)=(0,1)

In fact, these resonances have never been individually observed!

• Position
• Depth
• Shape
  teach everything about the dynamics taking place during the dissociation.
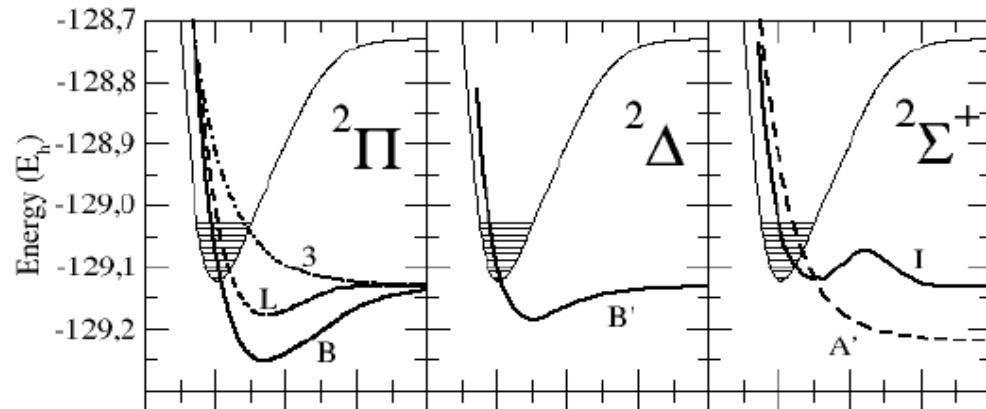
D. Zaifman, et al., DR2004 Mosbach

Recombination calculation and theory H_2^+ .....vibrational excitation

Potential energy curves in the (H_2^+, e^-) system

COMPUTATIONS vs MEASUREMENTS: H_2^+/H_2

Ngassam et al 2003   Fifirig et al 2003

Dissociative recombination

I. Schneider, et al., DR2004 Mosbach

Different energy region

Recombination NO+

Tennyson et al 1996-2000

$^2\Pi$ $^2\Delta$ $^2\Sigma^+$

$HD^+(v=0) + e \rightarrow HD^{**} \rightarrow H(n) + D(n') + E_k$

## Comparison with ASTRID

Schneider et al 2000

$NO^+(X^1\Sigma^+ v_i=0)$ dissociative recombination
MQDT modelling based on R–matrix molecular data v. experiment

Vejby–Christensen et al 1998

Mul & McGowan 1979

Present modelling

Walls & Dunn 1974

HD+

Sun & Nakamura 1990
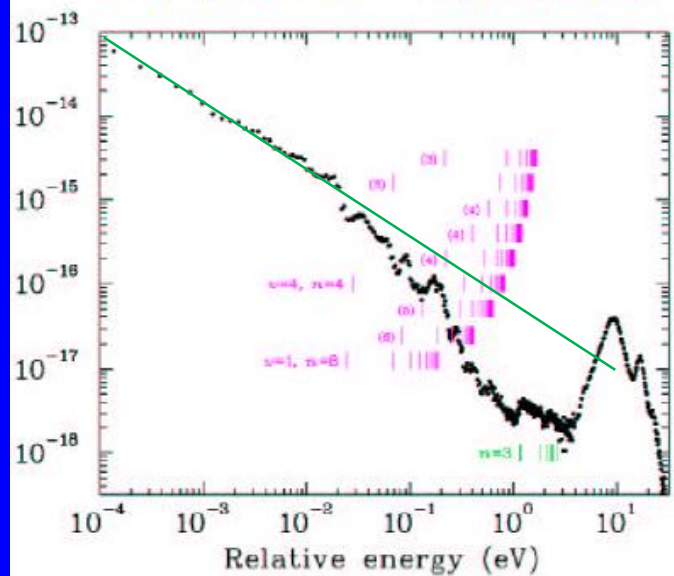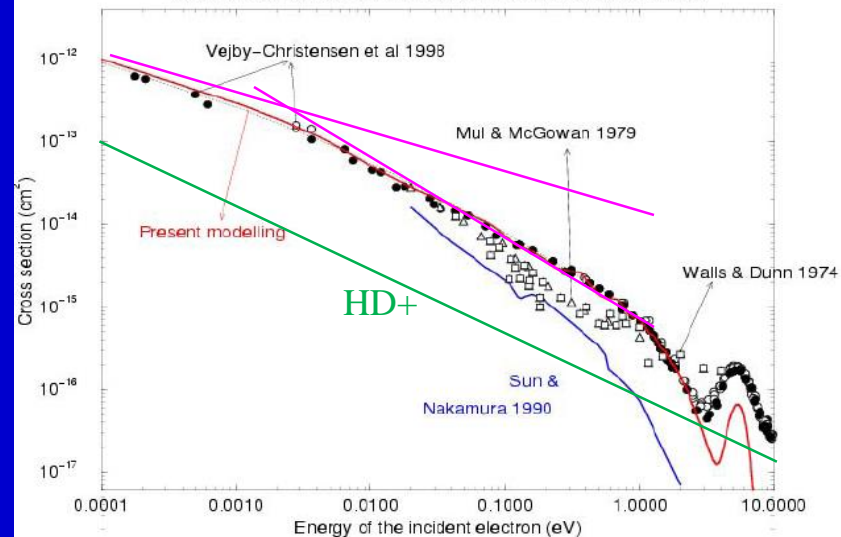
Theoretical background

Dissociative Recombination without a Curve Crossing

Theory predicted: DR rate coefficient is vary small ~ 10^{-11} cm^{3}s^{-1}
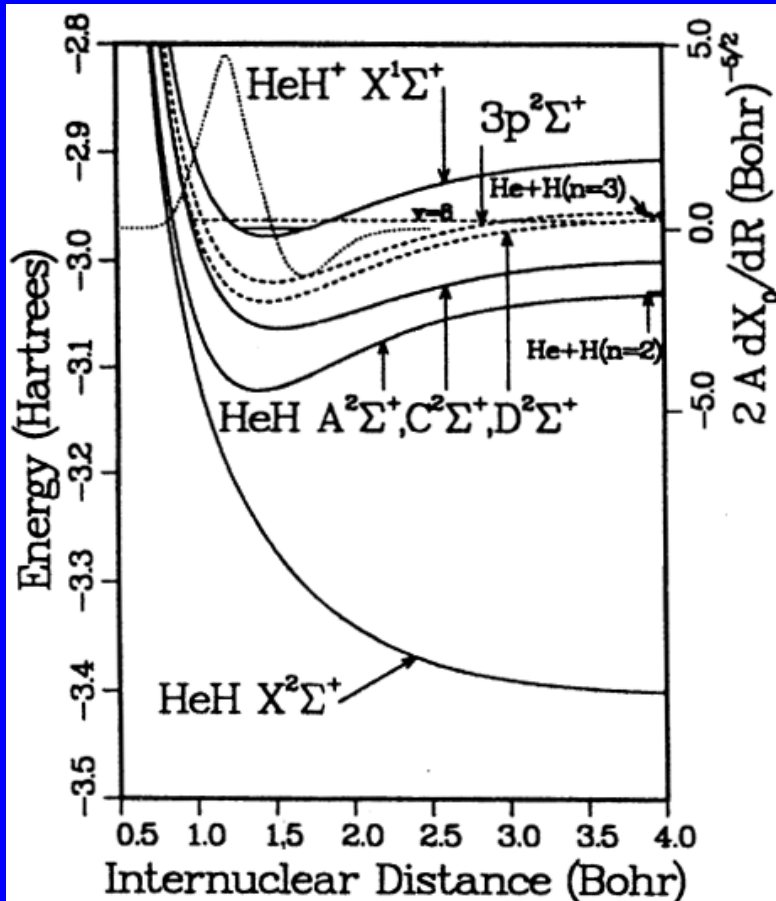
HeH$^+$ and HCO$^+$ ions-examples of a non-crossing case. However, experiments gave $\alpha \approx 2\times10^{-8}$ and $\alpha \approx 2\times10^{-7}$ cm^{3}s^{-1}

A new mechanism has been proposed!

Multi-step indirect dissociative recombination ("tunneling mode" recombination)

2019

Quantum-state-selective electron recombination studies suggest enhanced abundance of primordial HeH+

Oldřich Novotný[1]*, **Patrick Wilhelm[1]**, **Daniel Paul[1]**, **Ábel Kálosi[1,2]**, **Sunny Saurabh[1]**, **Arno Becker[1]**, **Klaus Blaum[1]**, **Sebastian George[1,3]**, **Jürgen Göck[1]**, **Manfred Grieser[1]**, **Florian Grussie[1]**, **Robert von Hahn[1]**, **Claude Krantz[1]**, **Holger Kreckel[1]**, **Christian Meyer[1]**, **Preeti M. Mishra[1]**, **Damian Muell[1]**, **Felix Nuesslein[1]**, **Dmitry A. Orlov[1]**, **Marius Rimmler[1]**, **Viviane C. Schmidt[1]**, **Andrey Shornikov[1]**, **Aleksandr S. Terekhov[4]**, **Stephen Vogel[1]**, **Daniel Zajfman[5]**, **Andreas Wolf[1]**

[1]Max-Planck-Institut für Kernphysik, Saupfercheckweg 1, 69117 Heidelberg, Germany. [2]Charles University, 18000 Praha, Czech Republic. [3]Universität Greifswald, Institut für Physik, 17487 Greifswald, Germany. [4]Rzhanov Institute of Semiconductor Physics, Novosibirsk 630090, Russia. [5]Weizmann Institute of Science, Rehovot 76100, Israel.

*Corresponding author. Email: oldrich.novotny@mpi-hd.mpg.de

The epoch of first star formation in the early universe was dominated by simple atomic and molecular species consisting mainly of two elements: hydrogen and helium. Gaining insight into this constitutive era requires thorough understanding of molecular reactivity under primordial conditions. We used a cryogenic ion storage ring combined with a merged electron beam to measure state-specific rate coefficients of dissociative recombination, a process by which electrons destroy molecular ions. We found a dramatic decrease of the electron recombination rates for the lowest rotational states of HeH+, compared to previous measurements at room temperature. The reduced destruction of cold HeH+ translates into an enhanced abundance of this primordial molecule at redshifts of first star and galaxy formation.
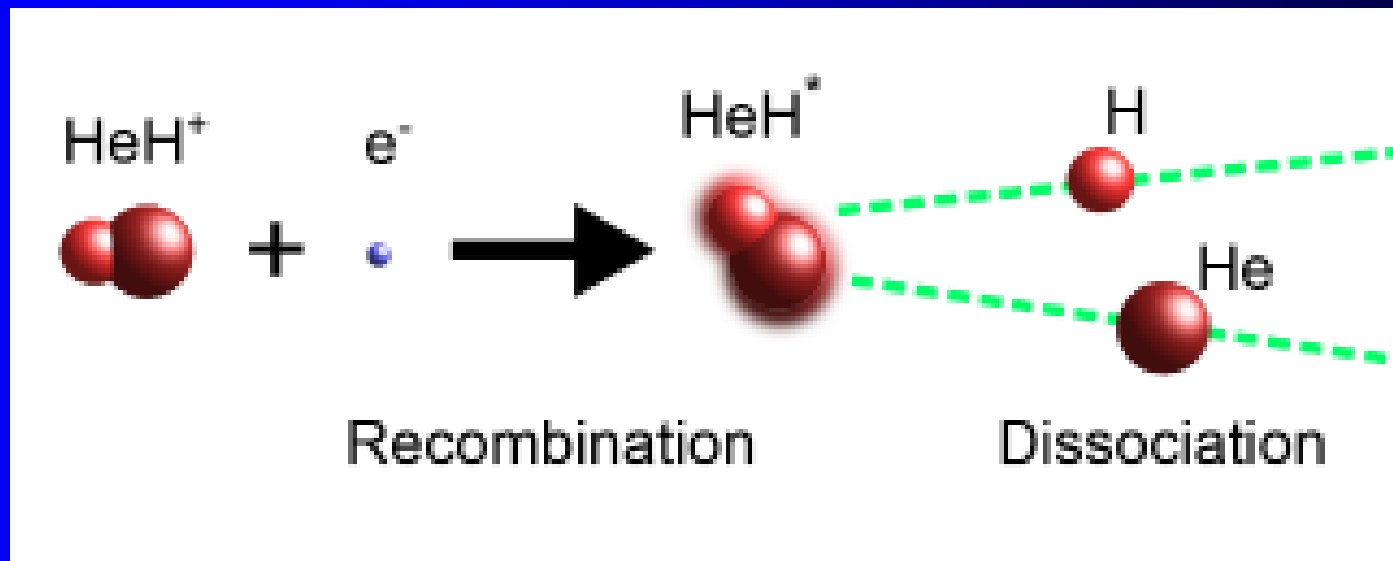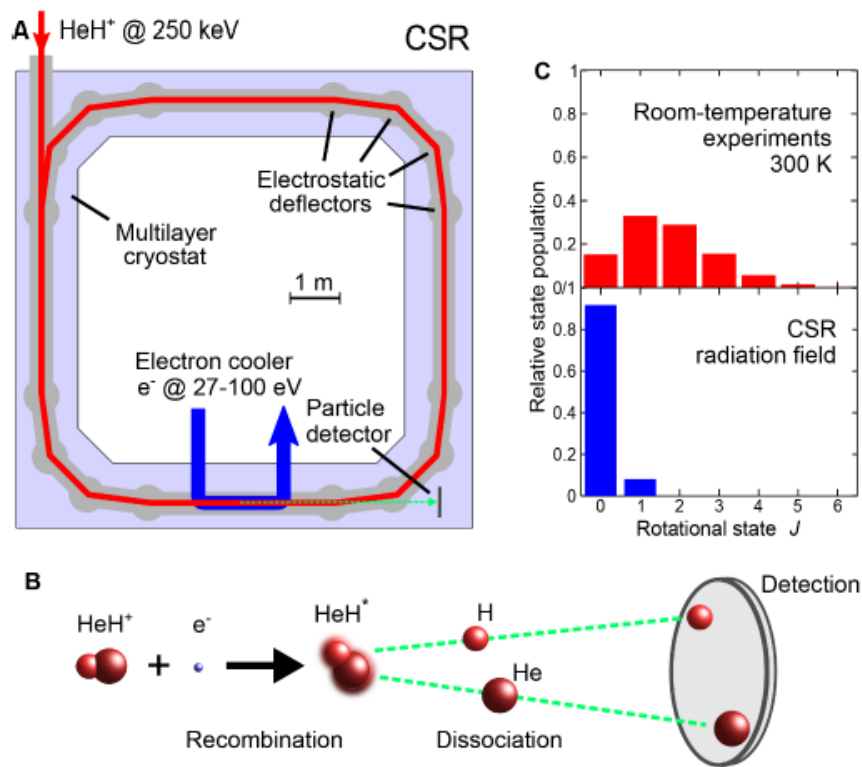
Fig. 1. Dissociative recombination in the cryogenic storage ring CSR. (**A**) Scheme of the CSR ring structure with injected and stored HeH⁺ ion beam (red), merged electron beam (blue), reaction products (green) and particle detector. (**B**) Reaction scheme and position-sensitive detection of coincident fragments. (**C**) Equilibrium rotational state populations of HeH⁺ for previous studies (300 K) and the estimated radiation field in the CSR.
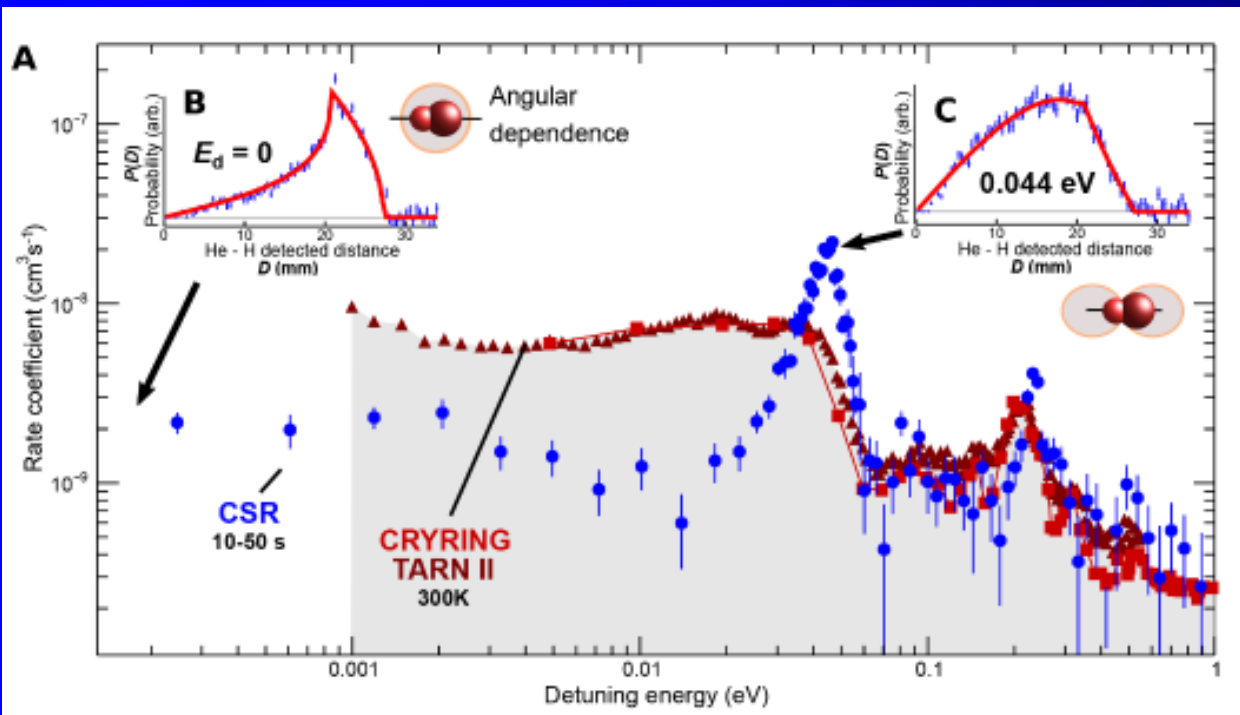
astro

Fig. 2. DR for rotationally cold HeH+. (A) Blue dots: merged-beams rate coefficient α_{DR} as a function of the detuning energy E_d after relaxation to >50% $J = 0$ (this experiment, 10 s < t < 50 s, mean ± SD); absolute scaling uncertainty ±20% (SEM). Red symbols: room-temperature data from Ref. (11) (squares, absolute scaling uncertainty ±10% SEM) and from Ref. (12) (triangles, scaled to Ref. (11) at 0.03 eV). (B) Fragment distance distribution projected into the detector plane for $E_d = 0$ (blue) with fit (19) for isotropic angular distribution (red). (C) Projected fragment distance distribution for E_d = 0.044 eV (blue) with fit (19) for a $|Y_{10}|^2$ angular distribution of the fragments (red). The angular dependences in (B) and (C) are indicated schematically.

astro

Fig. 4. Rotational-state selective DR rates for HeH⁺. (A) Merged-beams rate coefficients $\alpha_{DR}^J(E_d)$ for $J \leq 2$ and average for $J \geq 3$ (mainly 3 and 4; mean ± SD). The dashed lines mark the shift of the maximum as J increases. (B) Full lines: single-J plasma rate coefficients $\alpha_{DR,pl}^J(T_{pl})$ for $J \leq 2$ and average for $J \geq 3$ (mainly 3 and 4; mean with shaded areas as ± SD). Dotted: fully thermal rate coefficient $\alpha_{DR,therm}(T_{rot} = T_{pl})$. Dashed-dotted: values applied in early-universe models (21, 22) and astrochemistry databases (23–25). See (19) for further discussion, numerical fitting functions and parameters.
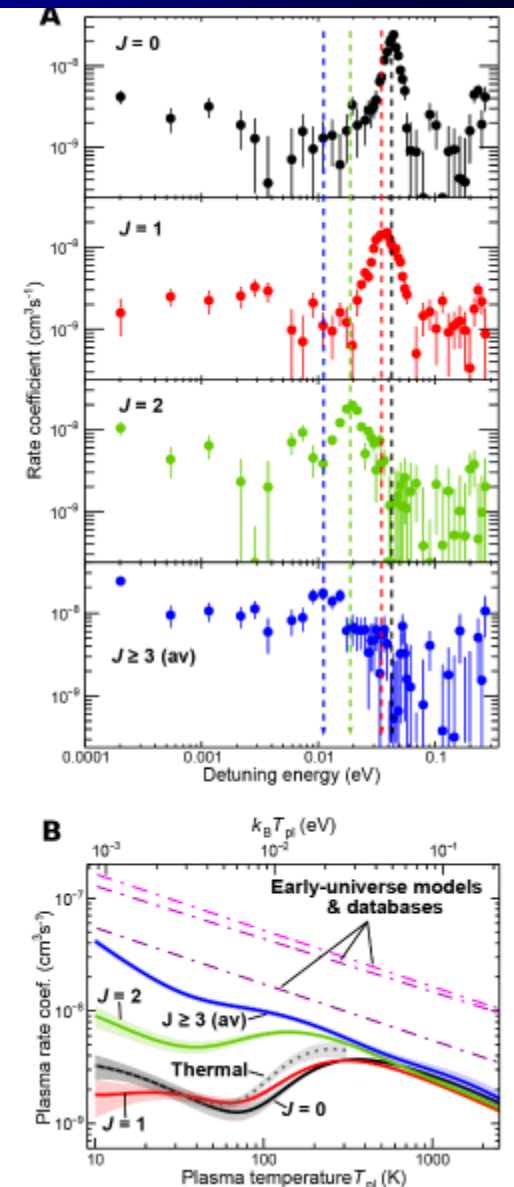
Dissociative recombination of N_2H^+ ions with electrons in the temperature range of 80–350 K

Dmytro Shapko,[1] Petr Dohnal,[1,a] Miroslava Kassayová,[1] Ábel Kálosi,[1] Serhiy Rednyk,[1] Štěpán Roučka,[1] Radek Plašil,[1] Lucie D. Augustovičová,[2] Rainer Johnsen,[3] Vladimír Špirko,[2,4] and Juraj Glosík[1]

$$N_2H^+ + e^- \xrightarrow{\alpha_{bin}} \text{neutral products}$$
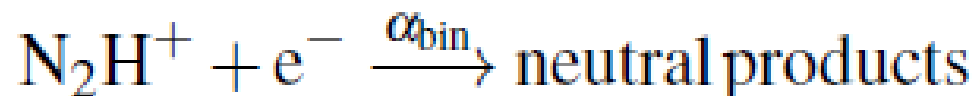
Recombination of N_2H^+ ions with electrons was studied using a stationary afterglow with cavity ring-down spectrometer. We probed in situ the time evolutions of number densities of different rotational and vibrational states of recombining N_2H^+ ions and determined the thermal recombination rate coefficients for N_2H^+ in the temperature range of 80 – 350 K. The newly calculated vibrational transition moments of N_2H^+ are used to explain the different values of recombination rate coefficients obtained in some of the previous studies. No statistically significant dependence of the measured recombination rate coefficient on the buffer gas number density was observed.

I. INTRODUCTION

N_2H^+, an important interstellar ion, has been observed in different interstellar environments such as dark and translucent clouds[1,2], protostellar cores[3], protoplanetary disks[4] and is considered to play a role in the atmospheric chemistry of Titan[5]. N_2H^+ serves as an important tracer for N_2 in dark clouds, therefore detailed information on production and destruction processes of N_2H^+ could help with the prediction of N_2 abundance in this environment. N_2H^+ in the interstellar medium is mainly produced in proton transfer from H_3^+ to N_2 and its main destruction mechanisms are proton transfer to CO and dissociative recombination with electrons[6].

astro

$$N_2H^+ + e^- \xrightarrow{\alpha_{bin}} \text{neutral products}.$$
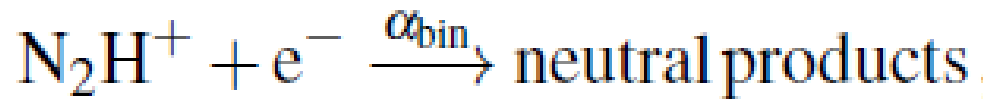
II. EXPERIMENT

The recombination rate coefficients[7,32] are measured in a stationary afterglow (SA) in conjunction with cavity ring-down spectroscopy (CRDS) to monitor the decay of the densities of different rotational and vibrational states of N_2H^+ ions. The plasma is generated in a pulsed microwave discharge in a fused silica tube (inner diameter ≈ 1.3 cm). The microwave generator is equipped with an external fast high-voltage switch to cut off the power to the magnetron within a fall time of less than 30 μs. A low microwave power in the range of $10 - 25$ W, with $\approx 40\%$ duty cycle, is used to avoid excessive heating of the gas during the discharge. The discharge tube temperature (T_{tec}) is measured by a thermocouple outside of the discharge and can be varied between 80 and 350 K.
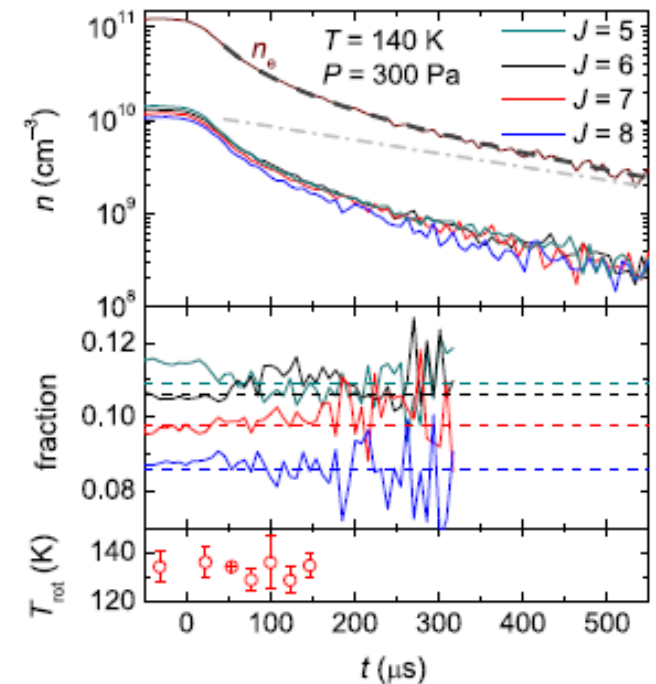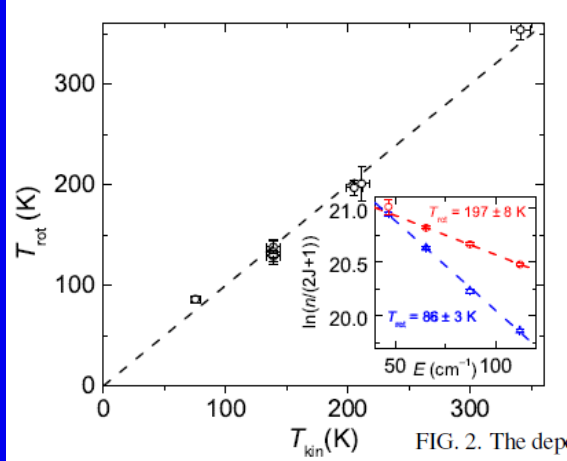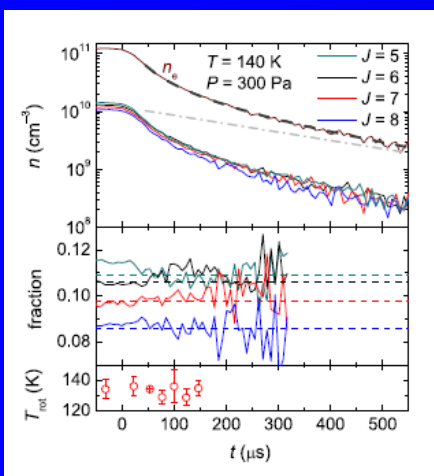
FIG. 2. The dependence of the rotational temperature measured during the discharge on kinetic temperature. All the displayed data were obtained in helium buffer gas. Insert: An example of the Boltzmann plots used for determination of the rotational temperature obtained at $T = 200$ K and $T = 78$ K.
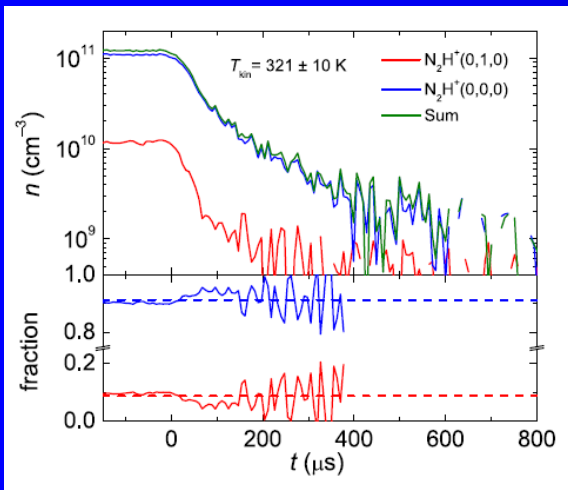
FIG. 3. An example of measured time evolutions of number densities of N_2H^+ ions in the ground and the first excited vibrational state. The lower panel shows the relative fractions of the vibrational states and the dashed lines denote the corresponding fraction in thermal equilibrium at temperature of 321 K. The particular vibrational states number densities were calculated from the measured number densities of the $J = 6$ rotational state of the ground vibrational state and of $J = 9$ state of the (01^10) vibrational state under the assumption of the same rotational temperature in both vibrational states.

FIG. 4. Dependence of the measured vibrational temperature T_{vib} on kinetic temperature T_{kin} of the N_2H^+ ions measured in the discharge. The kinetic temperature was obtained from the Doppler broadening of the P(6) line of the $(200) \leftarrow (000)$ vibrational band of N_2H^+. It was assumed that the rotational temperature of (000) and (010) states is equal to T_{kin}. The vibrational temperature was then evaluated from the P(6) line of the $(200) \leftarrow (000)$ vibrational band and from the R(9)^f line of the $(210) \leftarrow (010)$ vibrational band of the N_2H^+ ion. The full line denotes equality of $T_{vib} = T_{kin}$ and the dashed line indicates $T_{vib} = T_{kin} + 30$ K. The displayed errors are statistical errors of the fits.

astro
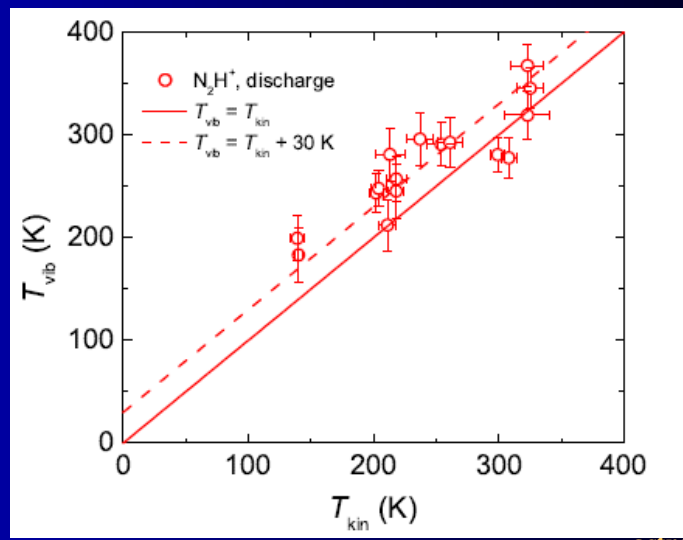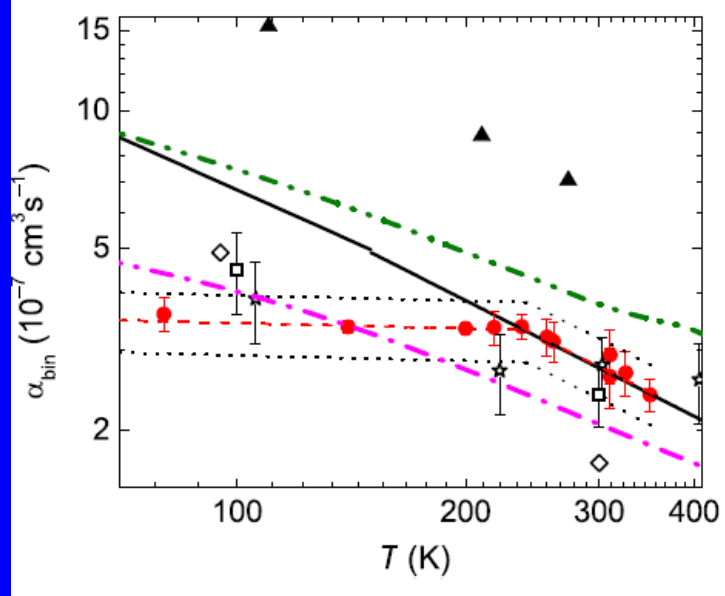
FIG. 8. The temperature dependence of the measured recombination rate coefficients of N_2H^+ (full circles, the value of α_{bin} at 350 K was obtained in H_2 buffer gas, for the rest of the data points, helium buffer gas was used) compared to values obtained in previous experiments. Rhomboids: FALP[11], squares: FALP[13], stars: FALP[14], triangles: stationary afterglow with absorption spectroscopy[17], full line: ion storage ring[6], double-dot-dashed line: merged beams[8] and to recent theoretical calculations by Fonseca dos Santos[21] (dot-dashed line, the rate coefficient was calculated from the cross sections for the direct and indirect recombination process in ref.[21]). The dashed line denotes fit to the data: $\alpha_{N_2H^+} = (2.81 \pm 0.04) \times 10^{-7}(T/300)^{-(0.81\pm0.10)}$ cm^{3}s^{-1} for $T > 240$ K and $\alpha_{N_2H^+} = (3.29 \pm 0.04) \times 10^{-7}(T/300)^{-(0.06\pm0.02)}$ cm^{3}s^{-1} otherwise. The dotted lines show 15% deviation from the fitted value (estimated systematic error of the measurement reflects mainly the uncertainty in the effective discharge column length and in the calculated vibrational transition moments).
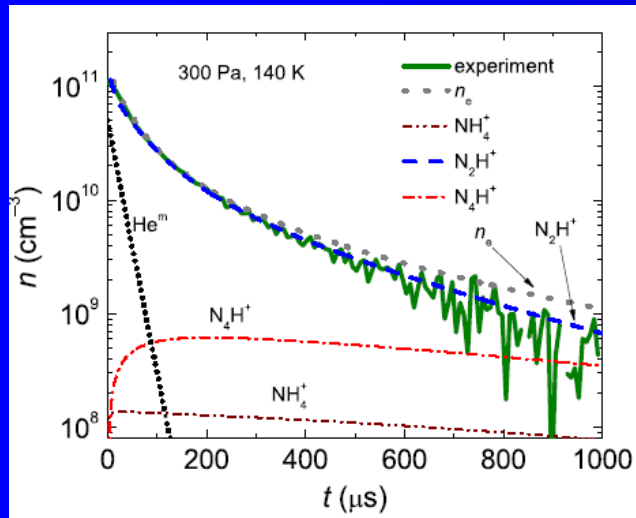
FIG. 9. Time evolution of the measured overall number density of N_2H^+ ions (full line) compared to the results obtained from the model of chemical kinetics. The data were obtained at $T = 140$ K, [He] = 1.5×10^{17} cm^{-3}, [Ar] = 2.5×10^{14} cm^{-3}, [H$_2$] = 5×10^{14} cm^{-3} and [N$_2$] = 4×10^{13} cm^{-3} (same as in Figure 1) and [NH$_3$] = 5×10^{11} cm^{-3}. [He^m]$(t = 0) = 1/3\, n_e(t = 0)$.

astro

Recombination of H_3^+

$$H_3^+ + e^- \rightarrow H + H + H$$
$$\rightarrow H_2 + H$$
$$\rightarrow H_3^* \quad (?)$$
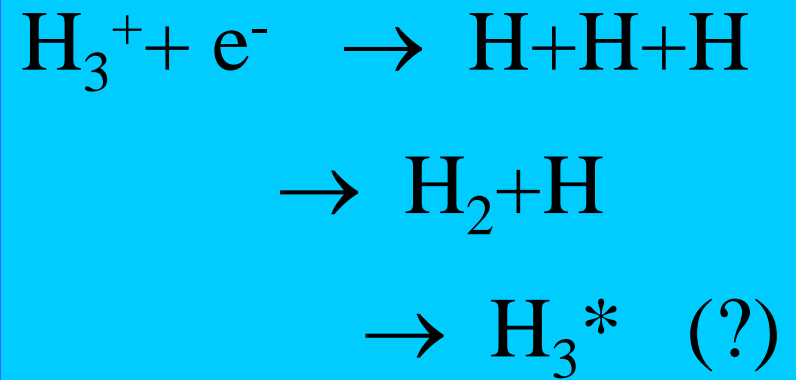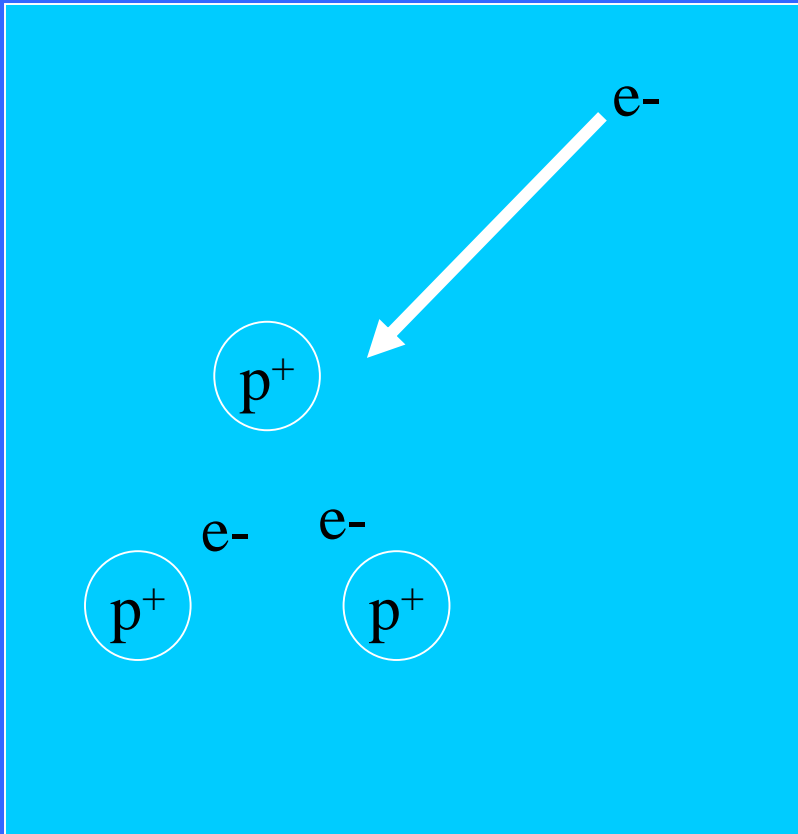
Tunneling dissociative recombination
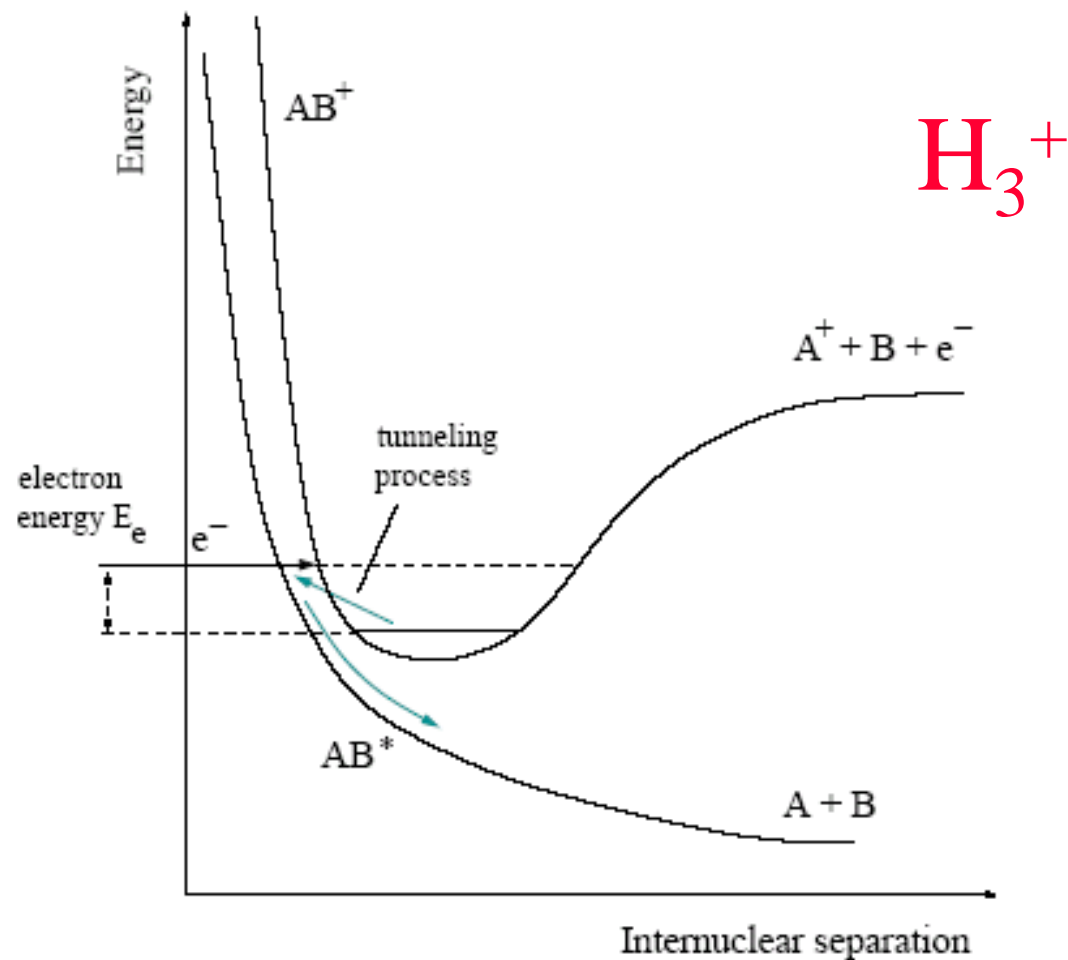
Figure 4.3: *Sketch of tunneling mode dissociative recombination.*

Tunneling dissociative recombination

H_3^+
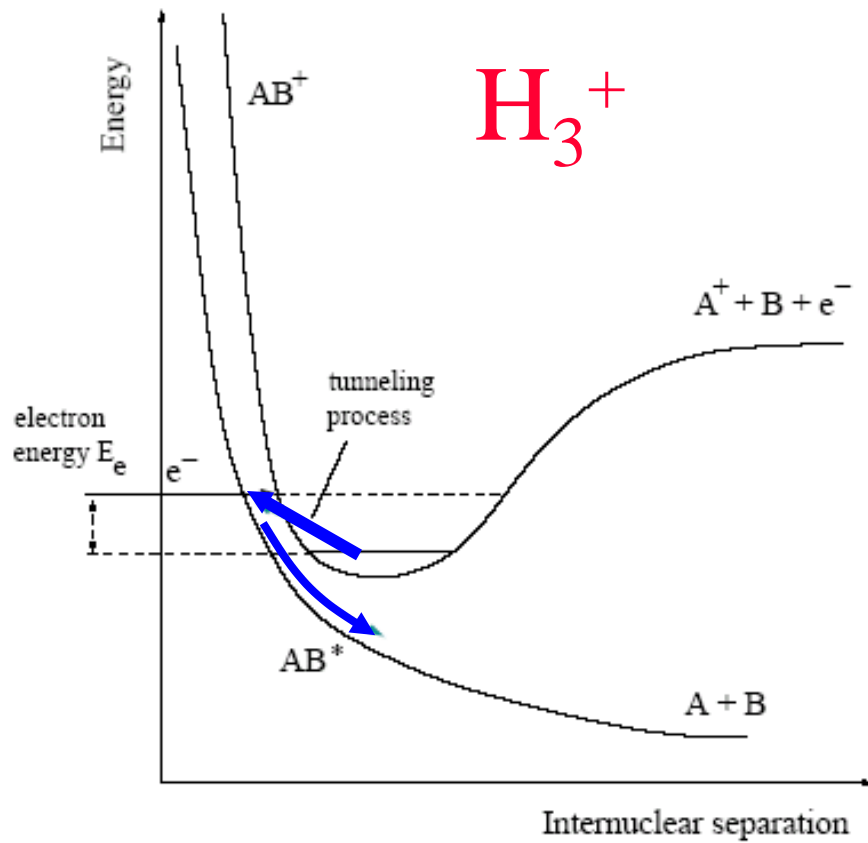
Figure 4.3: *Sketch of tunneling mode dissociative recombination.*
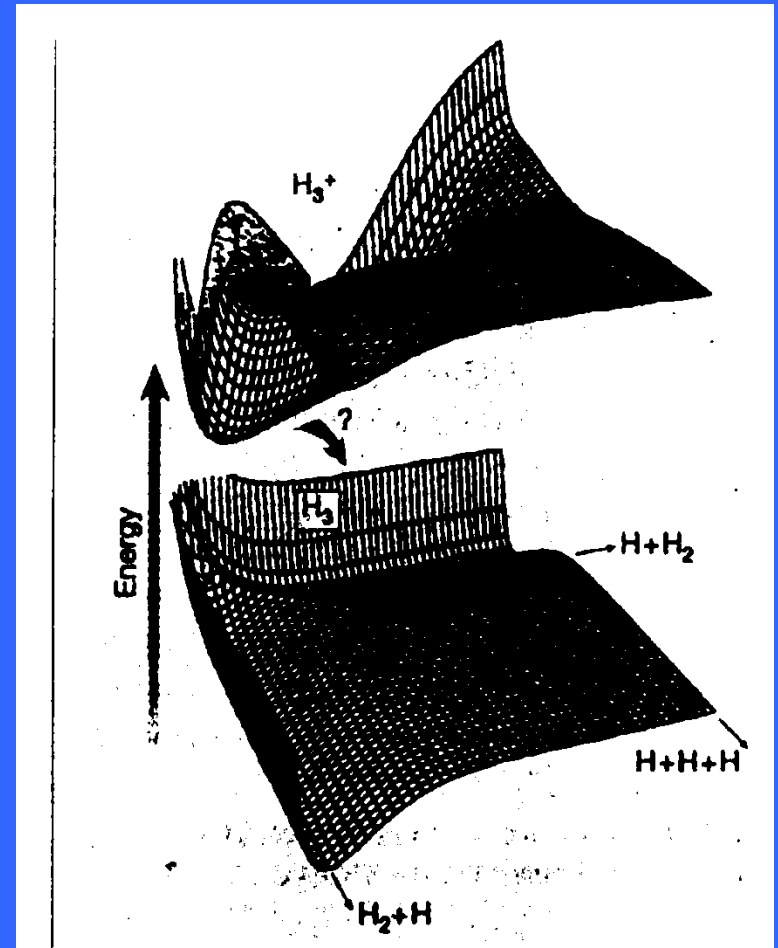
Dissociative recombination of H_3^+. Relevant potential curves
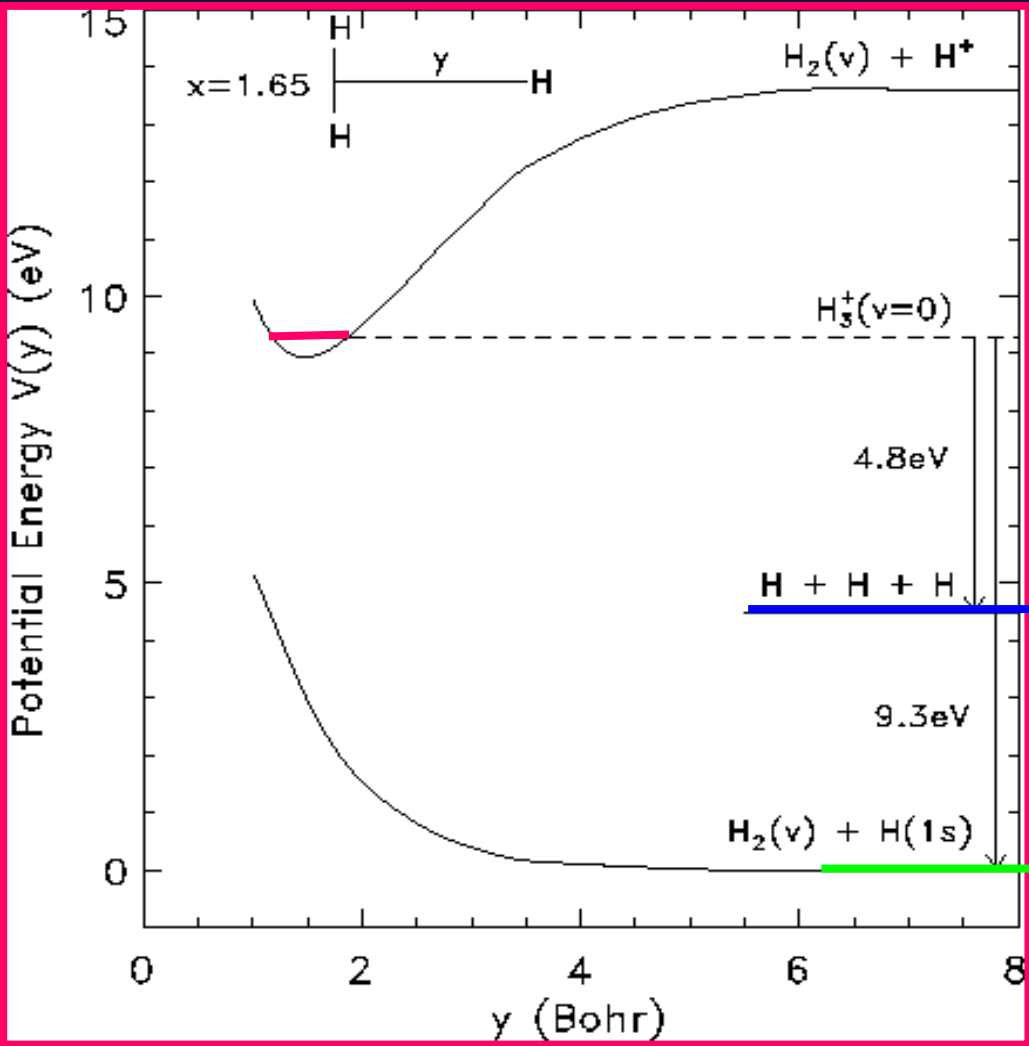
Dissociative recombination of H_3^+
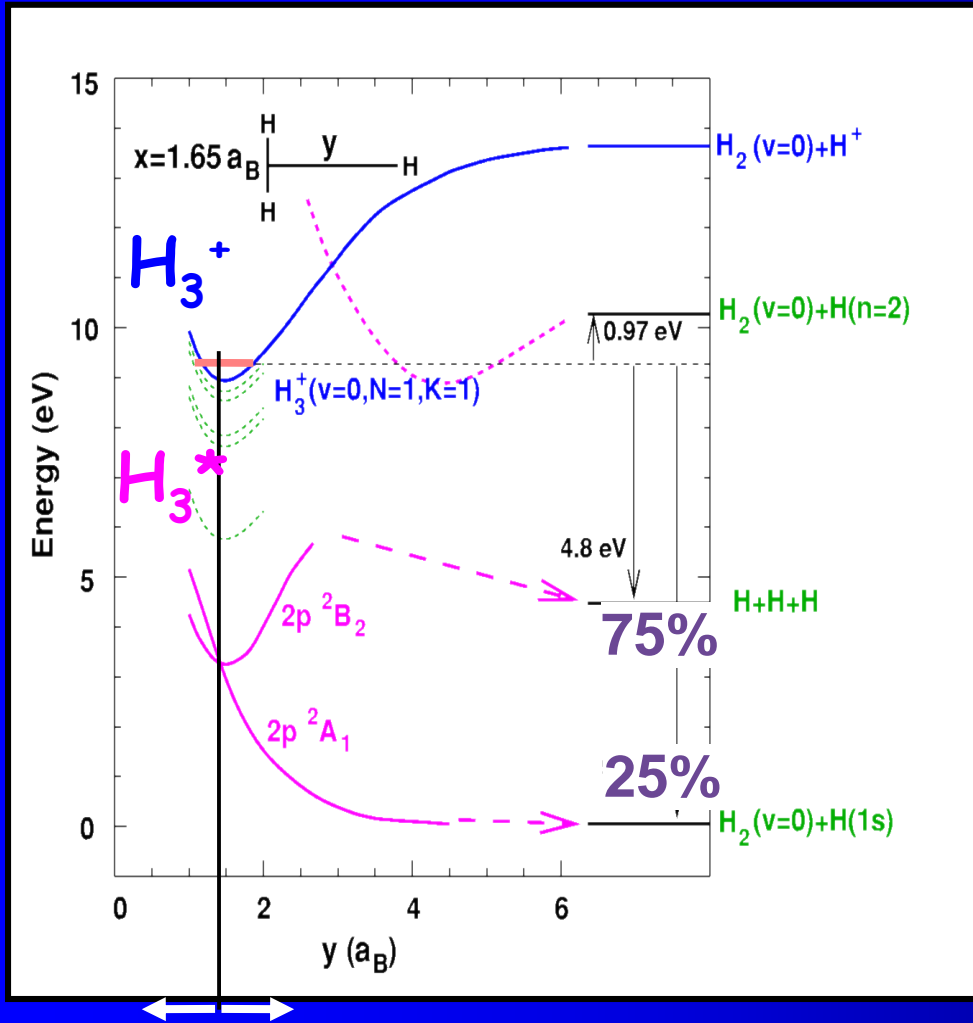
Remote curve crossing

Electron capture via Jahn-Teller coupling of electronic and ro-vibrational motion

Prototype system for electron capture and dissociation mechanisms in polyatomic species

Three atomic ions

Dissociative recombination of H_3^+

Prototype system for electron capture and dissociation mechanisms in polyatomic species

H_3^+

H_3^*

$x = 1.65\, a_B$

$H_2(v=0) + H^+$

$H_2(v=0) + H(n=2)$

$H_3^+(v=0, N=1, K=1)$

0.97 eV

4.8 eV

$2p\,{}^2B_2$

$2p\,{}^2A_1$

H+H+H

75%

25%

$H_2(v=0) + H(1s)$

Energy (eV)

$y\ (a_B)$

Symmetric deformation
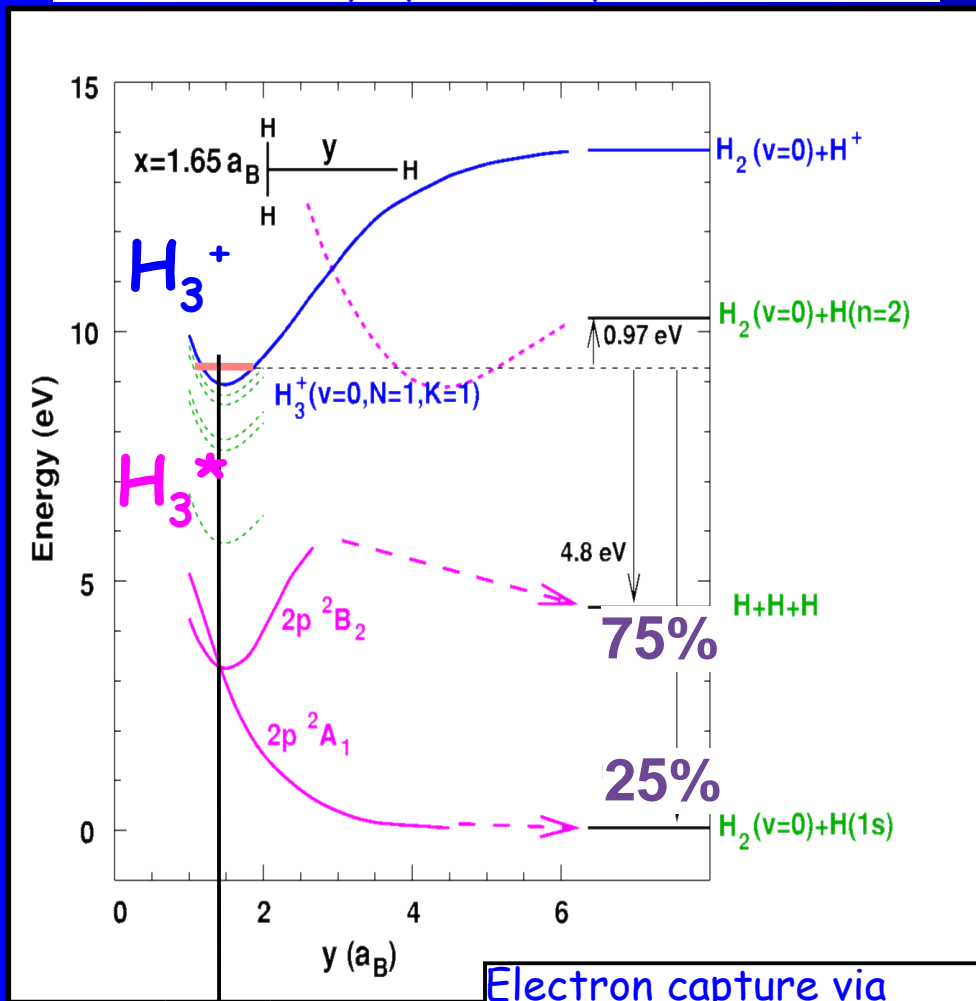
Electron capture via Jahn-Teller coupling of electronic and ro-vibrational motion

FIG. 4. The figure demonstrates how the Jahn-Teller effect produces a high rate of dissociative recombination. One $2p\sigma$ potential surface and two $2p\pi$ potential surfaces [47] of the neutral molecule are shown. The conical intersection is produced by Jahn-Teller coupling. When an electron arrives, it scatters first into a low-lying vibrationally excited Rydberg state $\{01^1\}$. Then, after the nuclei vibrate, the system finds its way with high probability into a $2p\pi$ state having high vibrational excitation, near the point of conical intersection. The contour plot at the bottom of the figure represents the lowest $2p\pi_1$ surface. All three potential surfaces are shown in the reduced 2D space of dimensionless normal coordinates. The coordinates used here are the normal asymmetric Q_x, Q_y coordinate, with ρ and ϕ their polar components [17,18]. The third vibrational coordinate—the symmetric stretch coordinate Q_1—is kept constant for this graph.

FIG. 1. The problem of DR of H_3^+ in the hyperspherical adiabatic approximation. The lowest hyperspherical adiabatic potential (thick full line) of the H_3^+ and number of hyperspherical adiabatic potentials of the neutral molecule (thin lines). Lower family of lines (darker lines) dissociate to the H_2+H channel; the upper family (lighter lines) dissociate to the $H+H+H$ channel. To calculate hyperspherical adiabatic curves we used the three-dimensional H_3^+ potential from Ref. [48] and the H_3 potential from Refs. [35–37]. Since the density of hyperspherical states is high, only every tenth H_3 potential curve is shown in the figure. The dashed line shows the position of the ground vibrational level of the ion, which is the only one populated in the relevant experiments.

FIG. 4. The figure demonstrates how the Jahn-Teller effect produces a high rate of dissociative recombination. One $2p\sigma$ potential surface and two $2p\pi$ potential surfaces [47] of the neutral molecule are shown. The conical intersection is produced by Jahn-Teller coupling. When an electron arrives, it scatters first into a low-lying vibrationally excited Rydberg state $\{01^1\}$. Then, after the nuclei vibrate, the system finds its way with high probability into a $2p\pi$ state having high vibrational excitation, near the point of conical intersection. The contour plot at the bottom of the figure represents the lowest $2p\pi_1$ surface. All three potential surfaces are shown in the reduced 2D space of dimensionless normal coordinates. The coordinates used here are the normal asymmetric Q_x, Q_y coordinate, with ρ and ϕ their polar components [17,18]. The third vibrational coordinate—the symmetric stretch coordinate Q_1—is kept constant for this graph.

$e^- + H_3^+$

Capture

Autoionization

H_3^* resonant state(s)

predissociation

To get high recombination rate, we need

(a) efficient capture

(b) predissociation faster than auto-ionization

Cosmic-ray ionisation rate $\gamma \sim 3 \times 10^{-17} s^{-1}$

Dense Clouds

Barnard 68 (João Alves)

Formation

$$H_2 \xrightarrow{h\nu} H_2^+ \xrightarrow{H_2} H_3^+$$

$$d[H_3^+]/dt \sim \gamma \cdot [H_2]$$

Diffuse Clouds

Cygnus OB2 (POSS)
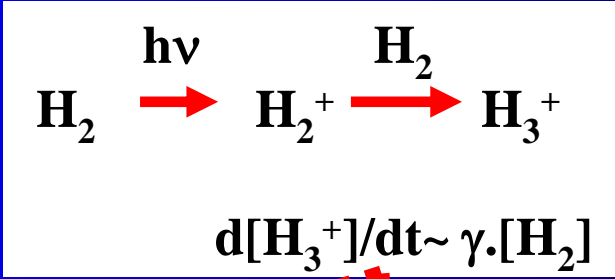
a) DENSE CLOUDS:

$H_3^+ + CO$ $d[H_3^+]/dt \sim -k_{CO}x[H_3^+]x[CO]$

$(k_{CO}=2 \times 10^{-9} cm^3 s^{-1})$

$[H_3^+]=\gamma/k_{CO} \cdot [H_2]/[CO]=$ **~1x10^{-4}cm^{-3}**

~OK with observation

b) DIFFUSE CLOUDS:

$H_3^+ + e^-$ $d[H_3^+]/dt \sim -\alpha_{DR}[H_3^+][e^-]$

$\alpha_{DR}=2 \times 10^{-7} cm^3 s^{-1} x(T/300)^{-0.65}$ (the value from 2005)

$[H_3^+]=\gamma/\alpha_{DR} \cdot [H_2]/[C]=$ **~1x10^{-7}cm^{-3}**

~ NO with observation

… history is repeating itself ….

$$H_3^+ + e^- \implies H + H_2, 3H$$

RSDM 2012

DR 2013

$\alpha(T=300\ K)$
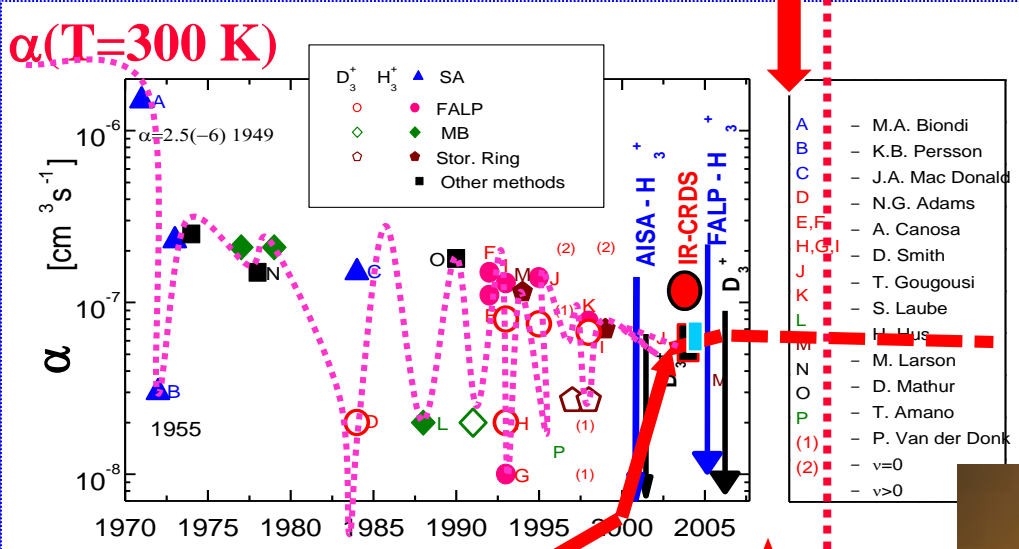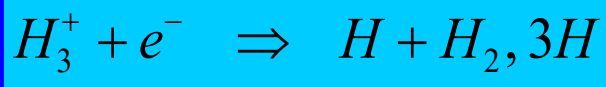
THEORY OF DR

Doubts 2011

"Presently no rate coefficient measurement with a confirmed temperature below 300 K exists".

Petrignani *et al*. Phys. Rev. A (2011)

and … history repeated itself .

M. Larsson et al, CP Letters (2008)

… One remaining problem is to understand the plasma afterglow experiments.

Plasma in TDE
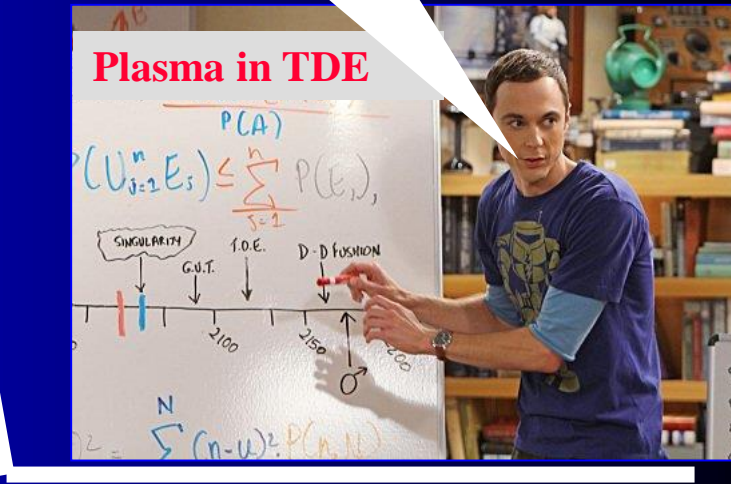
…. many times it was concluded, that the task was finished….

… and the caravan is on its way

p/o

Calculated life time from Slava

Slava 30 08 07

$$H_3^+ + e \rightarrow H_3^*$$

$$H_3^+ + e \Leftrightarrow H_3^* \rightarrow$$
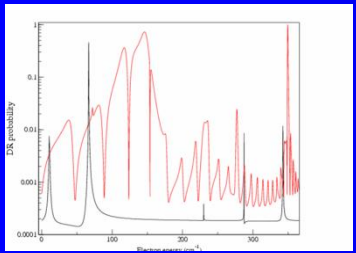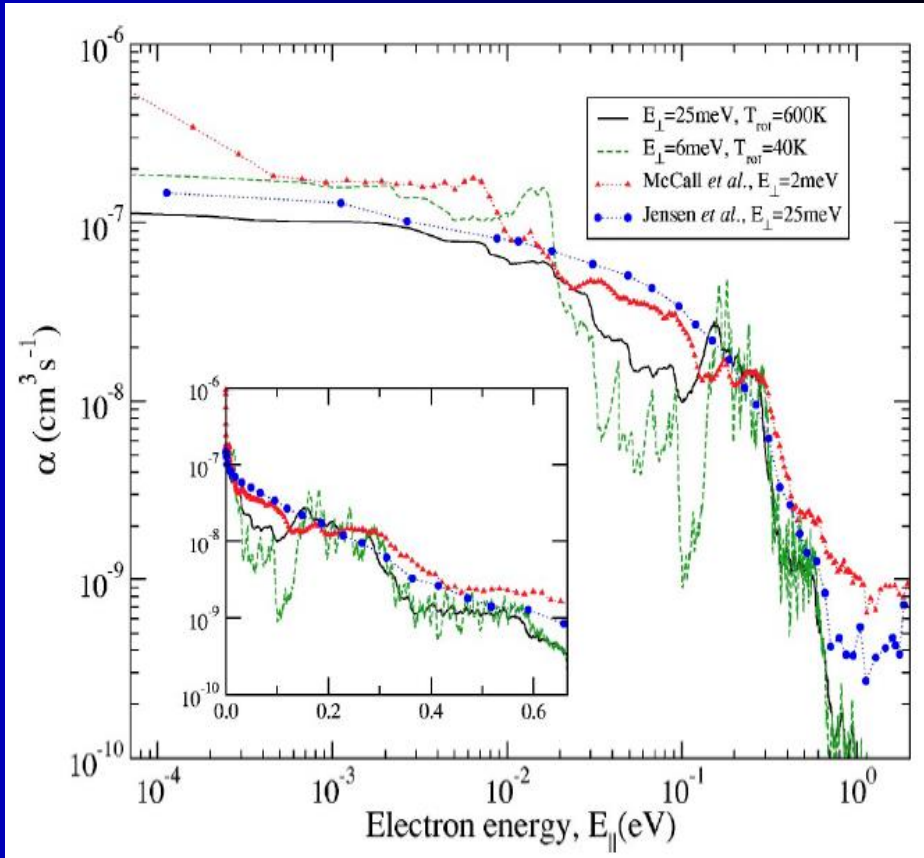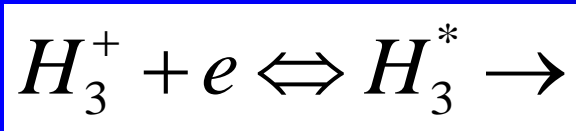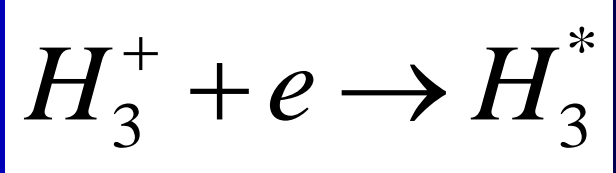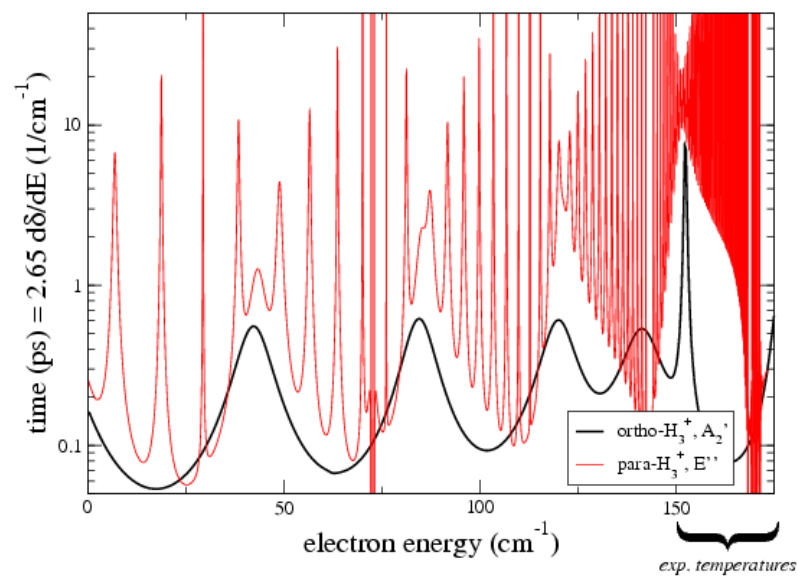
Dear Juraj and Chris, I'm sending you the figure with the DR probabilities for two different symmetries (red and black curves). The red curve corresponds to the rotational autoionization region. Fro this figure you can have an idea about the widths of the resonances. With best wishes, Slava

Recombination rate coefficients
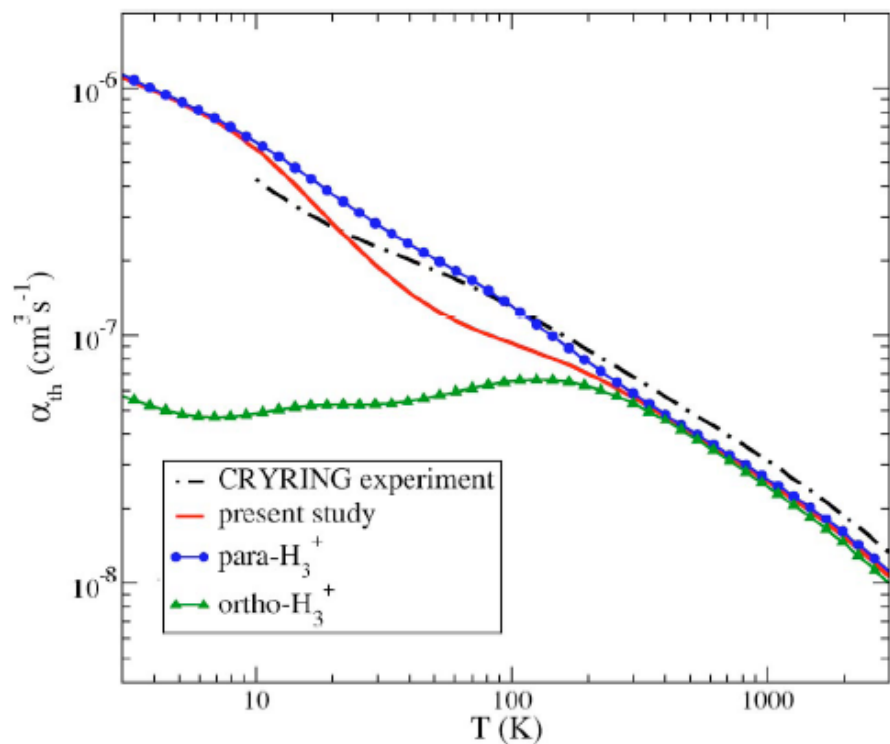
FIG. 5. (Color online) The present theoretical thermal rate coefficient for dissociative recombination of H_3^+ is compared with the experimental rate coefficient deduced from the storage ring experiment of McCall and co-workers (Refs. 9 and 10).
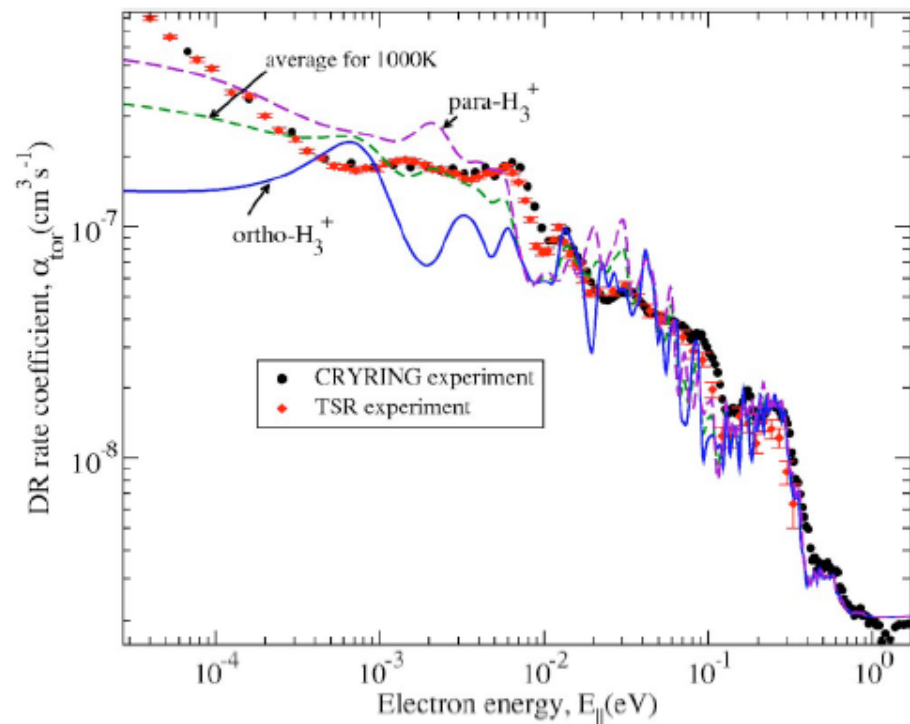
FIG. 3. (Color online) This figure compares the theoretical DR rate coefficient to the high-resolution storage ring experiment of Kreckel et al.[12] carried out at TSR. The experimental resolution parameters are $\Delta E_\parallel$ and $\Delta E_\perp$ are 25 μeV and 0.5 meV, respectively. The theoretical curve shown has been calculated with these parameters and rotational temperature T_{rv} =1000 K. The figure also shows the theoretical DR rate coefficients calculated separately for ortho- and paraconfigurations of H_3^+ with the same parameters $\Delta E_\parallel$, $\Delta E_\perp$, and T_{rv}.

The battle ship enters the stage

FALP

10^{-8}

Πλασμα

Perseus   Rho Ophiuchus
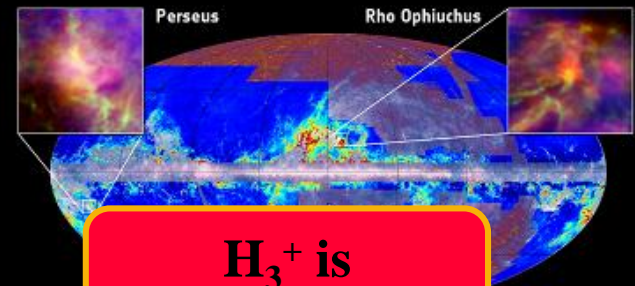
H_3^+ is
fundamental

Cryo-NIR-CRDS

AISA

Cryo-FALP

AISA

...versity Prag...

Pumping   He/Ar/H₂

Laser   LN₂

Pulsed
RF

Pressure dependence
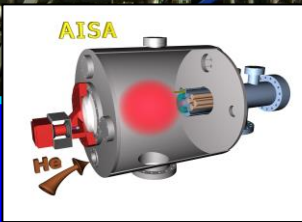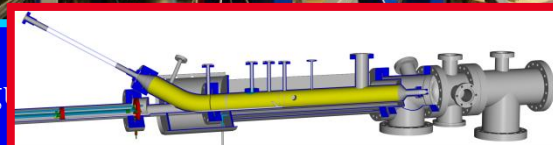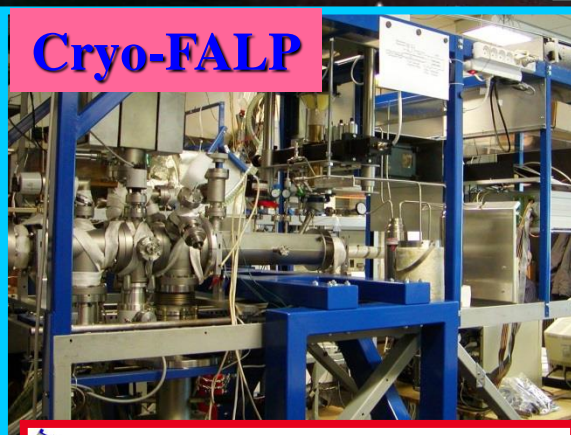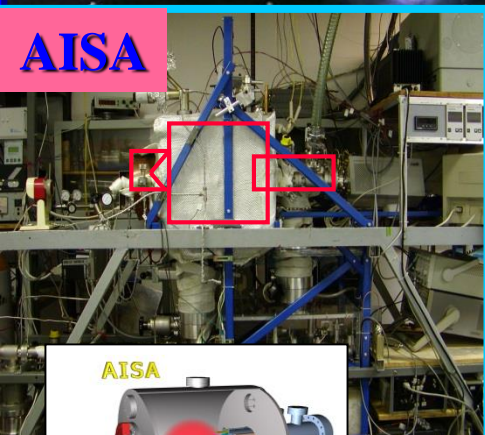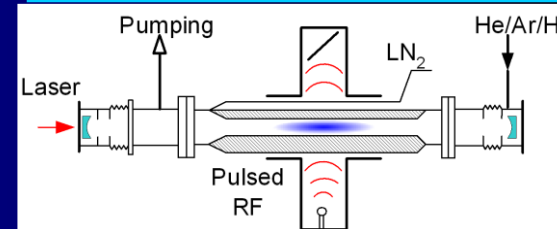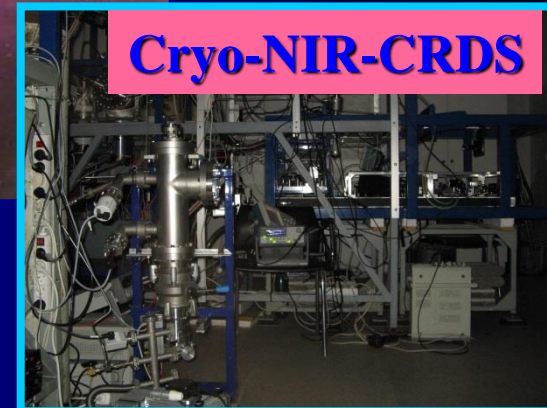
Pulsed (stationary) afterglow

Discharge pulse

microwave, UV, x-ray, e-beam
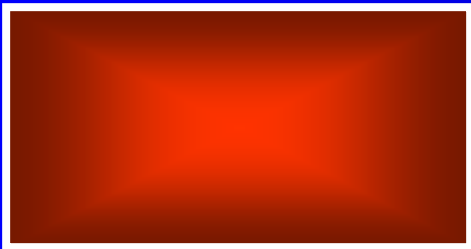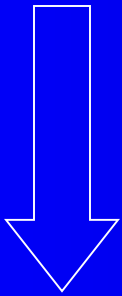
Plasma chamber
He: ~ 1 –20 Torr
Ar: 10 to 30 %
        + molecules

Measure $n_e(t)$
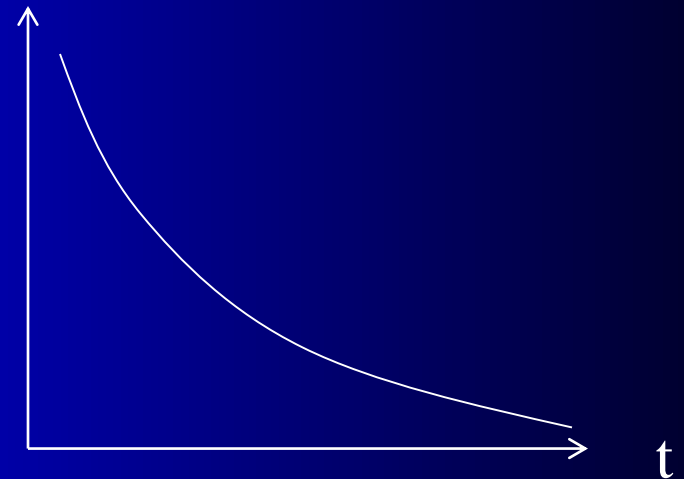
Get:

$$\frac{dn_e}{dt} = -\alpha n_e{}^2 + (diffusion)$$

$$n_e(t) = \frac{n_{e0}}{1 + \alpha n_{e0} t}$$

t

We measure effective – apparent binary recombination rate coefficient

p_{tot} = 6,2 Torr

$[H_2] = 4 \times 10^{14}$ cm^{-3}

Quasineutral H$_3^+$ dominated plasma
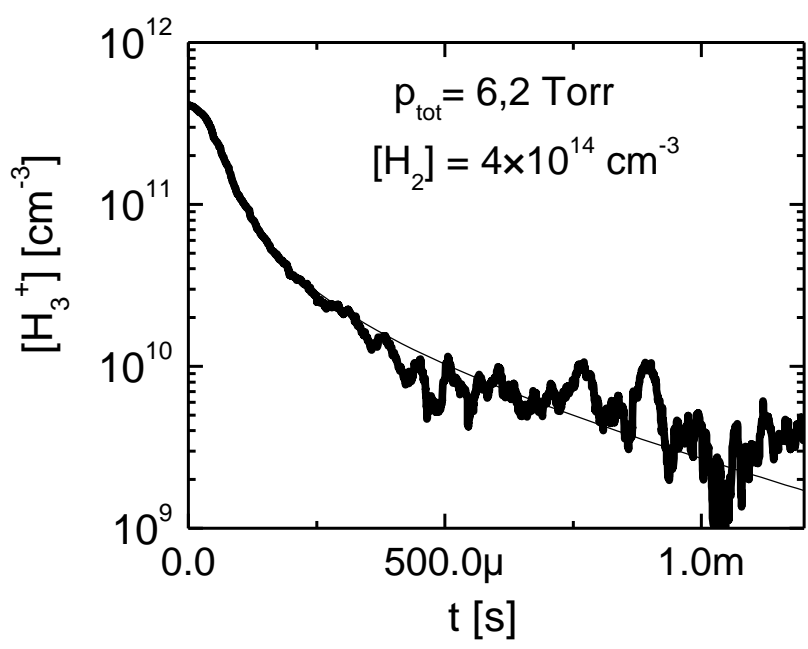
$$\frac{\mathrm{d}n_e}{\mathrm{d}t} = -\alpha_{\mathrm{eff}} n_e^2 - \frac{n_e}{\tau_L}$$

$$\frac{1}{[H_3^+]} = \frac{1}{[H_3^+]_0} + \alpha t$$

We measure effective – apparent binary recombination rate coefficient

p_{tot} = 6,2 Torr
$[H_2] = 4 \times 10^{14}$ cm^{-3}
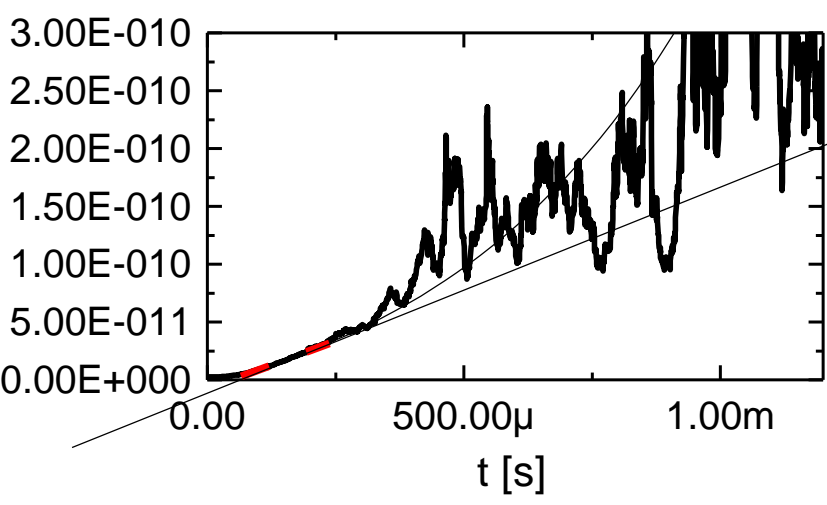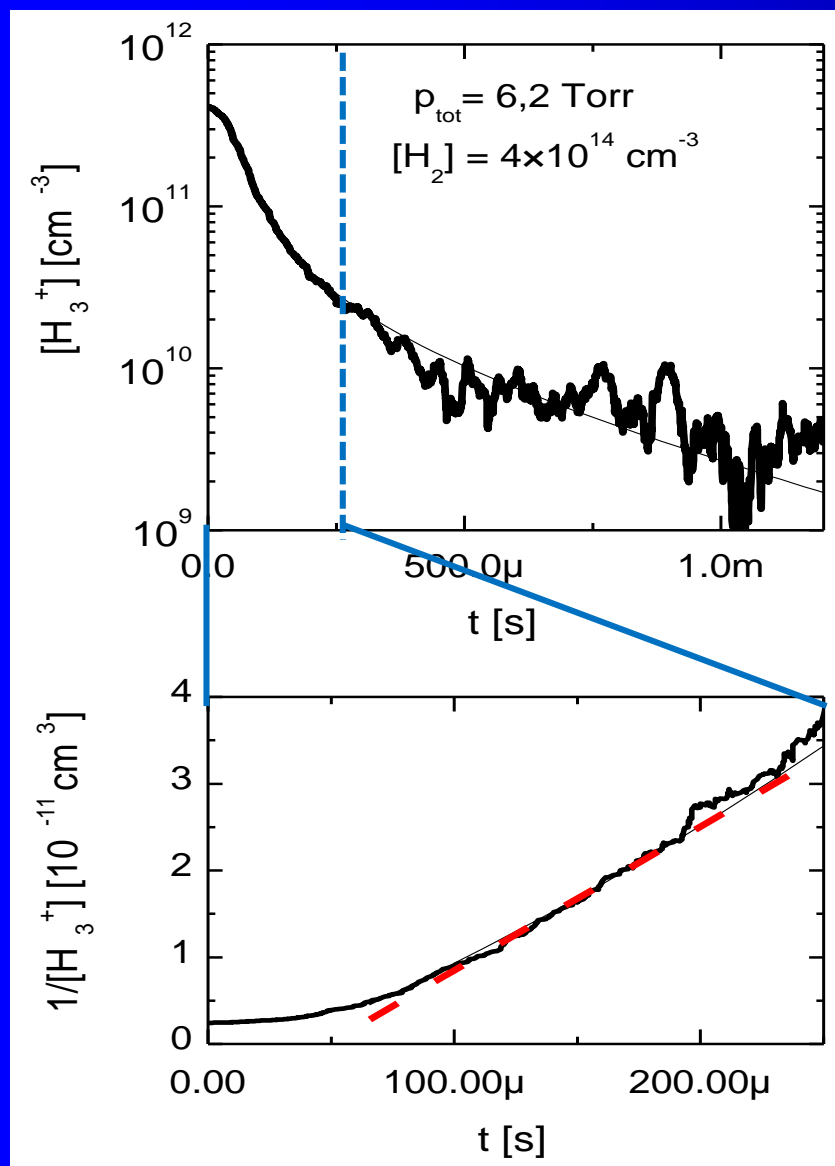
Quasineutral H_3^+ dominated plasma

$$\frac{dn_e}{dt} = -\alpha_{eff} n_e^2 - \frac{n_e}{\tau_L}$$

$$\frac{1}{[H_3^+]} = \frac{1}{[H_3^+]_0} + \alpha t$$

Decay in <u>diffusion</u> and <u>recombination</u> governed plasma

$$\frac{dn_e}{dt} = -\alpha \, n_e^2 - \frac{D_a}{\Lambda^2} \, n_e$$
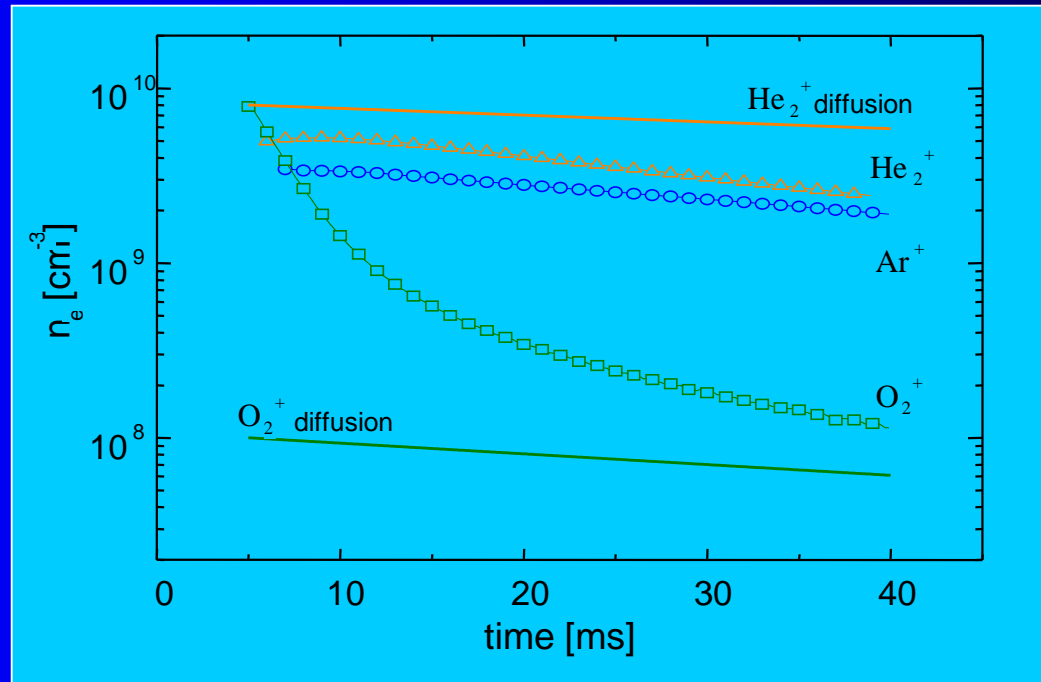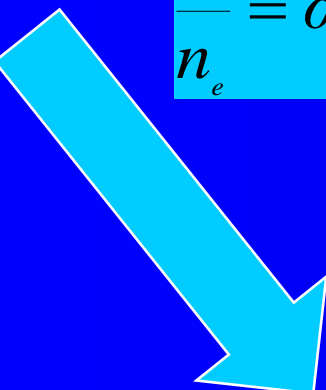
$$\frac{1}{n_e} = \alpha \, \frac{\exp(\nu t) - 1}{\nu_D} + \frac{1}{n_0} \exp(\nu_D t)$$

Decay in diffusion and recombination governed plasma

$$\frac{dn_e}{dt} = -\alpha \, n_e^2 - \frac{D_a}{\Lambda^2} n_e$$

$$\frac{1}{n_e} = \alpha \, \frac{\exp(\nu t) - 1}{\nu_D} + \frac{1}{n_0} \exp(\nu_D t)$$

Limit for t -->0

$$\frac{1}{n_e} = \alpha \, \frac{(1 + \nu_D t) - 1}{\nu_D} + \frac{1}{n_0}(1 + \nu_D t)$$

$$\frac{1}{n_e} = \alpha t \; + \frac{1}{n_0}(1)$$

Limit for large t

$$\frac{1}{n_e} = (\frac{\alpha}{\nu_D} + \frac{1}{n_0}) \exp(\nu_D t)$$
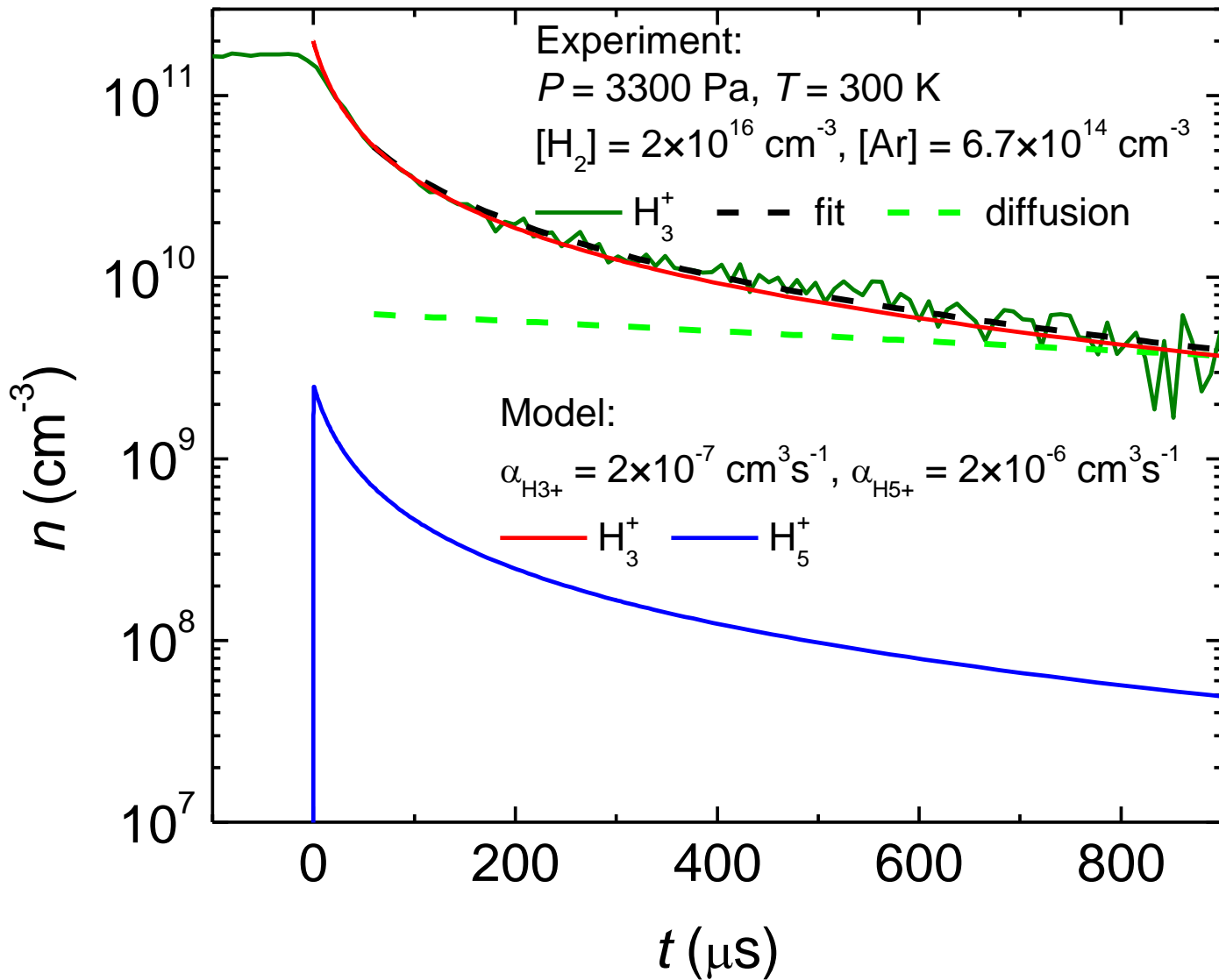
Srovnani modelu a experimentu. Pocatecni podminka: $[H_3^+] = n_e = 2 \times 10^{11} \, cm^{-3}$.

Experiment:
P = 3300 Pa, T = 300 K
$[H_2]$ = 2×10^16 cm^-3, $[Ar]$ = 6.7×10^14 cm^-3
—— H_3^+ - - - fit   - - - diffusion

Model:
α_{H3+} = 2×10^-7 cm^3s^-1, α_{H5+} = 2×10^-6 cm^3s^-1
—— H_3^+ - · - H_5^+ - · · - He^m

$$\frac{dn_e}{dt} = -[\alpha_1 n_1(t) + \alpha_2 n_2(t)]n_e$$

$$\Rightarrow \alpha_{eff}(t) = [\alpha_1 f_1(t) + \alpha_2 f_2(t)]$$

$$f_1 + f_2 = 1$$

Model + data. Pocatecni podminka: n_e = He^m = $[H_3^+]$.
Poznamka. Namerene τ difuznich ztrat 1.6 ms. Teoreticke τ pri danem tlaku je 1.8 ms (odpovida cca 4×10^10 cm^-3 koncentraci necistot (pri 2×10^-9 cm^3s^-1 rychlosti reakce H_3^+ s necistotami). Namerena koncentrace vody $[H_2O]$ = 5×10^10 cm^-3 ($[He]$ = 8×10^17 cm^-3).

If there are 2 or more ion species, the fast recombining species disappears first

$$\frac{dn_e}{dt} = -[\alpha_1 n_1(t) + \alpha_2 n_2(t)]n_e$$

$$\Rightarrow \alpha_{eff}(t) = [\alpha_1 f_1(t) + \alpha_2 f_2(t)]$$

$$f_1 + f_2 = 1$$

Diffusion and recombination

$$\frac{dn_e}{dt} = -\alpha\, n_e^2 - \frac{D_a}{\Lambda^2}\, n_e$$

$$\frac{1}{n_e} = \alpha\, \frac{\exp(\nu t) - 1}{\nu} + \frac{1}{n_0}\exp(\nu t)$$

$NH_4^+.(NH_3)_2 + e^-$

- ■ 9 Torr, Φ_{NH_3} = 0.17 sccm
- ● 9 Torr, Φ_{NH_3} = 0.44 sccm
- ▲ 9 Torr, Φ_{NH_3} = 0.72 sccm
- ▼ 11.5 Torr, Φ_{NH_3} = 1.4 sccm

$n_e\ [m^{-3}]$

$1/n_e\ [m^3]$

L [cm]

TRANSITIONAL REGION
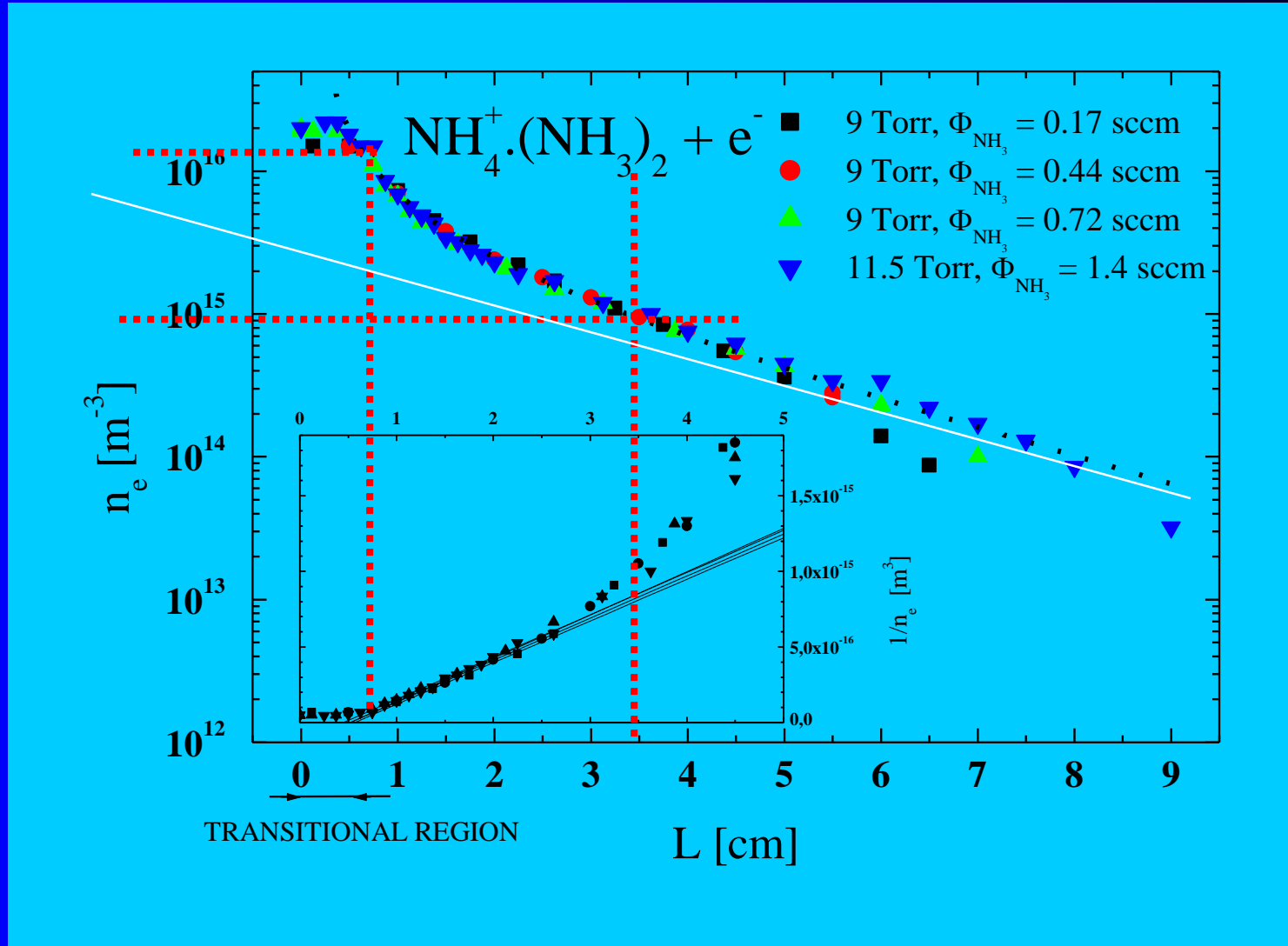
J. Glosík, G. Bánó, R. Plašil, A. Luca, P. Zakouril,
Study of the electron ion recombination in high pressure flowing afterglow. Recombination of $NH_4^+.(NH_3)_2$,
International J. Mass Spectrom., **189**, 103-113 (1999)

Advanced analyze O_2^+

$$dn_e / dt = -\alpha[O_2^+]n_e - \nu_D n_e - \nu_R n_e = -\alpha n_e^2 - \nu_D n_e - \nu_R n_e$$

$$\frac{1}{n_e} - \frac{1}{n_0} = \alpha(t_e - t_0)$$

$$-n_e'/n_e^2 = \alpha + (\nu_D + \nu_R)/n_e$$
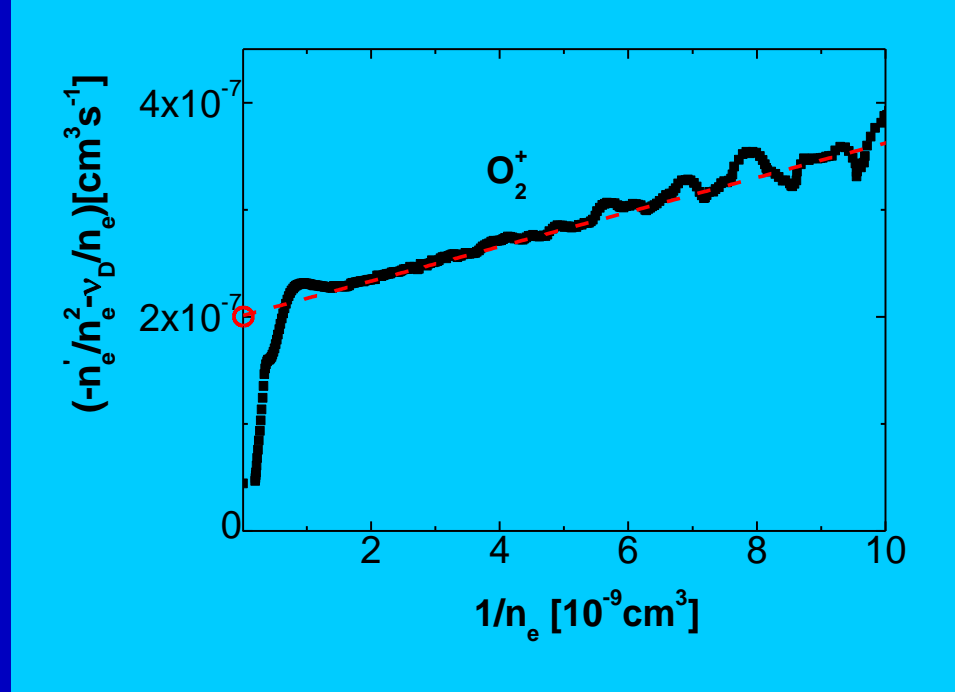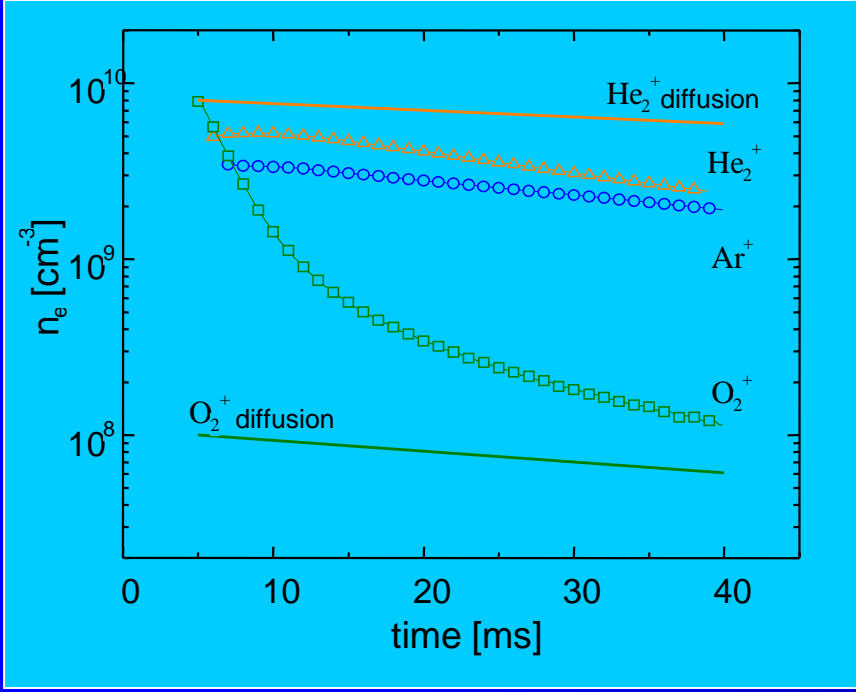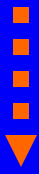
Stationary afterglow (M. Biondy, R. Johnsen)
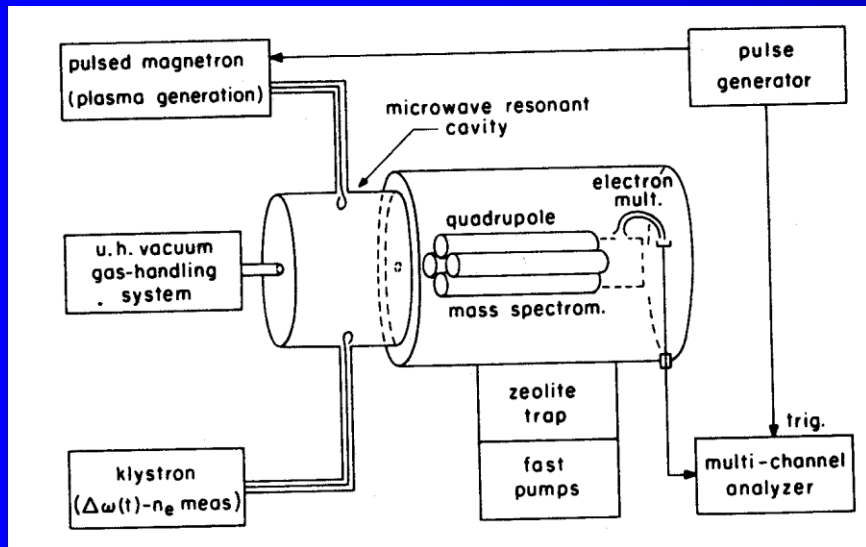
M.T.Leu, M.A. Biondy, R. Johnsen recombination of H_3^+ and H_5^+

μw SA
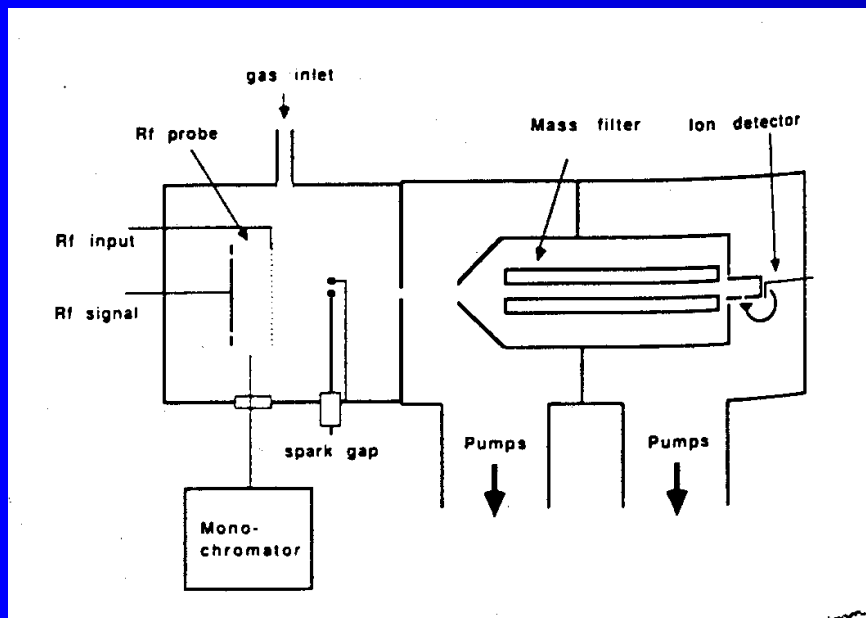
R. Johnsen N4+ recombination at 300-800 Torr $a= 2.6 \times 10^{-6} cm^3 s^{-1}$

High pressure SA

RF probe, spark discharge

ADVANCED INTEGRATED STATIONARY AFTERGLOW
AISA
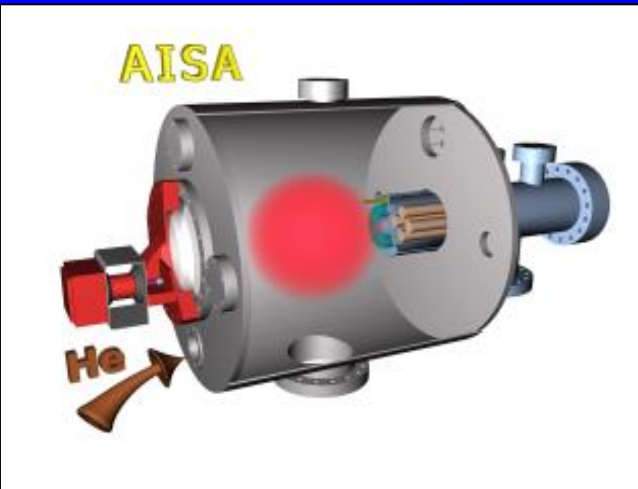
AISA

PULSED STATIONARY AFTERGLOW
20-100ms decay

Langmuir probe Ø 14μm

AISA

Window   Heating / Cooling system

He
Ar
H$_2$ flow in

Auxiliary
Probe

QMS

QMS

Magnetron
2.45 GHz
0..30 W
0..5 ms
25 Hz

Baratron

Turbo Pump

flow out

10 cm

Turbo Pump

40 cm diameter
UHV - 10^{-9} Torr
External magnetron
2 Torr of He/Ar/H$_2$
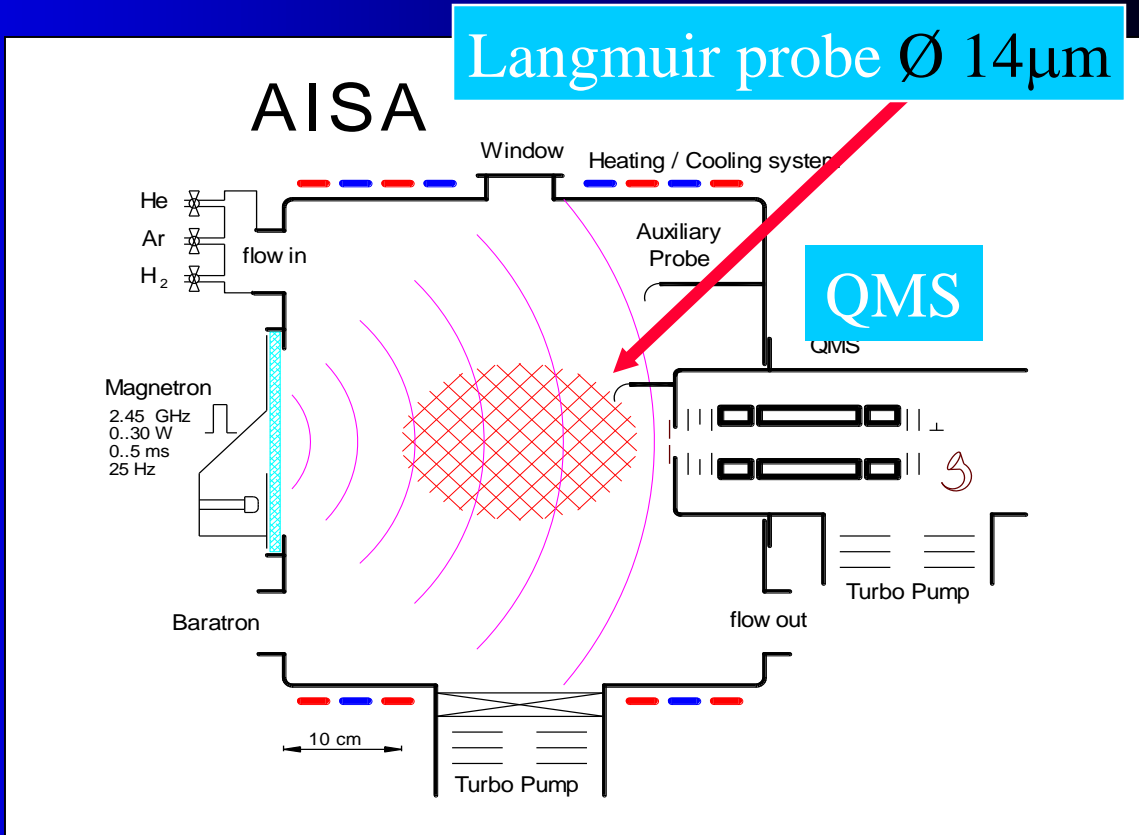
AISA - ADVANCED INTEGRATED STATIONARY AFTERGLOW
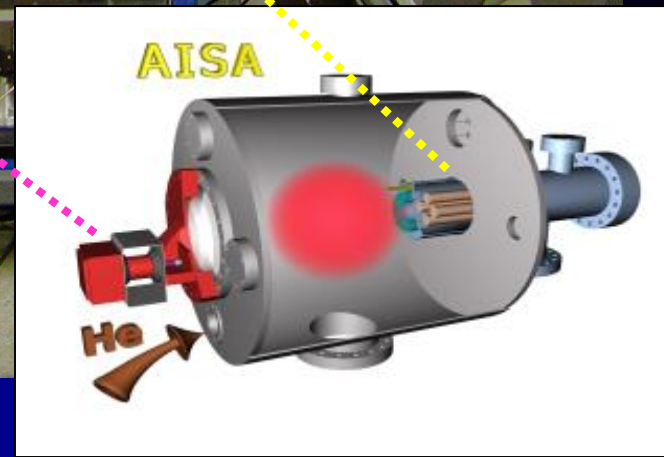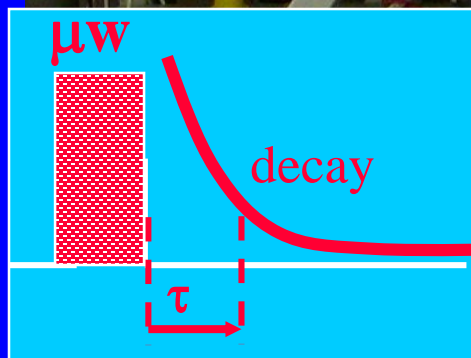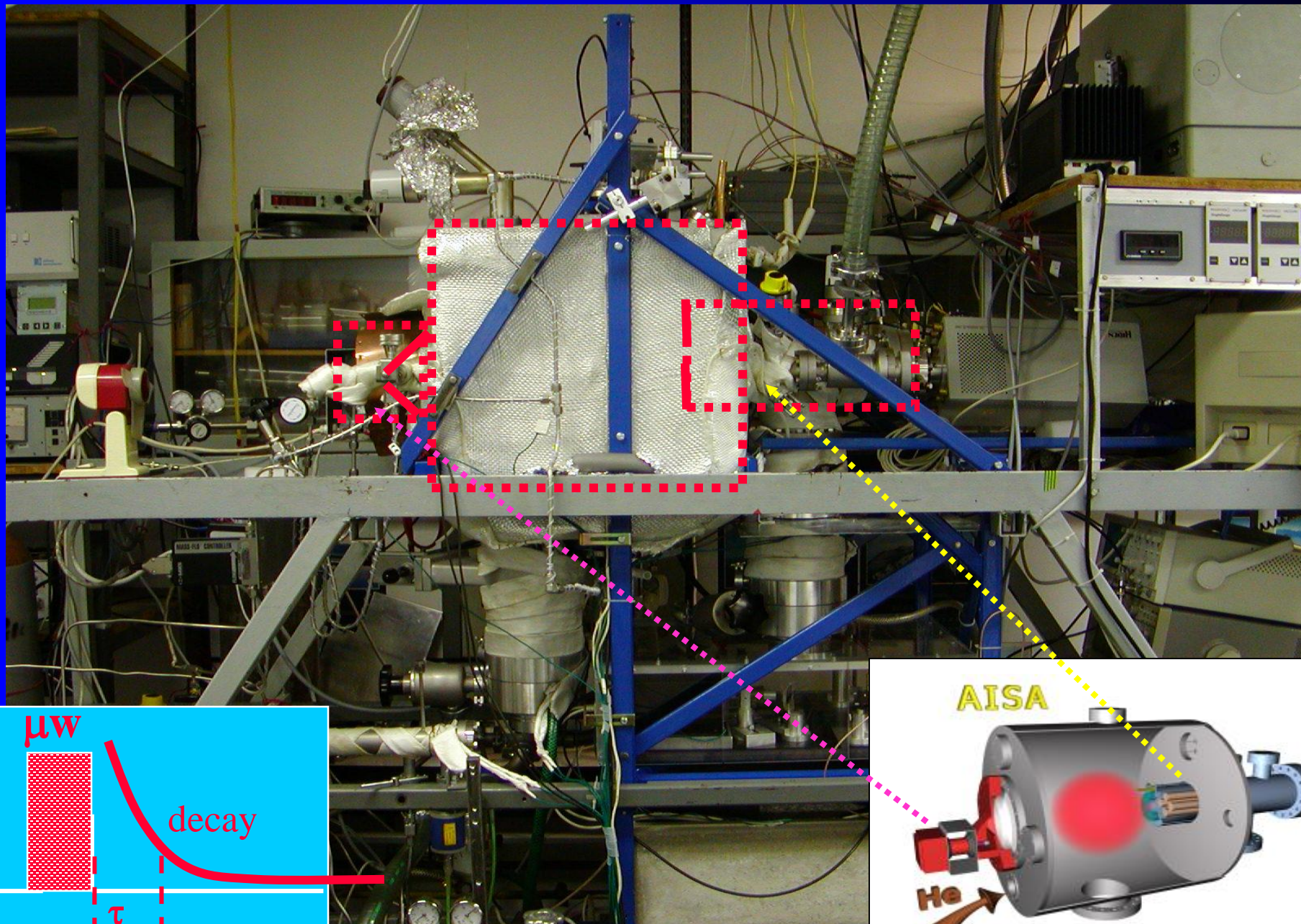
CALCULATION OF PLASMA DECAY IN CYLINDER
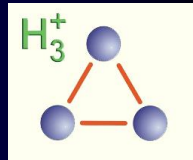
DIFFUSION AND RECOMBINATION

$\tau_D = 60$ ms, $\alpha = 1 \times 10^{-7}$ cm^{3}s^{-1} and $\alpha = 5 \times 10^{-9}$ cm^{3}s^{-1}
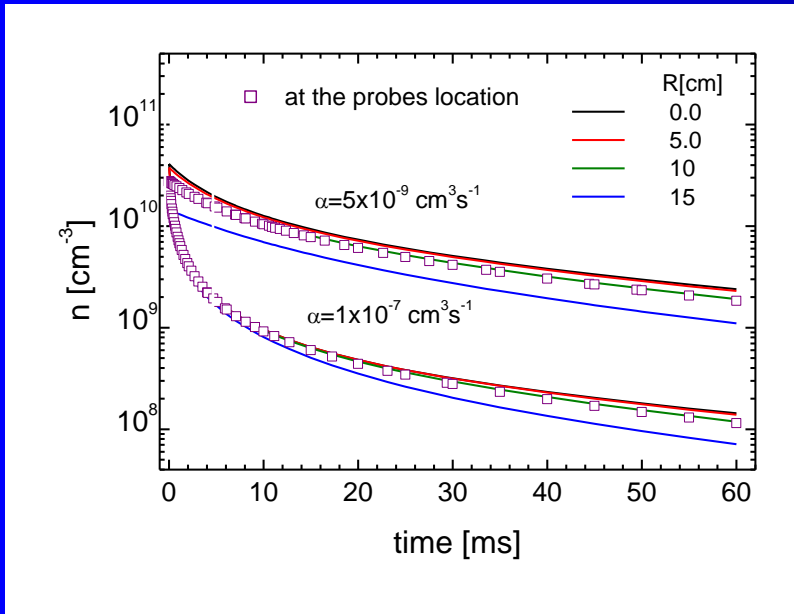
Time evolution
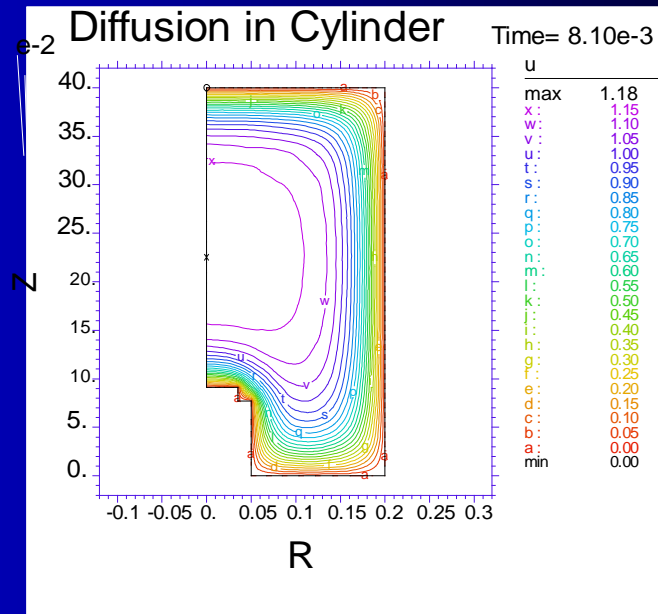
Spatial distribution after 8 ms
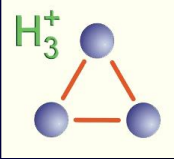
RECOMBINATION AND DIFFUSION
in He/O_2^+/e^- plasma (2 Torr, $\tau_D \sim 60ms$)

$$\alpha(O_2^+, 300K) = 2 \times 10^{-7} cm^3 s^{-1}$$

O_2^+

$$O_2^+ + e^- \Rightarrow neutral \quad products$$

$$\frac{d[O_2^+]}{dt} = -\alpha[O_2^+]n_e - \frac{n_e}{\tau_D}$$

Only recombination:

$$1/n_e = 1/n_{e0} + \alpha t$$

Only diffusion

$$n_e = n_{e0} \exp\left(-\frac{t}{\tau_D}\right)$$

With recombination and diffusion

$$n_e = \frac{1}{\alpha\tau_D \exp\left(t/\tau_D\right) + \frac{1}{n_0}\exp\left(t/\tau_D\right)}$$

He_2^+ diffusion

He_2^+

Ar^+

O_2^+

O_2^+ diffusion

n_e [cm^{-3}]

time [ms]

Formation of H_3^+ in He/Ar/H_2 mixture

$99/1/<0.01\%$ $(10^{17}/10^{14}/10^{11-14})$

microwave discharge

He^+, He^m, Ar^+, Ar^m, H_2^+, H^+

$He^+ \xrightarrow{He} He_2^+$

$He_2^+ \xrightarrow{Ar} Ar^+$

$He^m \xrightarrow{Ar} Ar^+$

$Ar^+ \xrightarrow{H_2} ArH^+, H_2^+ \xrightarrow{H_2} H_3^+$

$Ar^m \xrightarrow{+e^-(300K)} h\nu$

$H^+ \xrightarrow{+He+He} HeH^+$
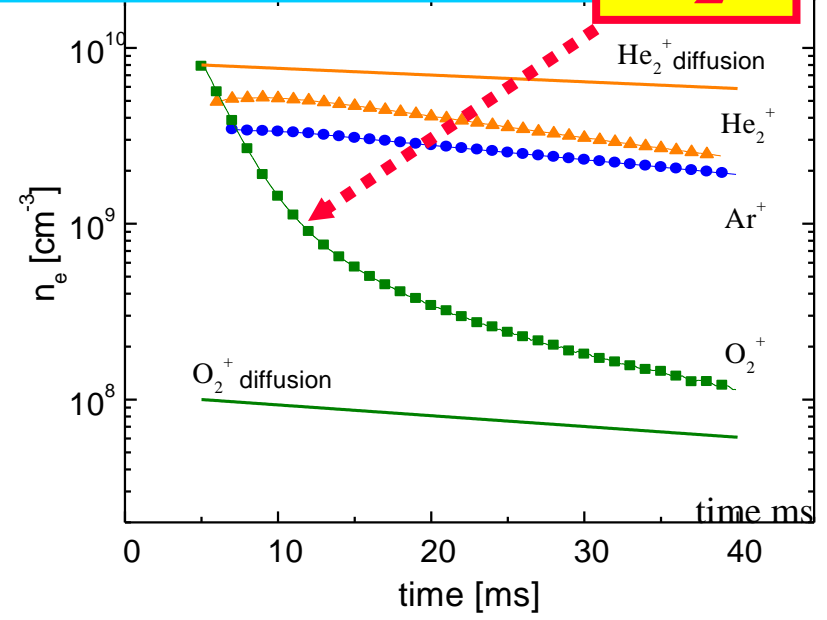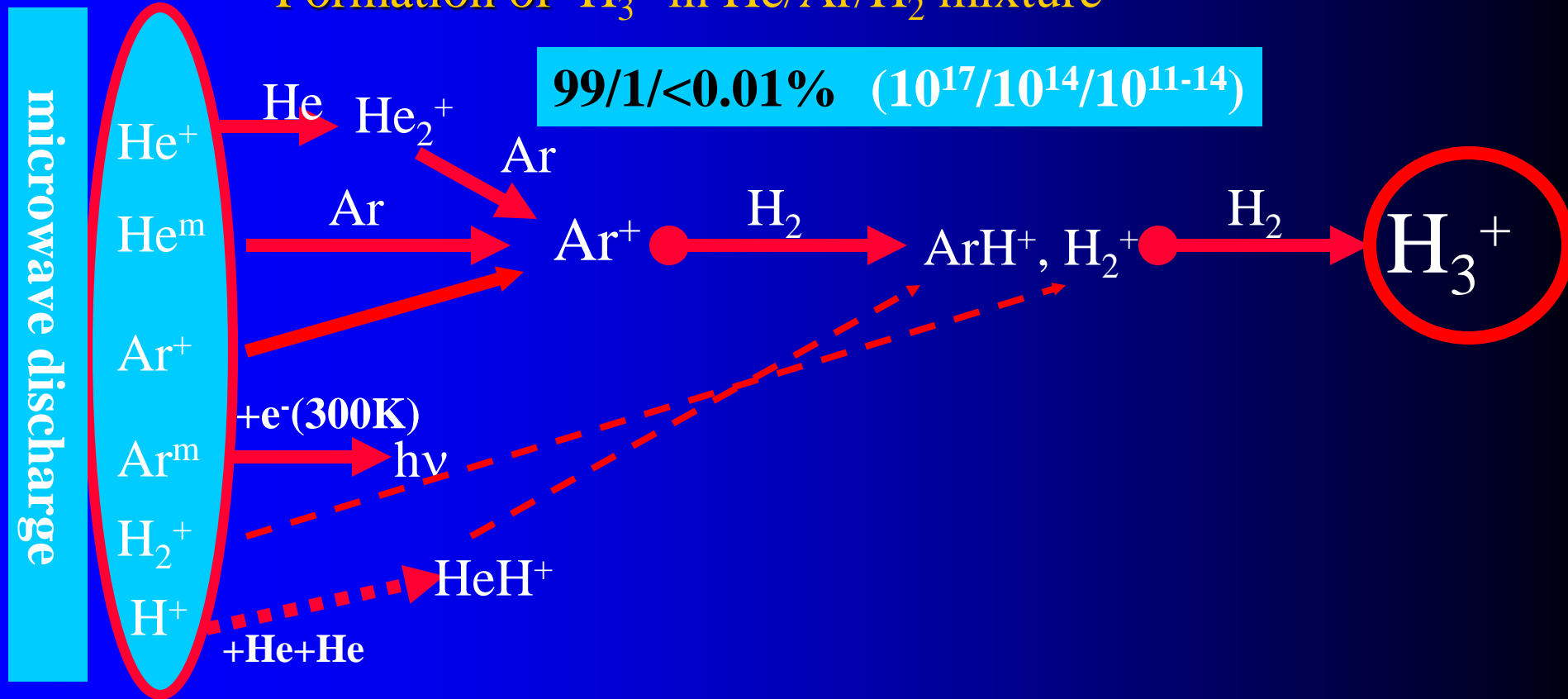
FORMATION:
Ion molecule reactions during the early afterglow

VT - AISA

$$dn_i/dt=-\alpha n_i n_e$$

He/Ar/H$_2$

$\alpha(T)$

H$_3^+$

T

e

40 cm diameter
UHV - 10^{-9} Torr
External magnetron
2 Torr of He/Ar/H$_2$

AISA

Liquid nitrogen

Window

He
Ar
H$_2$

Flow In

Magnetron
2.45 Ghz
0..30 W
0..5 ms
25 Hz

Baratron

Auxiliary
Probe

QMS

Flow Out

Turbo Pump

Turbo Pump

Cooling medium (LN)
Heating system
Thermal isolation

PULSED STATIONARY AFTERGLOW

20-100ms decay

$n_e(\tau), n_i(\tau)$

τ
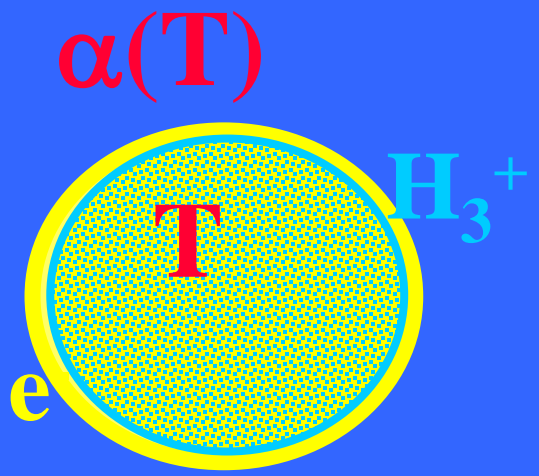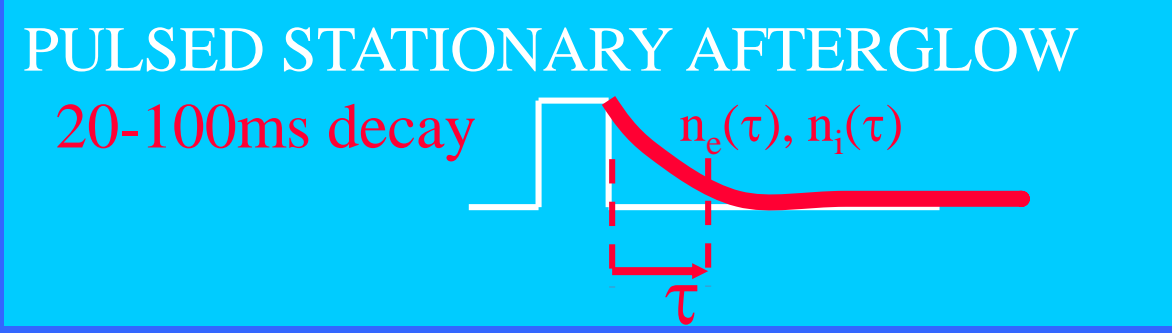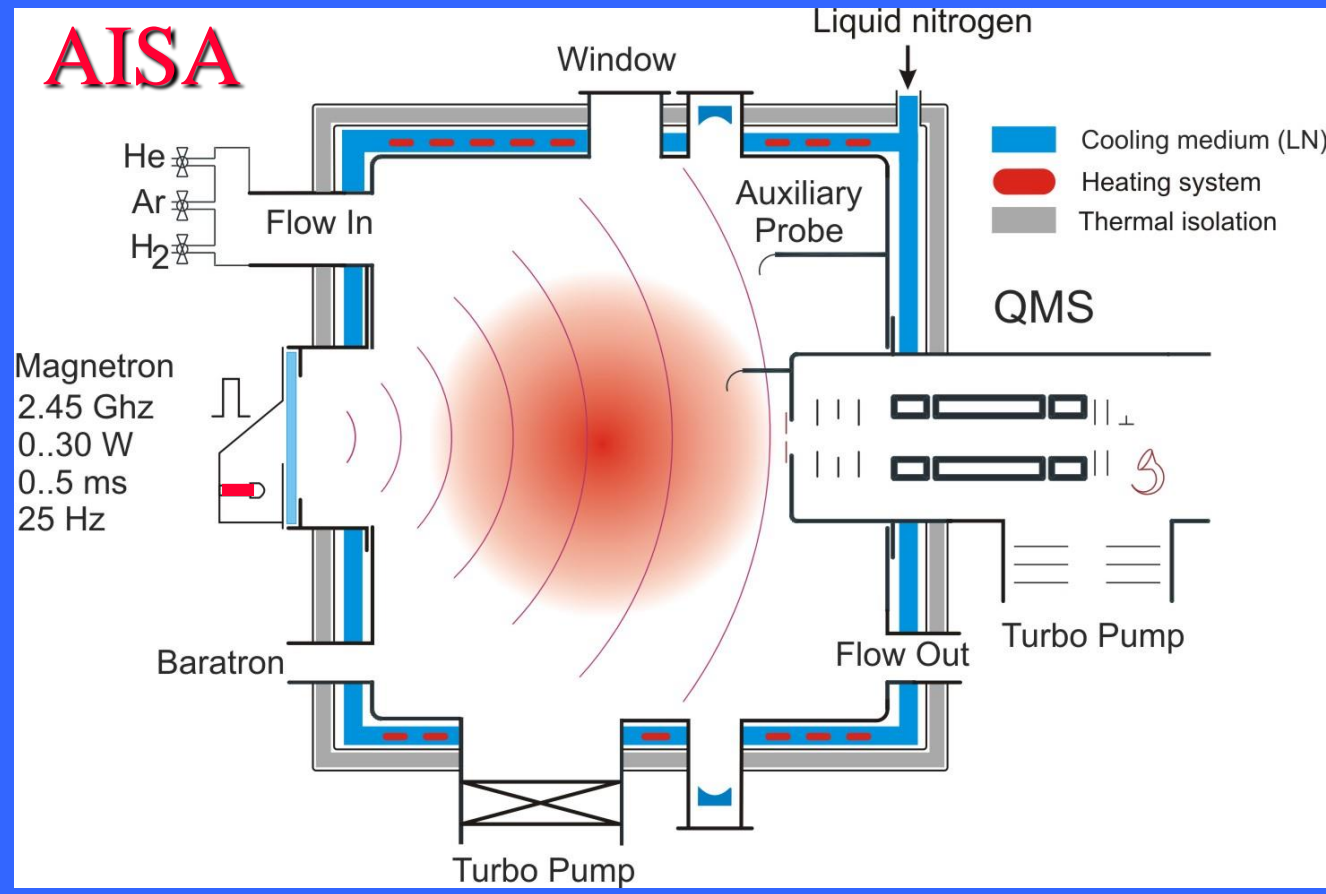
Formation of H_3^+ in He/Ar/H$_2$

99/1/<0.01%   ($10^{17}/10^{14}/10^{11-14}$)

He$^+$ → He → He$_2^+$

He^m → Ar → Ar$^+$ → H$_2$ → ArH$^+$, H$_2^+$ → H$_2$ → $H_3^+ + e^-$

e$^-$

Ar$^+$

Ar^m +e$^-$(300K) → hν

H$_2^+$

H$^+$ → HeH$^+$

+He+He

DECAY BY RECOMBINATION

microwave discharge

Time resolved mass spectra

e$^-$ Ar$^+$ H_3^+

He$^+$

FORMATION   RECOMBINATION

n_e [cm^{-3}]

H_3^+ Ar$^+$

O$_2^+$

$1/n_e$ [10^{-9}cm^3]

[H$_2$][10^{11}cm^{-3}]

♦ 6
■ 30

time [ms]
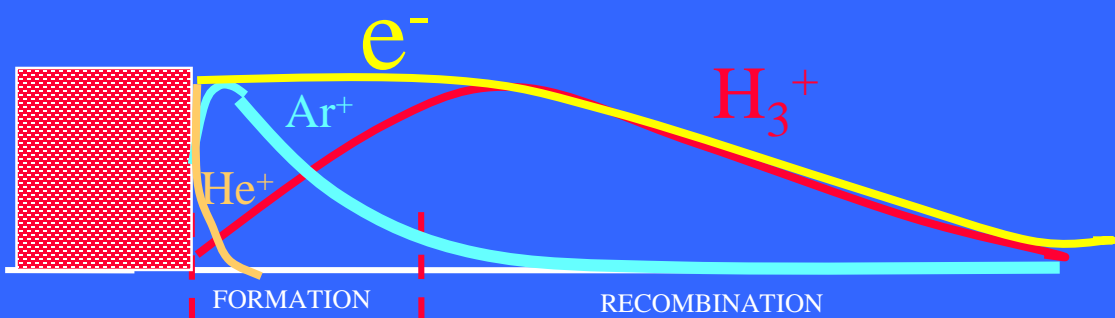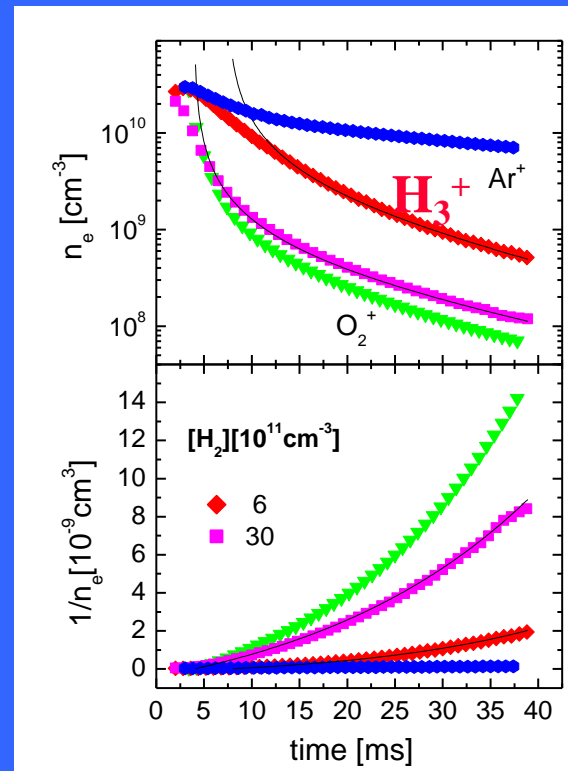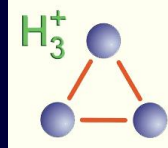
Formation of H_3^+ in He/Ar/H_2 mixture

$10^{17}/10^{14}/10^{11}$

microwave discharge

He$^+$
He^m
Ar$^+$
Ar^m
H_2^+

$$He^+, He^m, Ar^+, Ar^m, H_2^+ \xrightarrow{Ar} Ar^+ \xrightarrow{H_2} ArH^+, H_2^+ \xrightarrow{H_2} H_3^+$$
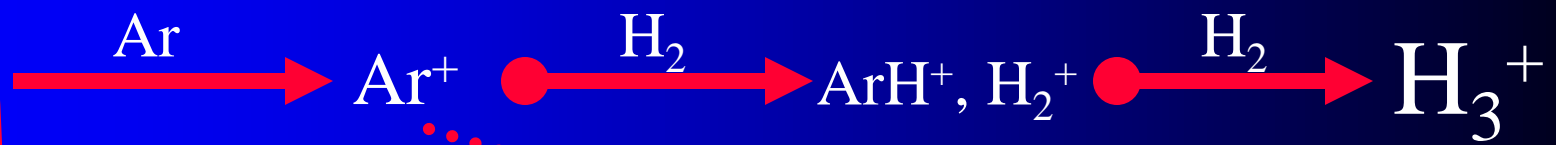
Changes due to the ion molecule reactions during the early afterglow

He/Ar

He/Ar/H_2 H_3^+

He/Ar/D_2 D_3^+
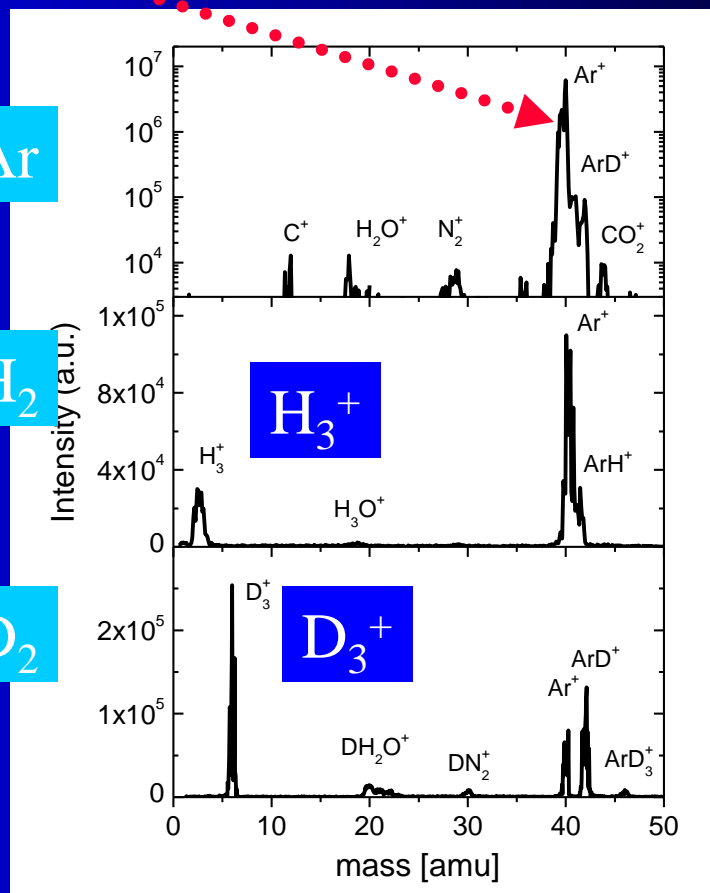
From over 30 years of systematic studies of kinetics of IMR follows:

Kinetics of formation of H_3^+ is clear

IT IS NOT A MYSTERY !!

Table of reactions

R. No	Reaction	Rate coef. [cm³ s⁻¹] or [cm⁶ s⁻¹]	Reactant number density [cm⁻³]	Reaction time [ms]	Ref.
1	$He^+ + 2He \rightarrow He_2^+ + He$	1E-31	6,5E16	2	
2	$He^M + He^M \rightarrow He_2^+ + e$	5E-9	5E10 (assumption)	4	
3	$He^M + Ar \rightarrow Ar^+ + He + e$	7E-11	1E14	0,14	
4	$He_2^+ + Ar \rightarrow Ar^+ + 2He$	2E-10	1E14	0,05	
5	$Ar^+ + H_2 \rightarrow ArH^+ + H$ $\rightarrow H_2^+ + Ar$	8E-10 ArH^+ is dominat	2E11	6,3	
6	$H_2^+ + Ar \rightarrow ArH^+ + H$	2,3E-9	1E14	<0,01	
7	$H_2^+ + H_2 \rightarrow H_3^+ + H$	2,1E-9	2E11	2,4	
8	$ArH^+ + H_2 \rightarrow H_3^+ + Ar$	1.5E-9	2E11	3,3	
9	$H_3^+ + H_2 + He \rightarrow H_5^+ + He$	<1E-29	2E11; 6,5E16	>8000	
10	$H_3^+ + H_2 + H_2 \rightarrow H_5^+ + H_2$	4,6E-30; 210K	2E11	>1E9	
11	$H^+ + He + He \rightarrow HHe^+ + He$	0,9E-31	6,5E16	2,6	

VT - AISA

2 Torr of He/Ar/H$_2$

AISA

Liquid nitrogen

Window

He
Ar
H$_2$

Flow In

Auxiliary
Probe

Cooling medium (LN)
Heating system
Thermal isolation

QMS

Magnetron
2.45 Ghz
0..30 W
0..5 ms
25 Hz

Baratron

Flow Out

Turbo Pump

Turbo Pump
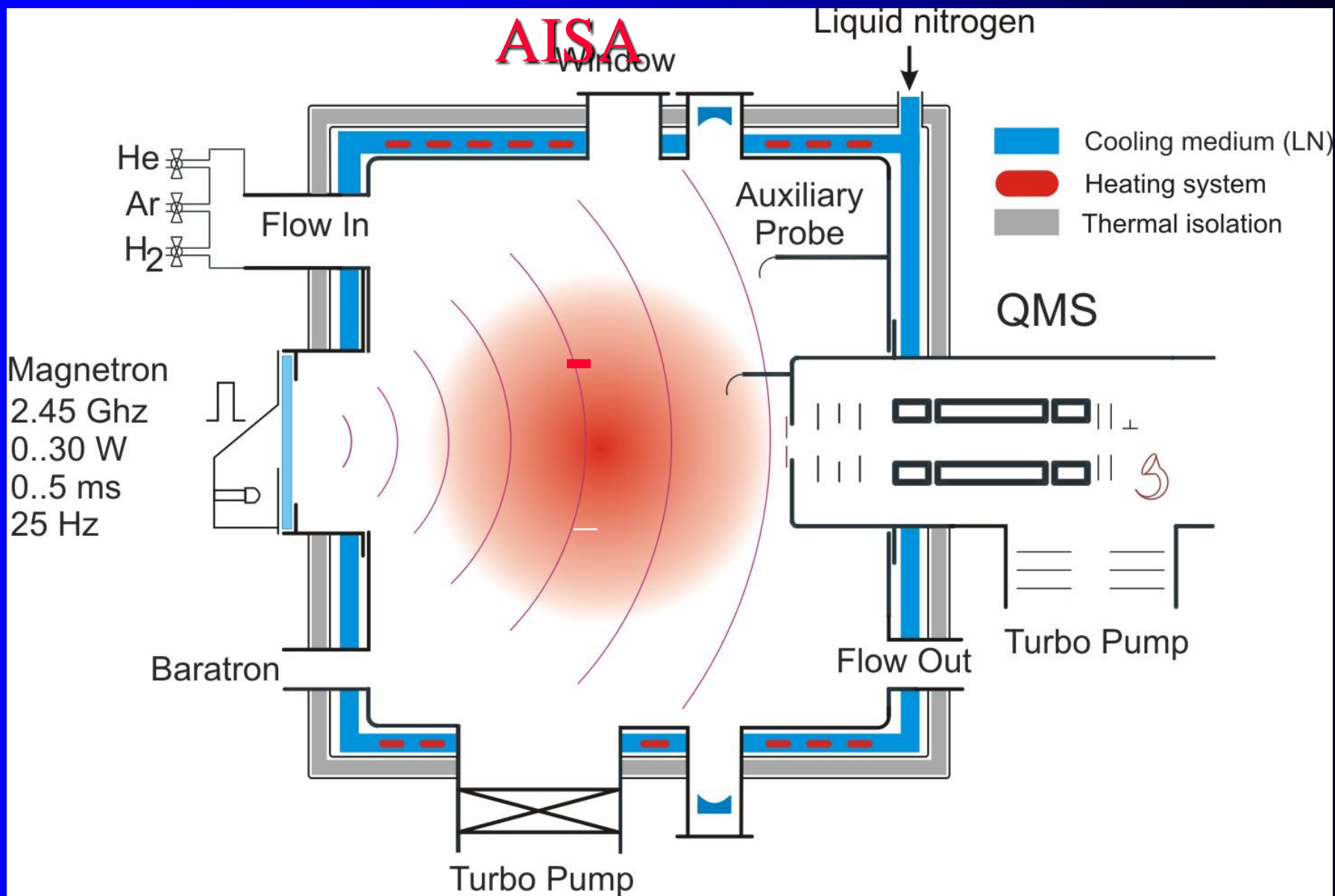
Formation of H_3^+ in He/Ar/H_2 mixture
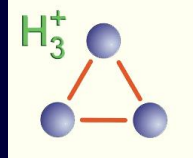
Calculated from kinetic model

He^+
He^m, Ar^m
Ar^+

Ar, H_2 → Ar^+ → H_2 → ArH^+, H_2^+ → H_2 → H_3^+

Formation of H_3^+ in He/Ar/H_2 mixture
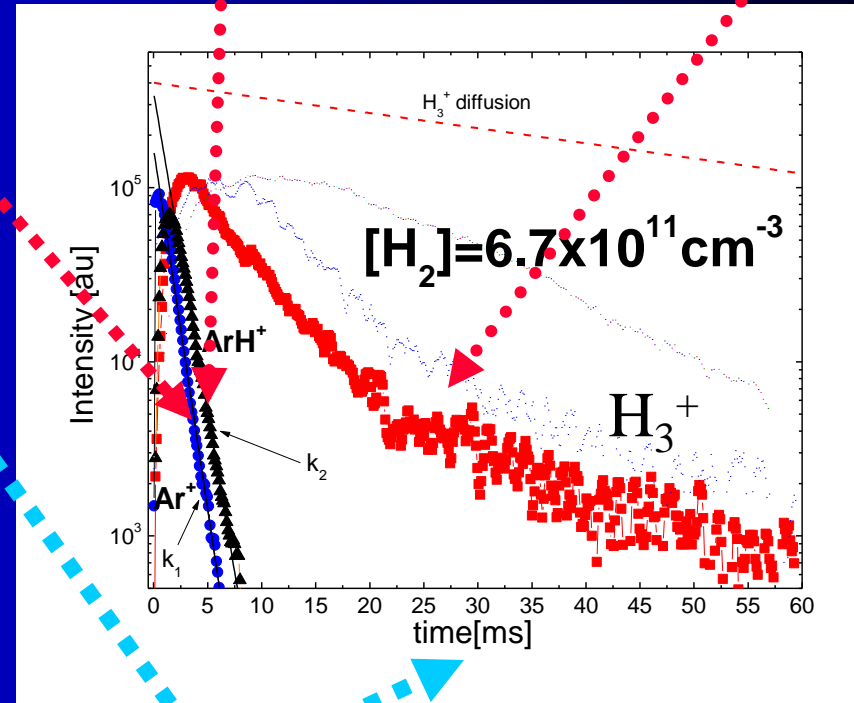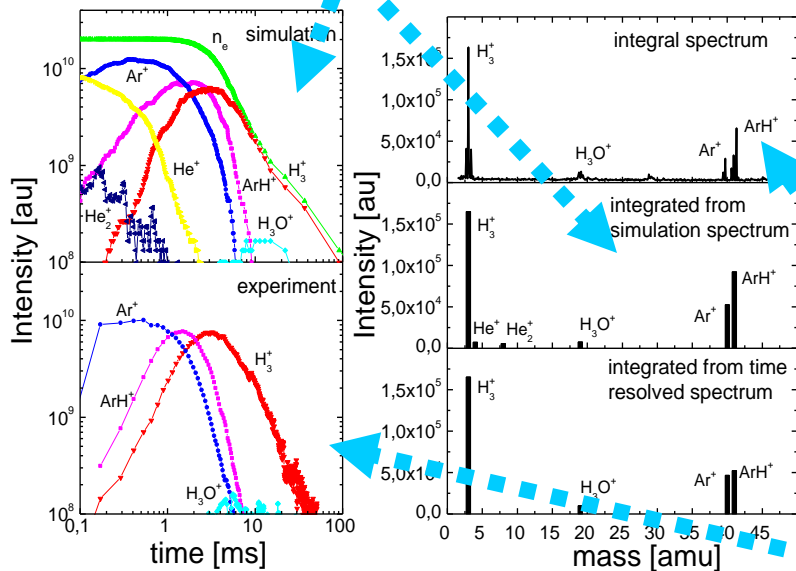
Time resolved mass spectra
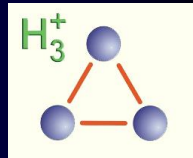
Rates of the decays are dependent on [H_2]
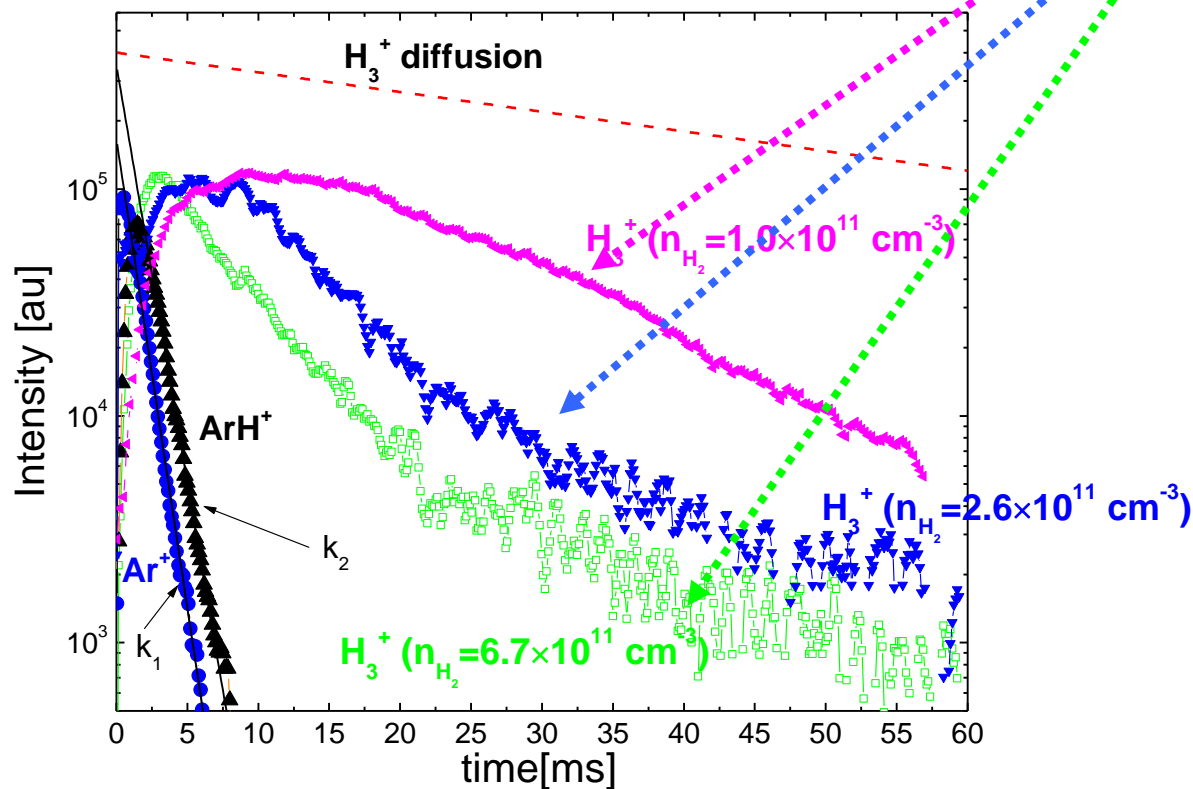
Time resolved mass spectra

$$\frac{dn_e}{dt} = -[\alpha_1 n_1(t) + \alpha_2 n_2(t)]n_e$$

$$\Rightarrow \alpha_{eff}(t) = [\alpha_1 f_1(t) + \alpha_2 f_2(t)]$$

$$f_1 + f_2 = 1$$

OBSERVED DEPENDENCE ON [H$_2$]!!
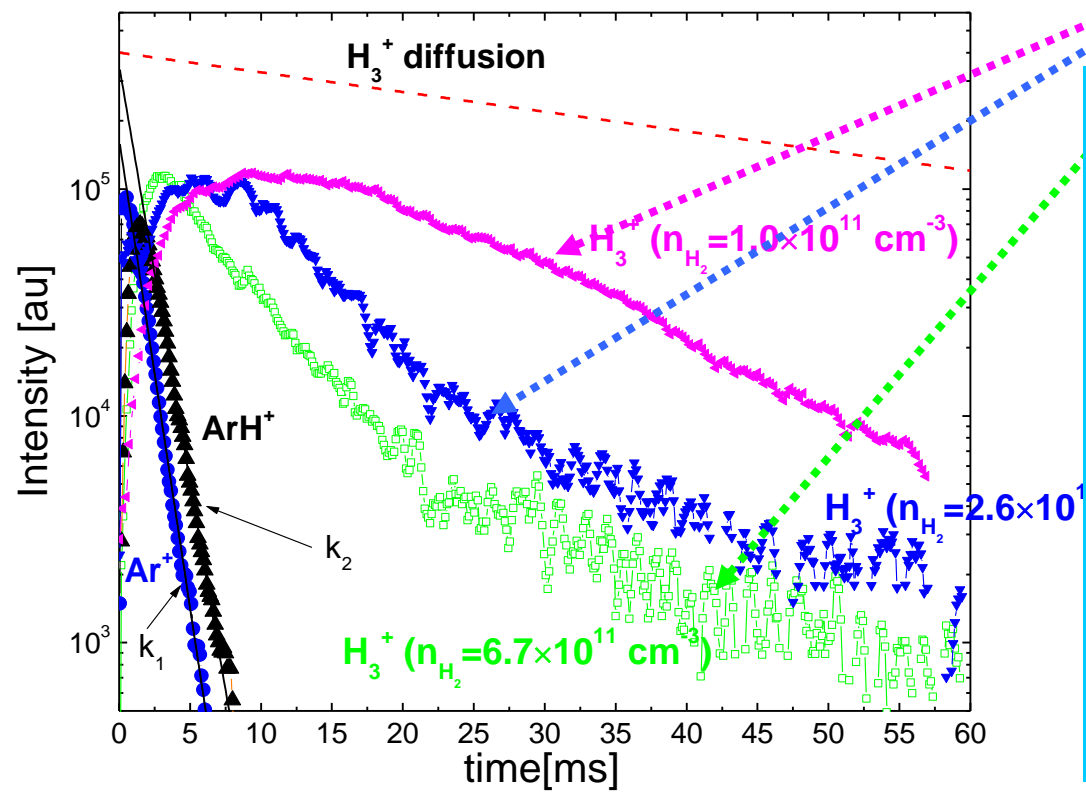
H$_3^+$ *fraction*
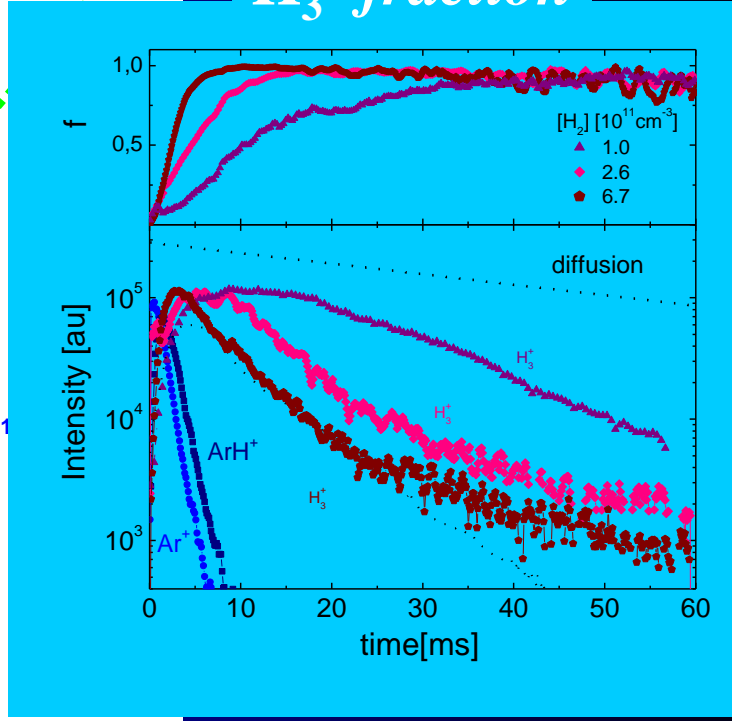
It is only qualitative information, not sufficient to obtain α

RECOMBINATION

FLOWING AFTERGLOW

Diffusion in FA

$$[A^+] = [A^+]_0 \exp(-Dt/\Lambda^2) = [A^+]_0 \exp(-Dpt/p\Lambda^2) = [A^+]_0 \exp(-D_0 p_0 L/vp\Lambda^2)$$

$$\sim [A^+]_0 \exp(-D_0 p_0 L/vp\Lambda^2) \sim [A^+]_0 \exp(-const.L/Q)$$

reaktant

$V_{GAS} = 50\text{-}100\text{m/s}$

Plasma source

Carrier gas
He

QMS
DETEKTOR

Movable Langmuir probe

Reaction region - L
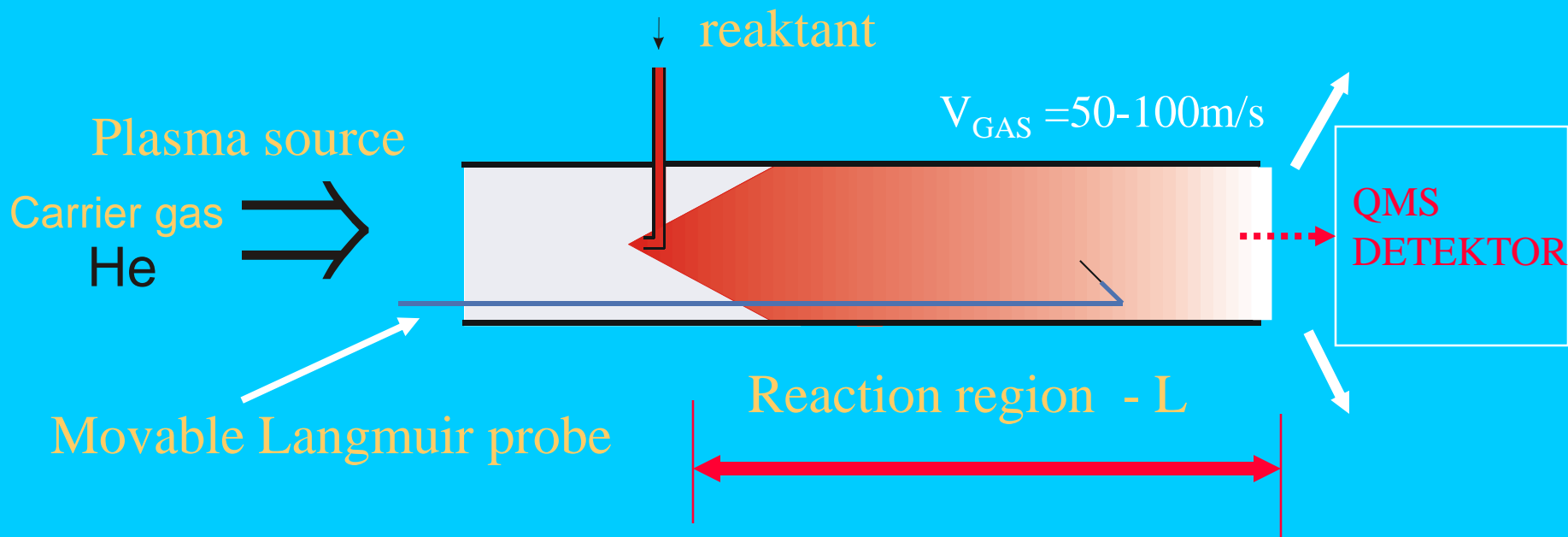
$$[A^+] \sim [A^+]_0 \exp(-const.L/Q)$$

FLOWING AFTERGLOW

FA

FA	E.E.Ferguson, Fehsenfeld, ~1965
FALP	J. Hasted, D. Smith, N. Adams, ….

reaktant B

Plasma source

V_{GAS} =50-100m/s

He + A

Carrier gas

A^+

$A^+ + B$

Rreaction region

$$A^+ \quad + \quad B \xrightarrow{\quad k \quad} \quad products,$$
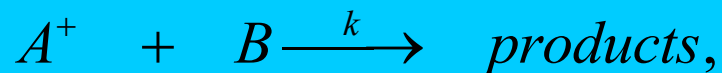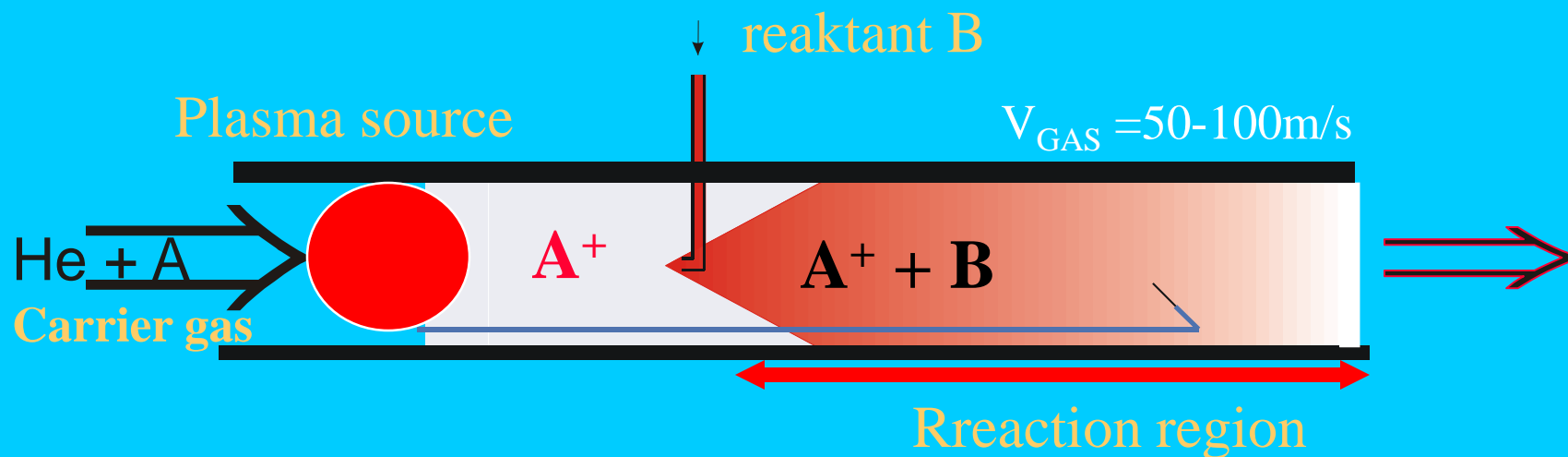
$$d[A^+]/dt = -k[B][A^+], \qquad at \ [A^+] << [B]$$

$$[A^+] = [A^+]_0 \exp(-k[B]t) = [A^+]_0 \exp(-k[B]L_0/v)$$

SIFT

, D. Smith, N. Adams, ….

Flowing Afterglow Langmuir Probe - FALP

Recombination Attachment

MW discharge

Ar

O_2

~0.5 - 10 Torr

He $\Rightarrow$ **He^+,e^-** **Ar^+,e^-** **$O_2^+ + e^-$** $\Rightarrow$

Langmuir probe

$n/exp(t)$

t

— ■ — He^+ — ▲ — Ar^+

— □ — He_2^+ — ★ — O_2^+

$He^+ + 2He \rightarrow He_2^+ + He$

$He_2^+ + Ar \rightarrow Ar^+ + 2He$

$He^m + Ar \rightarrow Ar^+ + He$
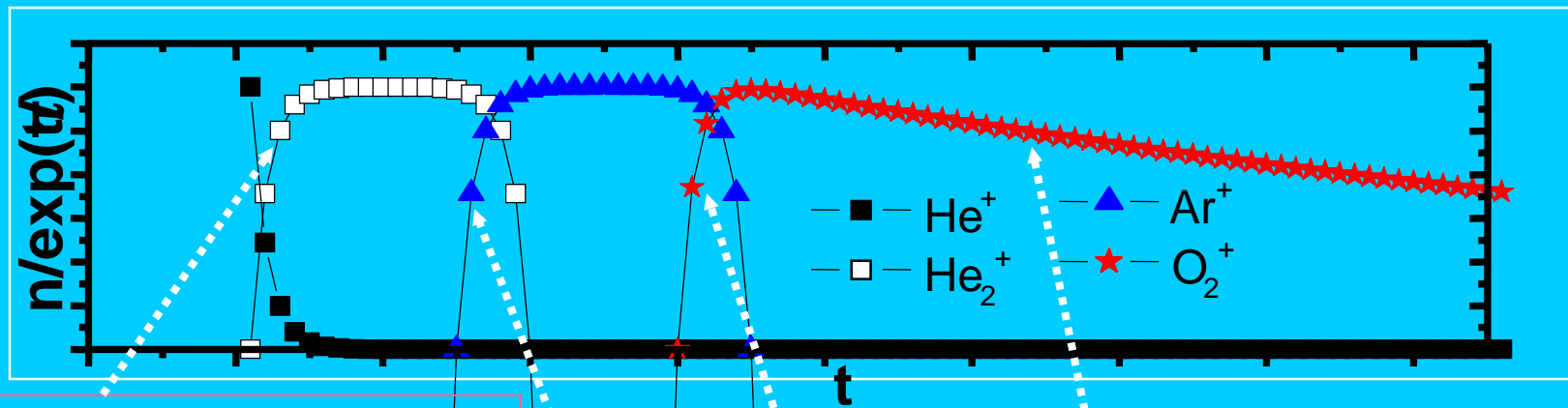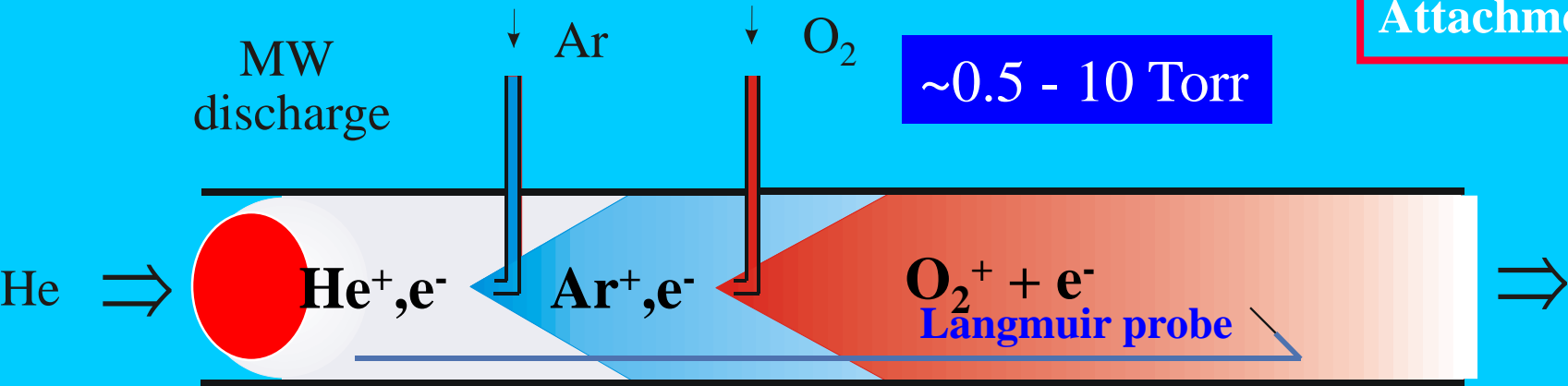
Diffusion, IMR Recombination

$Ar^+ + O_2 \rightarrow O_2^+ + Ar$

FALP - Formation of H_3^+ in He/Ar/H_2 mixture

H_3^+

microwave discharge

He^+
He^m
He_2^+

$\xrightarrow{\text{Ar}}$ Ar^+ $\bullet$ $\xrightarrow{H_2}$ ArH^+, H_2^+ $\bullet$ $\xrightarrow{H_2}$ H_3^+

Ar

H_2
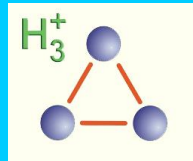
He
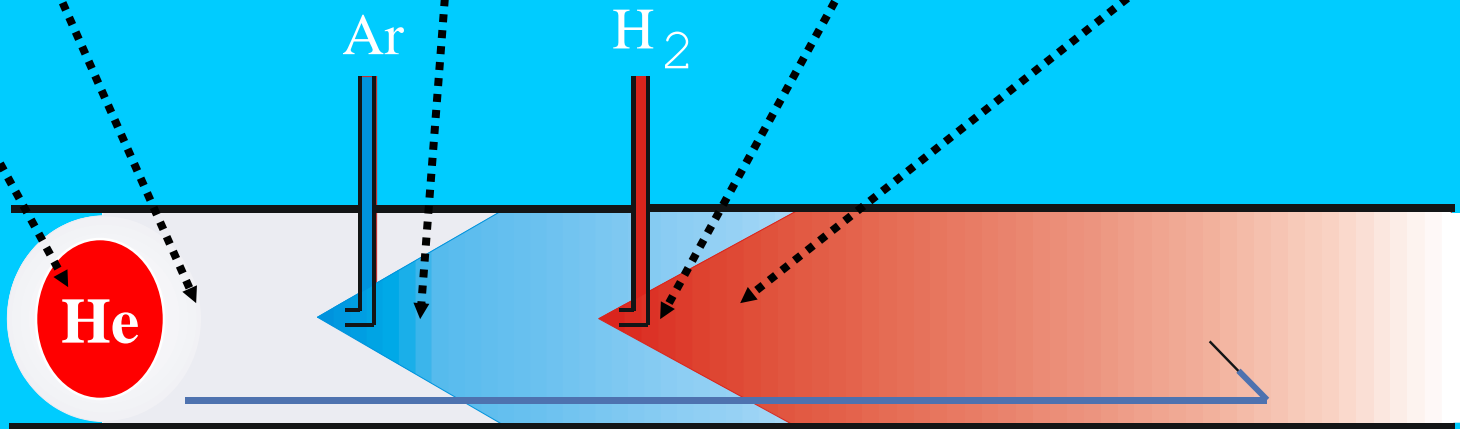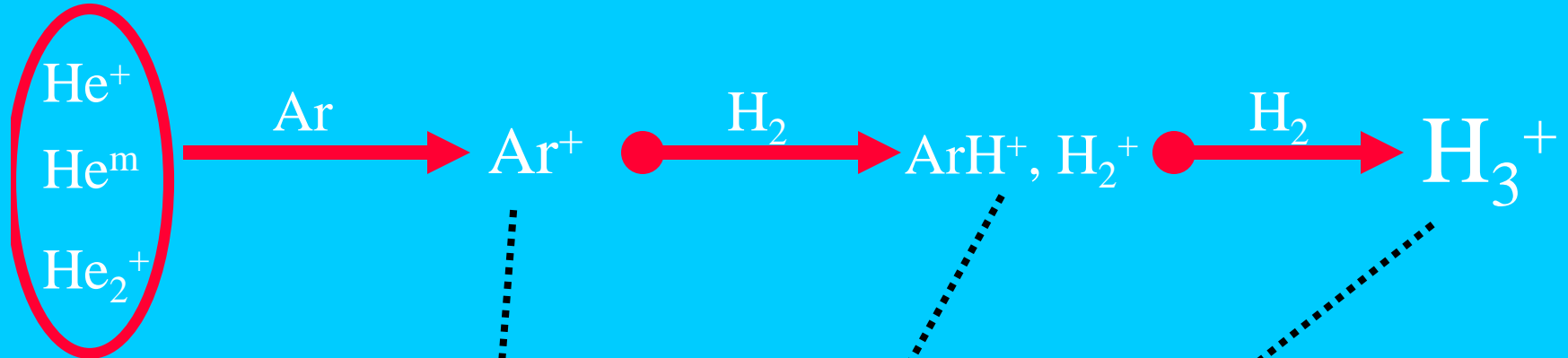
$T_e \sim 2eV$

$T_e = T_i = T_G = 300K$

FALP - RECOMBINATION OF H_3

MW discharge

Ar H_2

~10 Torr

He ⟹

Langmuir probe

⟹

$n/exp(t/\tau)$

t

- ■ - He^+
- □ - He_2^+
- ▲ - Ar^+
- ★ - H_3^+

$He^+ + 2He \rightarrow He_2^+ + He$

$He_2^+ + Ar \rightarrow Ar^+ + 2He$
$He^m + Ar \rightarrow Ar^+ + He$

$Ar^+ + H_2 \rightarrow ArH^+\ldots$
$ArH^+ + H_2 \rightarrow H_3^+ \ldots$

$H_3^+ + H_2 + He \rightarrow H_5^+\ldots$

$H_3^+ + e^- \rightarrow \ldots$

$H_5^+ + e^- \rightarrow \ldots$
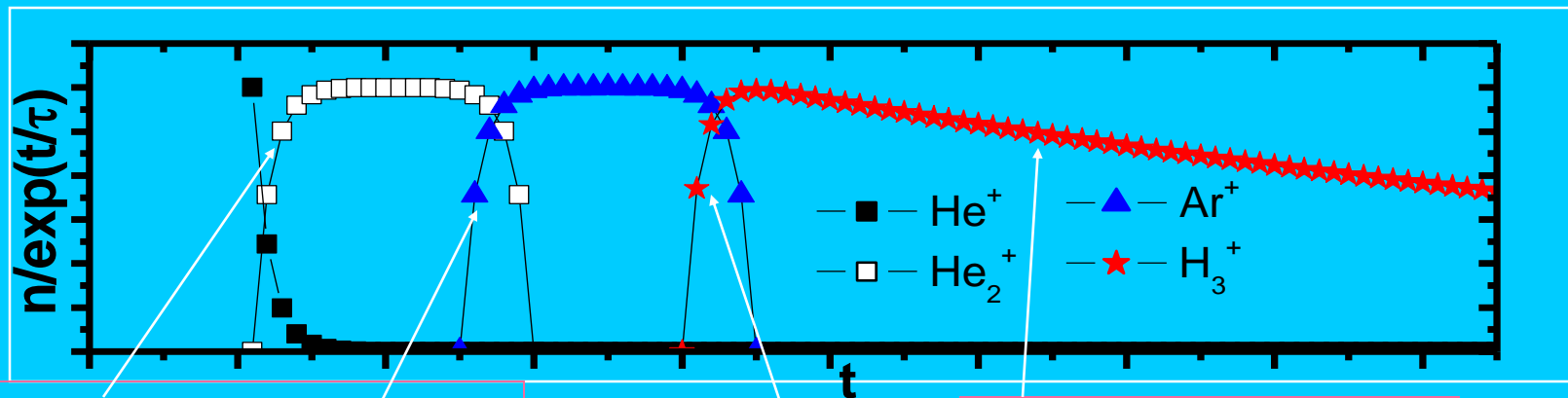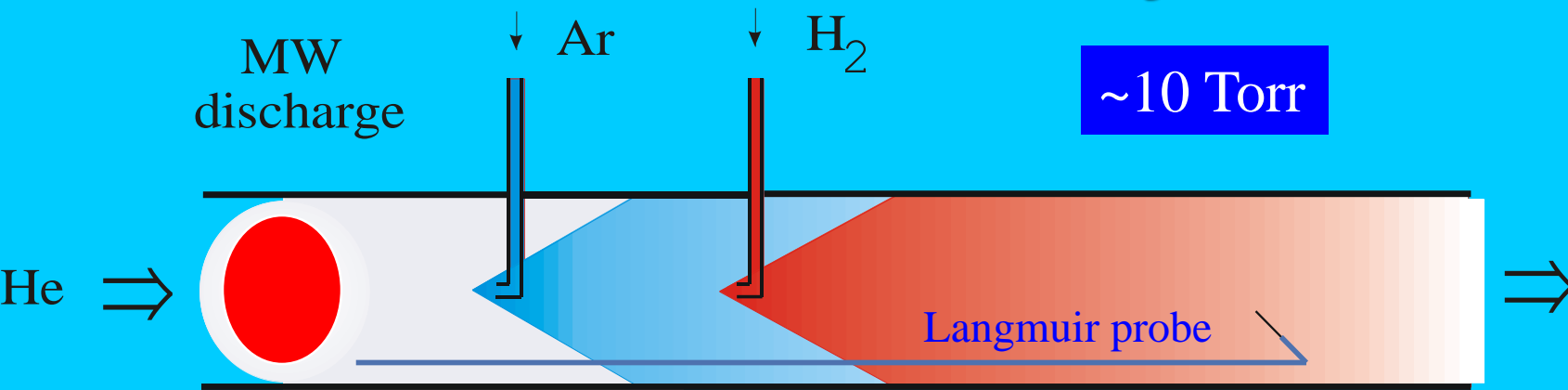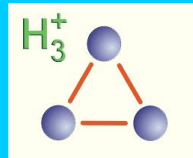
Flowing afterglow/Langmuir probe (FALP)
D. Smith, N. G. Adams and P. Spanel

- A schematic diagram of the **FALP apparatus** showing the relative positions of the microwave discharge that generates the afterglow plasma and the three reactant gas entry ports **P1**, **P2** and **P3**. The distance (z) scale is referenced to the downstream mass spectrometer sampling orifice. The complete flow tube is surrounded by a **vacuum jacket** to facilitate high and low temperature operation (ranging from 80 to 600K).
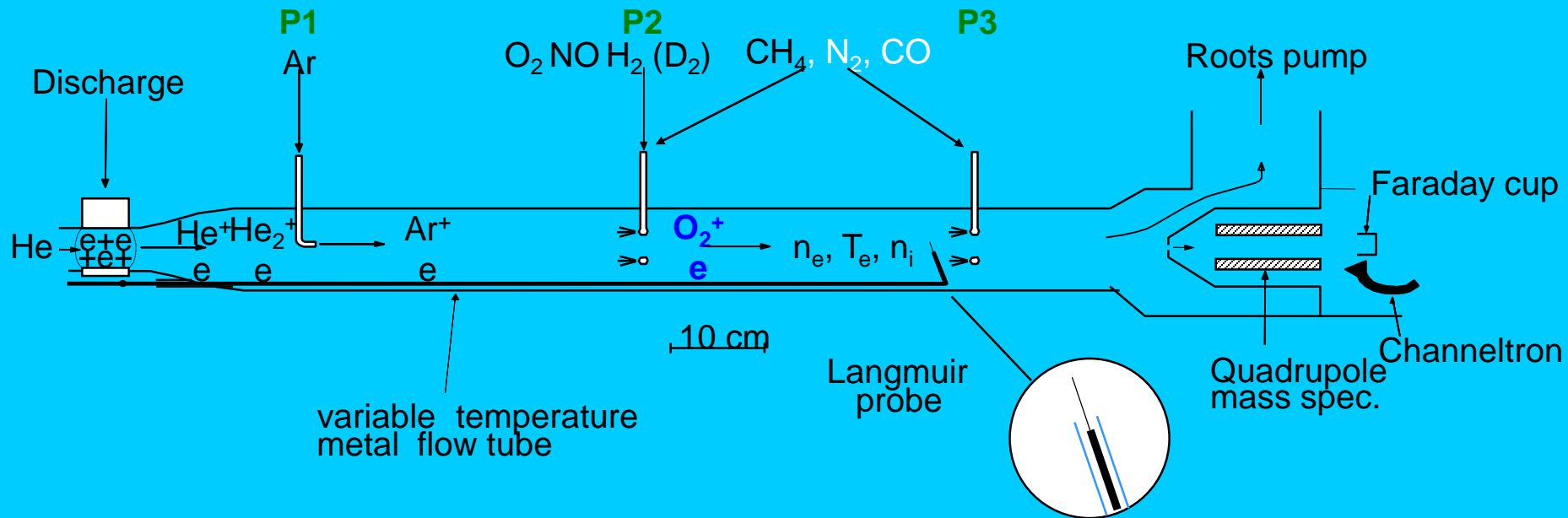
Positive ion/electron dissociative recombination

- e.g. $NO^+ + e \rightarrow N + O$

$$\frac{dn_e}{dt} = -\alpha\, n_e^2 + D_a \nabla^2 n_e \quad \text{diffusion}$$

$$\frac{dn_e}{dt} = -\alpha\, n_e^2 - \frac{D_a}{\Lambda^2} n_e$$

$$\frac{1}{n_e} - \frac{1}{n_0} = \alpha(t_e - t_0)$$

$$\frac{1}{n_e} = \alpha\; \frac{\exp(\nu t)-1}{\nu} + \frac{1}{n_0}\exp(\nu t)\; ; \nu = D_a/\Lambda^2$$

... SA... ... ...n experiments (CRDS)

FALP studies of the dissociative recombination coefficients for O_2^+ and NO^+ within the electron temperature range 300–2000 K[1]

Patrik Španěl, Libuše Dittrichová[†], David Smith*
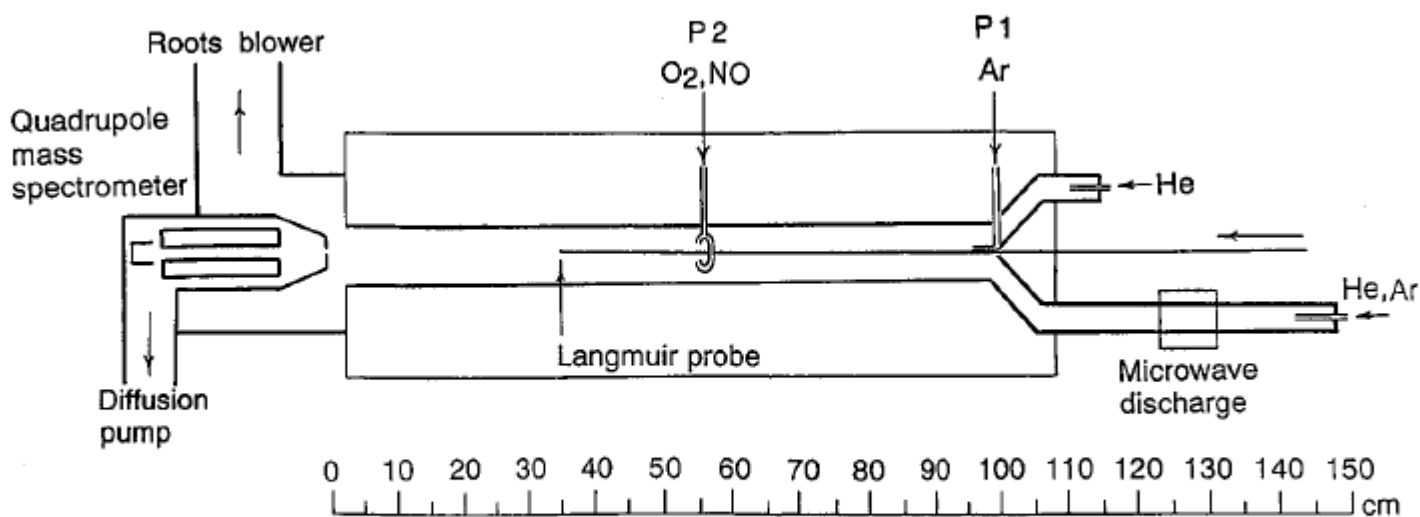
Fig. 1. A line diagram (approximately to scale) of the FALP apparatus, indicating the positions of the microwave discharge, the entry port of helium coolant gas (for the argon afterglow plasmas), the entry ports P1 for argon (for the helium afterglow plasmas) and P2 for O_2 and NO, and the mass spectrometer. The Langmuir probe can be positioned at any point on the axis of the flow tube. Also indicated is the outline of the vacuum jacket which facilitates the heating and cooling of the complete flow tube.
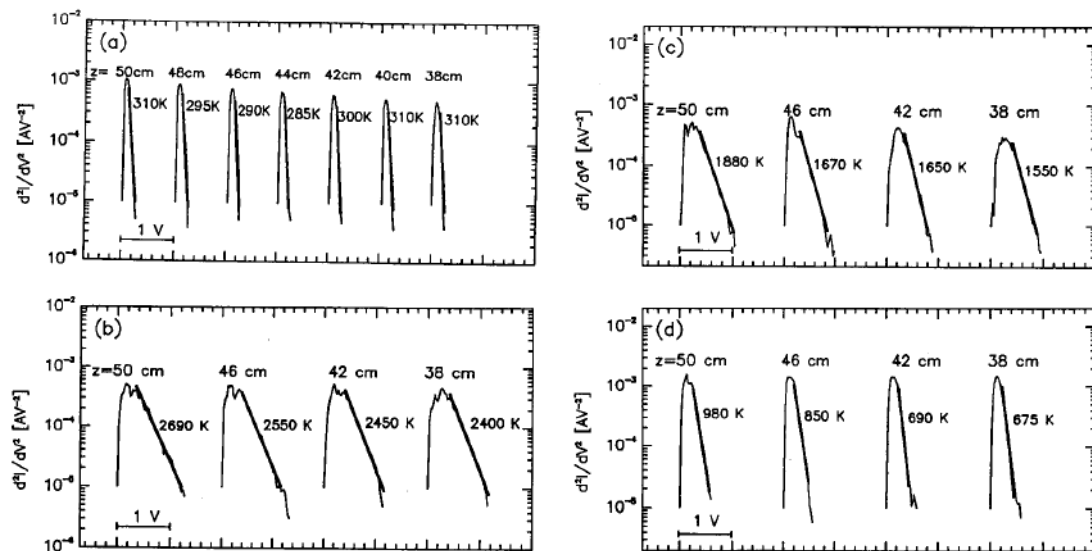
Fig. 2. Representative plots of d^2i/dV^2 against V obtained from the Langmuir probe current (i)–voltage (V) characteristics from which electron temperatures T_e are obtained. In every case the carrier gas temperature is 300 K. The good linearity of a plot is indicative of a Maxwellian electron energy distribution function (EEDF). The z values are the positions of the probe along the axis of the flow tube (referenced to the mass spectrometer sampling orifice; see Fig. 1). The entry port P2 via which the O_2 and NO ion source gases were introduced into the afterglows is located at $z = 56$ cm. (a) Obtained in helium afterglows (at a pressure of 1 Torr) with a small admixture of argon to destroy helium metastable atoms. Note the excellent linearity of the plots and the small scatter of T_e about T_g ($= 300$ K) along z. (b) Obtained in pure argon afterglows (at a pressure of 0.7 Torr). Note the much higher T_e values (compared with those in (a)) and the small (but obvious) T_e gradient along z. (c) Obtained in argon afterglows into which O_2 (partial pressure of ≈ 5 mTorr) has been added to generate an O_2^+/electron plasma. Note the somewhat greater fractional decrease in T_e compared with that in the pure argon afterglow in (b), this being due to the additional cooling of the electron gas on the O_2 molecules. (d) Obtained in argon afterglows into which first helium (partial pressure 50 mTorr) has been added to cool the electron gas (see Fig. 1), and then into which O_2 (partial pressure 5 mTorr) has been added to produce the O_2^+/electron plasma at a lower T_e than that in (c). Note that the fractional decrease in T_e is greater than in (c) because of the combined cooling effects of the helium and the O_2. It is this T_e gradient along the reaction zone which limits the T_e resolution in these experiments.

$$v_p \frac{dn_e}{dz} = -\alpha n_e^2 + D_a \nabla^2 n_e \qquad (4)$$

As a reasonable approximation, we assume that diffusive loss is via the fundamental mode only and then

$$v_p \frac{dn_e}{dz} = -\alpha n_e^2 - \frac{D_a}{\Lambda^2} n_e \qquad (5)$$

where D_a is the ambipolar diffusion coefficient and Λ is the characteristic diffusion length (for the flow tube used here, $\Lambda^2 = 2.76$ cm^2), and v_p is the plasma flow velocity (1.1×10^4 cm s^{-1}). When recombination is the dominant loss process, such as is the case in these studies of both $\alpha(O_2^+)$ and $\alpha(NO^+)$ at the lower T_e, (and certainly at 300 K in the helium carrier gas), then the diffusion term in Eq. (5) can be neglected, and the solution to Eq. (5) is then

$$\frac{1}{n_t} - \frac{1}{n_0} = \frac{\alpha(z_t - z_0)}{v_p} \qquad (6)$$

Electron temperature measurement

D.Smith and P.Spanel

(a) Obtained in **helium** afterglow (at a pressure of 1 Torr) with a small admixture of argon to destroy helium metastable atoms.

(b) Obtained in pure **argon** afterglow (at a pressure of 0.7 Torr).

(c) Obtained in **argon** afterglow into which O_2 (partial pressure of ~5mTorr) has been added to generate an O_2^+/electron plasma.
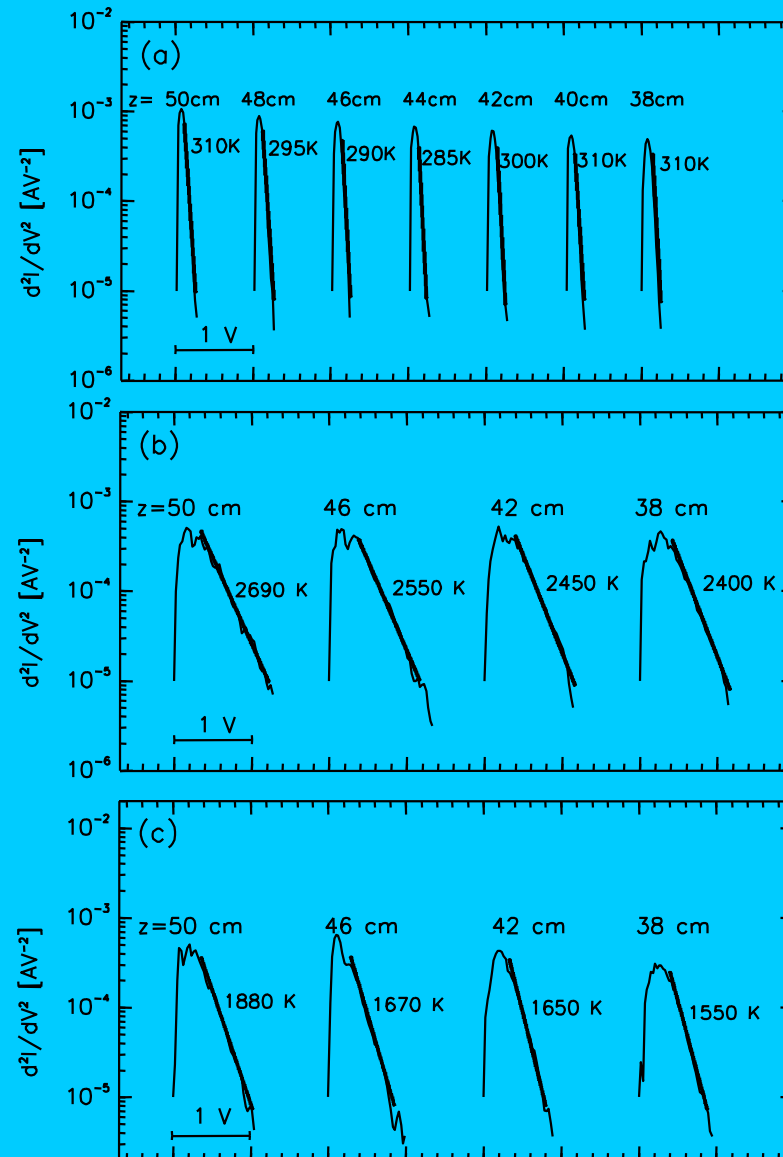
Electron temperature dependence

Plots of $1/n_e$ against the distance z along the flow tube obtained in O_2^+/electron afterglow plasmas from which values for $\alpha(O_2^+)$ are obtained.

The data indicated by filled circles were obtained in helium carrier gas when $T_e = T_i = T_g = 300$ K; the linearity of the plot over a factor of about ten indicates that dissociative recombination is the dominant loss process for electrons and ions.

The data represented by open circles (T_e=650 K) were obtained in argon carrier gas at $T_g = 300$ K, and at elevated T_e.

O_2^+/electron

Ar carrier, T_g=300 K

T_e=650 K

He carrier T_e=300 K

$1/n_e$ [10^{-10}cm^3]

z (cm)
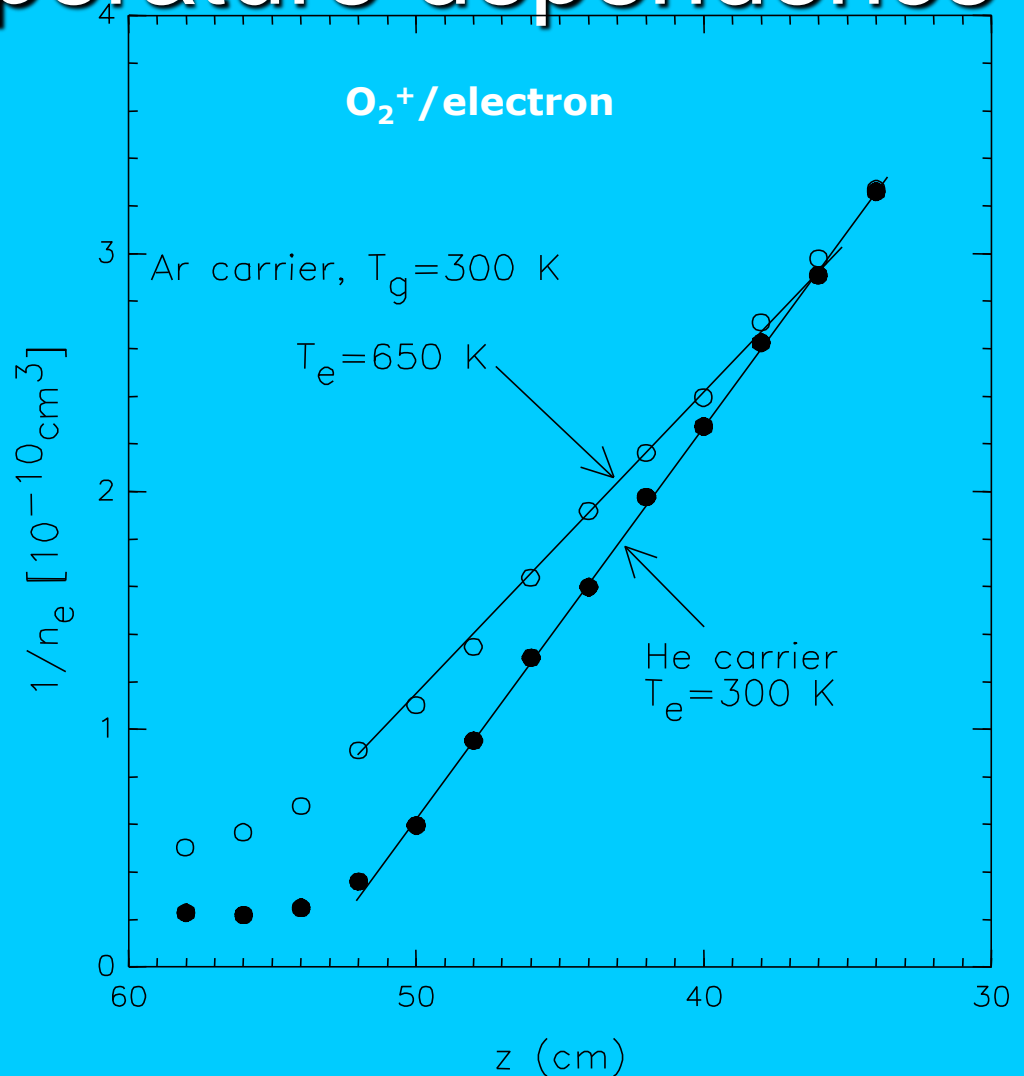
FALP and in-situ data

The points indicated by blue triangles are the $\alpha(NO^+)$ deduced from in-situ satellite data by

M. R. Torr, J. P. St-Maurice and D. G. Torr, J. Geophys. Res., **82** (1977) 3287.

The agreement between these data and the laboratory data is remarkable.
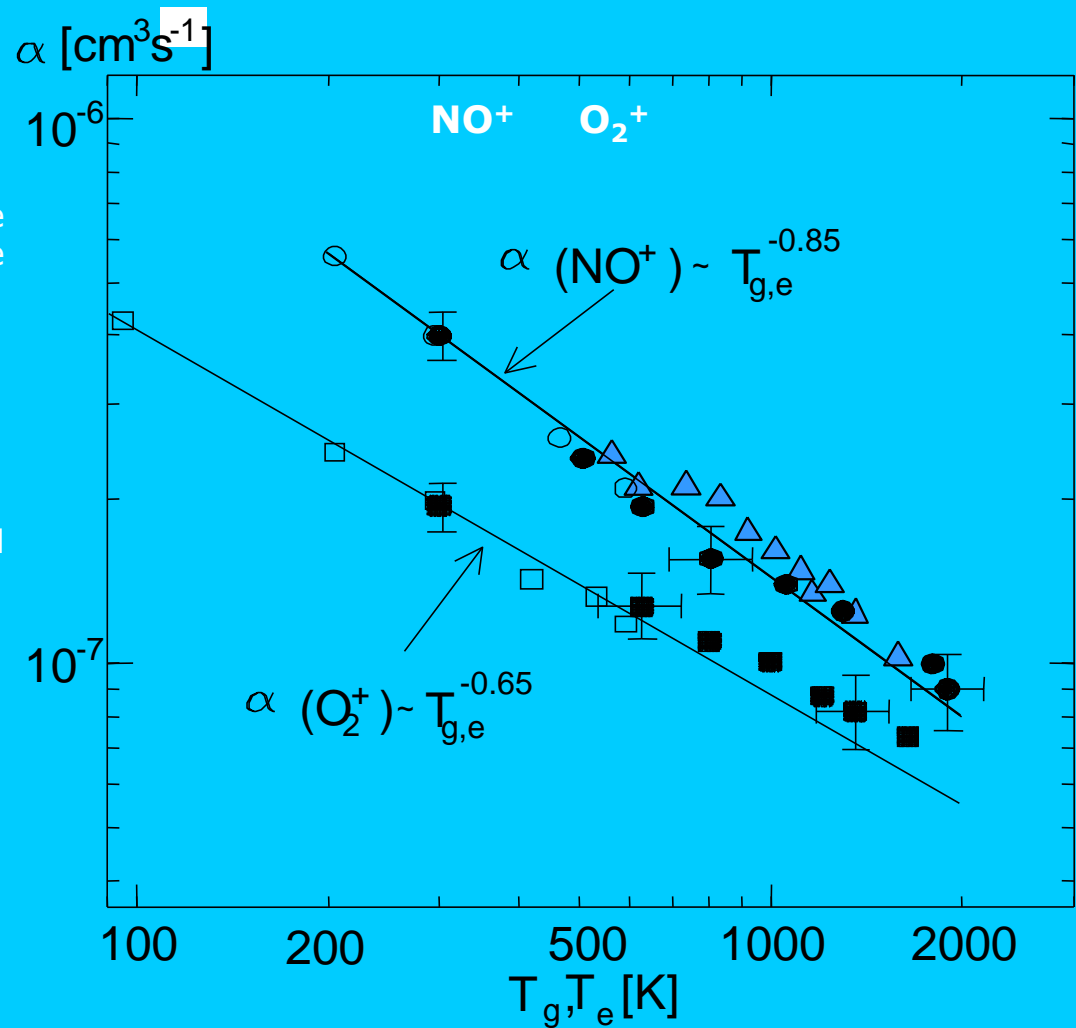
Dissociative recombination of different ions
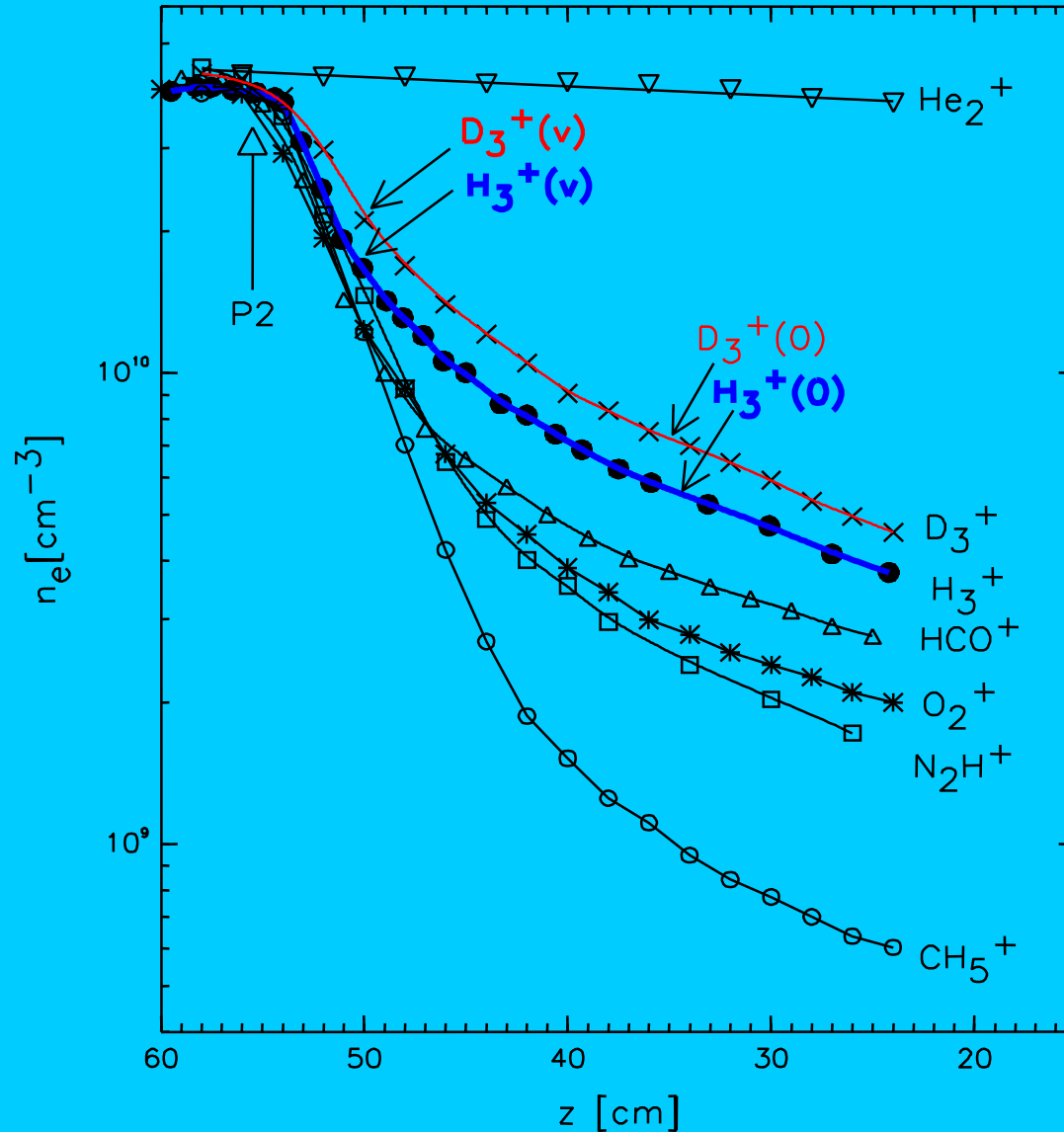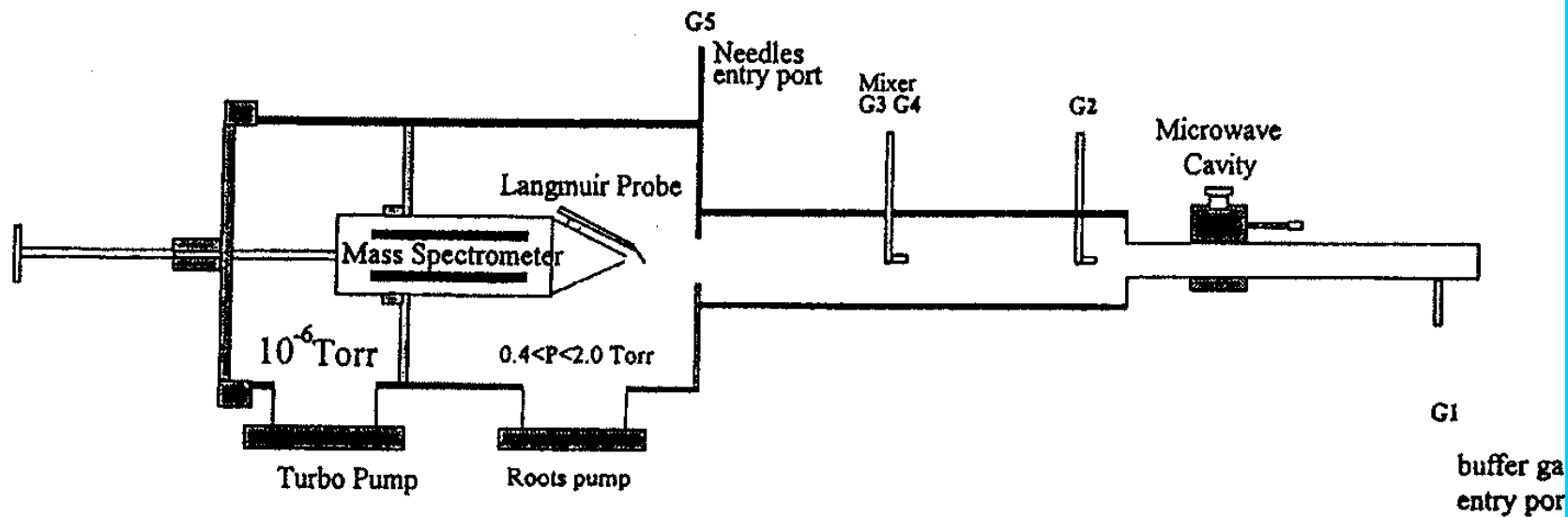
Figure 1. Sketch of the FALP apparatus.

RENNES absorption studies

FIG. 1. Sketch of the apparatus.

Movable Langmuir probe

Roots blower

N_2 entry port

Ar entry port

Microwave discharge

Helium entry port

$\bullet$: $Q_{N_2} = 0$ cm^3 min^{-1}atm

$\circ$: $Q_{N_2} = 100$ cm^3 min^{-1}atm

N_e (cm^{-3})

Distance z (cm)
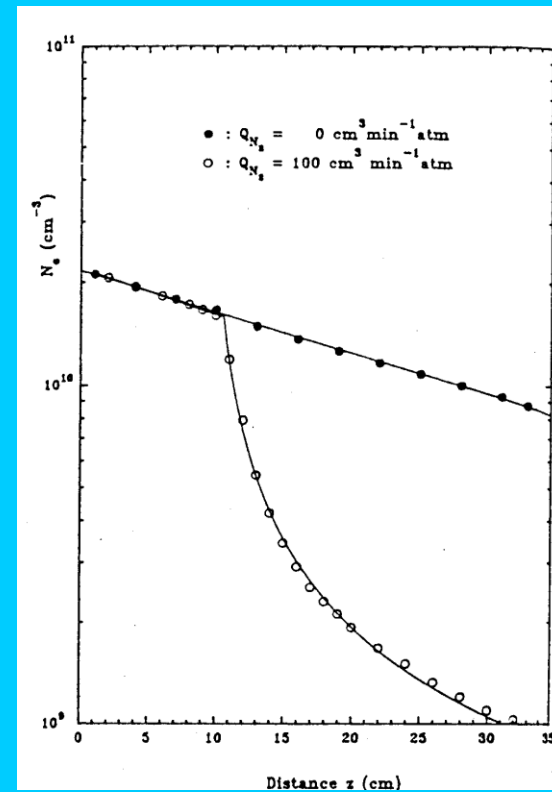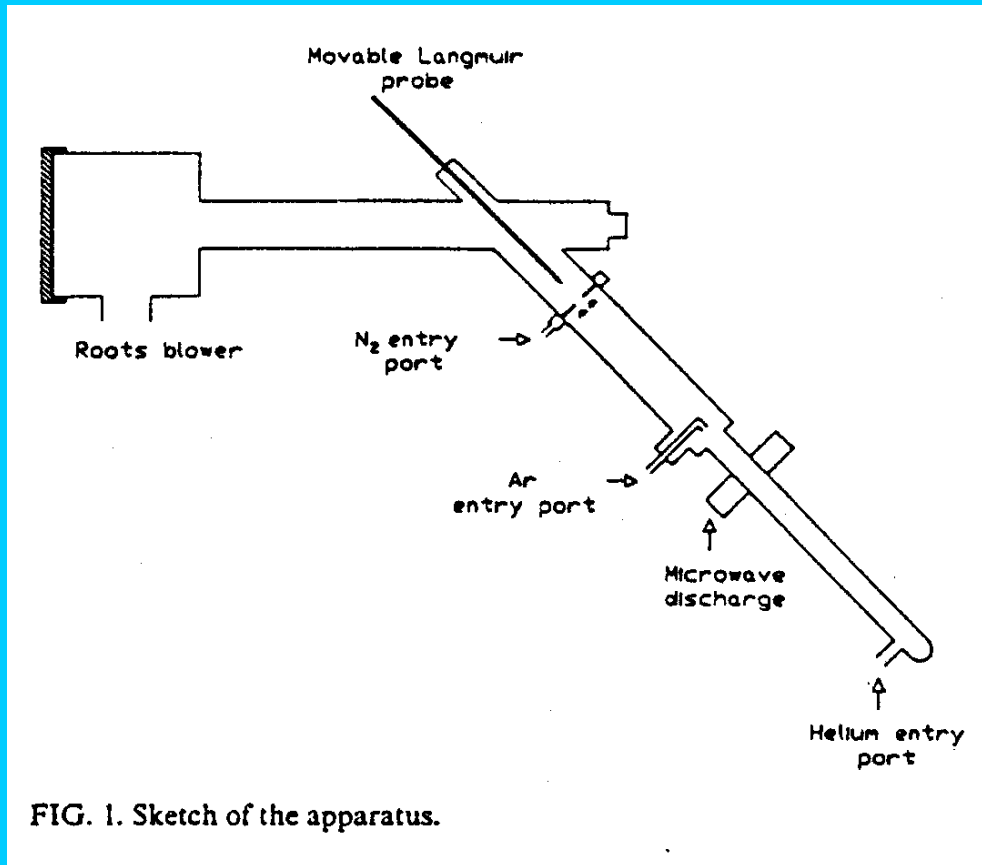
Pittsburg Rainer Johnsen FALP

Emission spectroscopy for identification products of recombination collisional radiative recombination of argon ions

$$Ar^+ + e^- + e^- \rightarrow Ar + e^-$$

He

Movable microwave discharge

Reagent inlet (H_2, N_2, COS)

Movable Langmuir probe

Laser beam

Mass spectrometer

Movable NO_2 inlet

He*

Ar

Quartz window

PMT

Ar

Roots pump

Turbopump
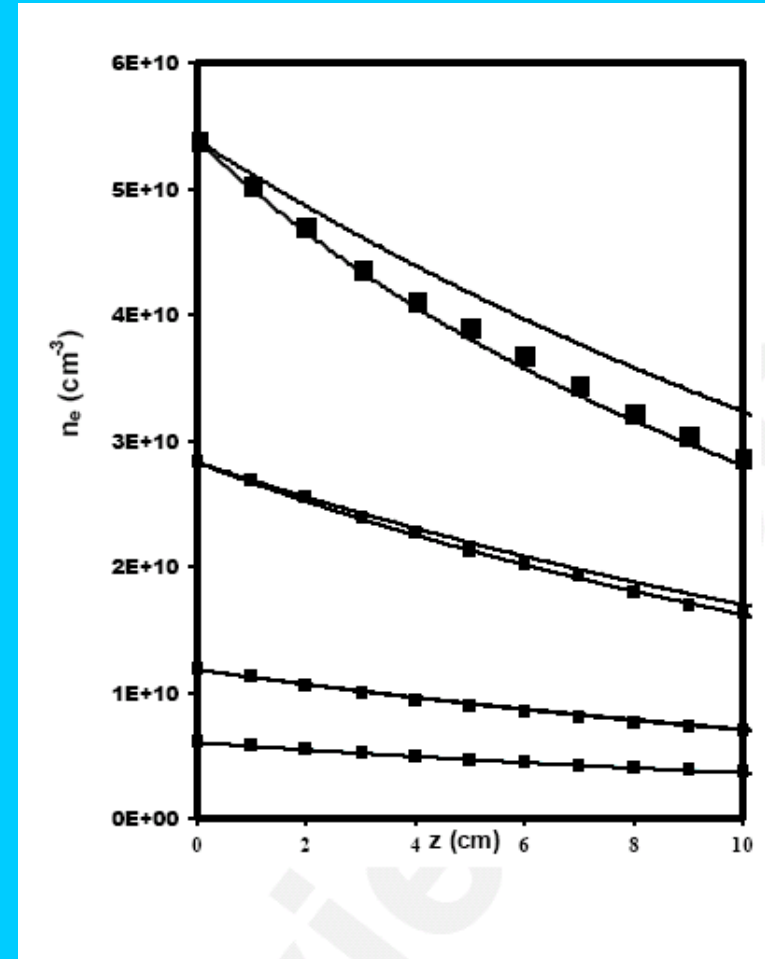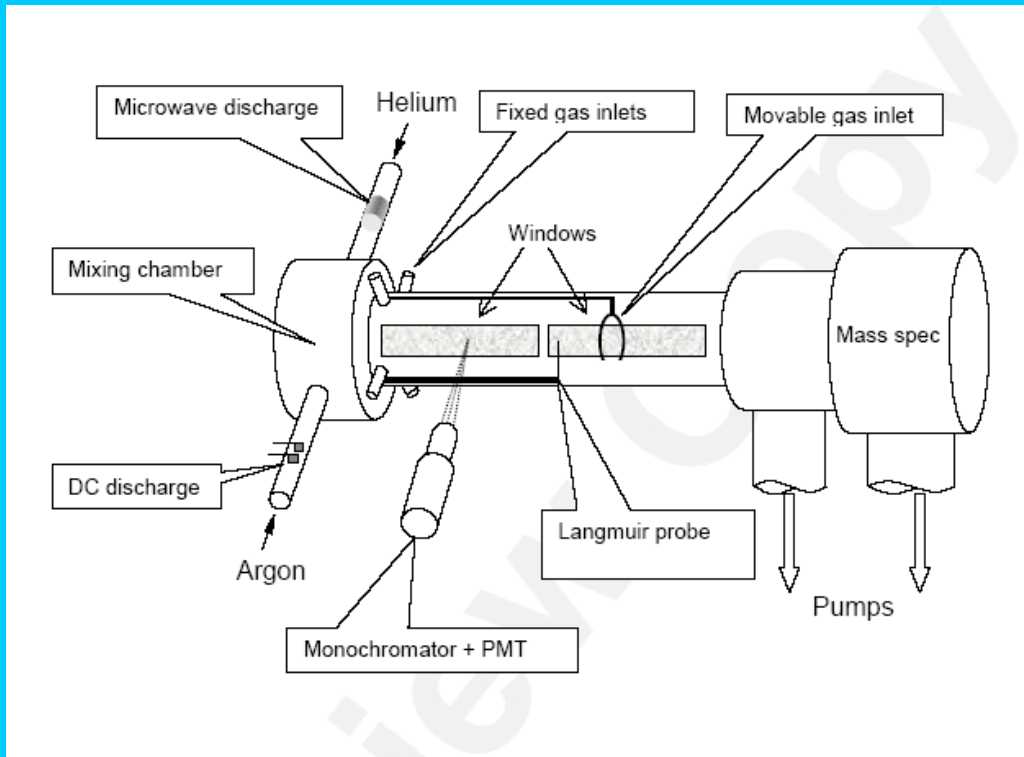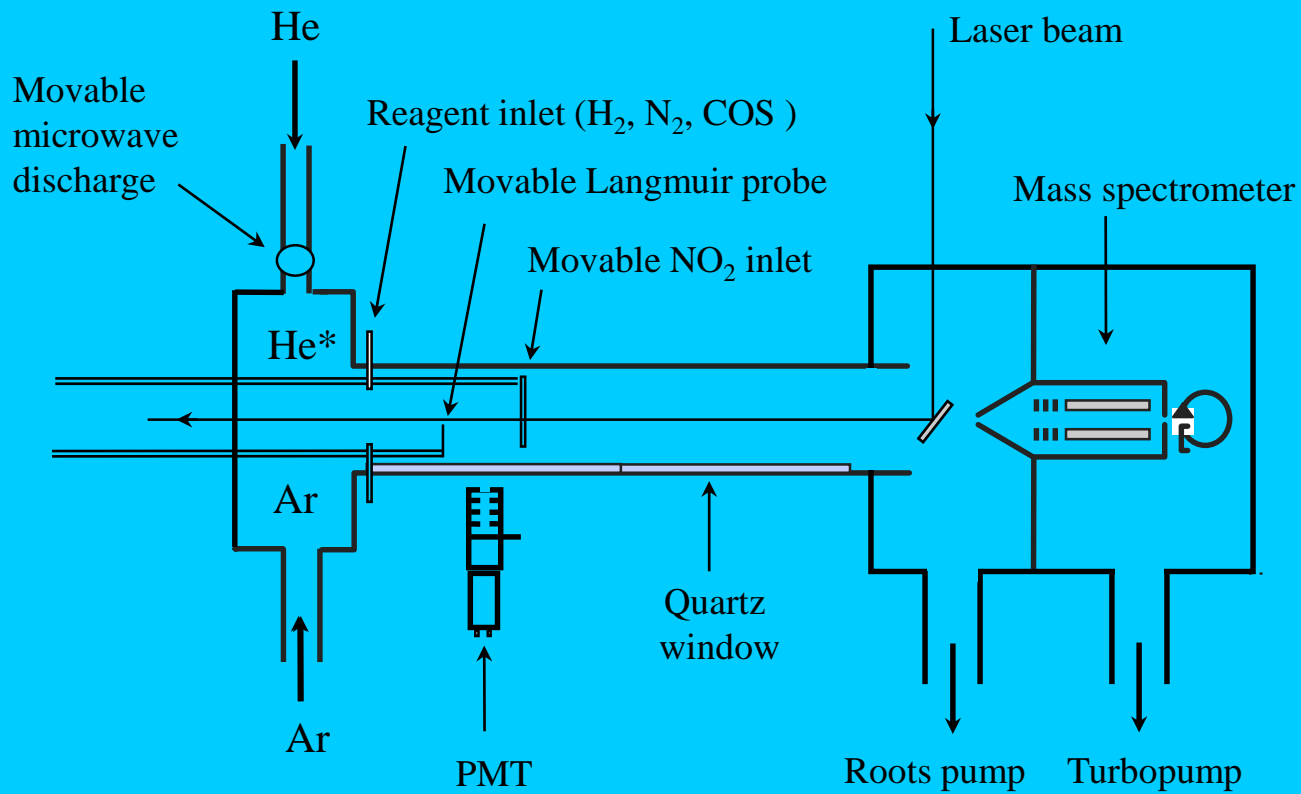
The Pittsburgh flow tube
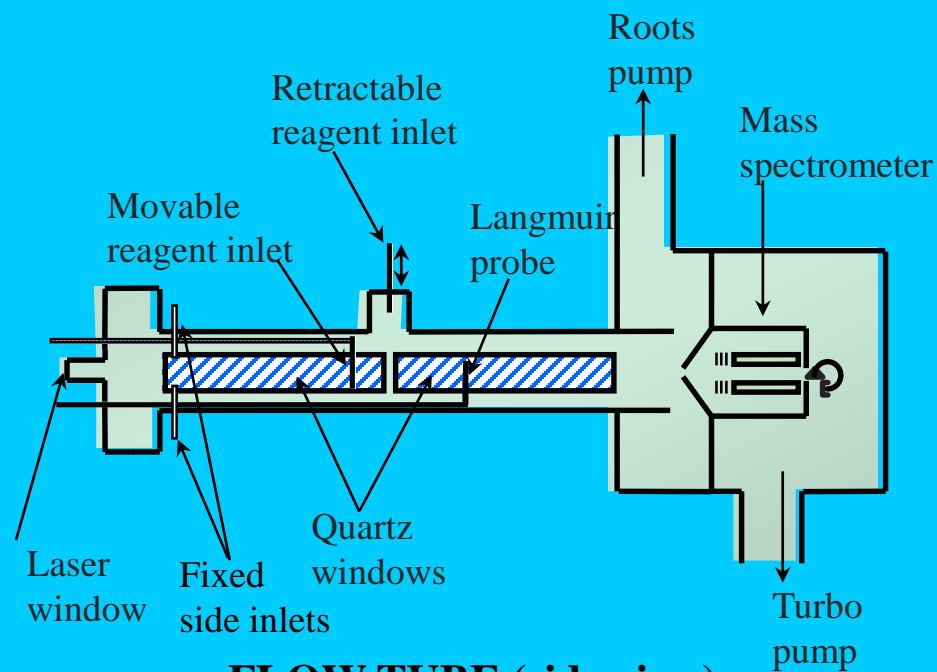
FLOW TUBE (side view)

FLOW TUBE (top view)

$$Ar^+ + H_2 \rightarrow Ar H^+ + H \quad (+ 1.53 eV)$$

$$ArH^+ + H_2 \rightarrow Ar + H_3^+ \quad (+ 0.57\ eV)$$
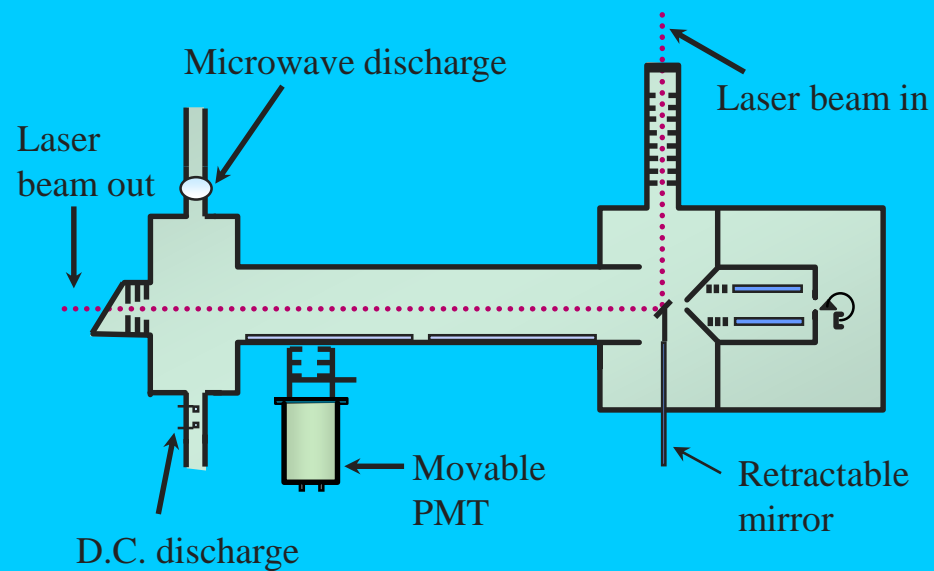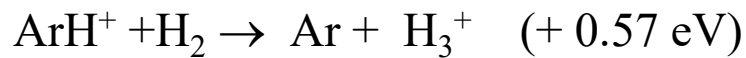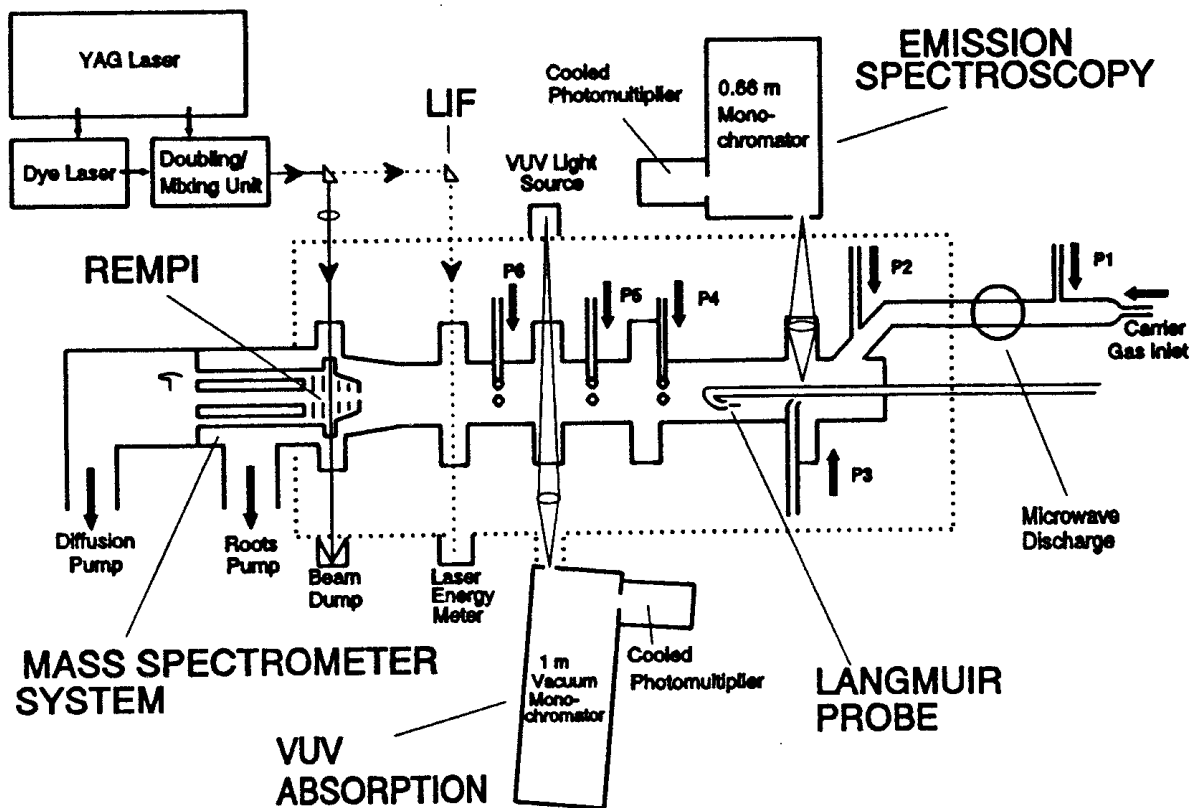
Figure 1. A schematic of the University of Georgia flowing afterglow. Illustrated are the axially movable Langmuir probe, the downstream mass spectrometer, a 0.66 m monochromator with red sensitive photomultiplier for emission studies, a vuv light source and 1 m vacuum monochromator with uv enhanced photomultiplier for detection of atoms and a YAG pumped dye laser with doubling and mixing capabilities for detection of radical species by LIF and REMPI. All photomultipliers are cooled to reduce the background noise and photon counting is used throughout. Further details of this apparatus are described in a separate review.[27]

FALP High pressure UHV version - PRAGUE
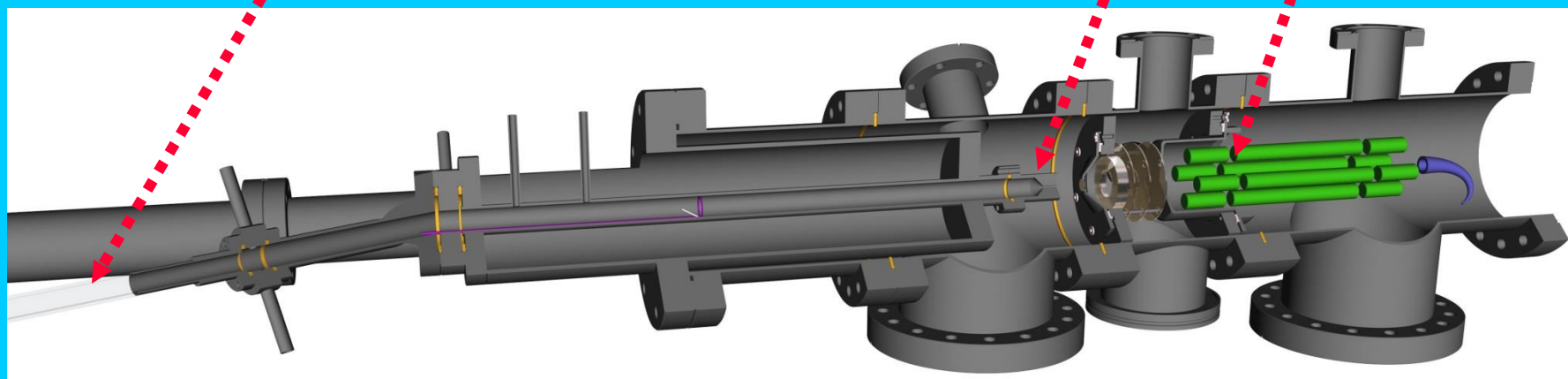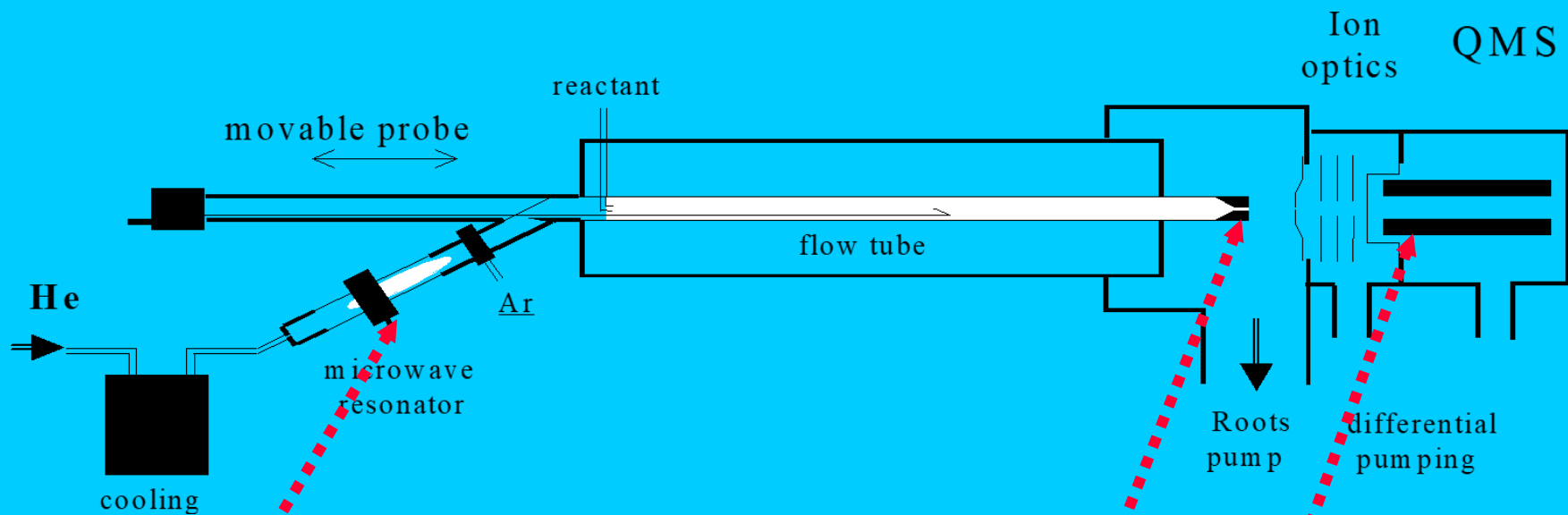
FALP – Ion detection system
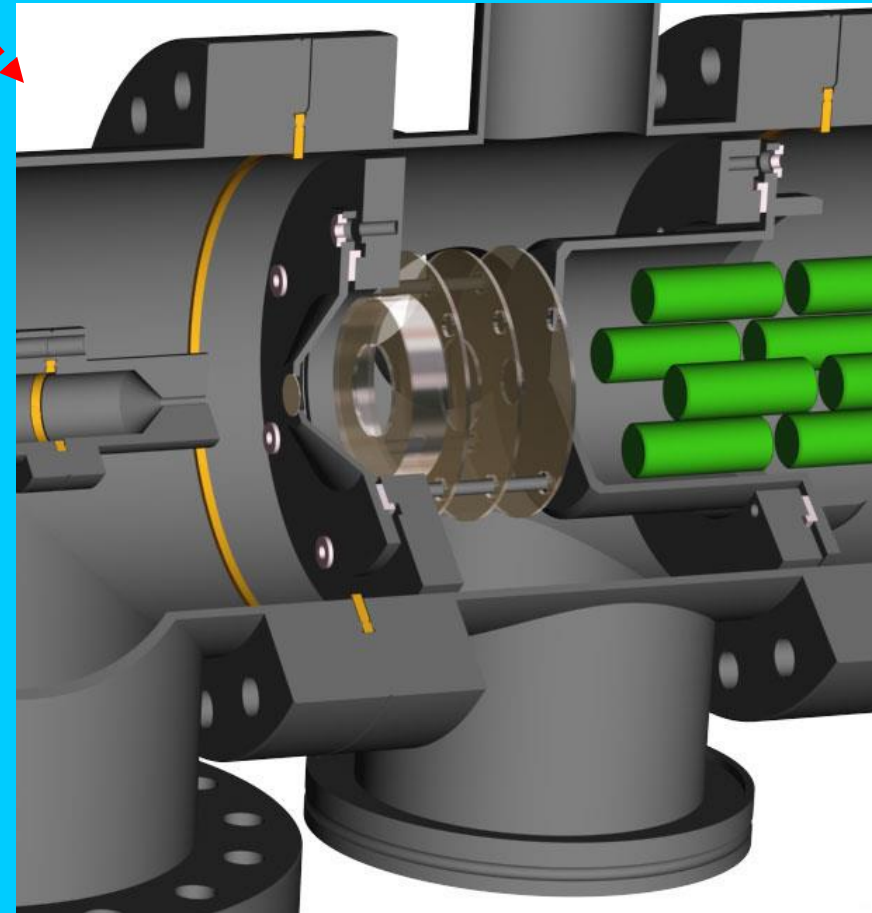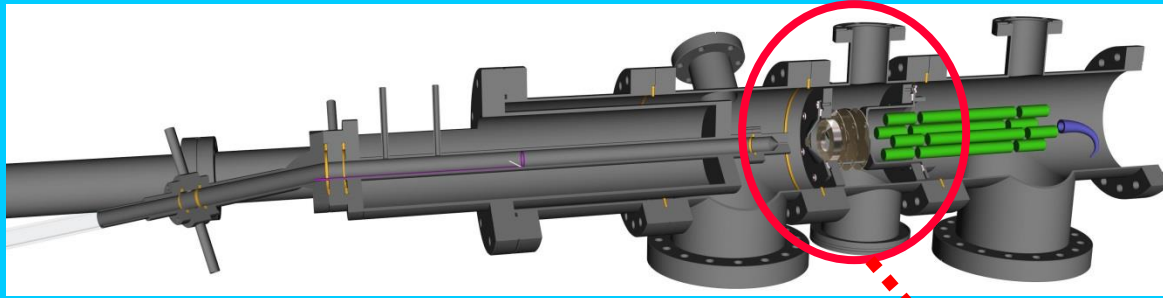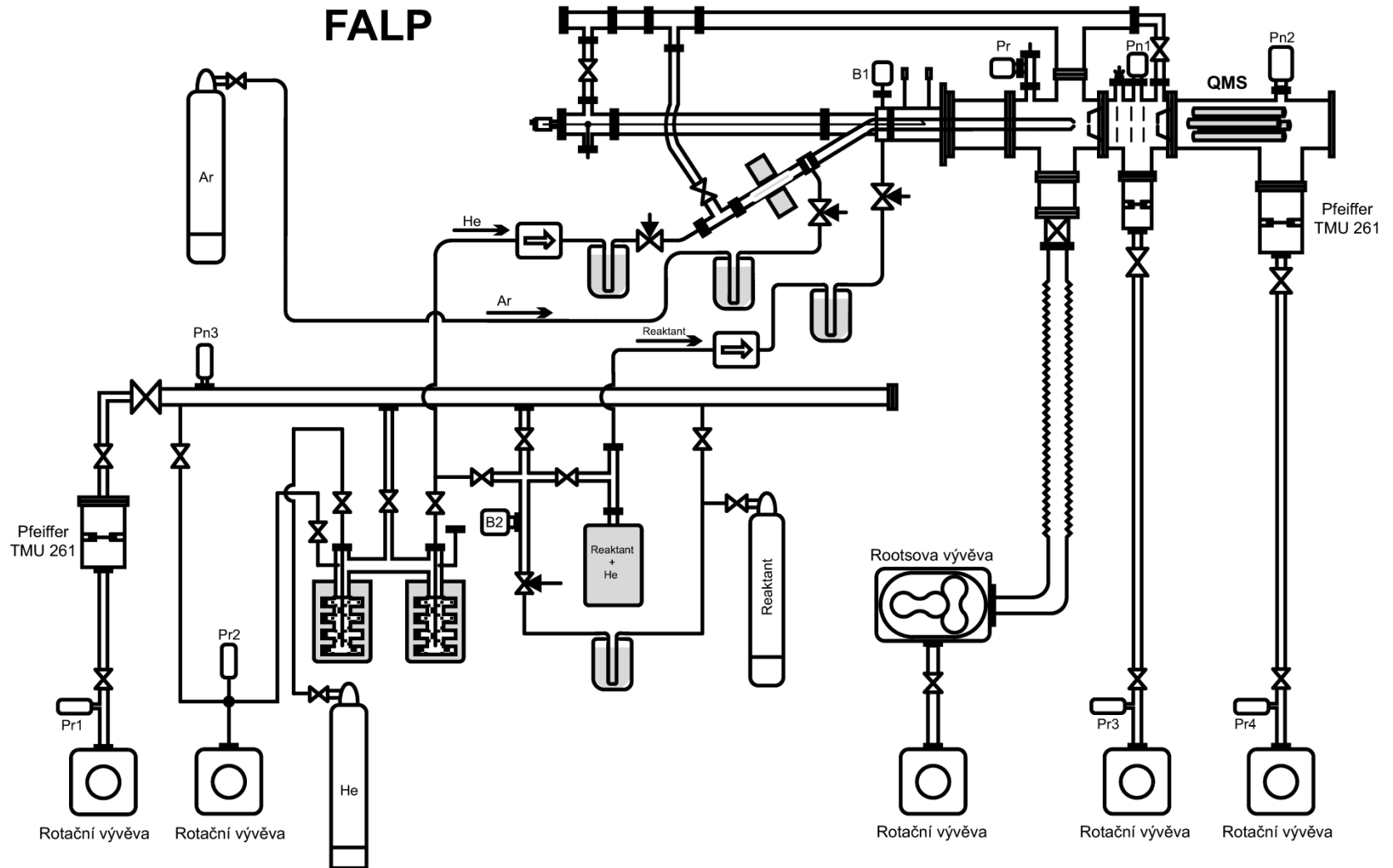
FALP high pressure version

To demonstrante how simple it is in reality

2 men experiment
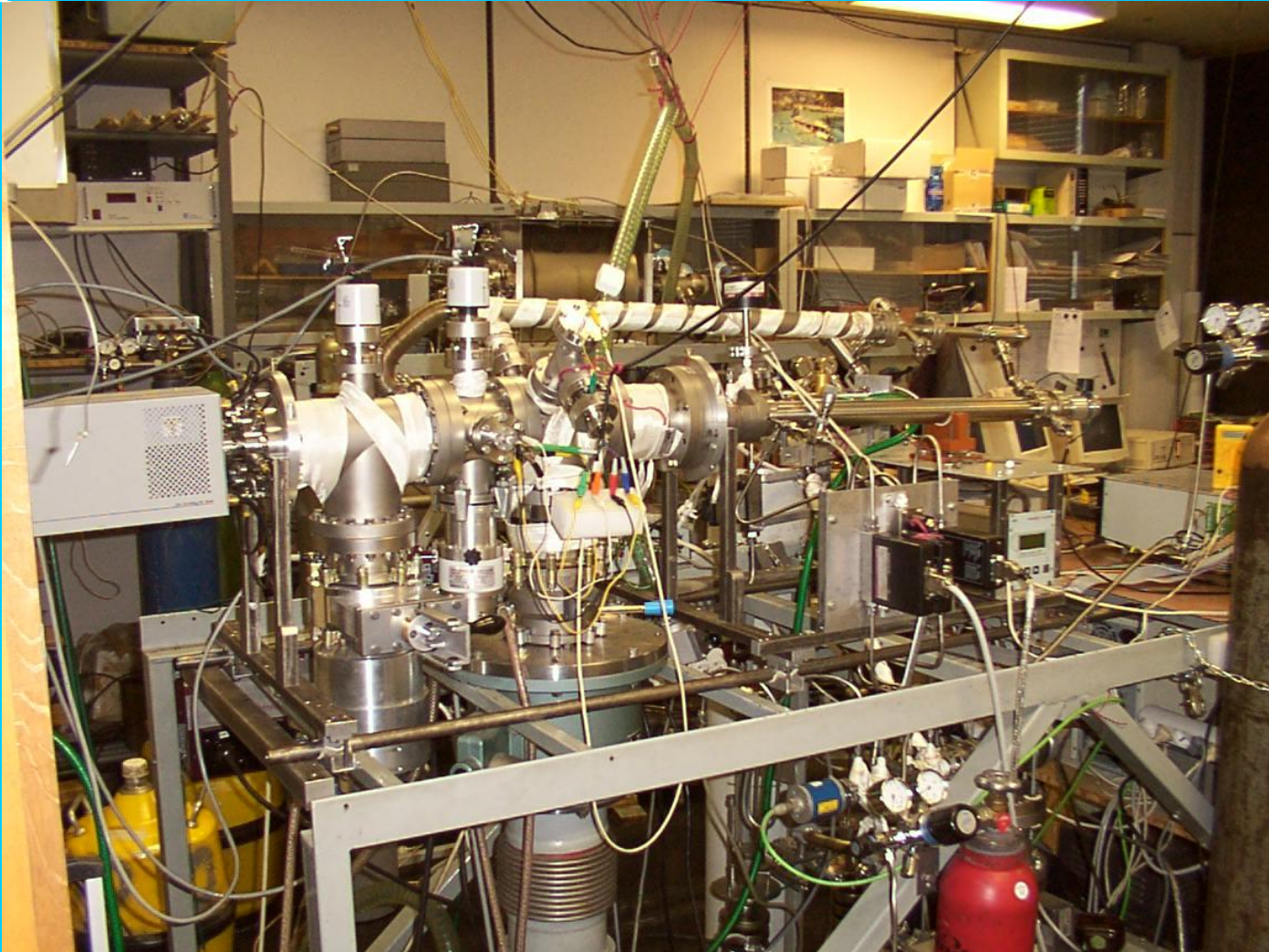
Variation of the probe characteristics along the flow tube
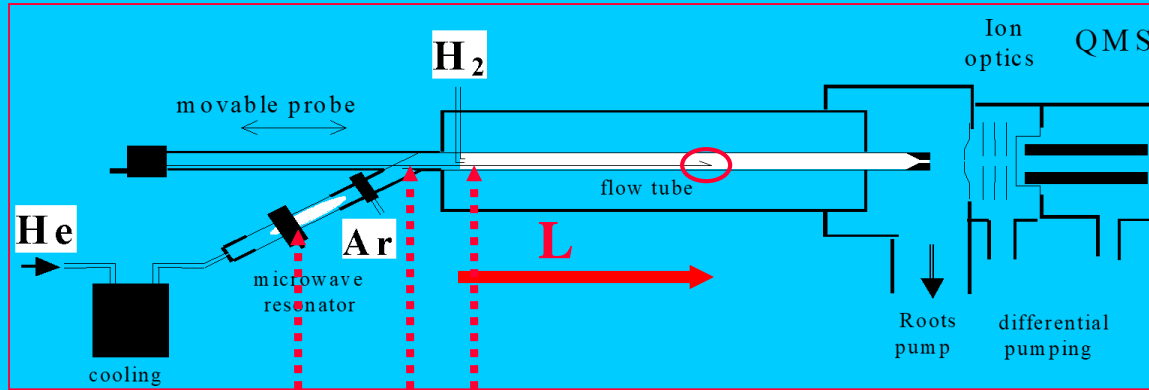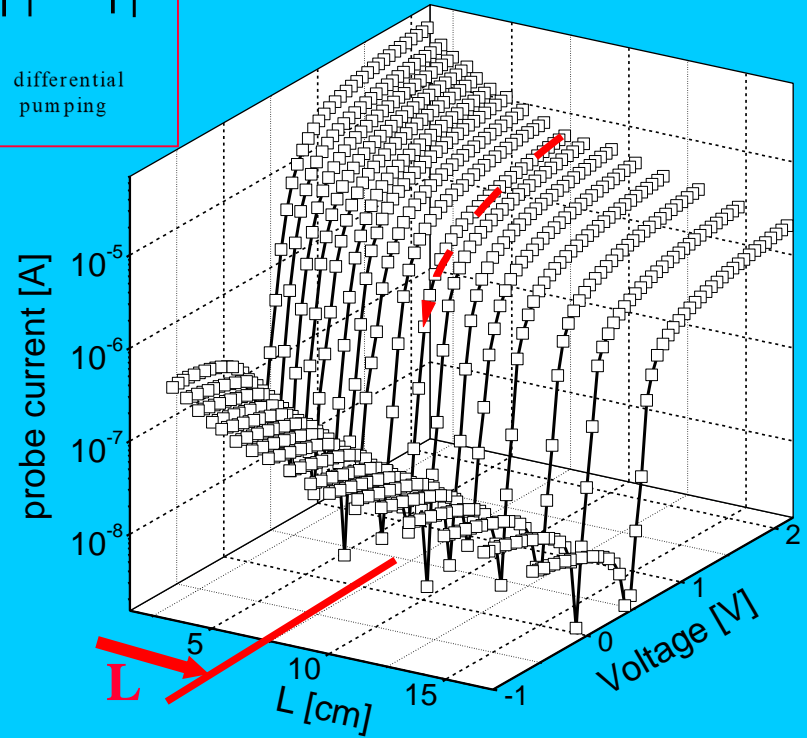
The decay time is correlated with the position in the flow tube.

He pressure 8.8 Torr, temperature 190 K, [Ar] 1.4 mTorr), [H$_2$] = 9.6×10^{14} cm^{-3}.

Evolution of the probe characteristics along the flow tube

Study of H₃⁺ and H₅⁺recombination
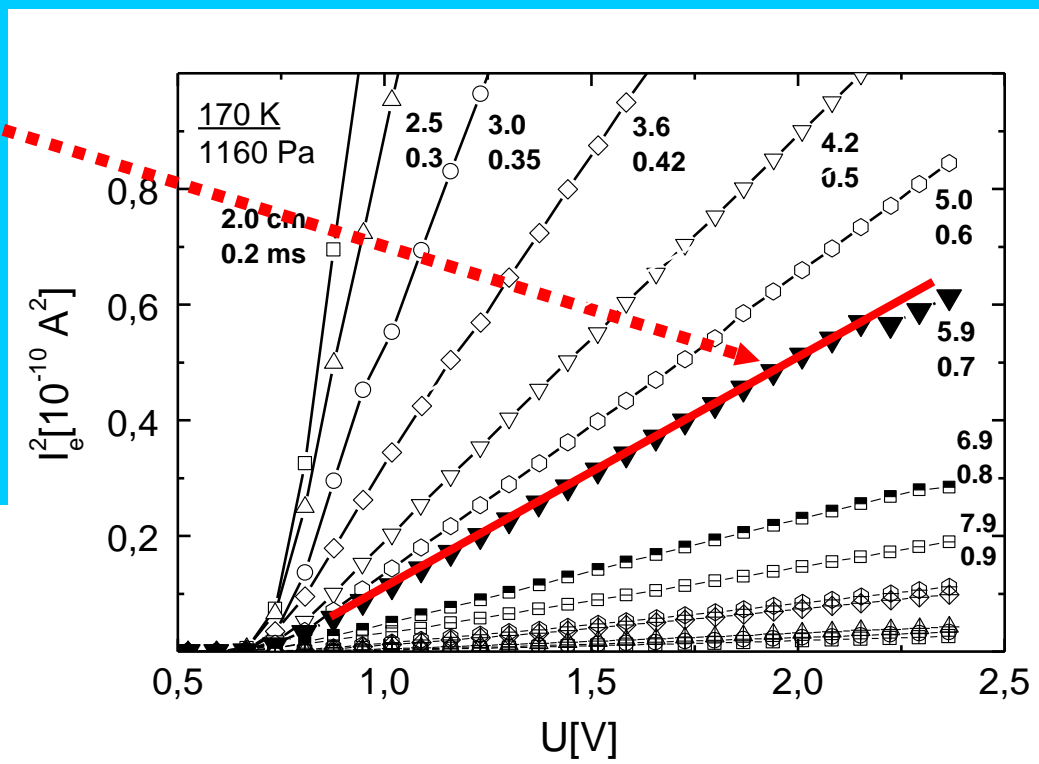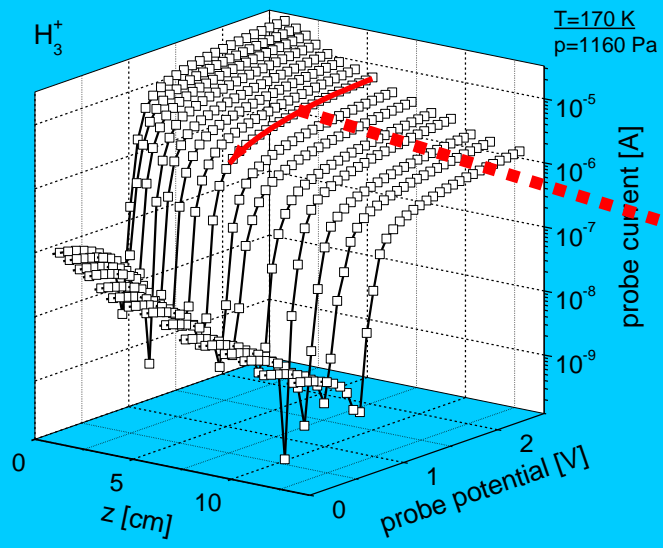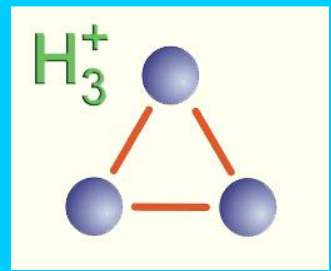
$$I_e^2 \sim n_e A_{Pr}(V_{probe} - V_{plasma})$$

PLASMA DECAY
H_3^+ and H_5^+ in thermodynamic equilibrium
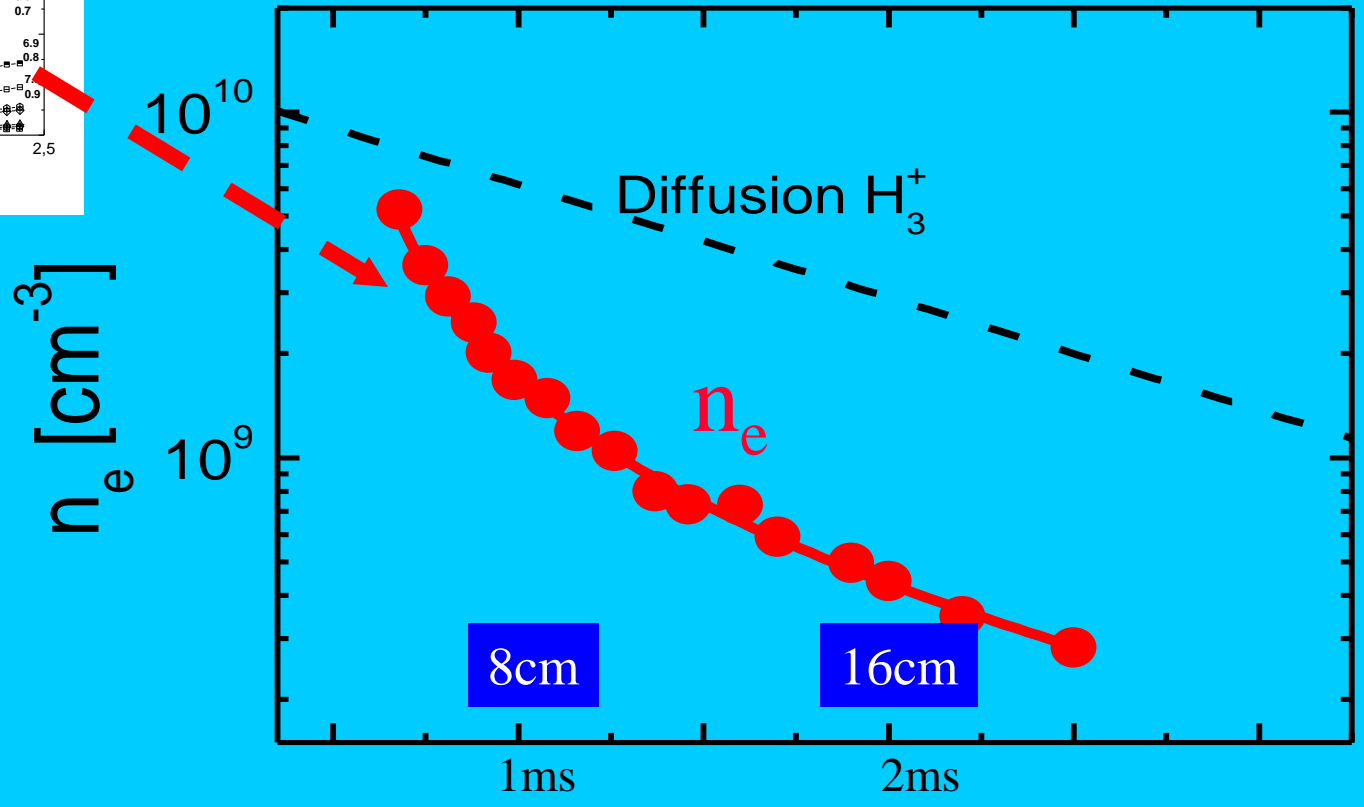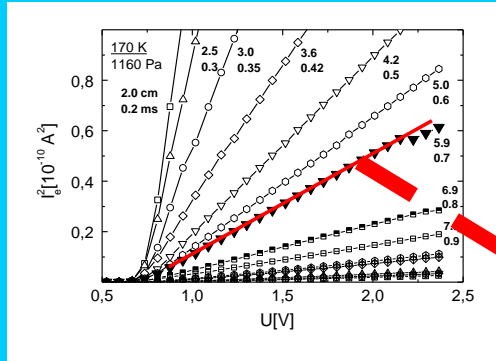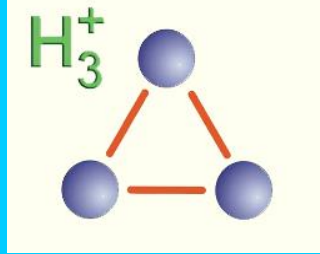
190 K,   9 Torr

Note very different time scale!!!

Plasma parameters along the flow tube

$$NH_4^+(NH_3)_2 + e^-$$

$$\vec{E_L}$$

$$V_P$$

$$T_e$$
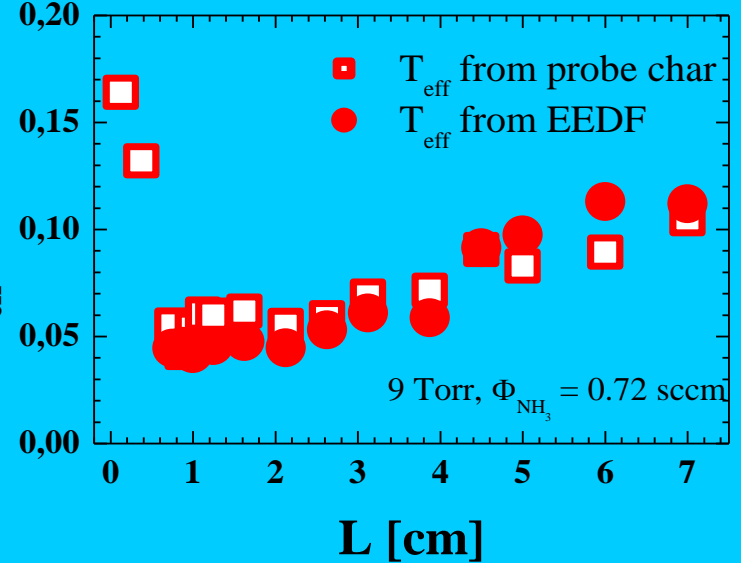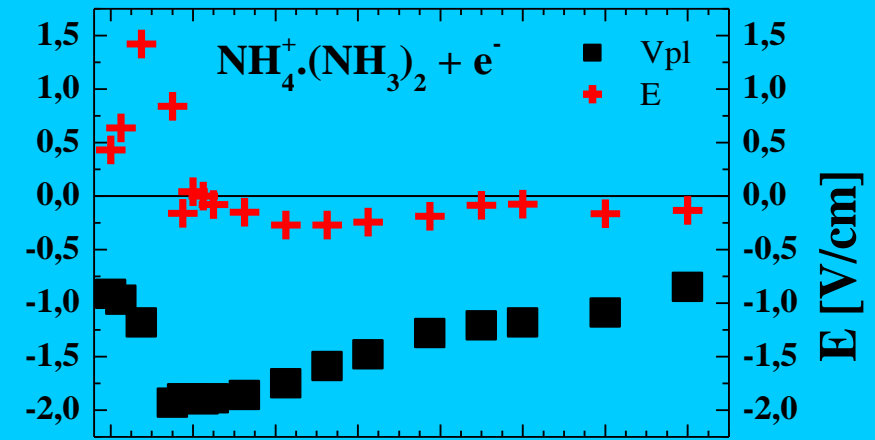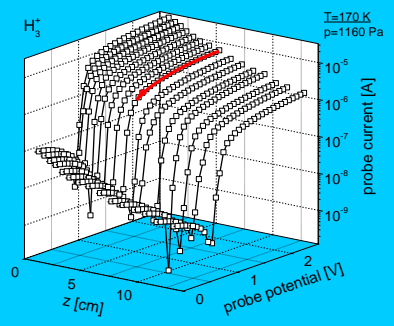
$$n_e$$
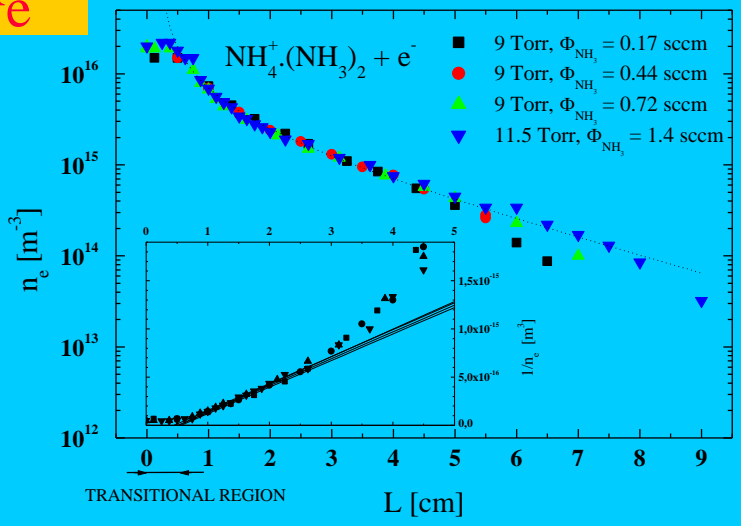
He buffer

EEDF measurements
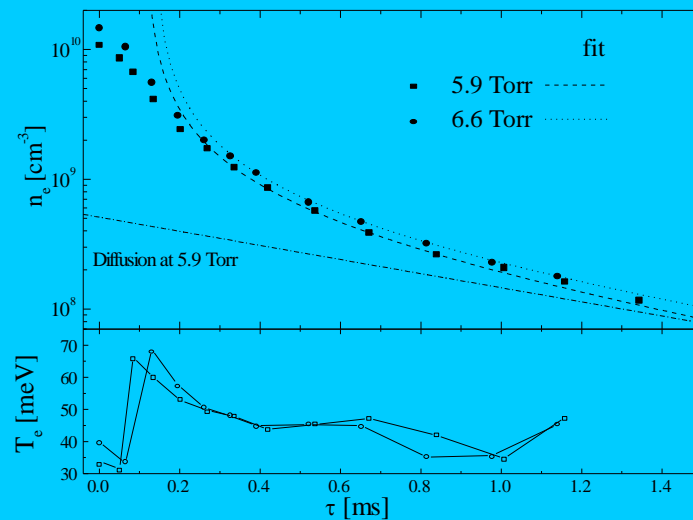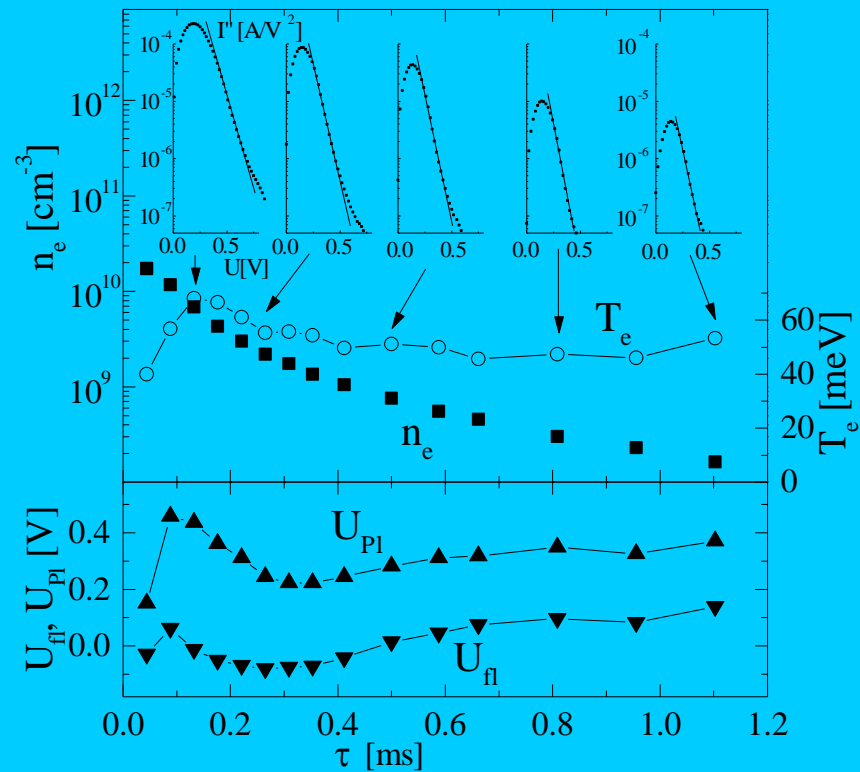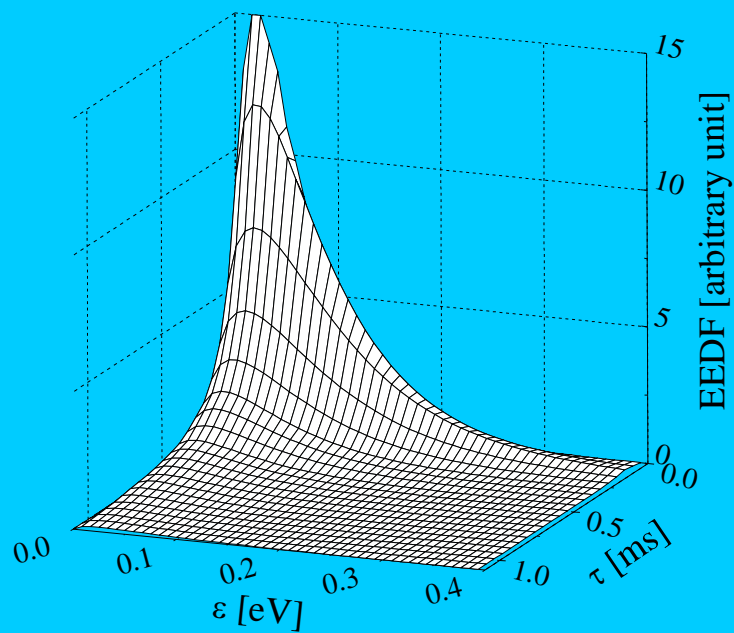
The time evolution of the EEDF in the recombination dominated FA plasma
In He (p= 9 Torr) with small admixture of HCOH (0.05 %).
EEDF is normalized to the electron number density.

Recombination of H⁺(HCOH)₂ + e⁻
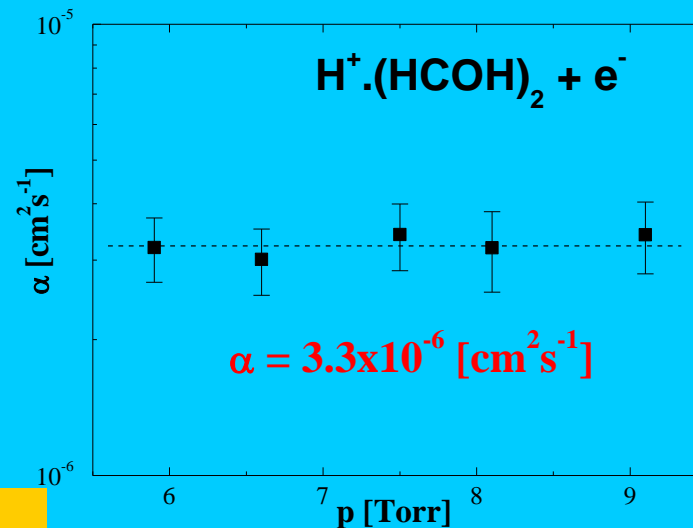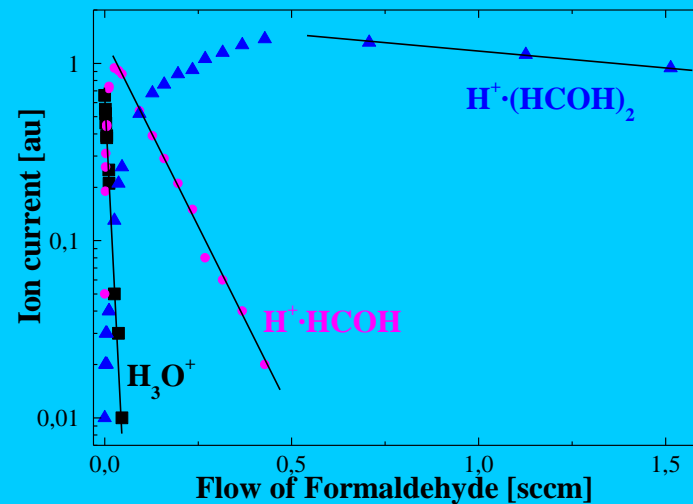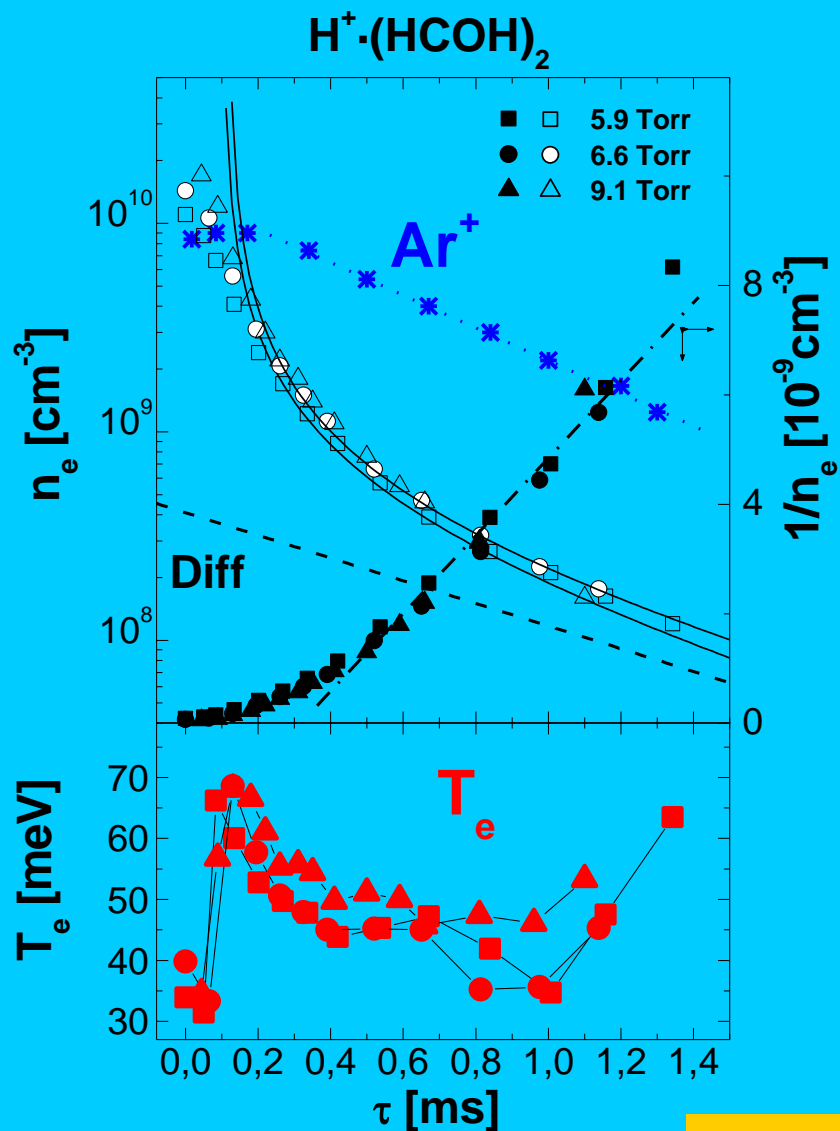
He buffer

Recombination aldehyde protonated dimmers with electrons

Conditions for measuring of therecombination
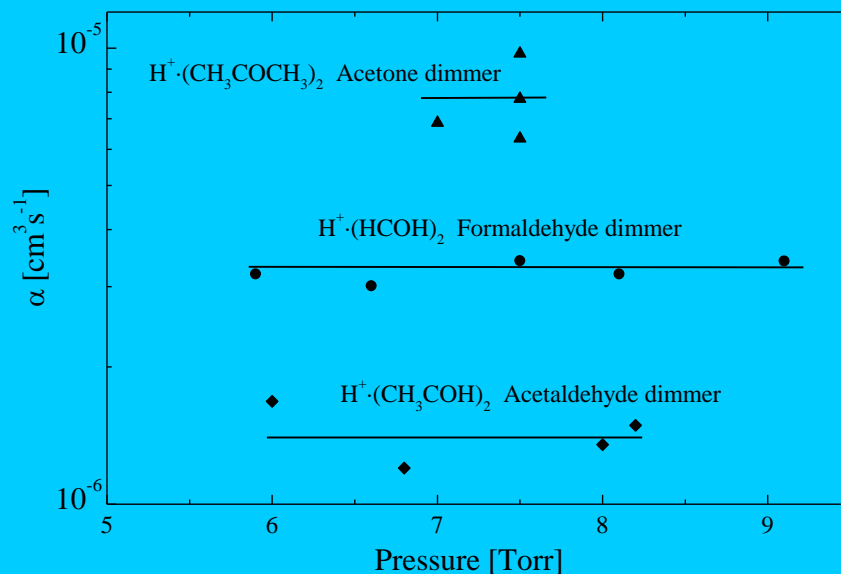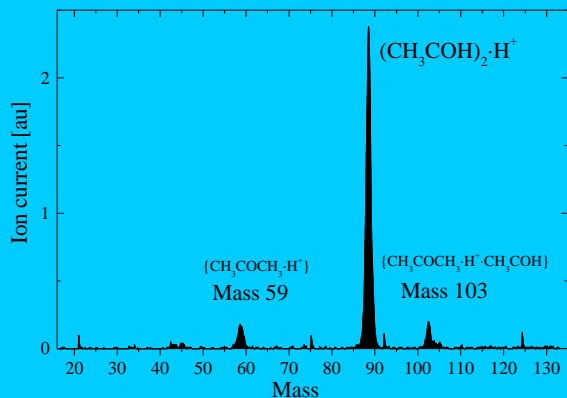
$H^+\cdot(HCOH)_2$ $\alpha = (3.3 \pm 1)\cdot10^{-6}$ [cm^{3}s^{-1}], at $T_e\sim400$ K

$H^+\cdot(CH_3COH)_2$ $\alpha = (1.4 \pm 1)\cdot10^{-6}$ [cm^{3}s^{-1}], at $T_e\sim500$ K

$H^+\cdot(CH_3COCH_3)_2$ $\alpha = (8 \pm 2)\cdot10^{-6}$ [cm^{3}s^{-1}], at $T_e\sim400$ K

Dissociative electron attachment $CF_3Br + e^-$

Smith and Spanel
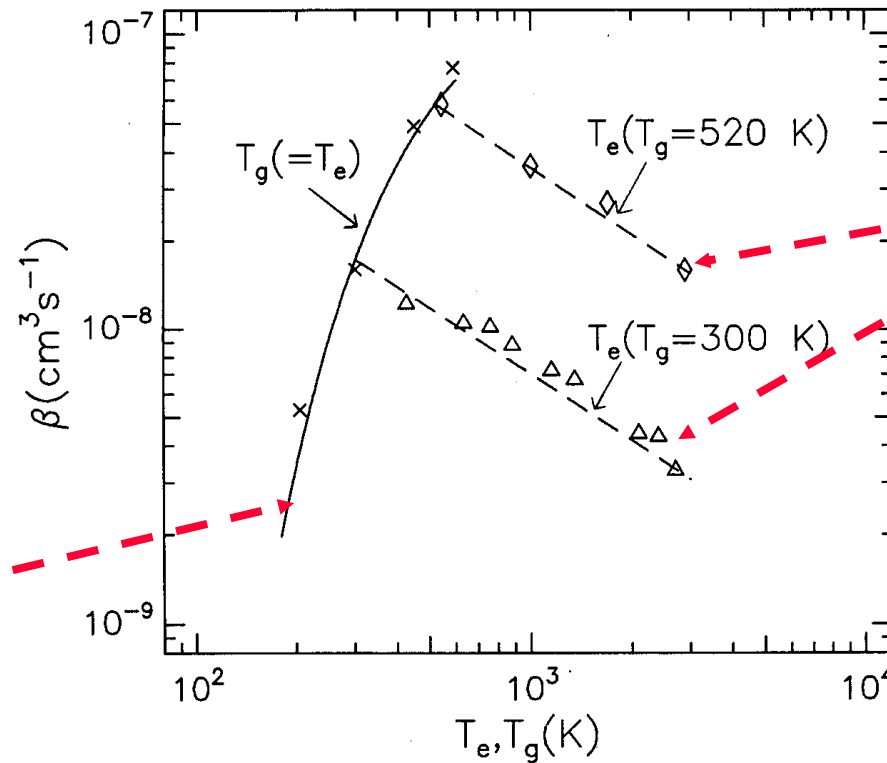
Fig. 4. Plots of the rate coefficient β for dissociative electron attachment to CF_3Br as a function of the attaching gas temperature T_g (= the carrier gas temperature) and the electron temperature T_e. The data points indicated ($\times$), i.e. the β vs. $T_g(=T_e)$ data, are from a previous FALP study carried out in helium afterglows [11]. The points indicated ($\triangle$) are for $T_g = 300$ K and those indicated ($\diamond$) are for $T_g = 520$ K; these data were obtained largely in argon afterglows (see text); (———) is described by Eq. (2) for the condition that $T_e = T_g$; (− − −) are described by the same equation but for the fixed T_g values of 300 and 520 K and for variable T_e.

T_e dependence

T_G dependence

buffer He/Ar mixture

CRESU

The CRESU technique at Rennes

Carrier gas (He, Ar or N_2) + reactants

Kinetics of Reaction in Supersonic Uniform Flows (CRESU)

T_{res}

$$c_p T_0 = c_p T + \tfrac{1}{2} u^2$$

Laval nozzle

$T_{=cte}$

Vacuum chamber

Throat diameter
3 mm – 5 cm

Supersonic uniform flow
$T = 15 - 220$ K
$n = 10^{16} - 10^{18}$ cm^{-3}
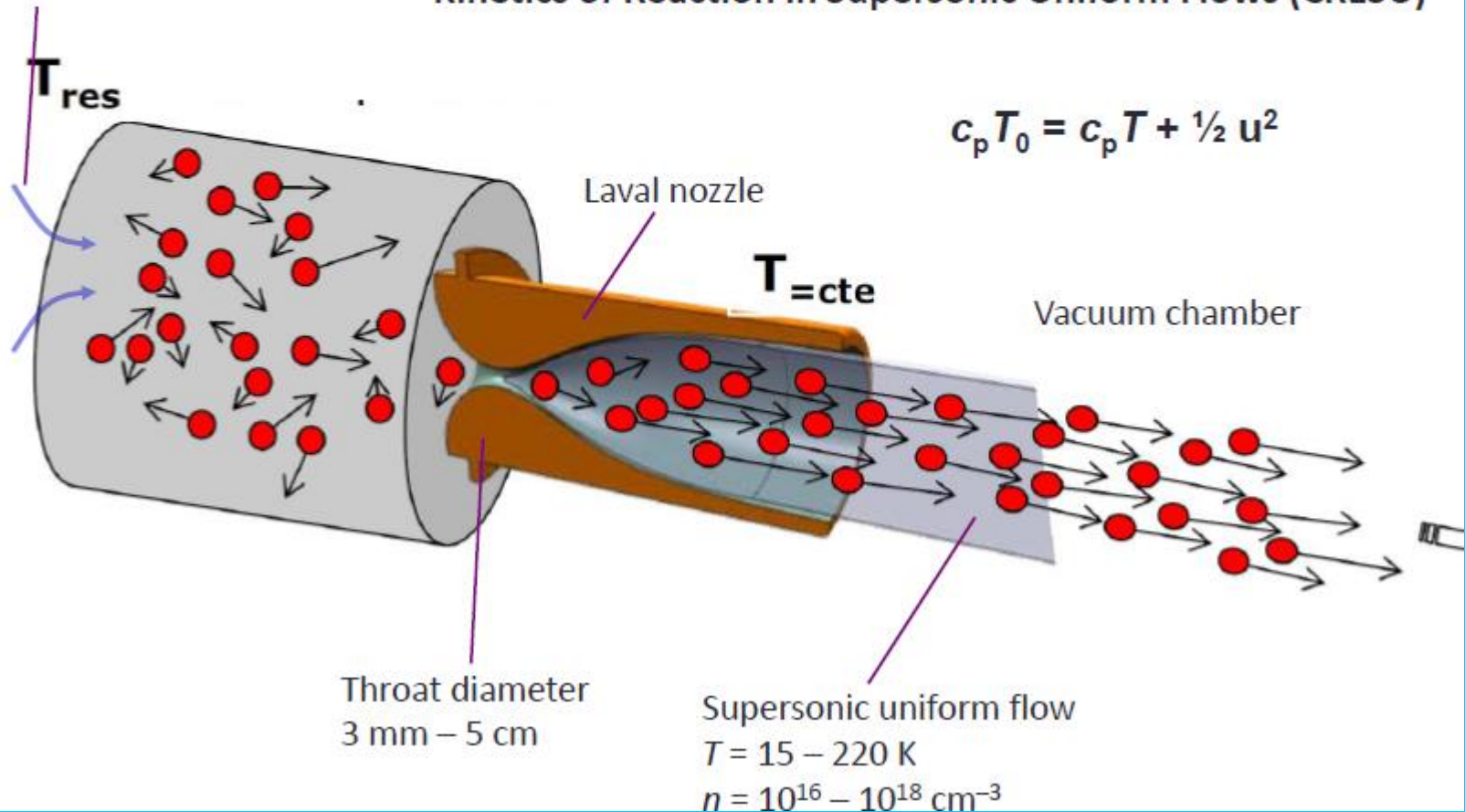
Kinetics of anion-molecule reactions at low temperature

Electron gun
(200 µA, 12.5 kV)

moveable reservoir

moveable quadrupole mass filter

Laval nozzl

10^9 e/cm^3

P_0

P_{res}

e

P_s

P_{ch}

He buffer gas

20 cm

He – BrCN mixture   He – HC$_3$N mixture
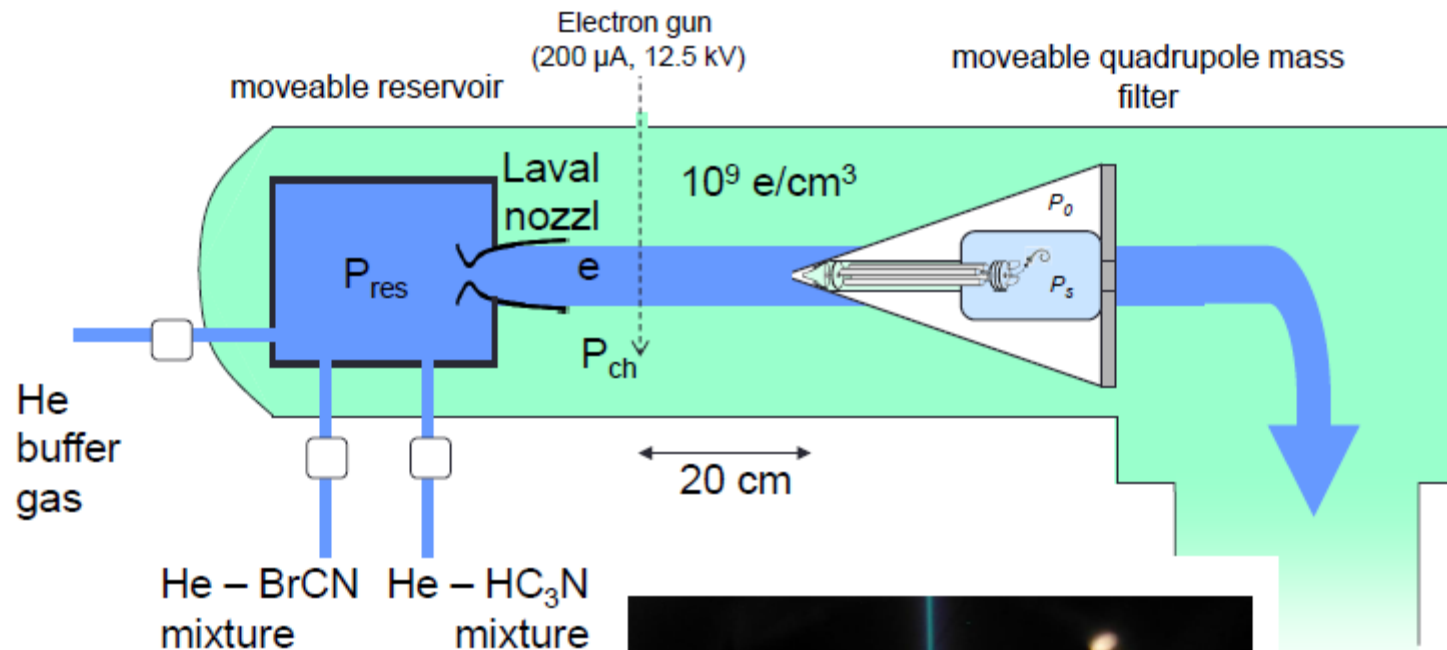
- CN$^-$ + HC$_3$N (L. Biennier, S. Carles, J-C Guillemin et al. Icarus, 227, 123, 2014)

- C$_3$N$^-$ + HC$_3$N (in progress)

- Collaboration with C. Alcaraz and co-workers (Orsay and Prague)
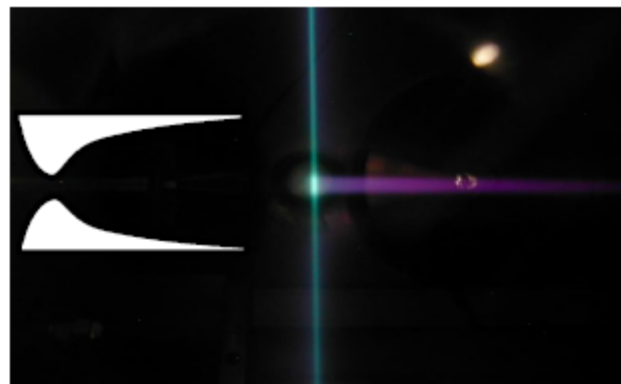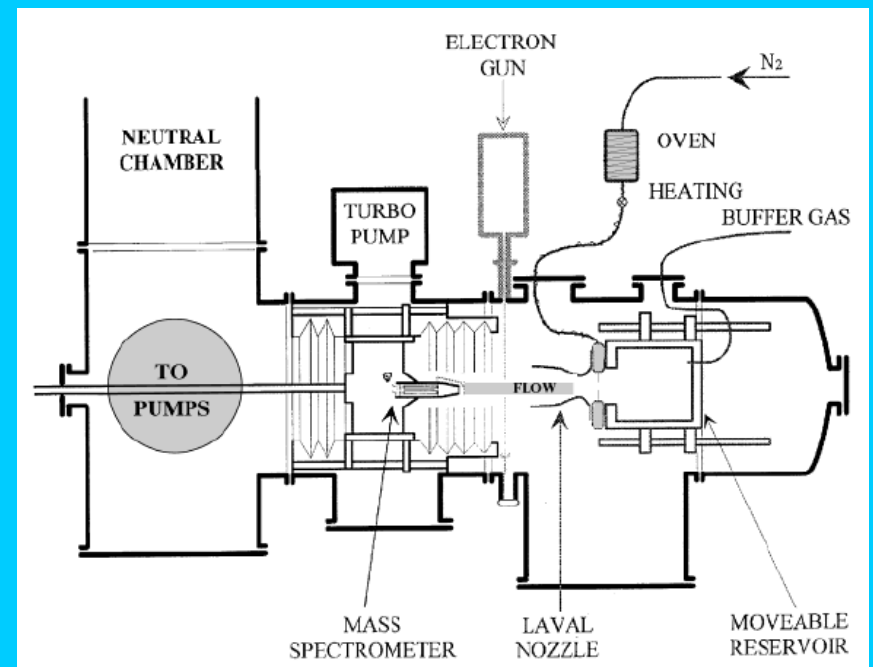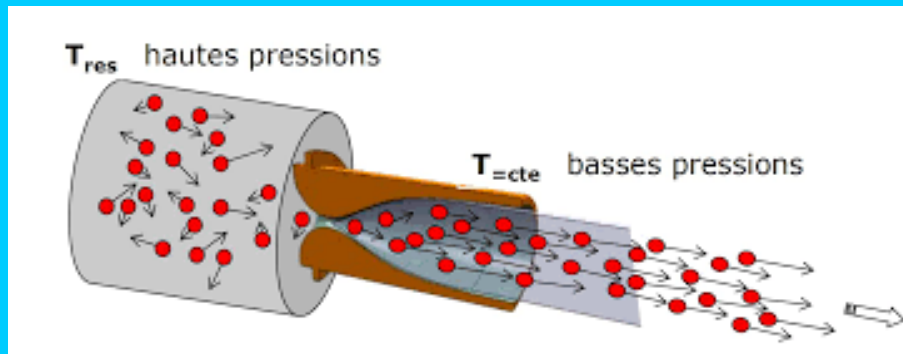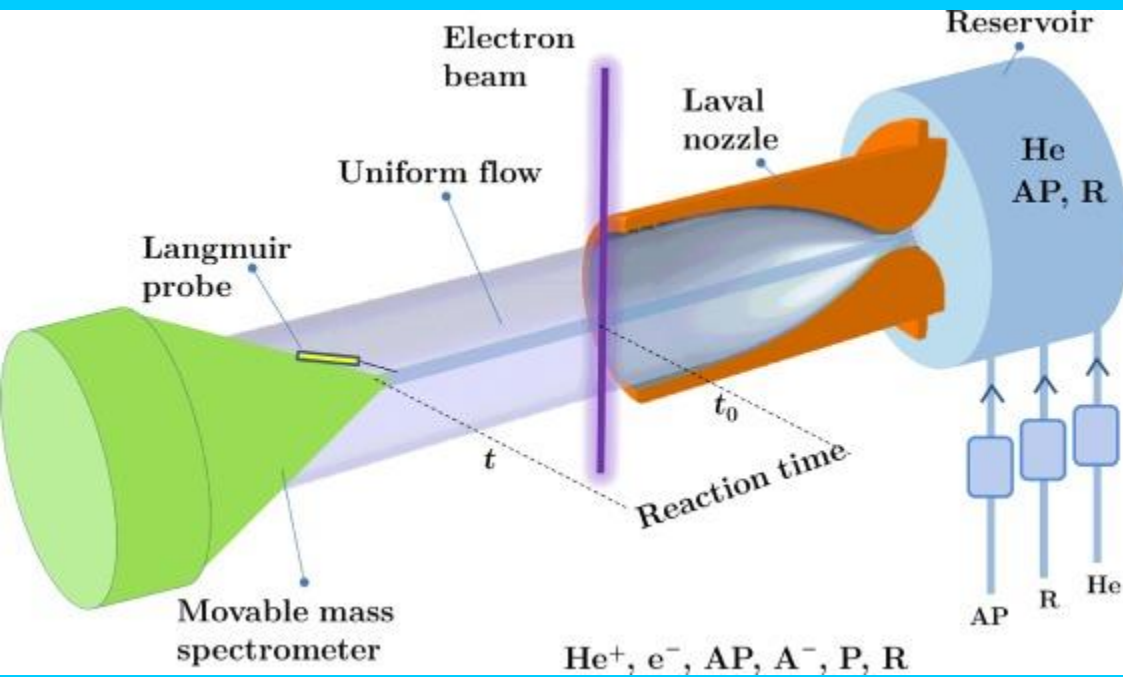
astro

Electron beam

Uniform flow

Langmuir probe

Laval nozzle

Reservoir

He
AP, R

t_0

Reaction time

t

Movable mass spectrometer

AP   R   He

He^+, e^-, AP, A^-, P, R

T_{res} hautes pressions

$T_{=cte}$ basses pressions

ELECTRON GUN

N_2

NEUTRAL CHAMBER

TURBO PUMP

OVEN

HEATING

BUFFER GAS

TO PUMPS

FLOW

MASS SPECTROMETER

LAVAL NOZZLE

MOVEABLE RESERVOIR

Outlook: Electron-beam collision studies

Electron capture and dissociation
Dissociative recombination

ABC^+

Fast (stored) molecular ion beam

e

T_{env}

T_e

Fragment detectors

C

AB
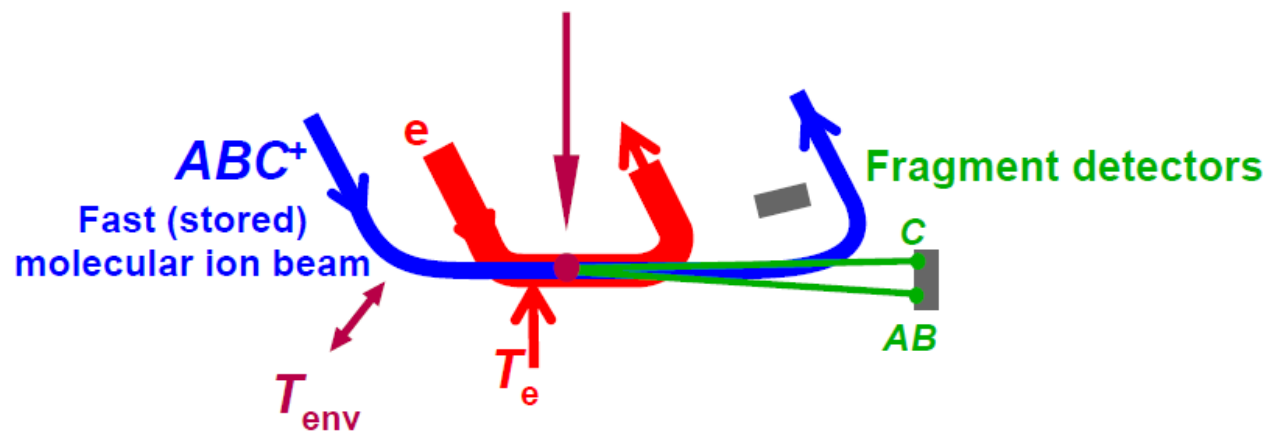
$$E_{coll} = \tfrac{1}{2}\, m_e\, (v_e - v_i)^2$$

can be scanned from ~ 1 meV … 50 eV

Experiments

PLASMA experiments SA and FA   - multi collisions $\{\alpha(T)\}$

Crossed beam experiments   - single collisions $\{\sigma(v_r)\}$

Marched beam, Storage rings - TSR, Cryring, Astrid   - single collisions $\{\sigma(v_r)\}$

$$\mathbf{H_3^+ + e^- \rightarrow H,\ H_2}$$
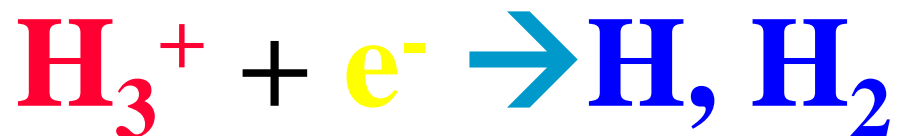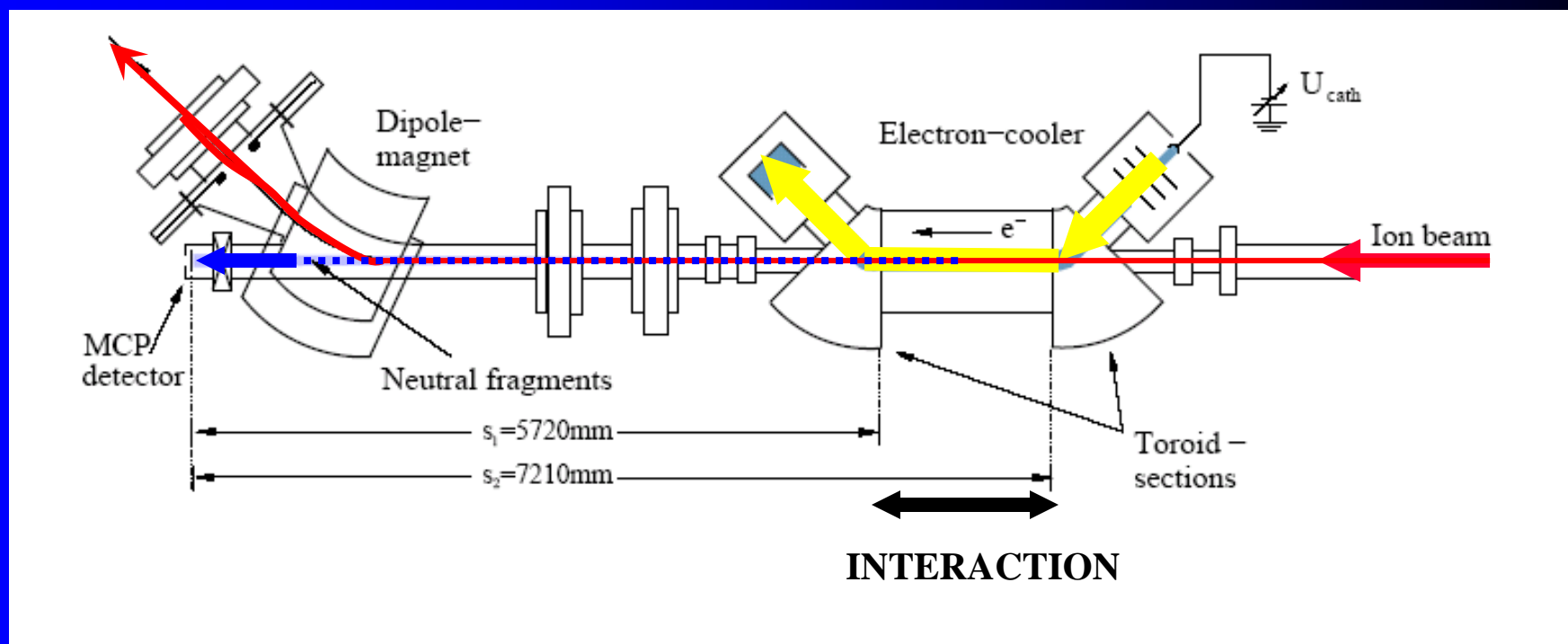
Electron-cold molecular ion reaction: Dissociative Recombination

Merged Beam Kinematics

Electrons E_e, m_e

Ions E_i, m_i
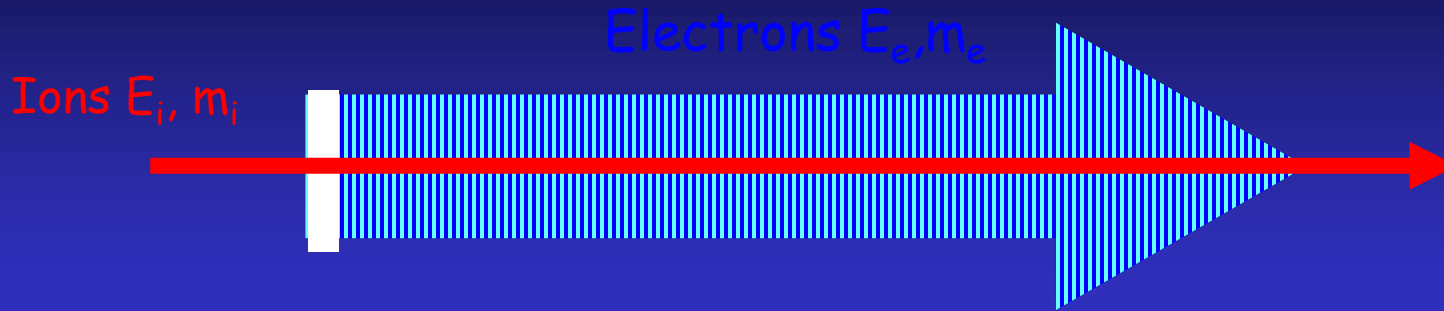
$$E_{cm} = \frac{1}{2} m_e v_{cm}^2 \approx \left[\sqrt{\frac{m_e}{m_i}} E_i - \sqrt{E_e} \right]^2$$

Center of mass resolution:

$$\Delta E_{cm} = \left\{ \left[\left(1 - \frac{v_e}{v_i}\right) \frac{m_e}{m_i} \Delta E_i \right]^2 + \left[\left(1 - \frac{v_i}{v_e}\right) \Delta E_e \right]^2 \right\}^{1/2}$$

~ meV resolution for zero relative kinetic energy!

TSR electron target

Neutral atom detectors

Ion detectors

Electron source
Cryogenic (77 K) photocathode
or
thermal emission (1300 K)

Cathode magnetic field up to 4 T (magnetic expansion up to 100)

Adiabatic acceleration
($\Gamma_{e\parallel} \rightarrow \sim 10$)

Electron temperature lower limits:
longitudinal ~ 0.1 K (0.01 meV)
transverse ~ 1 K (0.1 meV)

Electron energy: up to 20 keV
Interaction energy: up to 40 keV (counterpropagating operation)

Stored ion beam

Reality - TSR (MPIK Heidelberg)

Injection of INTERNALY COLD H$_3^+$ IONS(12-50K) with kinetic energy 1-2 MeV

TSR

electron cooler

neutral fragment detector

chopper

collimators

D: dipole magnet
Q: quadrupole magnet

0 1 2 3 4 5 m
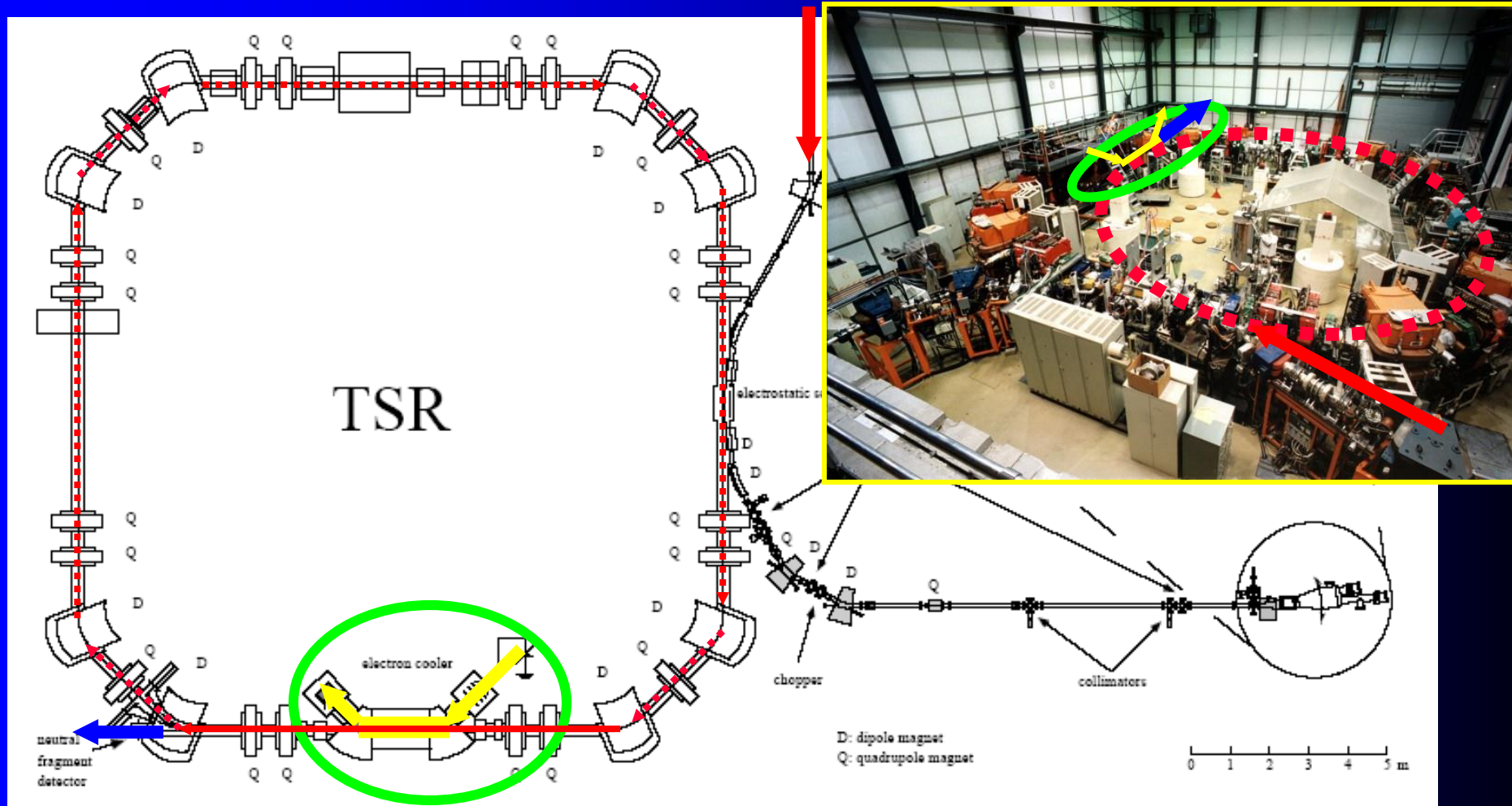
Detection of neutrals

INTERACTION at meV collision energies

Detection of H$_3^+$(v,j)

Recombination

TSR (MPIK Heidelberg)

Dipole–magnet

Electron–cooler

U_{ca}

e^-

Ion beam

MCP detector

Neutral fragments

$s_1=5720mm$

$s_2=7210mm$

Toroid – sections

INTERACTION
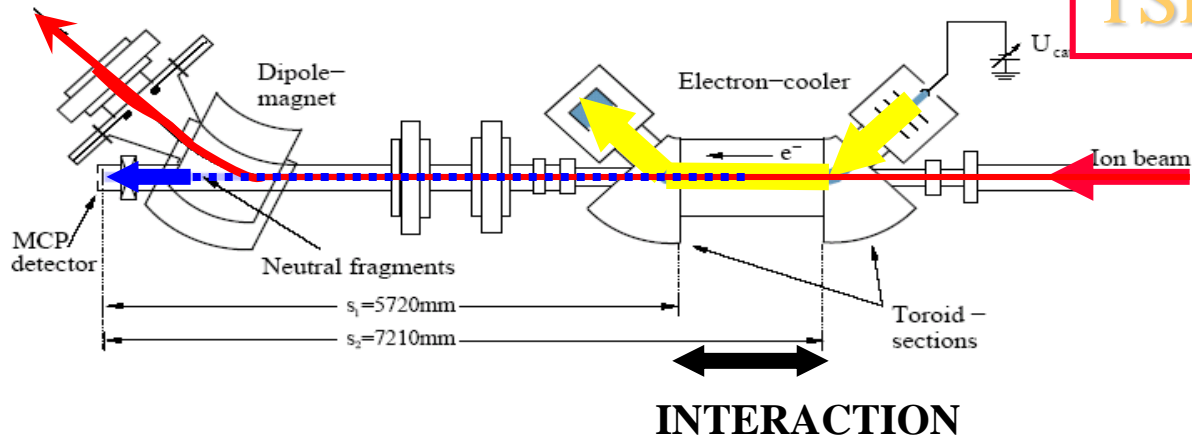
Kumulativní prstenec
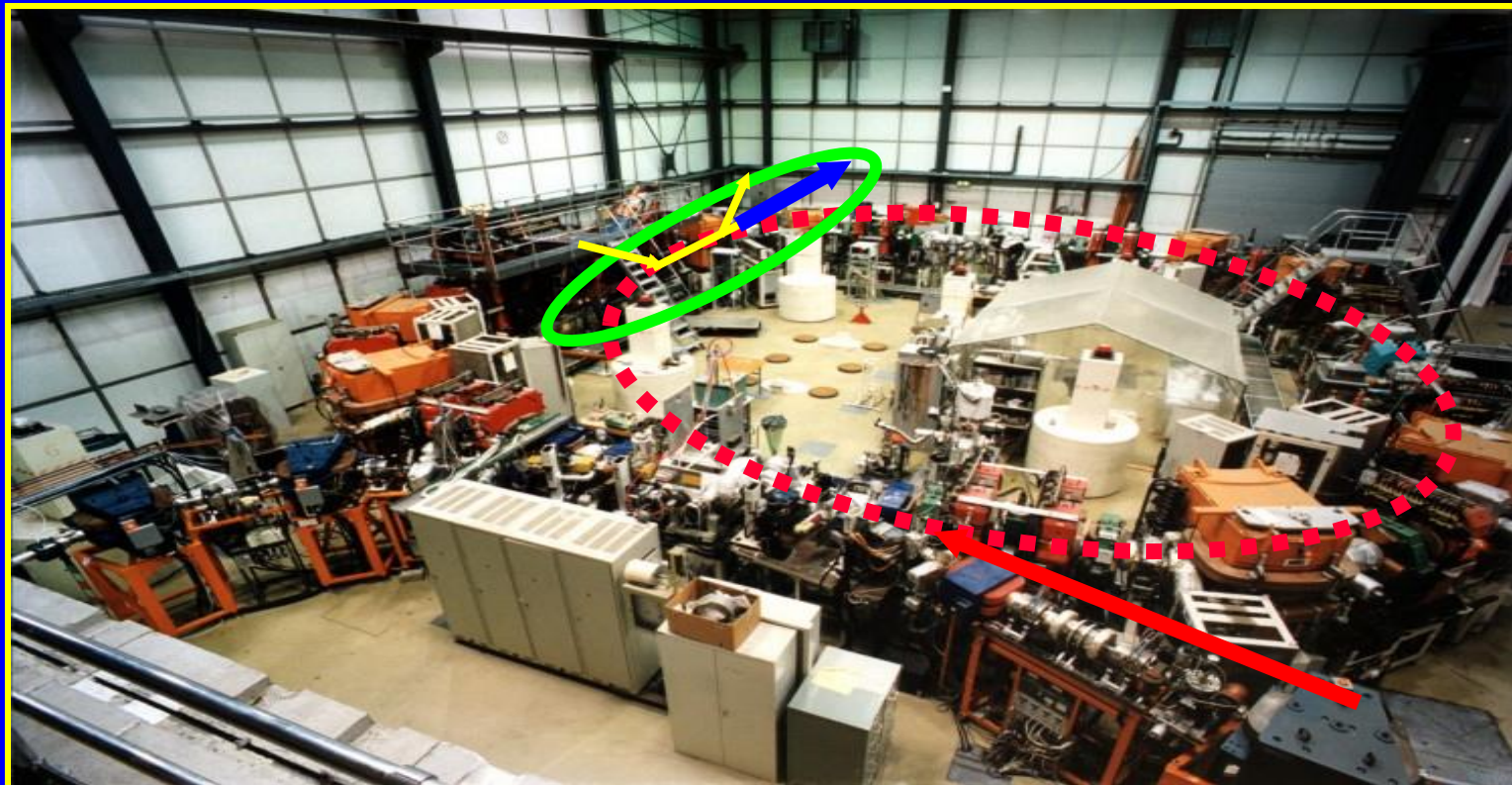
Ion storage rings

TSR, Heidelberg

H_2^+, HD^+, D ,
H_3^+, H_2D^+, D_2H^+, D_3^+,
He_2^+,
LiH_2^-, ...

Mass limit
RFQ: q/A ≤ 9

Post Accelerator
~ 25 MV

~ 10 MV

High current injector
Linac   RFQ

TSR

15 m

Bρ=1.5 Tm

Pressure ~ 3·10^{-11} mbar

10 m
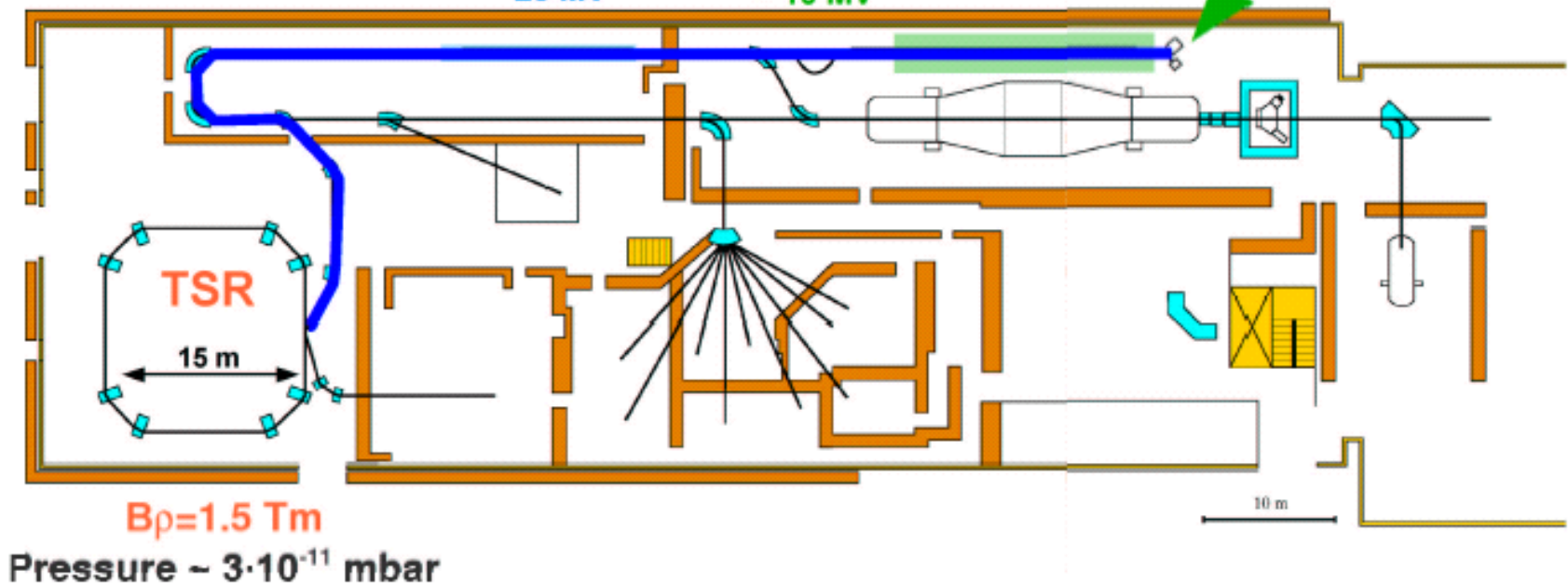
Ion storage rings

Ion storage rings

Mean storage lifetimes of molecular ions in the TSR
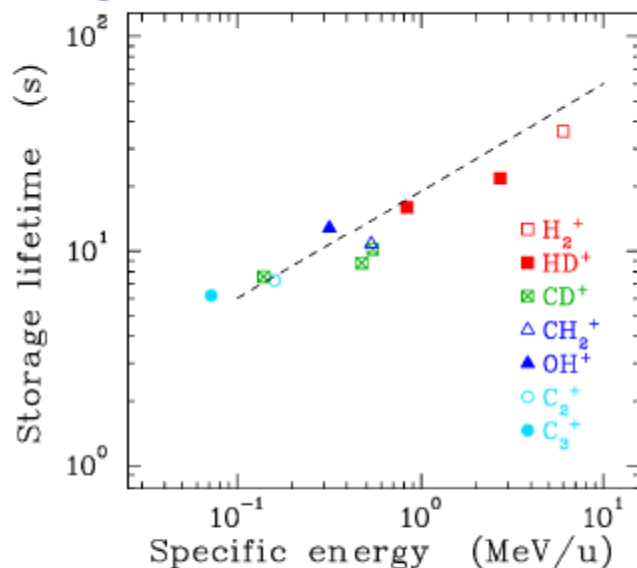
DR with electrons can reduce the beam lifetime !

Legend:
- H_2^+
- HD^+
- CD^+
- CH_2^+
- OH^+
- C_2^+
- C_3^+

Axes:
- Storage lifetime (s)
- Specific energy (MeV/u)

Internal cooling

Asymmetrical molecules: Cooling by spontaneous electric dipole radiation (typ. ~0.1 sec for vibration, ~1-10 sec for rotation) Thermal equilibrium with blackbody radiation (300 K)

Symmetrical molecules: No significant cooling by radiation
Internal cooling by electrons (present electron temperature ~ 20 ... 200 K)

TSR instrumentation

Storage ring instrumentation

Charles University Prague
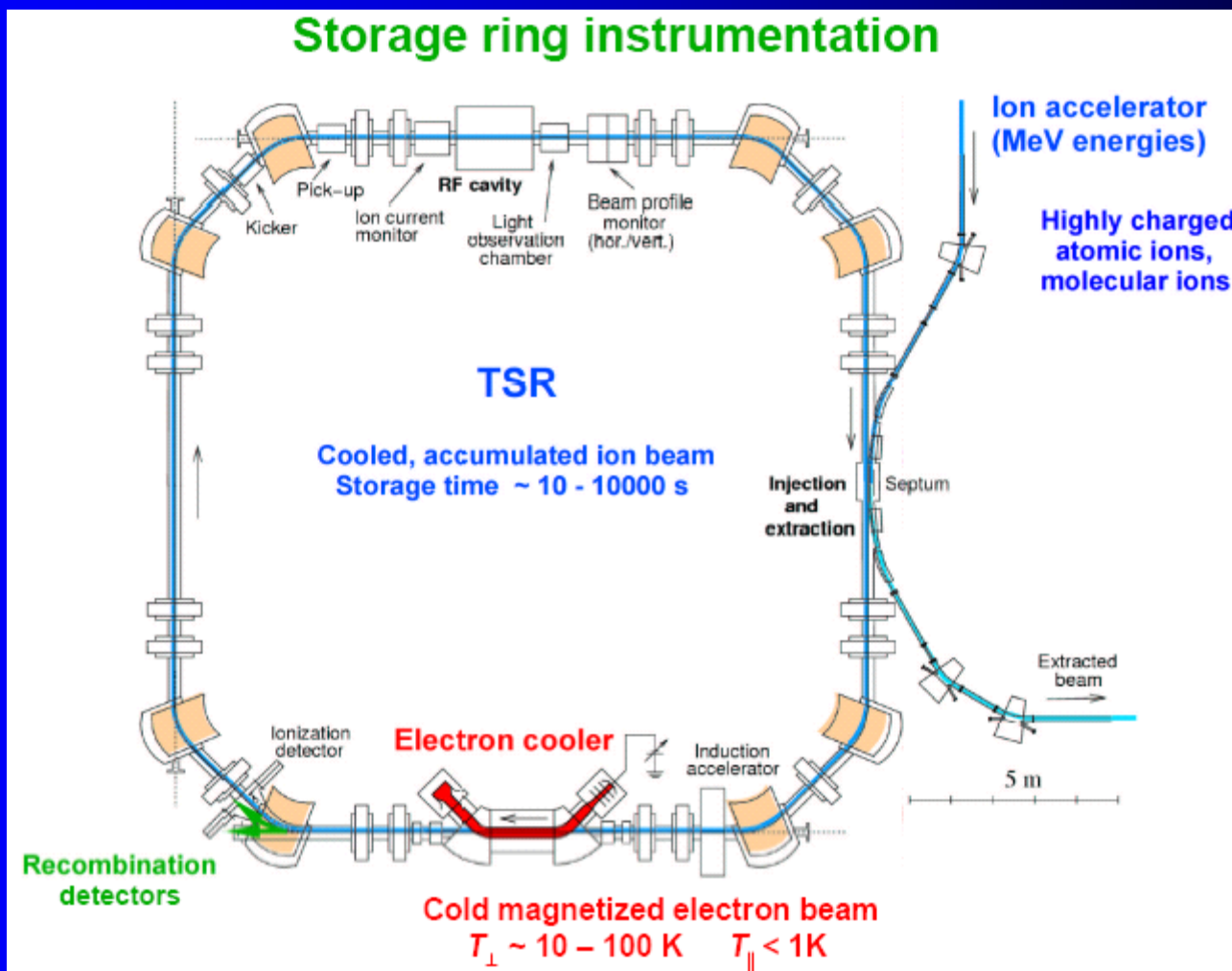
Electron cooling

Electron cooling

Electron velocity distribution
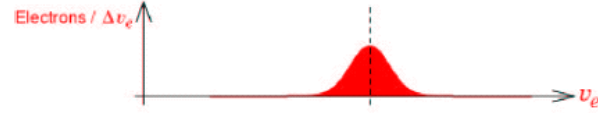
Friction force
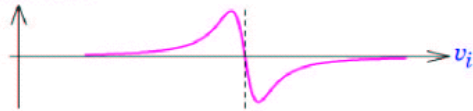
Ion velocity distribution

~1 sec
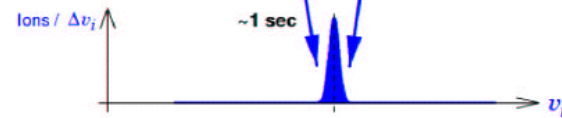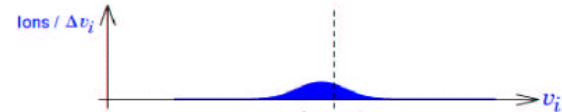
Electron cooling

Correlated 2-hit events on imaging detector

D_2^+ 1.9 MeV (TSR)

10 mm

$E_k [v,n]$
$\Downarrow$
D_{max}
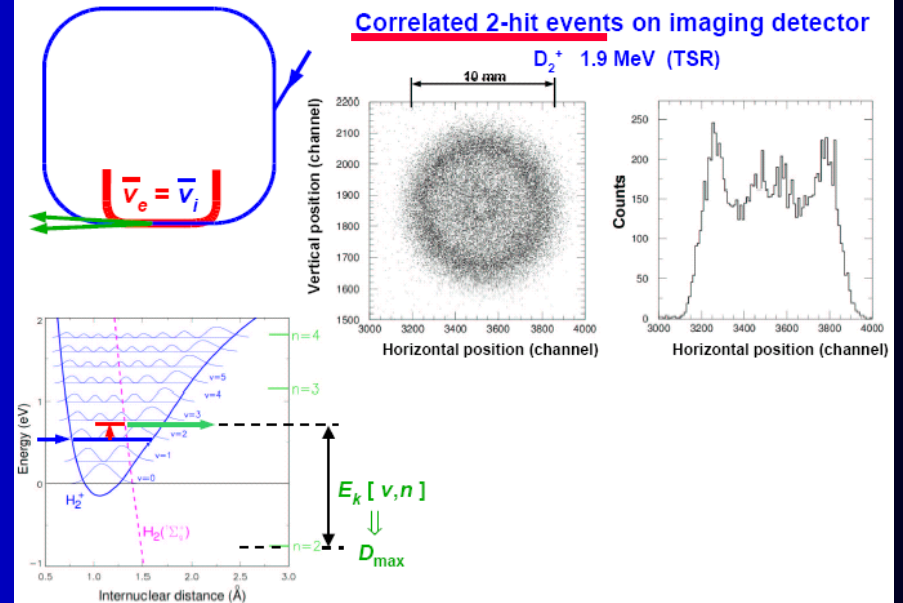
Electron cooling

Fragment center-of-mass impact position

D_2^+ 1.9 MeV (TSR)

2 mm

0-1 s   1- 2 s   2- 3 s

2 mm

3- 4 s   4- 5 s   5- 6 s

$n_e = 5.5 \times 10^6$ cm^{-3}
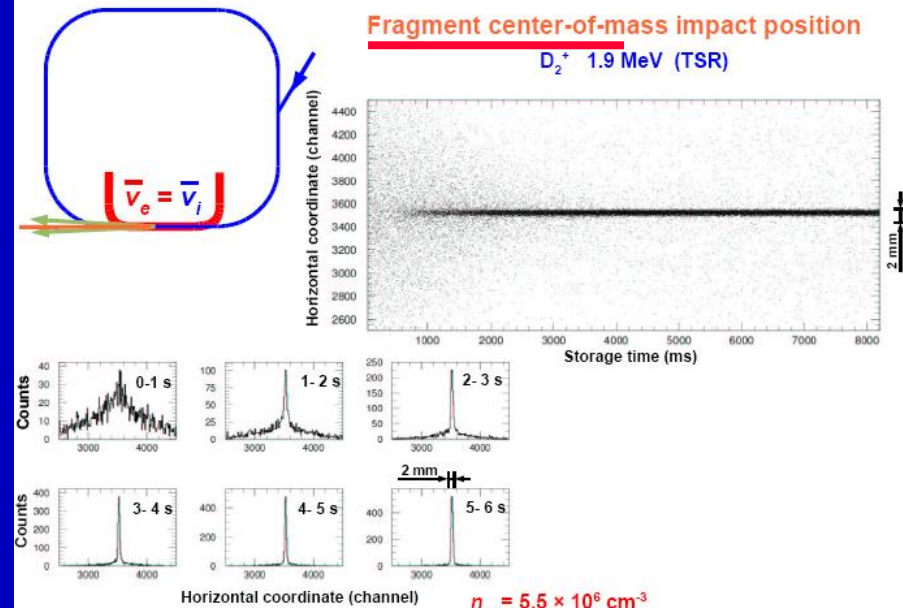
State diagnostics

State diagnostics methods at the TSR
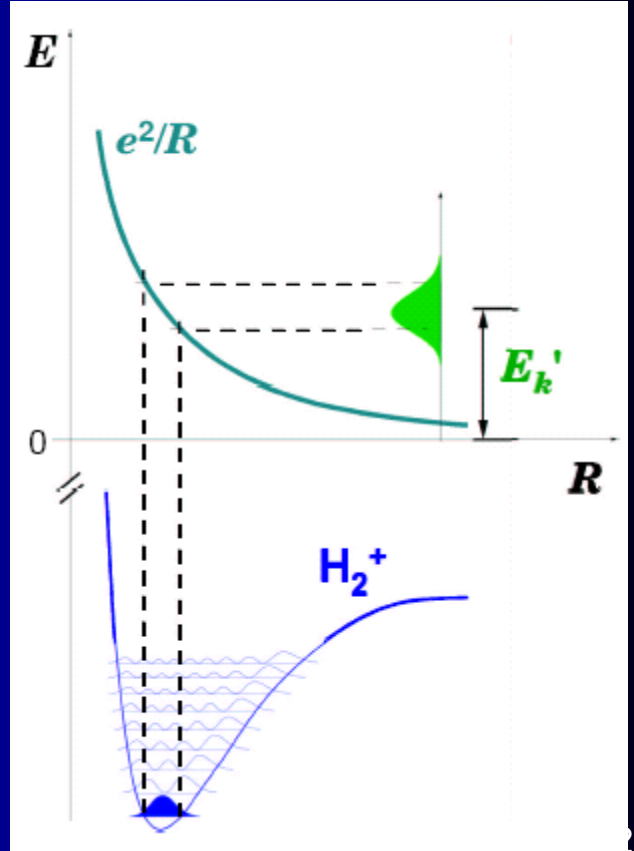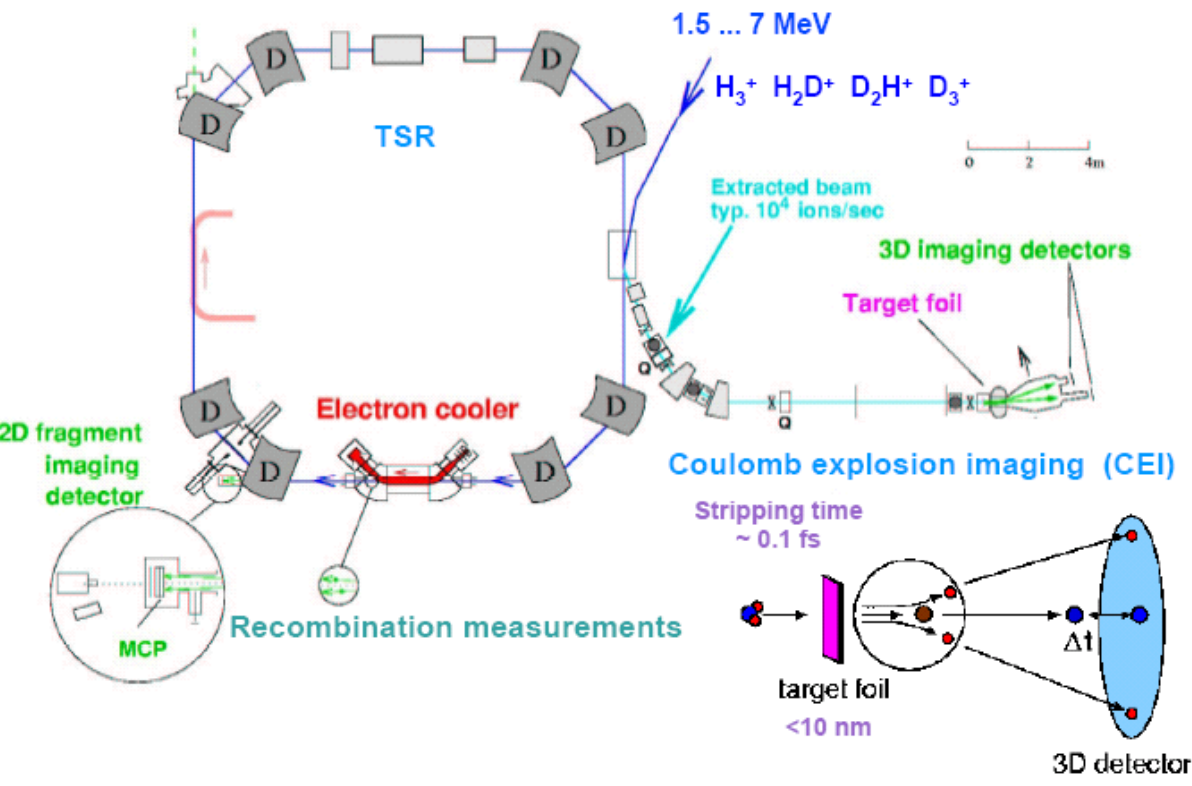
Recombination H_2^+
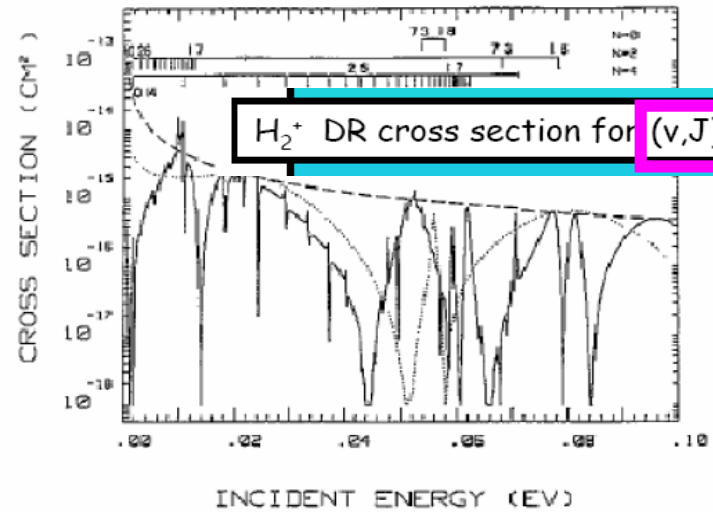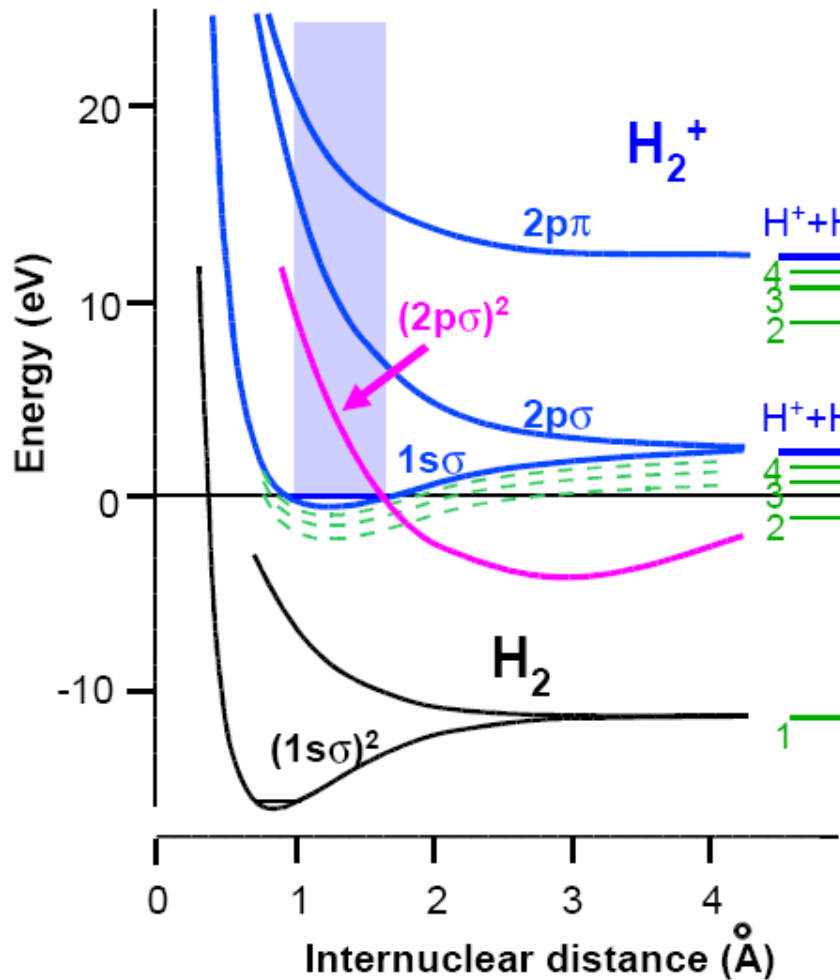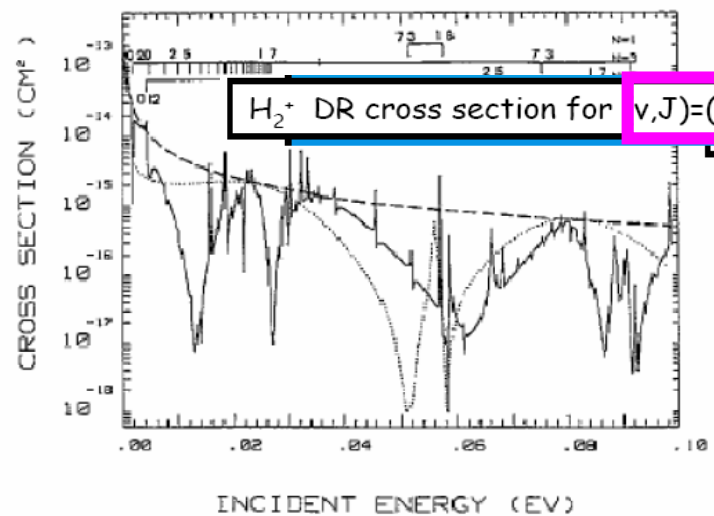
Electron collisions with H_2^+

H. Takagi, J. Phys. B, 26, 4815 (1993)

H_2^+ DR cross section for (v,J)=(0,0)

H_2^+ DR cross section for (v,J)=(0,1)

Thanks for your attention!

CSR team

A. Becker	C. Krantz	S. Saurabh
K. Blaum	H. Kreckel	S. Schippers
C. Breitenfeldt	S. Kumar S.	C. D. Schröter
F. Fellenberger	M. Lange	D. Schwalm
S. George	J. Lion	L. Schweikhard
J. Göck	S. Lohmann	K. Spruck
M. Grieser	C. Meyer	X. Urbain
F. Grussie	P. M. Mishra	S. Vogel
R. von Hahn	O. Novotný	A. Wolf
P. Herwig	P. O'Connor	D. Zajfman
J. Karthein	R. Repnow	

מכון ויצמן למדע
WEIZMANN INSTITUTE OF SCIENCE

JUSTUS-LIEBIG-
UNIVERSITÄT
GIESSEN

UNIVERSITAS CATHOLICA LOVANIENSIS
SEDES SAPIENTIAE
1425

31

The CSR – overview

- circumference: **35 m**
- beam energy: **20 keV × q ...** **300 keV × q**
- temperature: **10 ... 300 K**
- res. gas press. (@ < 10 K): **10⁻¹⁴ mbar** ($\sim$ 100 cm⁻³)

- Beam profile monitors (3x)
- Current pickup
- Schottky pickup
- Position pickups (6x)

... with electron cooling
m/q range: **1 ... 160 u/e** (@ 300 kV)

Electrostatic ion optics (mass independent)

Fully cryogenic (10 K) beam line

Full set of diagnostic tools

Electron cooler phase space cooling up to 160 u/e

1 m

R. v. Hahn
M. Grieser
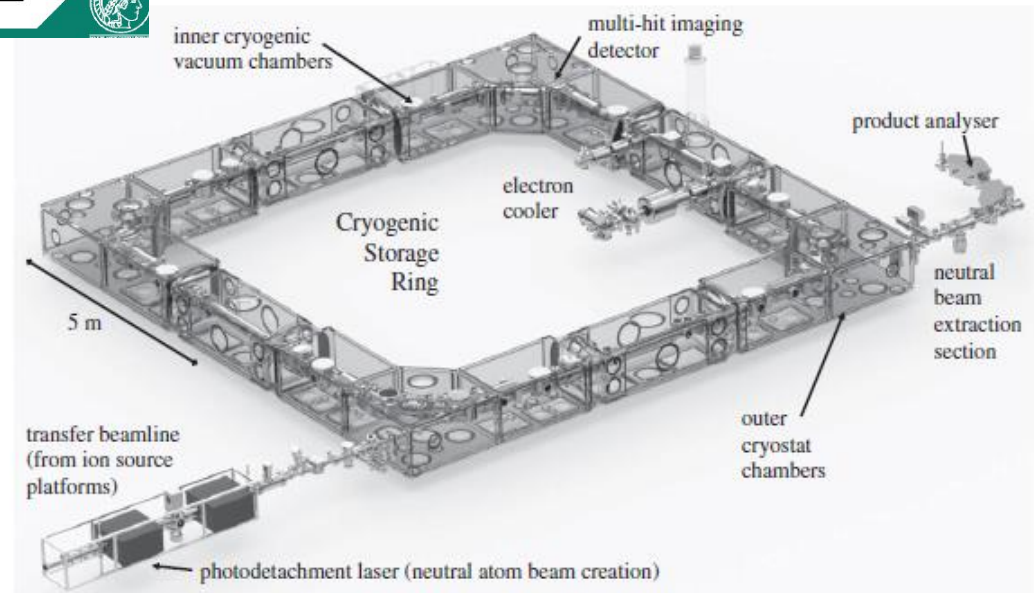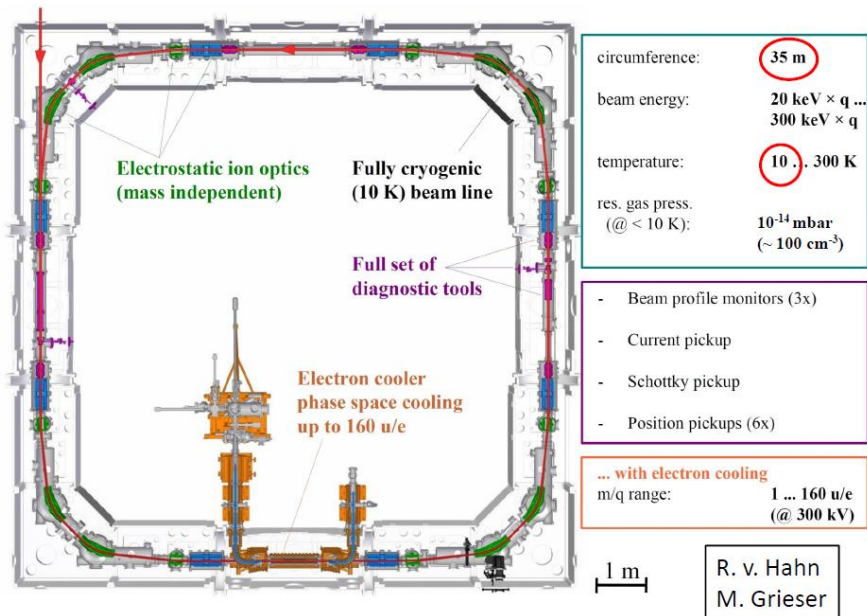
Figure 1. Overview of the CSR. The experimental set-ups relevant for astrochemical studies are labelled in the insets. The image includes the new low-energy electron cooler as well as the photodetachment section for the neutral beam creation in the injection beamline, the neutral beam extraction and some of the corresponding detector units.

The CSR – overview

circumference:	**35 m**
beam energy:	20 keV × q ... 300 keV × q
temperature:	**10 ... 300 K**
res. gas press. (@ < 10 K):	10^{-14} mbar (~ 100 cm^{-3})

- Beam profile monitors (3x)
- Current pickup
- Schottky pickup
- Position pickups (6x)

... with electron cooling
m/q range: 1 ... 160 u/e
(@ 300 kV)

Electrostatic ion optics (mass independent)

Fully cryogenic (10 K) beam line

Full set of diagnostic tools

Electron cooler phase space cooling up to 160 u/e

1 m

R. v. Hahn
M. Grieser

First cooldown
April 2015

6 K

astro

The CSR – storage lifetime

$$Ag_2^- \; (60 \text{ keV}) + \gamma \; (1.9 \text{ eV}) \rightarrow Ag_2 + e^-$$

$$\Rightarrow T_{CSR} = 2717(81) \text{ s}$$

18000 s = 5 h

EA (Ag_2^-) = 1.02 eV

$h\nu$

Ag2-

Ag2
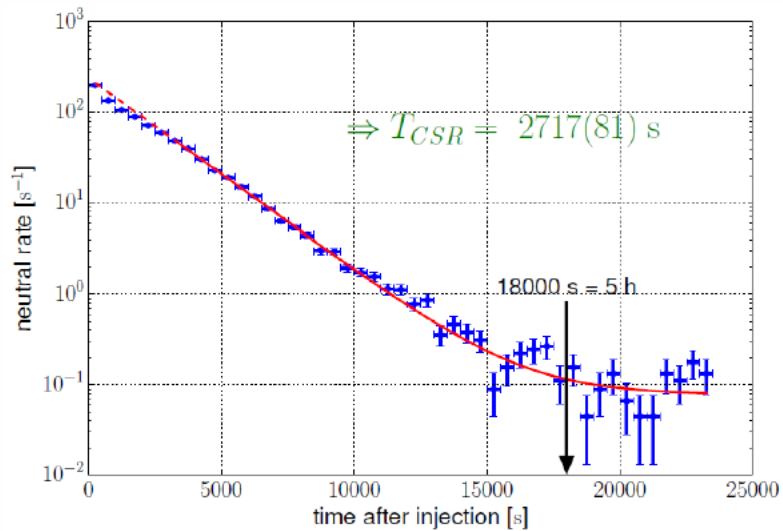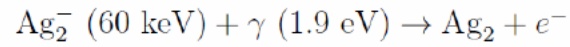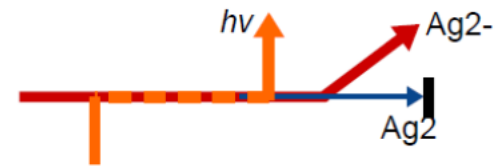
von Hahn et al.,
Rev. Sci. Instr. 87 (2016) 063115

A set-up for ion–atom collisions at the Cryogenic Storage Ring

$$H_3^+ + C \longrightarrow CH^+ + H_2, \quad H_3^+ + O \longrightarrow OH^+ + H_2$$
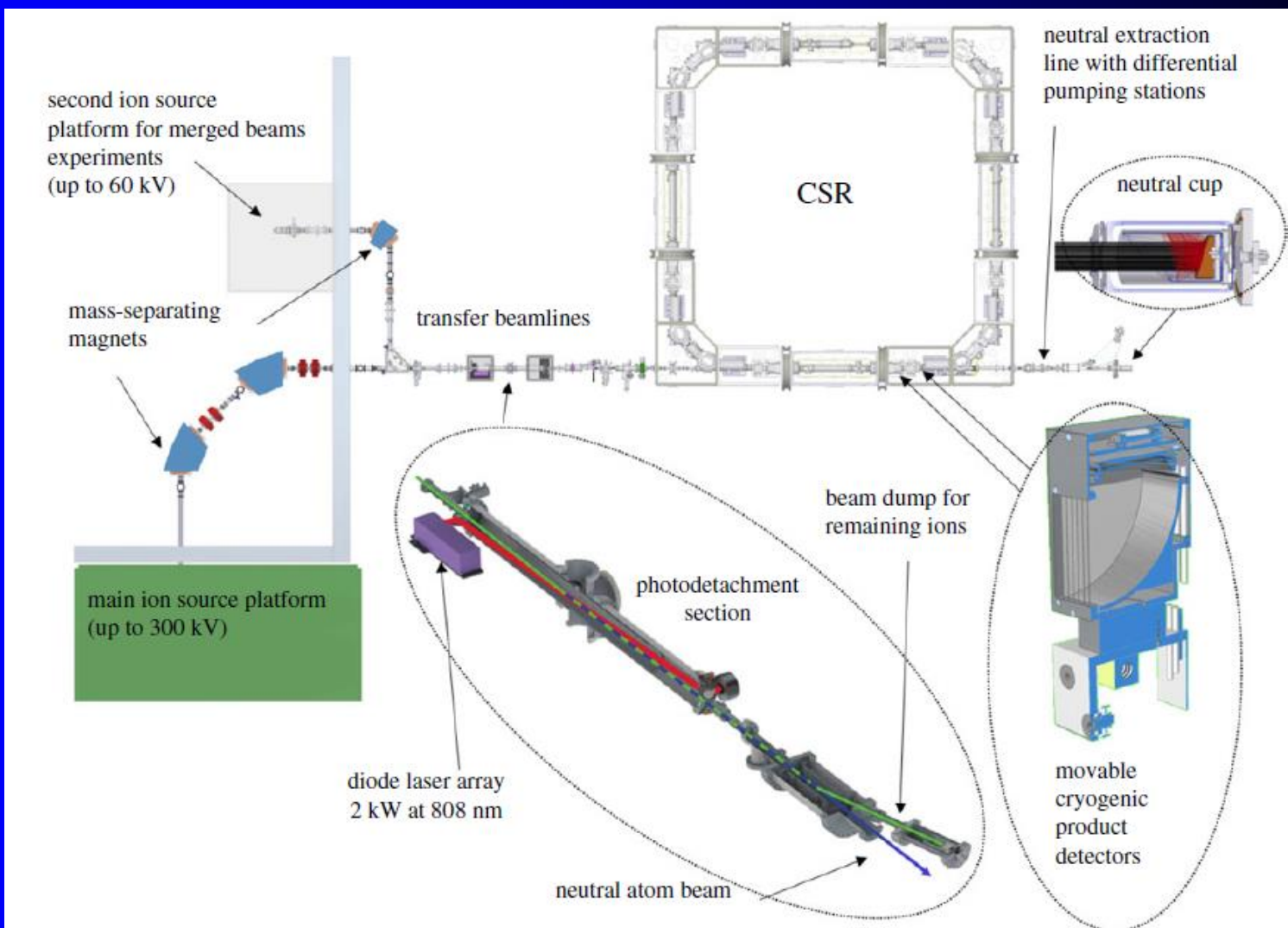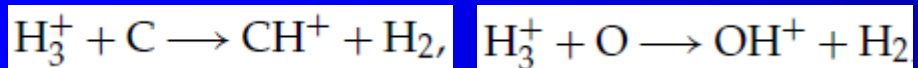
Figure 4. Overview of the CSR facility and the peripheral infrastructure for the ion–atom collision experiments.

astro
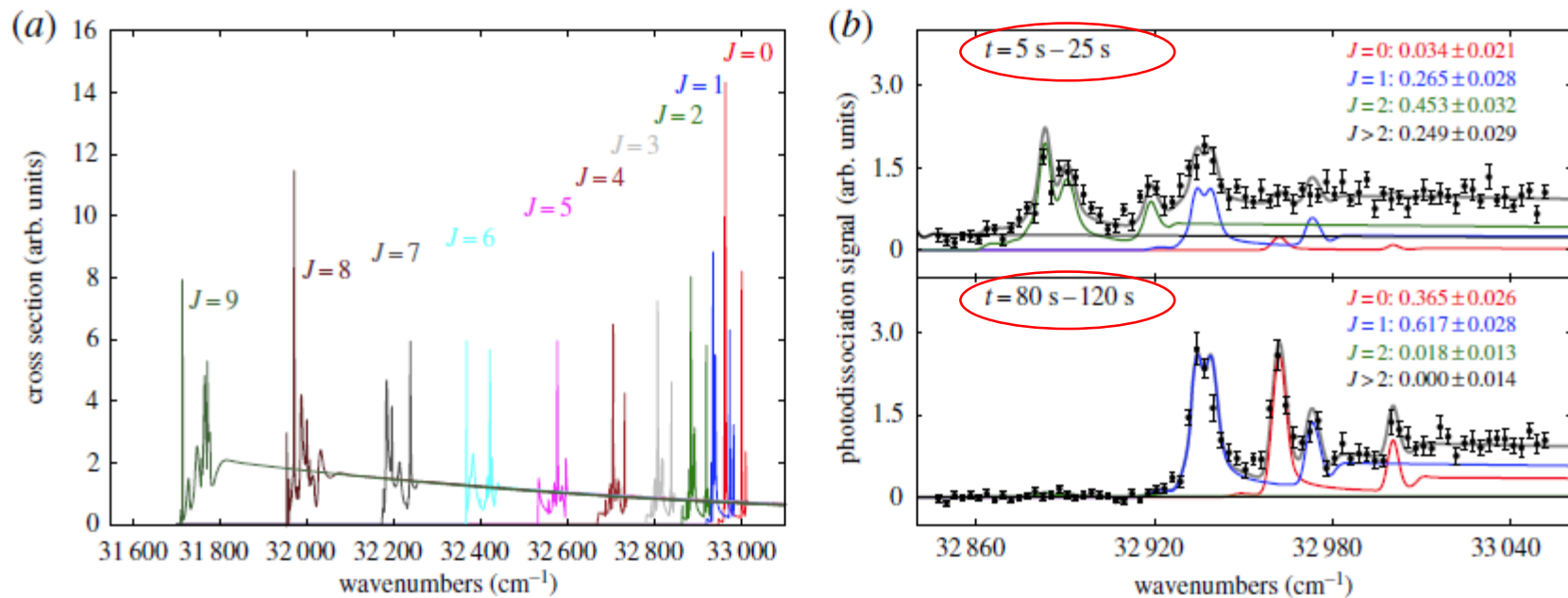
Figure 3. (a) Calculated Feshbach resonances for the photodissociation of CH^+ for rotational states $J = 0-9$. The window of resonances shifts with the rotational quantum number of the initial state. For the lowest rotational states ($J = 0-2$), some of the resonances overlap. This is the area of interest to monitor the rotational cooling inside the CSR. (b) Photodissociation spectrum of CH^+ measured for two different storage time intervals inside the CSR. The resonances can be fitted and assigned to individual rotational states. The resulting state populations are given in the insets.

Outlook: Electron-beam collision studies

Electron capture and dissociation
Dissociative recombination

ABC^+
Fast (stored)
molecular ion beam

T_{env} T_e

e

Fragment detectors

C

AB

$$E_{coll} = \tfrac{1}{2} m_e (v_e - v_i)^2$$

can be scanned from ~ 1 meV ... 50 eV

photocathode electron
source

room-temperature
sections

collector

cryogenic merged beams section with superconducting magnets
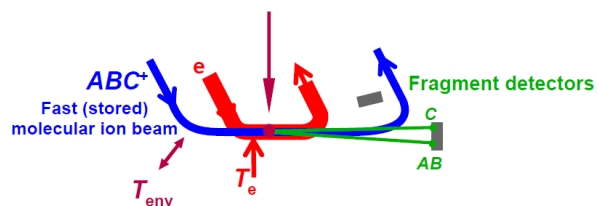
position-sensitive
multi-hit detector
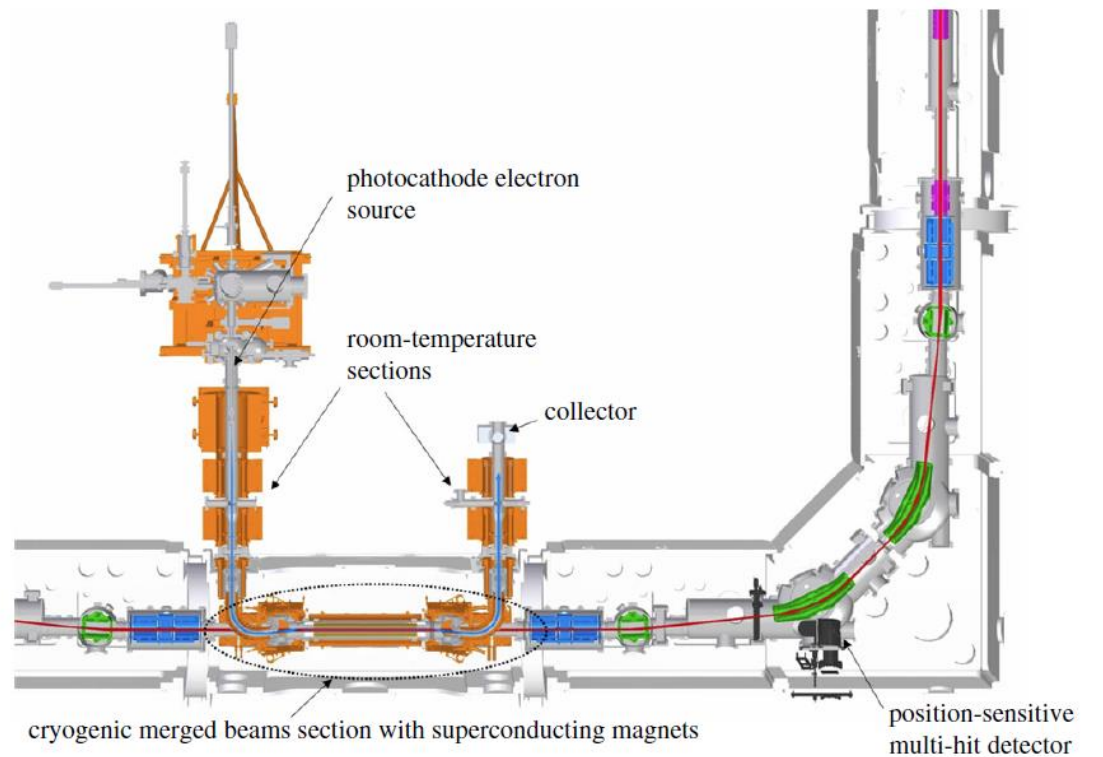
Figure 5. Detail of the straight section of the CSR that houses the low-energy electron cooler and the corresponding position-sensitive, multi-hit counting detector.

The CSR electron cooler

High Temp. Superconductors in cryogenic region

toroidal solenoid

ion beam

merging coils

room temperature copper solenoids

electron beam

interaction solenoid

B=125 G

ion beam correction coils

B=250 G

B=2.5 kG

second expansion (α ~ 2)

first expansion (α ~ 10)

interaction region (length ~ 0.8m)

photoelectron gun

electron collector

ion beam correction coils
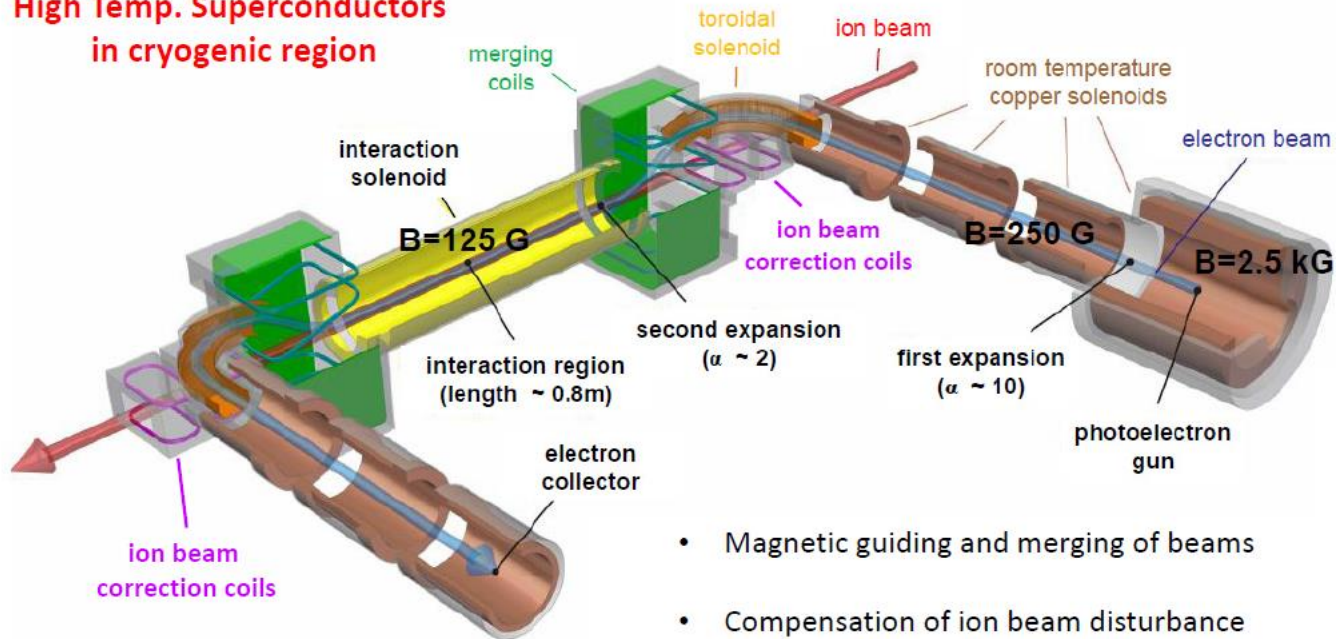
- Magnetic guiding and merging of beams
- Compensation of ion beam disturbance
- Variable electron energy (drift tube)
- Beam diagnostics (two wire scanners)

astro

The CSR electron cooler

ions

electrons

interaction region

electron collector
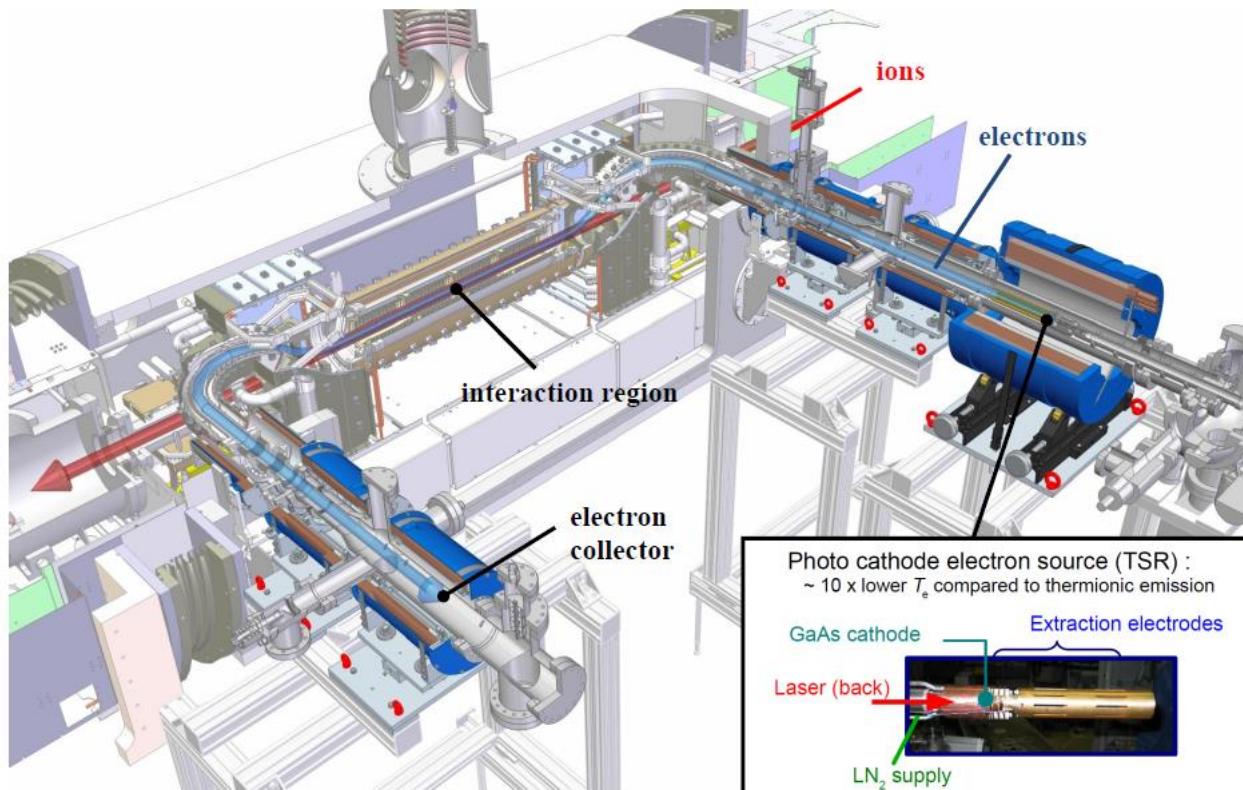
Photo cathode electron source (TSR) :
~ 10 x lower T_e compared to thermionic emission

GaAs cathode

Extraction electrodes

Laser (back)

LN_2 supply

astro
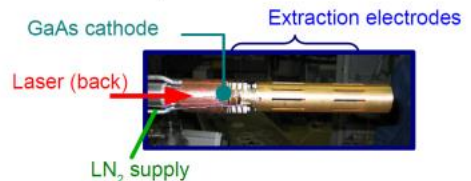
The CSR electron cooler
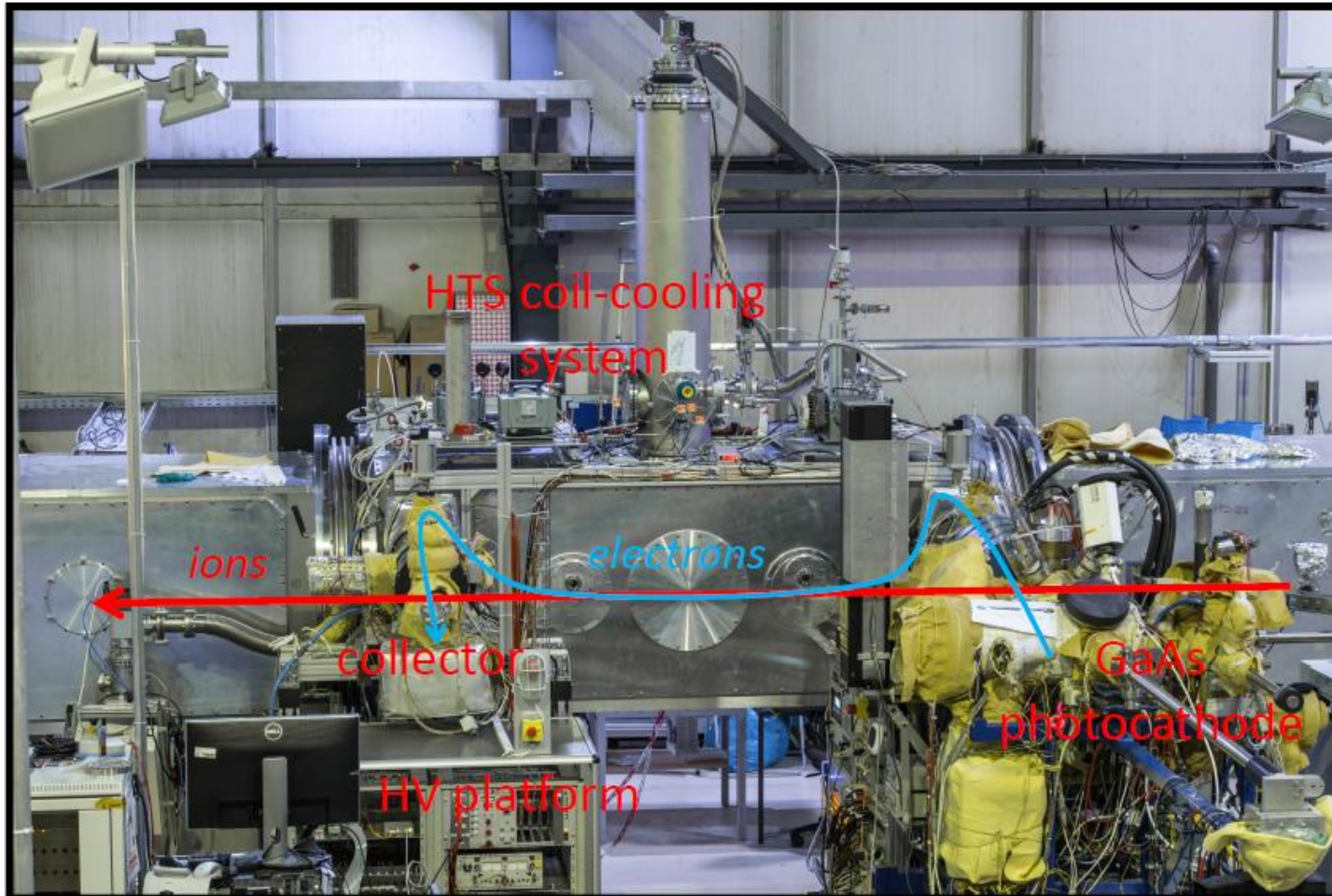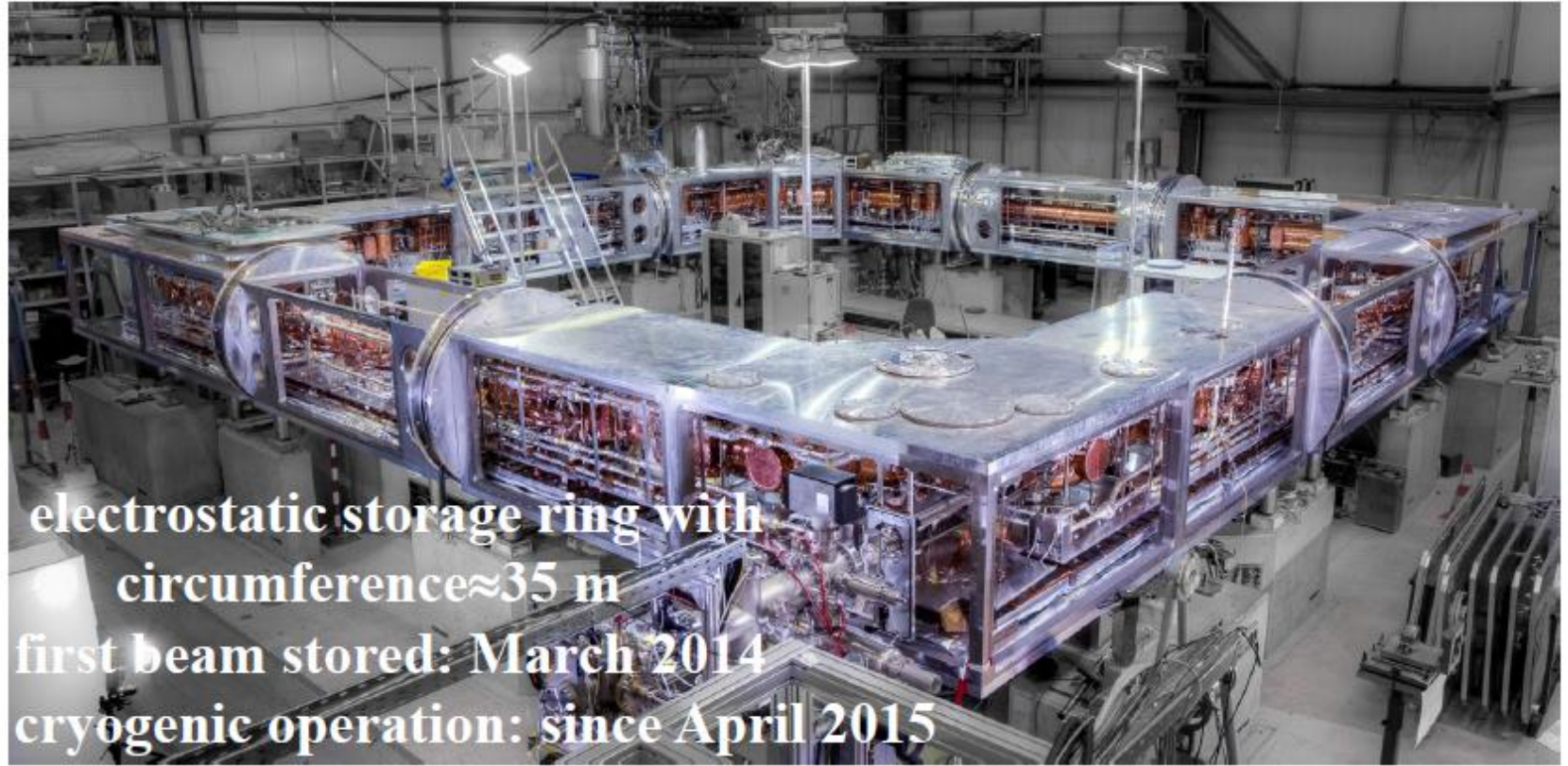
electrostatic storage ring with
circumference≈35 m
first beam stored: March 2014
cryogenic operation: since April 2015

High Voltage platforms

CSR main injector:
ion sources on a high
voltage plat form of ±300 kV
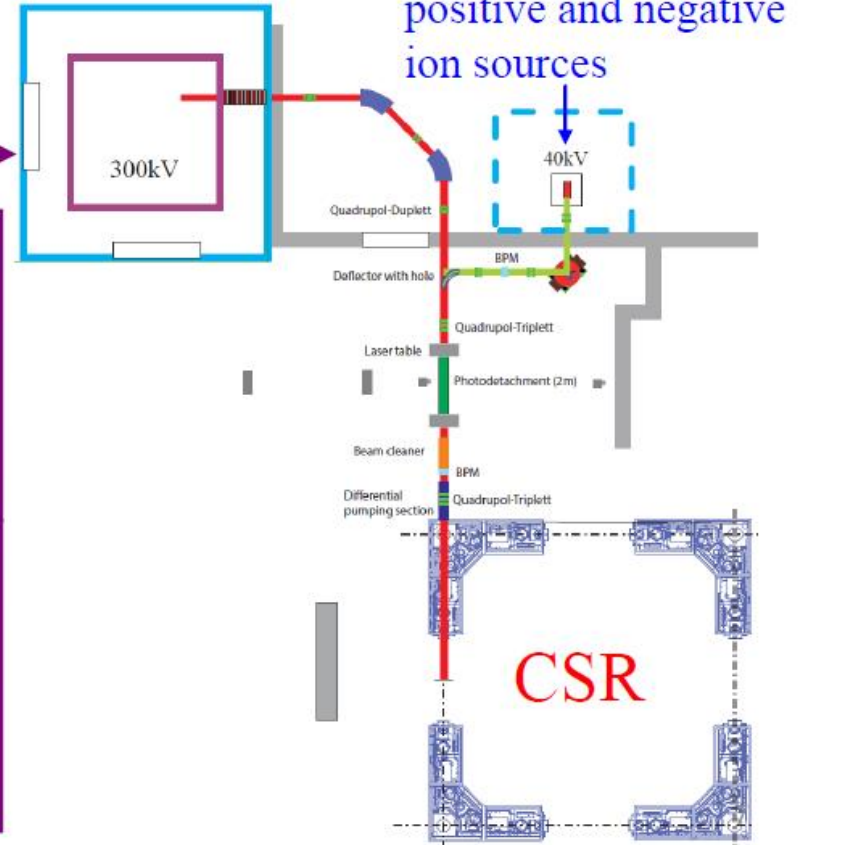
± 40 keV platform with
positive and negative
ion sources

astro

Thanks for your attention!

CSR team

A. Becker	C. Krantz	S. Saurabh
K. Blaum	H. Kreckel	S. Schippers
C. Breitenfeldt	S. Kumar S.	C. D. Schröter
F. Fellenberger	M. Lange	D. Schwalm
S. George	J. Lion	L. Schweikhard
J. Göck	S. Lohmann	K. Spruck
M. Grieser	C. Meyer	X. Urbain
F. Grussie	P. M. Mishra	S. Vogel
R. von Hahn	O. Novotný	A. Wolf
P. Herwig	P. O'Connor	D. Zajfman
J. Kartliein	R. Repnow	

מכון ויצמן למדע
WEIZMANN INSTITUTE OF SCIENCE

JUSTUS-LIEBIG-
UNIVERSITAT
GIESSEN

UNIVERSITAS·CATHOLICA·LOVANIENSIS
1425
SEDES·SAPIENTIAE

31

astro

The battle ship enters the stage

Perseus

Rho Ophiuchus

H_3^+ is fundamental

FALP

Πλασμα

10-8

Cryo-NIR-CRDS

AISA

Cryo-FALP

AISA

...versity Pragu...

Pumping

Laser

LN_2

He/Ar/H

Pulsed RF

Pressure dependence
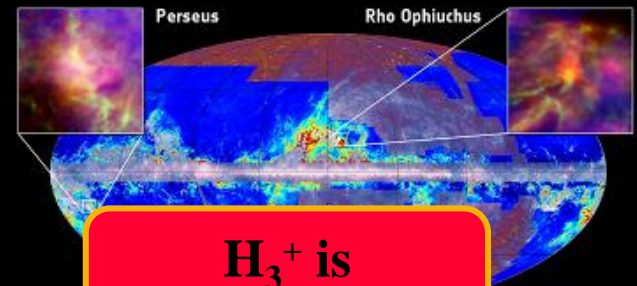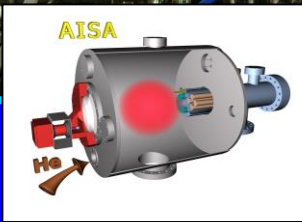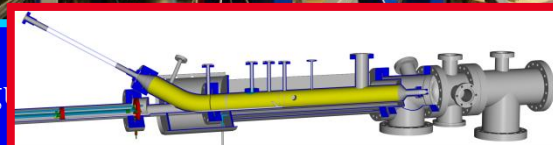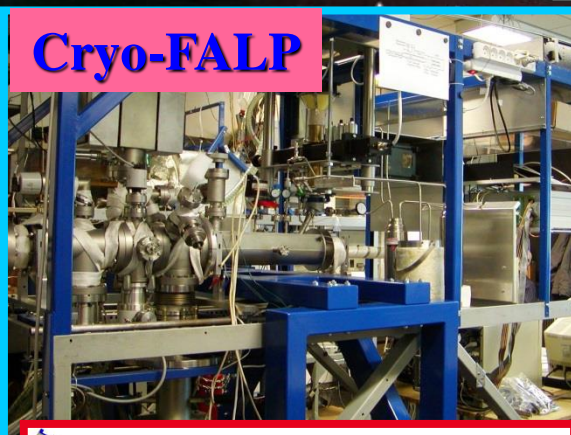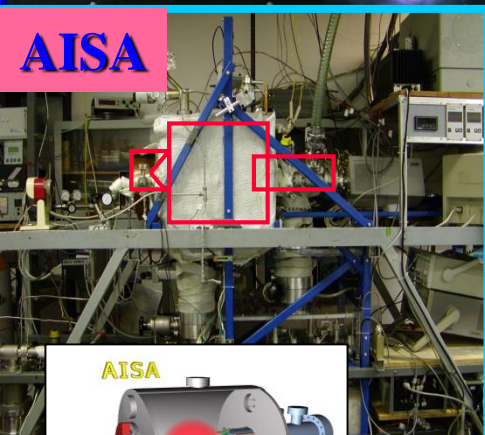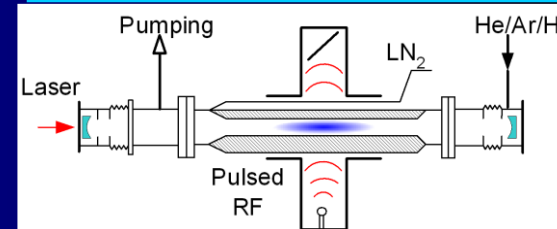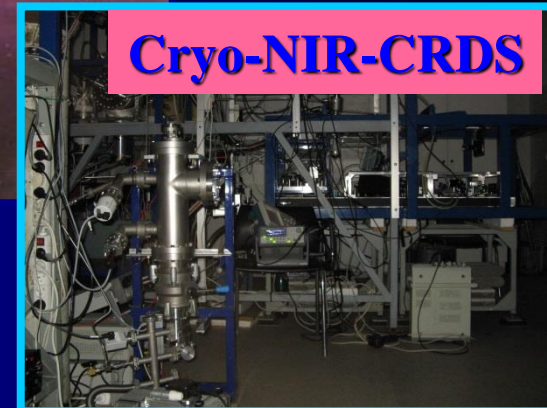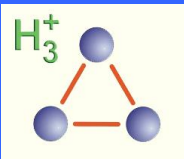
FALP – Flowing Afterglow Langmuir Probe

Formation of H_3^+ in He/Ar/H_2 mixture (10 Torr)

microwave discharge

He^+
He^m
e^-
He_2^+

Ar → Ar^+

H_2 → ArH^+, H_2^+

H_2 → $H_3^+ + e^-$

H_2

$H_5^+ + e^-$

μw

Ar

H_2

He

He

RECOMBINATION

$T_e \sim 2eV$

$T_e = T_i = T_G = 130 - 260K$
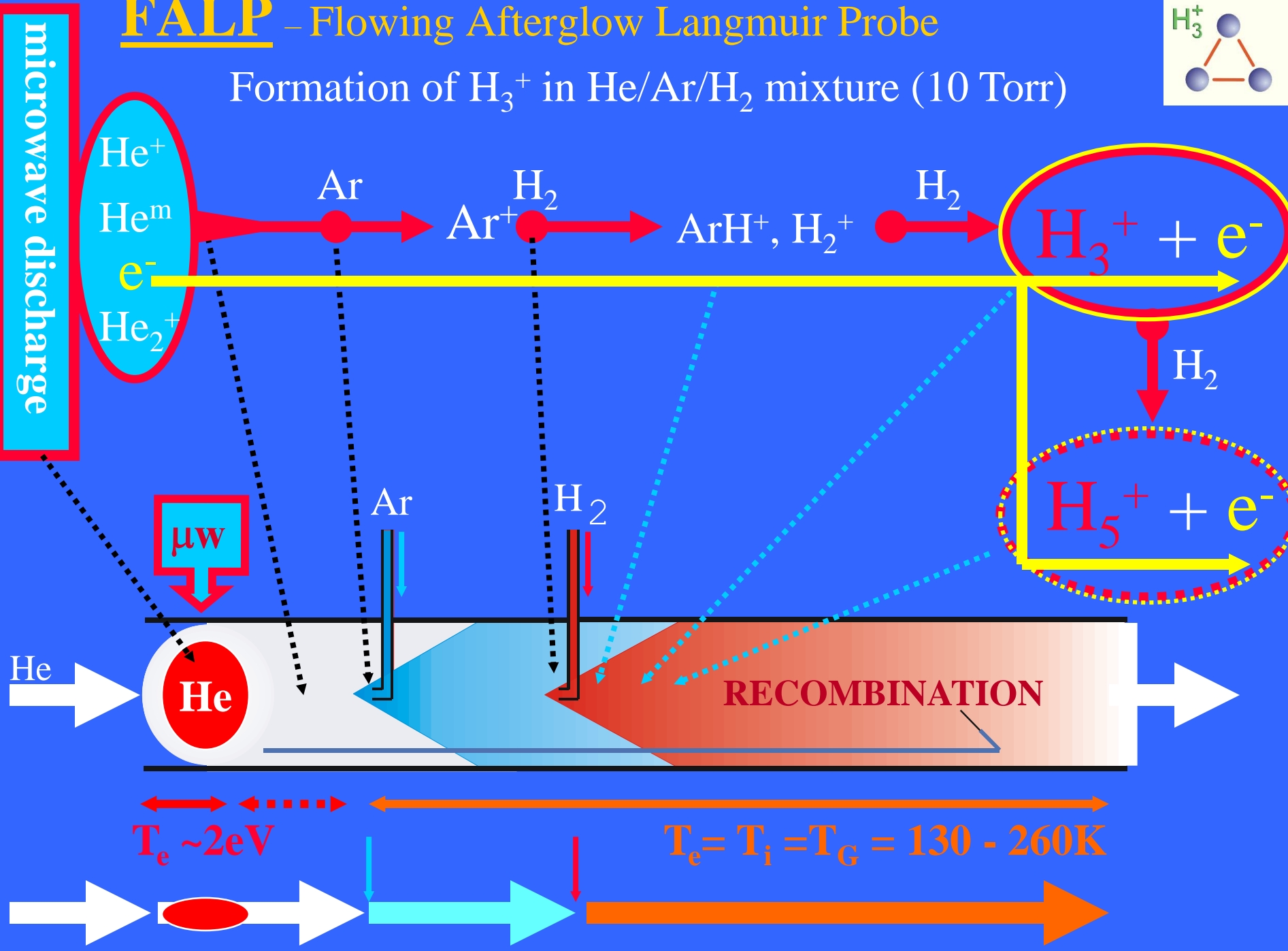
Line intensity H₃⁺

High sensitivity required

observed
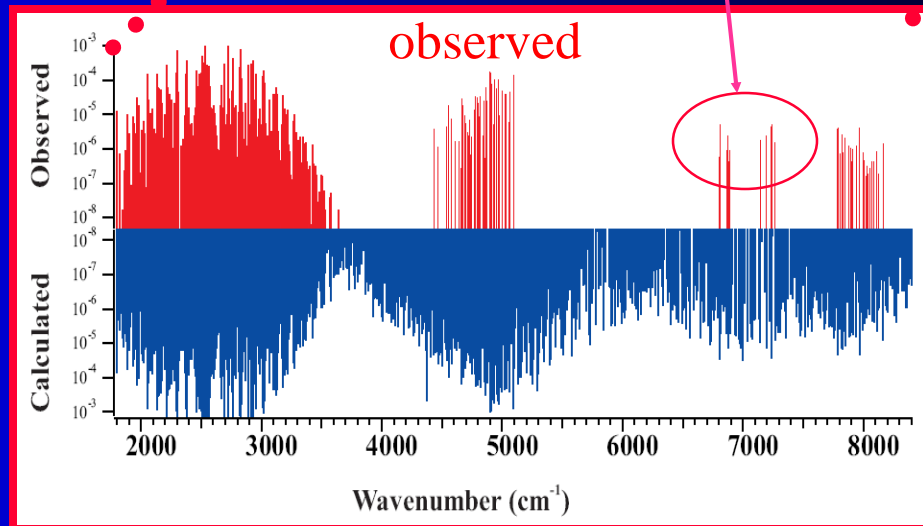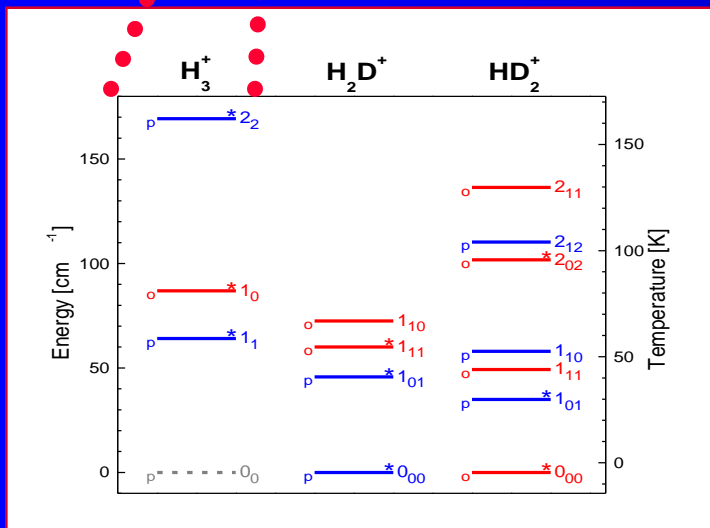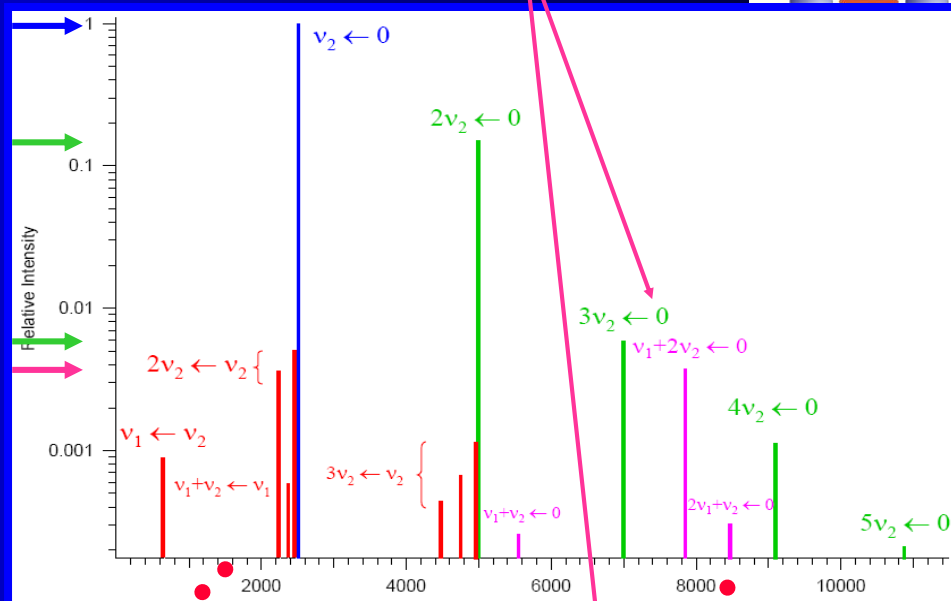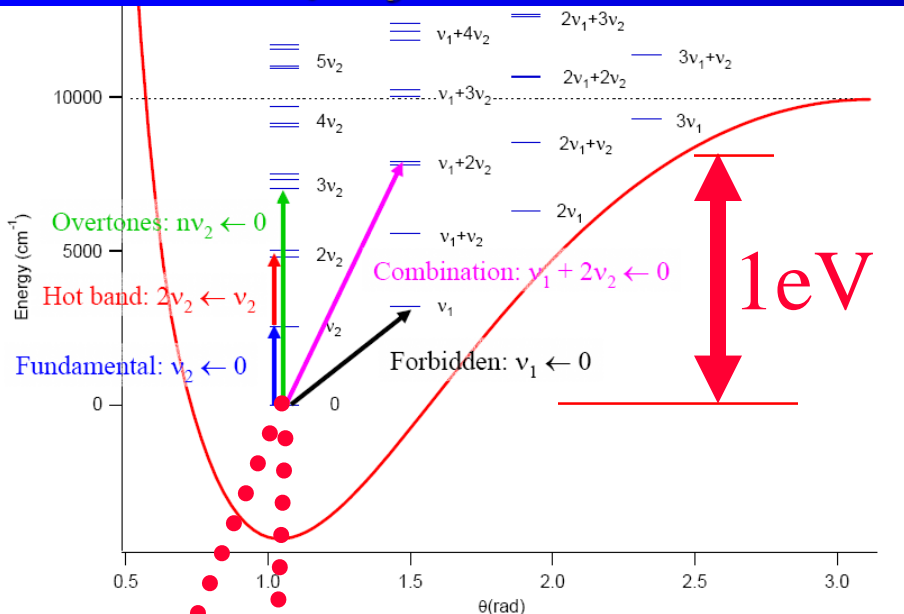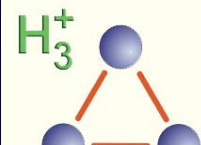
Stationary afterglow + Spectroscopic identification of recombining ions

$$\frac{d[H_3^+]}{dt} = -\alpha[H_3^+]n_e = -\alpha[H_3^+]^2$$

CRDS

5 ns

IR-CRDS
Laser absorption spectroscopy

(J, K)

361 K

32.9 K

mW pulse

IR Laser

He/Ar/H$_2$

He/Ar/H$_2$ pumping   D$_2$ He/Ar/H$_2$

Liquid N$_2$

Laser input
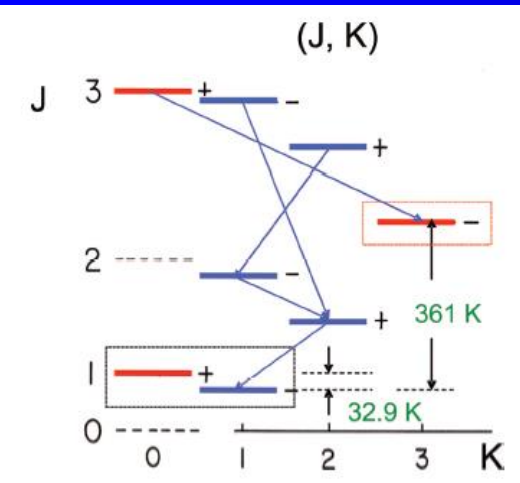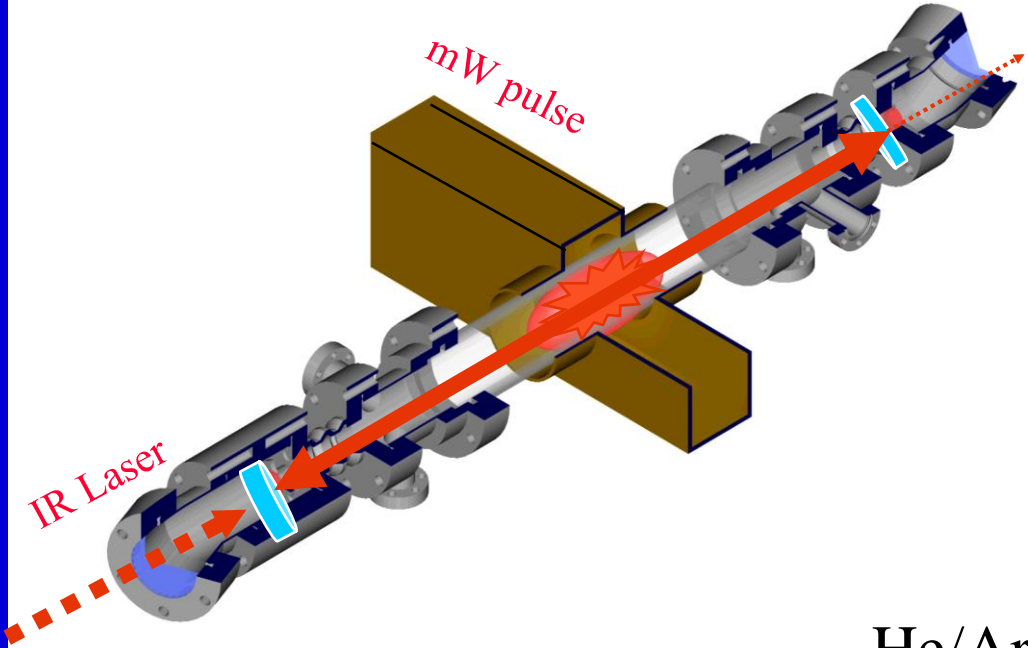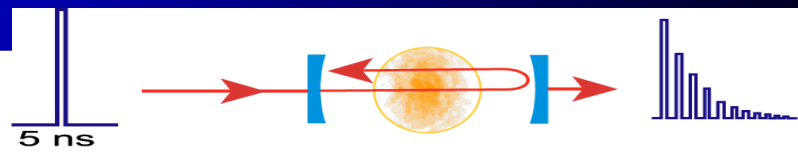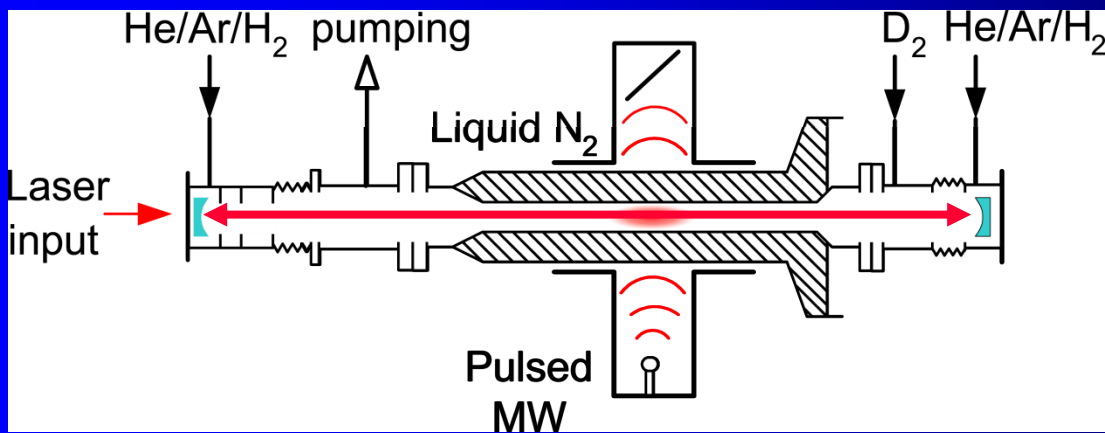
Pulsed MW

Pulsed discharge – plasma decay

n_e

H_3^+

$\nu_0 = 6877.546 \text{ cm}^{-1}$

$[H_3^+] = 1.88 \ 10^{11} \ [\text{cm}^{-3}]$
$T = 180 \text{ K}$
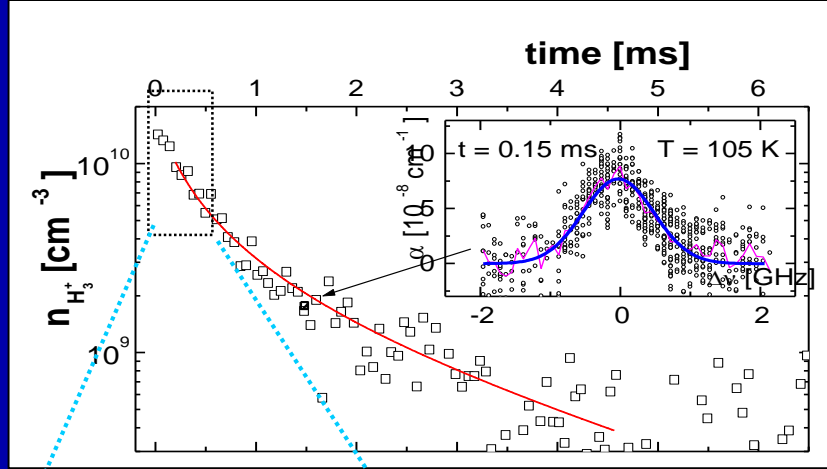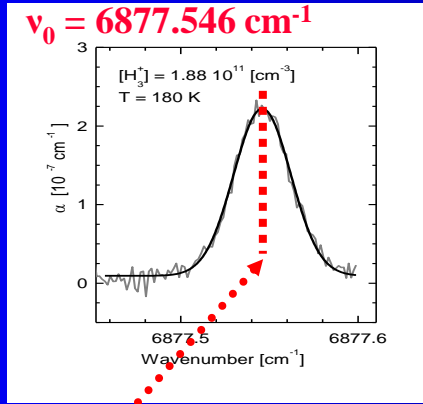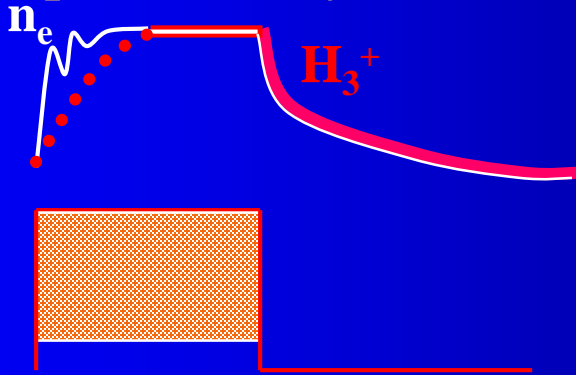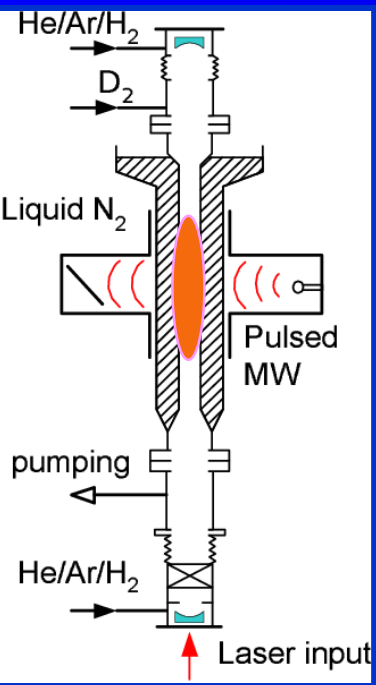
From Doppler broadening

Early Afterglow
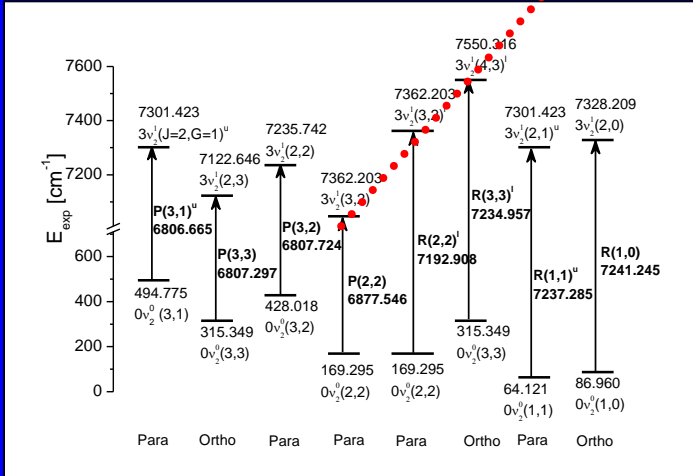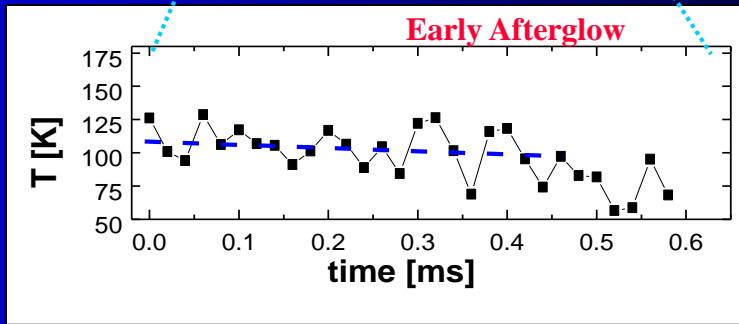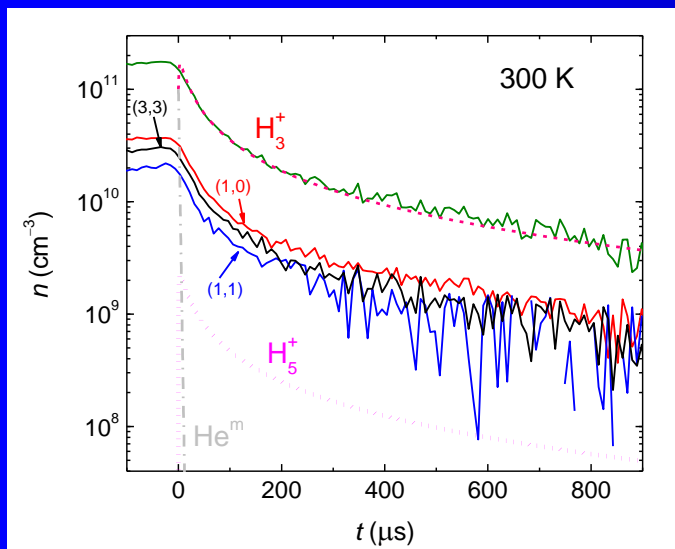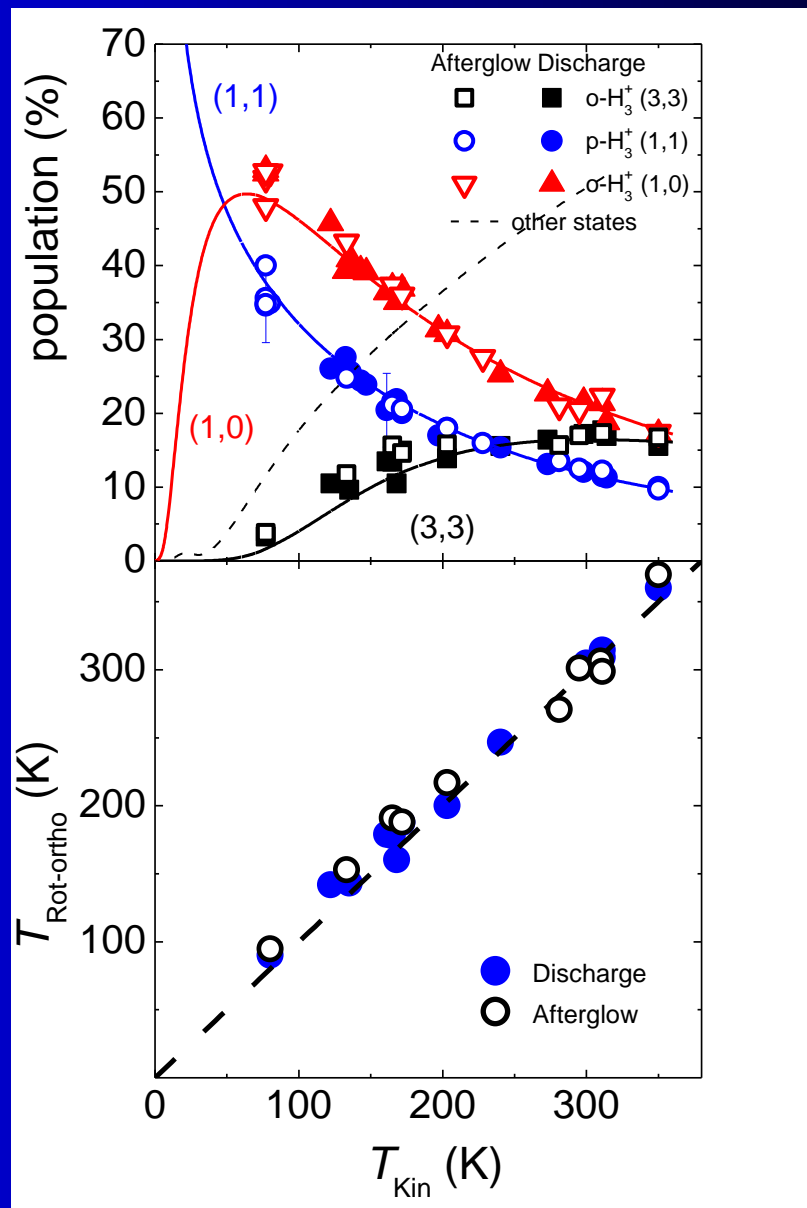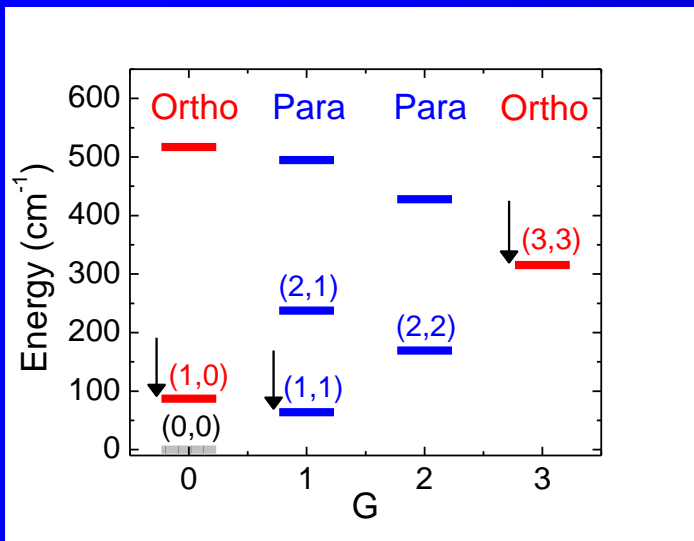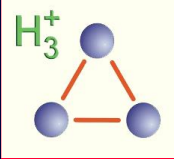
~300 K
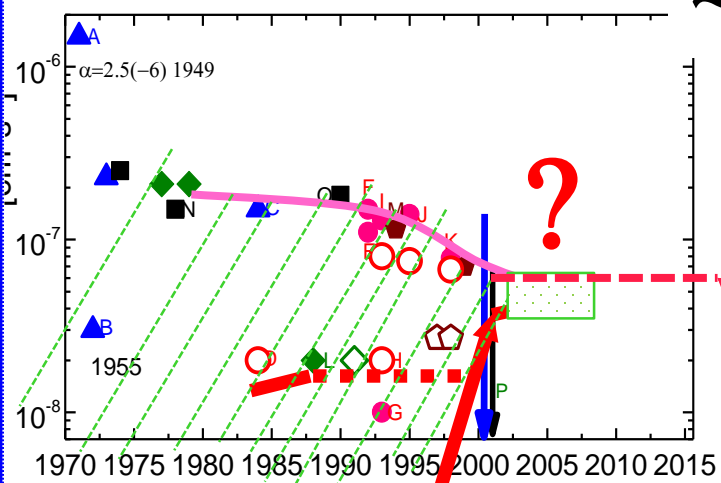
$$H_3^+ \quad PLASMA \quad EXPERIMENT$$

$$\alpha_{bin}(260K) = 7.5x10^{-8}\, cm^3 s^{-1}$$

THEORY OF DR

?

| Storage rings | TSR CRYRING |
| Afterglow | SA FALP |

Experiment:
$P = 3300$ Pa, $T = 300$ K
$[H_2] = 2 \times 10^{16}$ cm^{-3}, $[Ar] = 6.7 \times 10^{14}$ cm^{-3}

—— H_3^+ – – – fit   – – – diffusion

Model:
$\alpha_{H3+} = 2 \times 10^{-7}$ cm^{3}s^{-1}, $\alpha_{H5+} = 2 \times 10^{-6}$ cm^{3}s^{-1}

—— H_3^+ –·–·– H_5^+ –··–··– He^m

$$\frac{dn_e}{dt} = -[\alpha_1 n_1(t) + \alpha_2 n_2(t)]n_e$$

$$\Rightarrow \alpha_{eff}(t) = [\alpha_1 f_1(t) + \alpha_2 f_2(t)]$$

$$f_1 + f_2 = 1$$

Model + data. Pocatecni podminka: $n_e = $ He$^m = [H_3^+]$.
Poznamka. Namerene τ difuznich ztrat 1.6 ms. Teoreticke τ pri danem tlaku je 1.8 ms (odpovida cca 4×10^{10} cm^{-3} koncentraci necistot (pri 2×10^{-9} cm^{3}s^{-1} rychlosti reakce H_3^+ s necistotami). Namerena koncentrace vody $[H_2O] = 5 \times 10^{10}$ cm^{-3} ([He] = 8×10^{17} cm^{-3}).

If there are 2 or more ion species, the fast recombining species disappears first

$$\frac{dn_e}{dt} = -[\alpha_1 n_1(t) + \alpha_2 n_2(t)]n_e$$

$$\Rightarrow \alpha_{eff}(t) = [\alpha_1 f_1(t) + \alpha_2 f_2(t)]$$

$$f_1 + f_2 = 1$$

Stationary afterglow apparatus with CRDS for study of processes in plasmas from 300 K down to 30 K

R. Plašil,[1,a)] P. Dohnal,[1] Á. Kálosi,[1] Š. Roučka,[1] D. Shapko,[1] S. Rednyk,[1] R. Johnsen,[2] and J. Glosík[1]

astro

Nuclear spin dependence of H_3^+ recombination

H_3^+

B. J. McCall, et al. *Physical Review A* (2004)

H. Kreckel, J. Glosik, et al. Phys. Rev. Lett. 2005,

….2008, new improved calculations

Astronomy & Astrophysics
October 13, 2008

L. Pagani[1], C. Vastel[2], E. Hugo[3], V. Kokoouline[4], Chris H. Greene[5], A. Bacmann[6], E. Bayet[7], C. Ceccarelli[6], R. Peng[8], and S. Schlemmer[3]

M. Larsson, B.J. McCall, A.E. Orel (2008)

J. Glosik, R. Plasil, et al. *Phys. Rev. A*, 2009.

H. Kreckel, O. Novotny, et al., Phys. Rev. A（2010）.

K. N. Crabtree, N. Indriolo, et al., Astrophys. J. (2011)

J. Varju, M. Hejduk, J. Glosik, et al. *Phys. Rev. Lett.*, 2011.

P. Dohnal, M. Hejduk, J. Glosik, et al. *J. Chem. Phys.*, 2012.

Doubts 2011

"Presently no rate coefficient measurement with a confirmed temperature below 300 K exists".

Petrignani *et al.* Phys. Rev. A (2011)
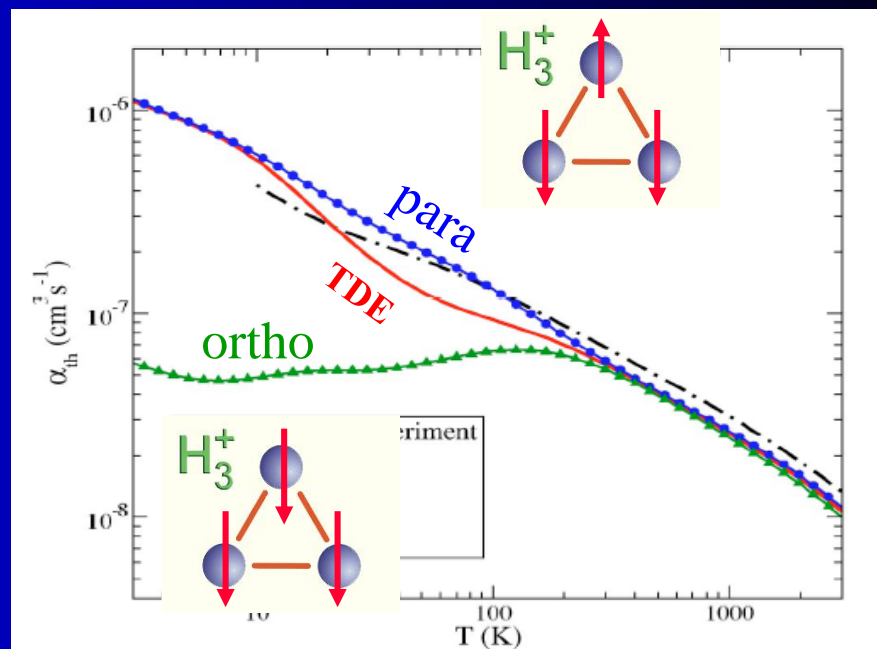
FIG. 5. (Color online) The present theoretical thermal rate coefficient for dissociative recombination of H_3^+ is compared with the experimental rate coefficient deduced from the storage ring experiment of McCall and co-workers (Refs. 9 and 10).

. Unfortunately the experiments on storage rings were stopped ….☹ ... ☹...

State of the art in 2013???

The dissociative recombination of H_3^+ – a saga coming to an end?

'Yes, the saga is coming to an end; but slowly.'

M. Larsson, B.J. McCall, A.E. Orel (2008)

..... Presently no reliable recombination rate coefficient for H3+ measured with storage rings below 300 K exists. .....

H. Kreckel, O. Novotny, K. N. Crabtree, et al., Phys. Rev. A（2010）.
A. Petrignani, S. Altevogt, M. H. Berg, et al., Phys. Rev. A（2011）.

The recent observations made towards several diffuse molecular clouds showed large difference between excitation temperatures T10(H2) and T(H3+), for details see ref. [cra11].

These observations lead to conclusion that in reliable chemical models the nuclear spin dependences of the reactions, including recombination of para- and ortho-H3+, have to be considered.
The dependences on spin, rotational excitation and temperature have to be measured.

K. N. Crabtree, N. Indriolo, H. Kreckel, B. A. Tom, and B. J. McCall, Astrophys. J. (2011)

… and the caravan is on its way

Help! Theory for H_3^+ Recombination Still Needed
…. We still badly need theory …

Takeshi Oka, DR2013

…. It is time to present some recent results from afterglow experiments … ☺

SA a FALP
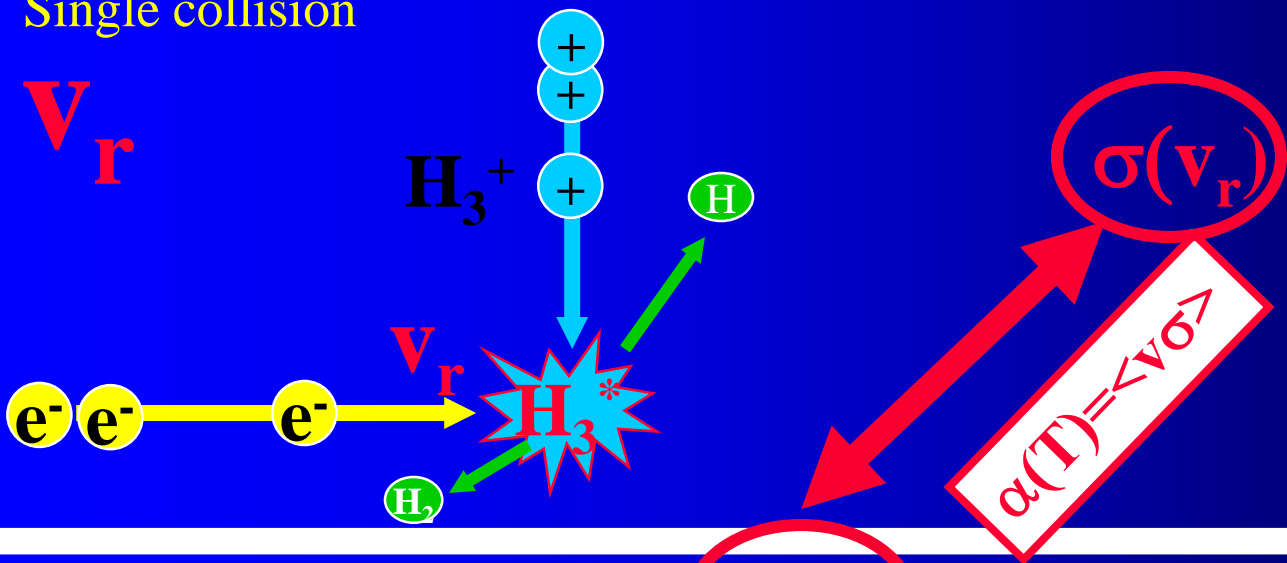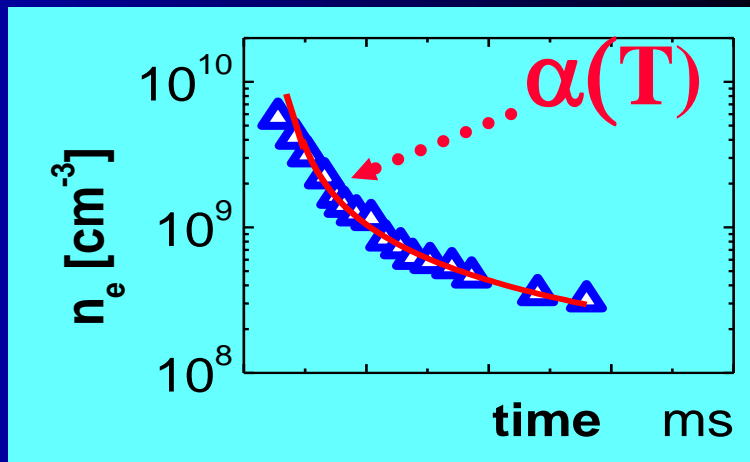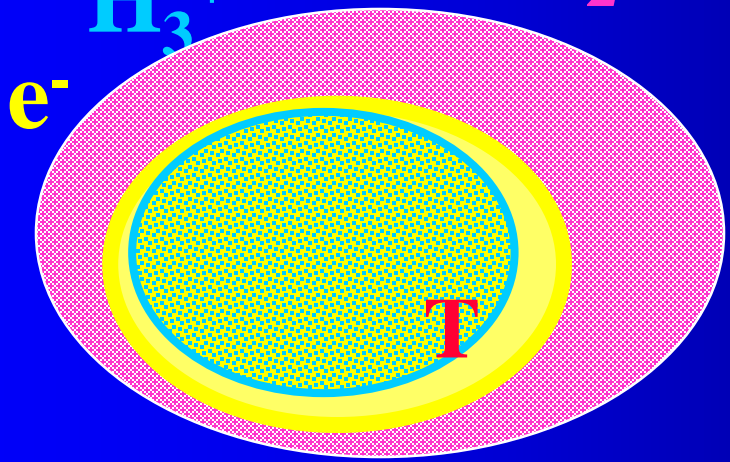
$$a_{eff} = a_{eff}(T_e, T_i, n_e, [He], [H_2], ^{o/p}f_2, ^{o/p}f_3)$$

$$a_{eff} = a_{eff}(T, [He])$$

$$\alpha_{eff} = \alpha_{bin} + K_{He}.[He]$$

$$H_3^+ + e \underset{\longleftarrow}{\overset{\alpha*}{\longrightarrow}} H_3^* \rightarrow products$$

He,

THEORY binary

para

ortho

Battle ships
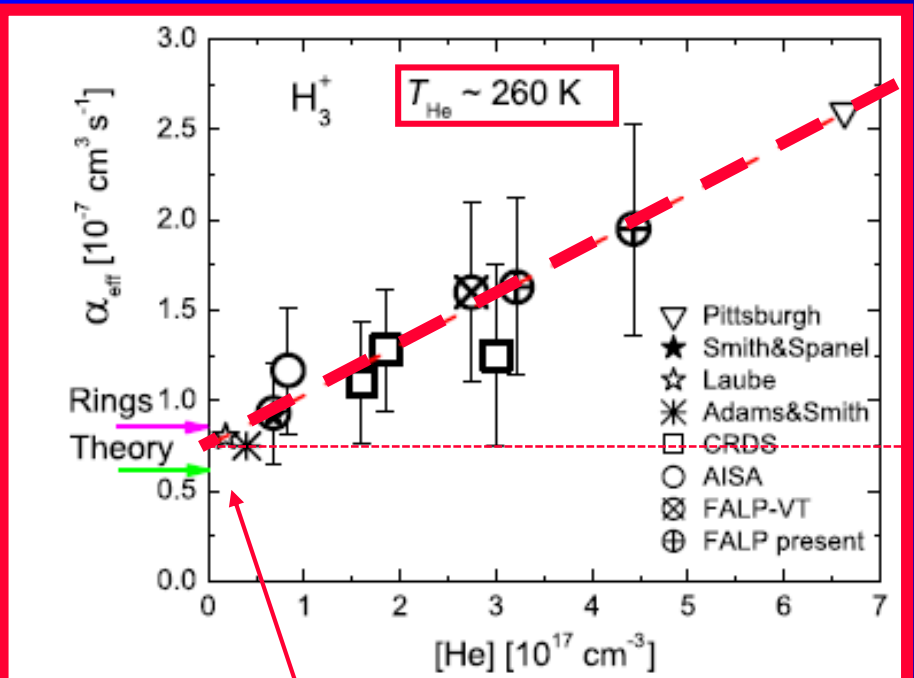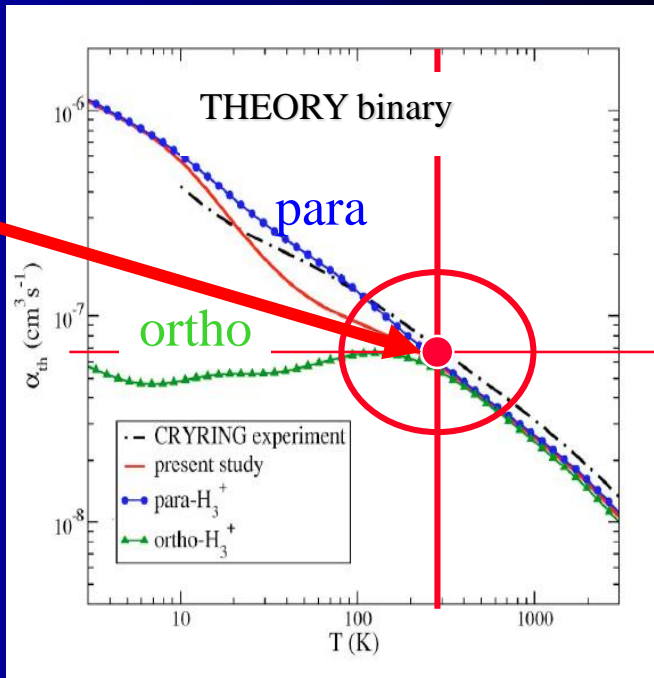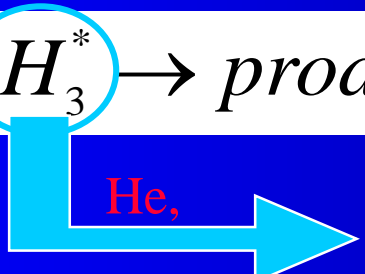
Binary + He assisted ternary recombination

$$\alpha_{eff} = \alpha_{bin} + K_{He}.[He]$$

$$H_3^+ + e^- \xrightarrow{\alpha_{Bin}} H_2 + H,.H + H + H$$

$$H_3^+ + e^- \underset{\tau_a}{\overset{\alpha_F}{\rightleftharpoons}} H_3^\# \xrightarrow[+He....ks_{He}]{} neutrals$$

$$H_3^+ \quad PLASMA \quad EXPERIMENT \quad \alpha_{bin}(260K) = 7.5x10^{-8} cm^3 s^{-1}$$

Just before splitting ☺
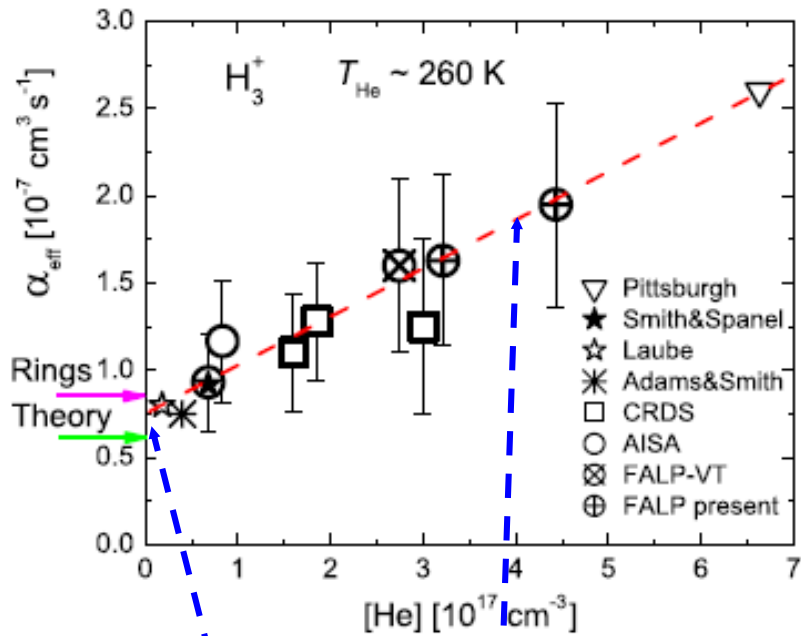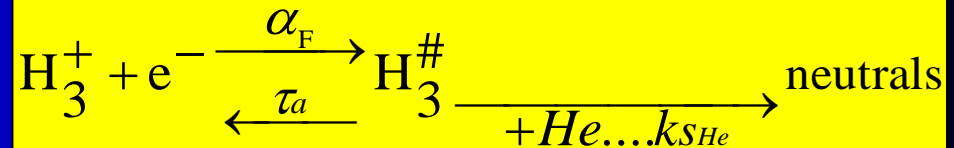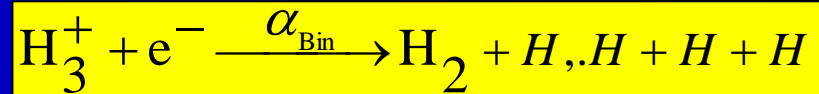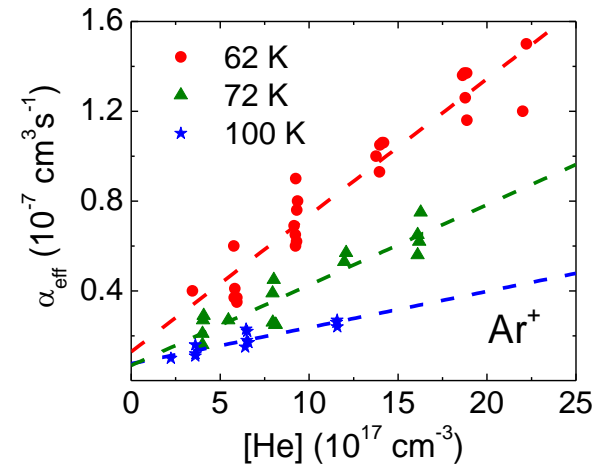
$$\alpha_{eff} = \alpha_{eff}(T_e, T_i, n_e, [He], [H_2], ^{o/p}f_3)$$
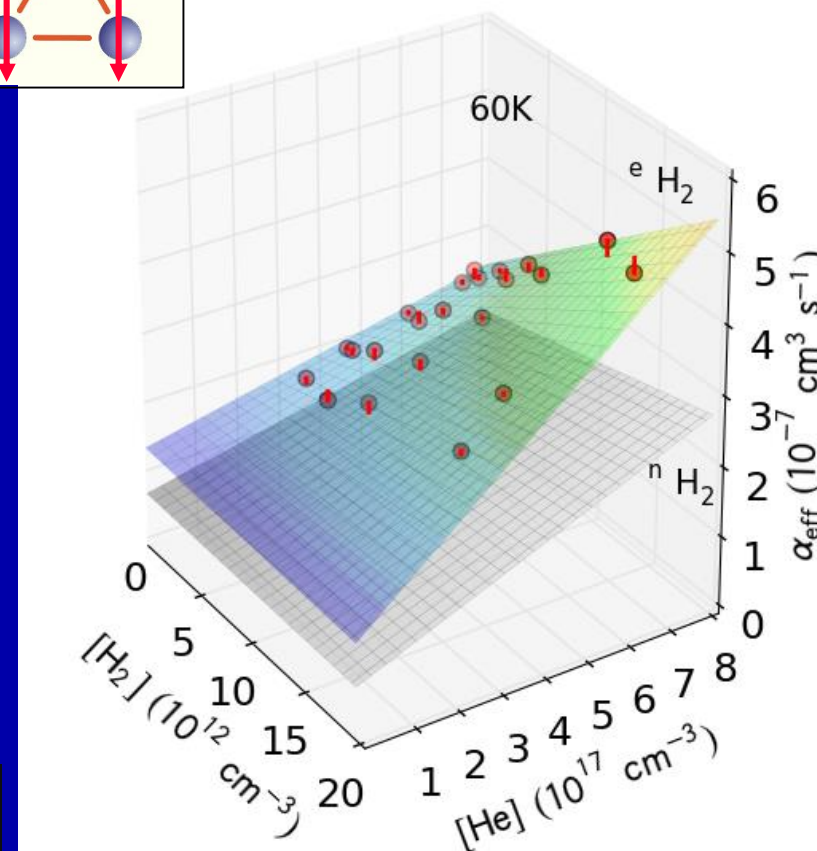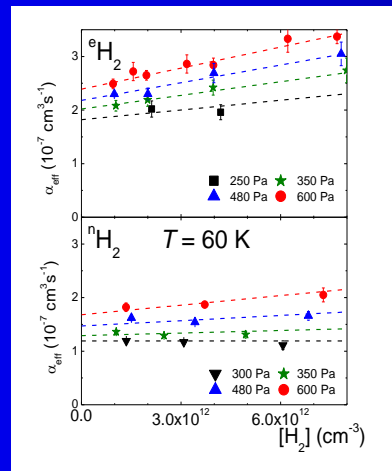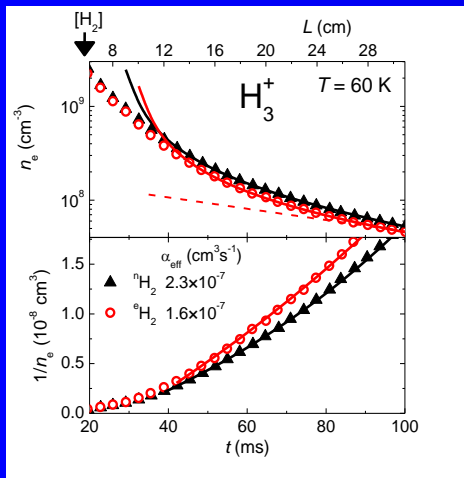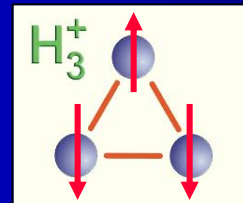
$$T = T_{wall} = T_{He} = T_e = T_{rot} = T_{kin\text{-}ion}$$

H_3^+

60K

Cryo-FALP II

model

Model

$$\alpha_{eff} = \alpha_{eff}(T_e, T_i, n_e, [He], [H_2], {}^{o/p}f_3)$$

$$H_3^+ + e^- \xrightarrow{\alpha_{Bin}} H_2 + H,.H + H + H$$

$$] \xrightarrow[\tau_a]{\alpha_F} H_3^{\#} \xrightarrow{H_2....k_{SH2}} neutrals$$
$$\xrightarrow{He....k_{SHe}}$$
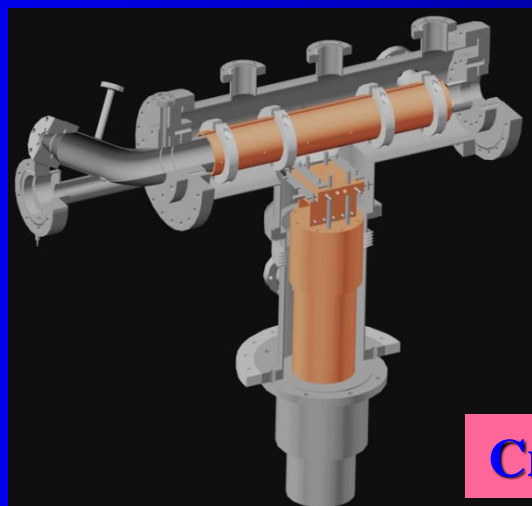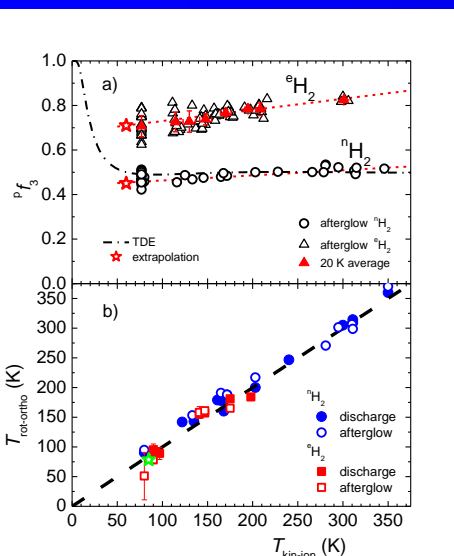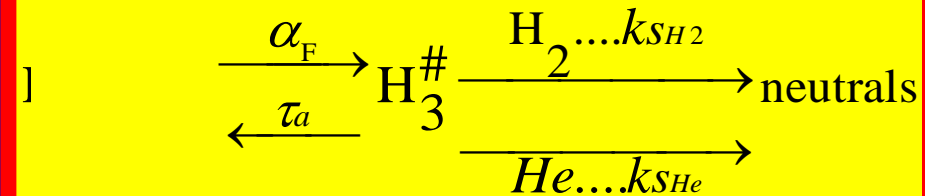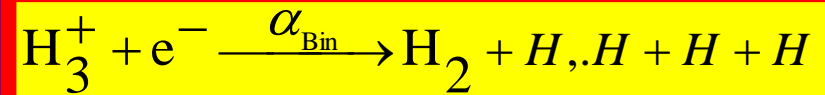
By solving the set of balance equations we obtain:

(He/Ar/H$_2$ mixture)

$$\frac{\partial n_e}{\partial t} = -(\alpha_{bin} - \alpha_F \frac{k_{SHe}[He] + k_{SH_2}[H_2]}{\frac{1}{\tau_a} + k_{SHe}[He] + k_{SH_2}[H_2]})[H_3^+]n_e$$

$$K_{He} = \alpha_F k_{SHe} \tau_a \qquad K_{H2} = \alpha_F k_{SH2} \tau_a$$

$$\alpha_{eff} = \alpha_{bin} + \alpha_F \frac{K_{He}[He] + K_{H2}[H_2]}{\alpha_F + K_{He}[He] + K_{H2}[H_2]}$$

In the low density limit ([He] and [H$_2$]$\rightarrow$ 0),   linear approximation

$$\alpha_{eff} = \alpha_{bin} + K_{He}[He] + K_{H2}[H_2]$$
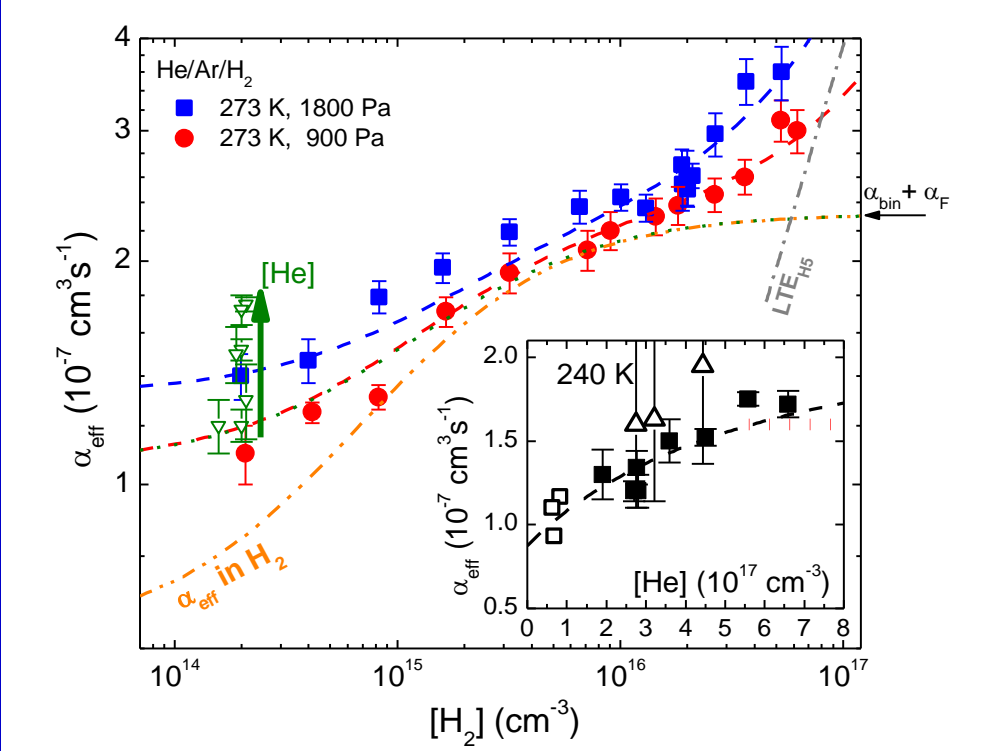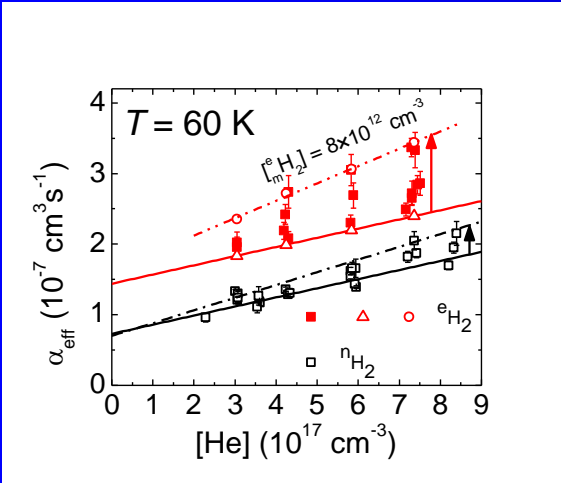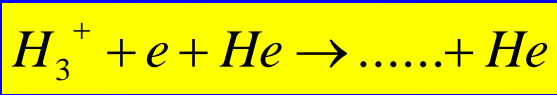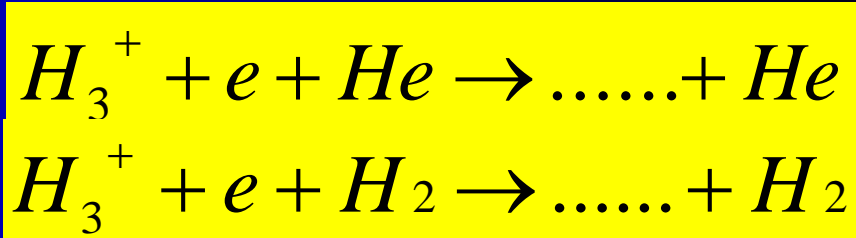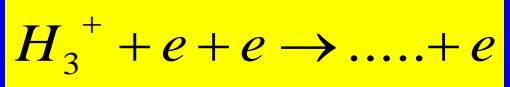
Experiments - State of the art in 2015

$$H_3^+ + e + He \rightarrow ...... + He$$

$$H_3^+ + e + He \rightarrow ...... + He$$

$$H_3^+ + e + H_2 \rightarrow ...... + H_2$$

CRR

$$H_3^+ + e + e \rightarrow ..... + e$$

$$\alpha_{\text{eff}} = \alpha_{\text{bin}} + \alpha_F \frac{K_{\text{He}}[\text{He}] + K_{\text{H2}}[\text{H}_2]}{\alpha_F + K_{\text{He}}[\text{He}] + K_{\text{H2}}[\text{H}_2]}$$
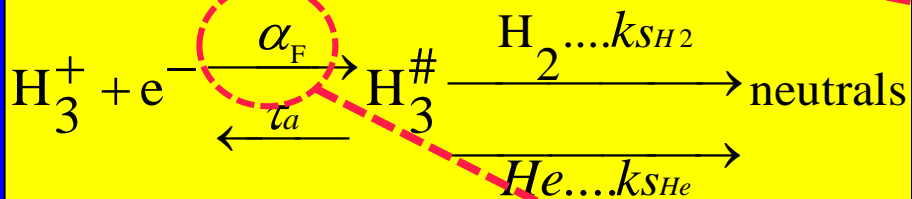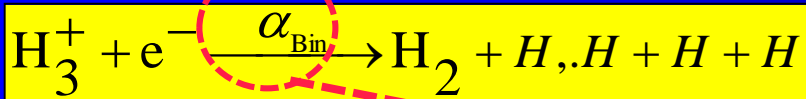
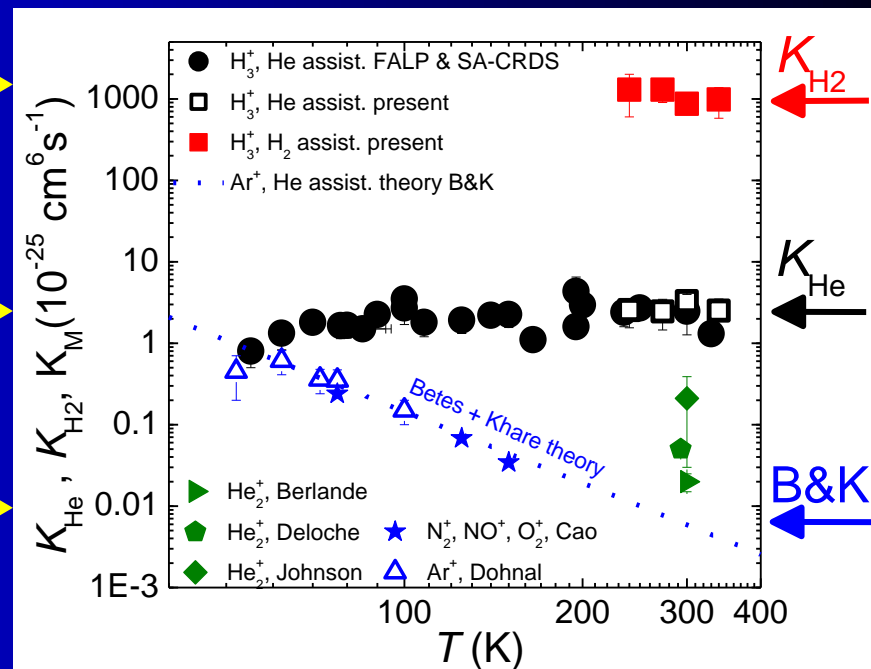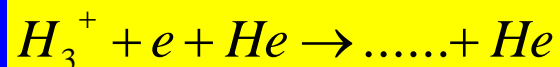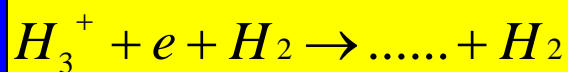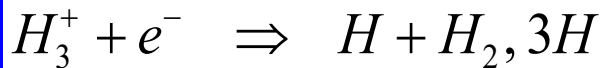$$H_3^+ + e^- \xrightarrow{\alpha_{Bin}} H_2 + H, .H + H + H$$

$$H_3^+ + e^- \underset{\tau_a}{\overset{\alpha_F}{\rightleftharpoons}} H_3^{\#} \xrightarrow{H_2 ....ks_{H2}} \text{neutrals}$$
$$\xrightarrow{He....ks_{He}}$$

para-H$_3^+$ and orto-H$_3^+$

(He/Ar/H$_2$ mixture)

$$H_3^+ + e^- \xrightarrow{\alpha_{Bin}} H_2 + H,. H + H + H$$

$$H_3^+ + e^- \xrightarrow{\alpha_F} H_3^{\#} \xrightarrow{H_2....k_{SH2}} \text{neutrals}$$
$$\xleftarrow{t_a} \qquad \xrightarrow{He....k_{SHe}}$$
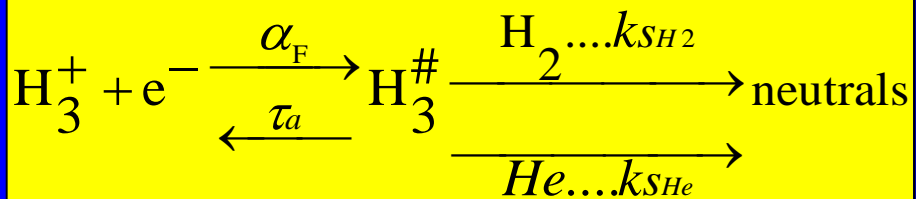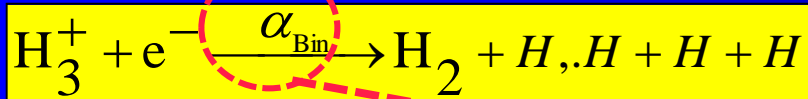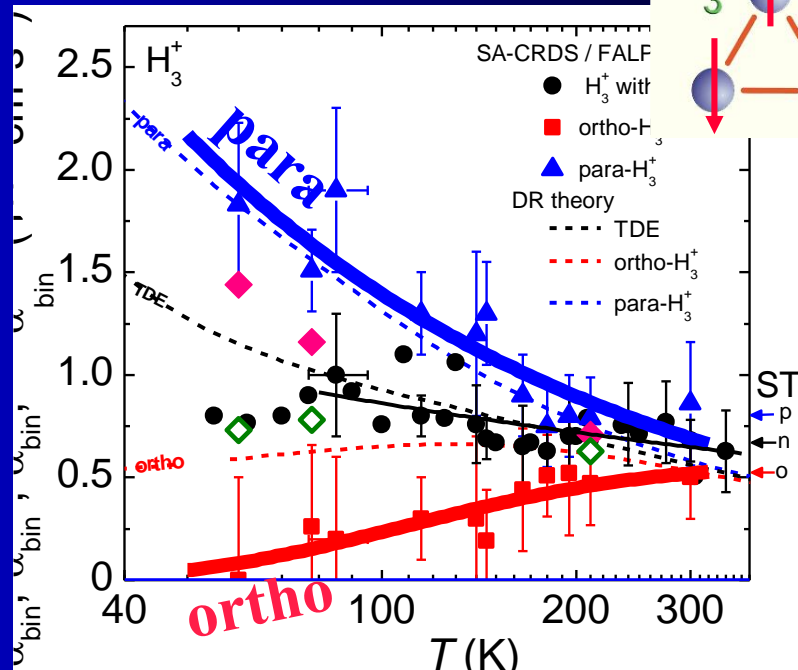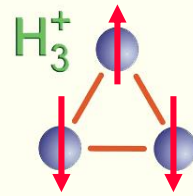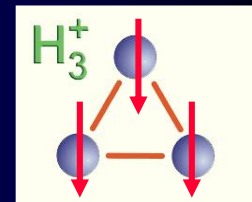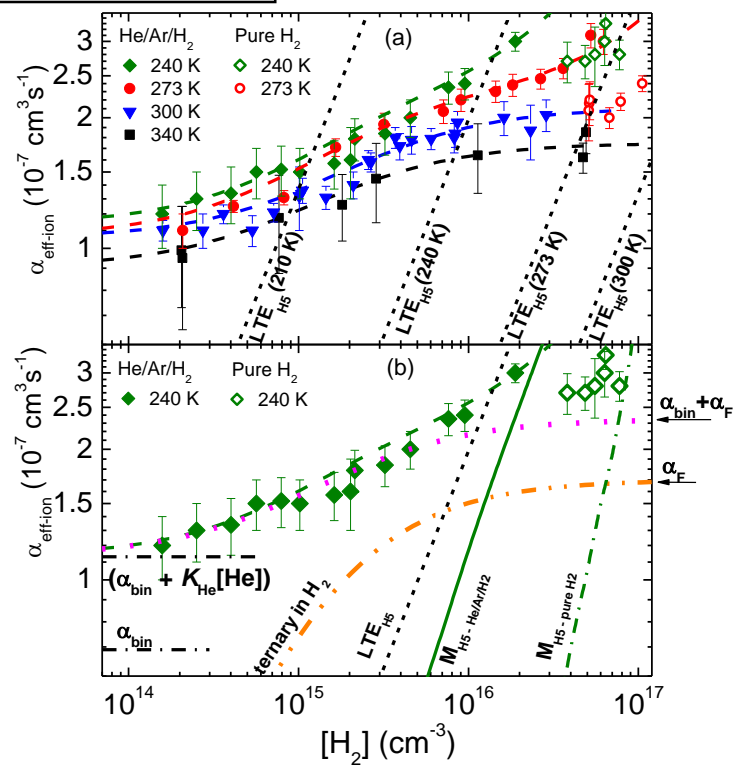
para-H$_3^+$ and orto-H$_3^+$
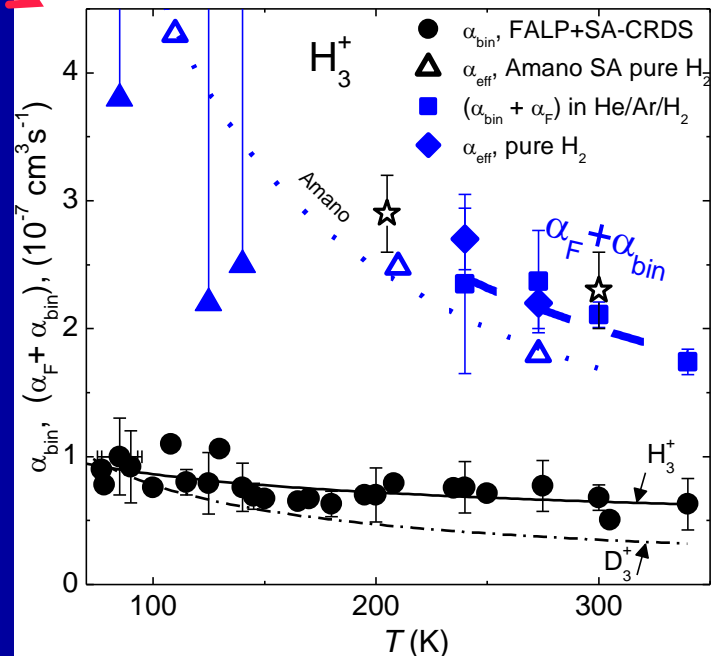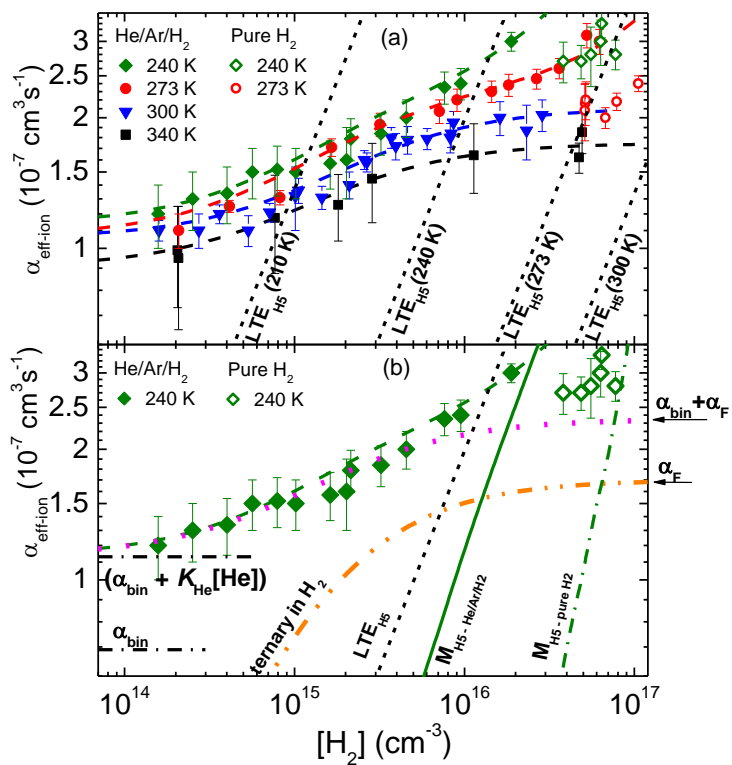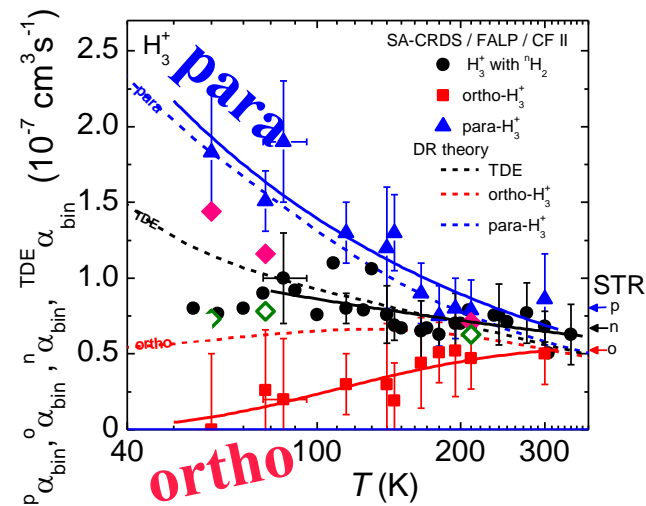
Rate coefficient ternary

$$H_3^+ + e^- \xrightarrow{\ \alpha_{Bin}\ } H_2 + H,.H + H + H$$

$$H_3^+ + e^- \xrightarrow[\tau_a]{\ \alpha_F\ } H_3^\# \xrightarrow[He....ks_{He}]{H_2....ks_{H2}} \text{neutrals}$$
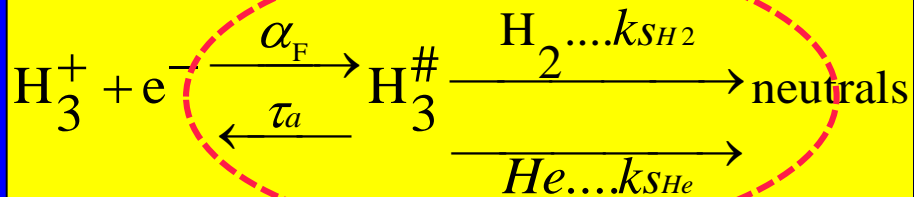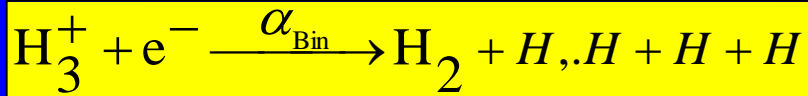
$$K_{He} = \alpha_F\, k_{SHe}\, \tau_a \qquad K_{H2} = \alpha_F\, k_{SH2}\, \tau_a$$

$$\alpha_{eff} = \alpha_{bin} + \alpha_F\, \frac{K_{He}[He] + K_{H2}[H_2]}{\alpha_F + K_{He}[He] + K_{H2}[H_2]}$$
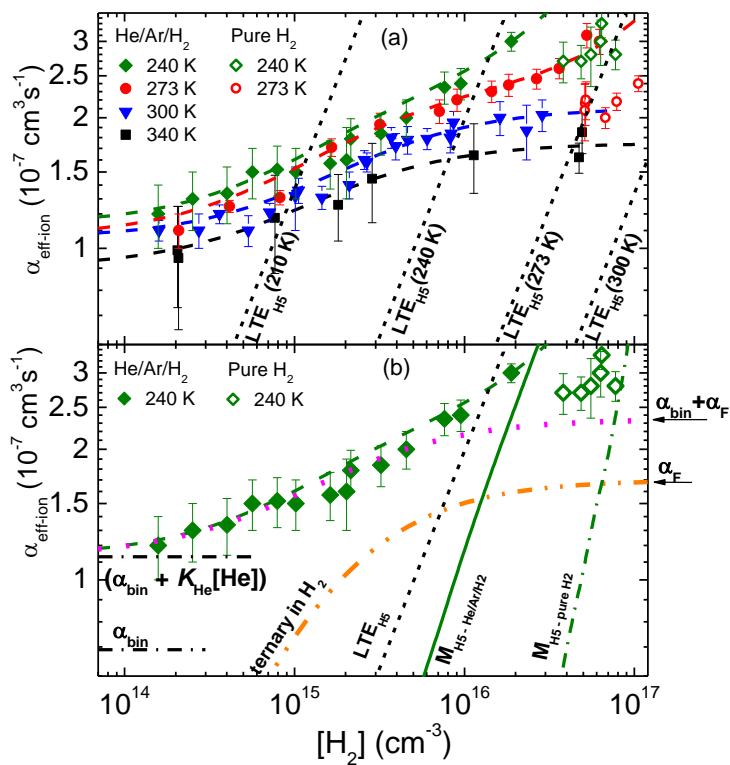
$$K_{He} \qquad K_{H2}$$
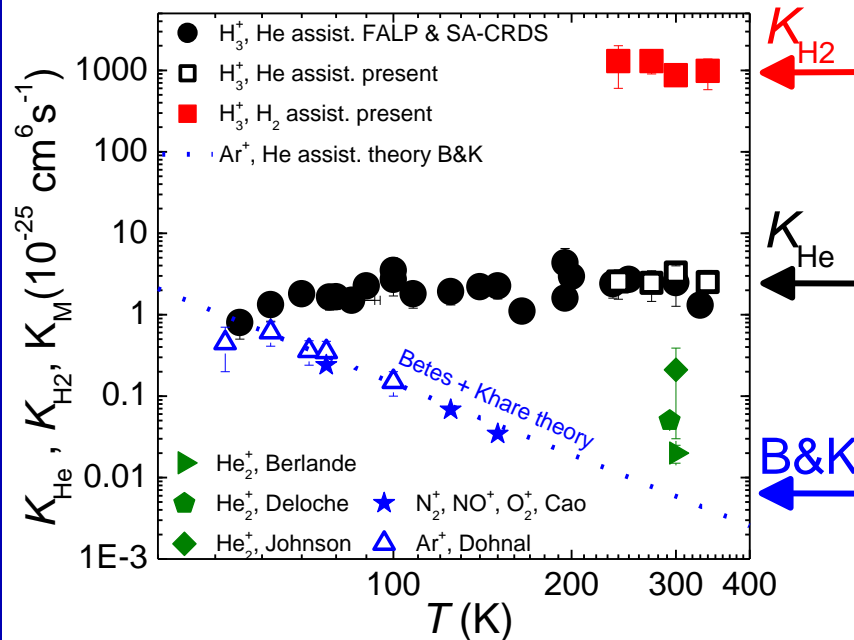
Recombination of H_3^+ ions with electrons in He/H$_2$ ambient gas at temperatures from 240 K to 340 K

J Glosík[1], P Dohnal[1], P Rubovič[1], Á Kálosi[1], R Plašil[1], Š Roučka[1] and R Johnsen[2]

$$K_{He} = \alpha_F \, k_{SHe} \, \tau_a \qquad K_{H2} = \alpha_F \, k_{SH2} \, \tau_a$$

$$H_3^{\,+} + e + H_2 \rightarrow \ldots\ldots + H_2$$

$$H_3^{\,+} + e + He \rightarrow \ldots\ldots + He$$

$$Ar^{\,+} + e + He \rightarrow \ldots\ldots + He$$

astro

H$_3^+$/e$^-$ plasma in He/Ar/H$_2$ gas mixture

$$H_3^+ + e^- \Rightarrow H + H_2, 3H$$

α(T=300 K)

$$\alpha_{\text{eff}} = \alpha_{\text{bin}} + \alpha_{\text{F}} \frac{K_{\text{He}}[\text{He}] + K_{\text{H2}}[\text{H}_2]}{\alpha_{\text{F}} + K_{\text{He}}[\text{He}] + K_{\text{H2}}[\text{H}_2]}$$
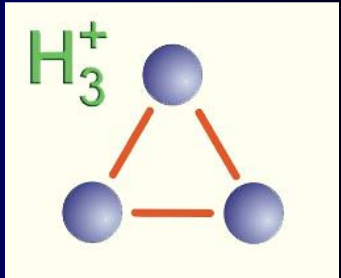
$$H_3^+ + e + H_2 \rightarrow \ldots\ldots + H_2$$

$$H_3^+ + e + He \rightarrow \ldots\ldots + He$$

$$Ar^+ + e + He \rightarrow \ldots\ldots + He$$
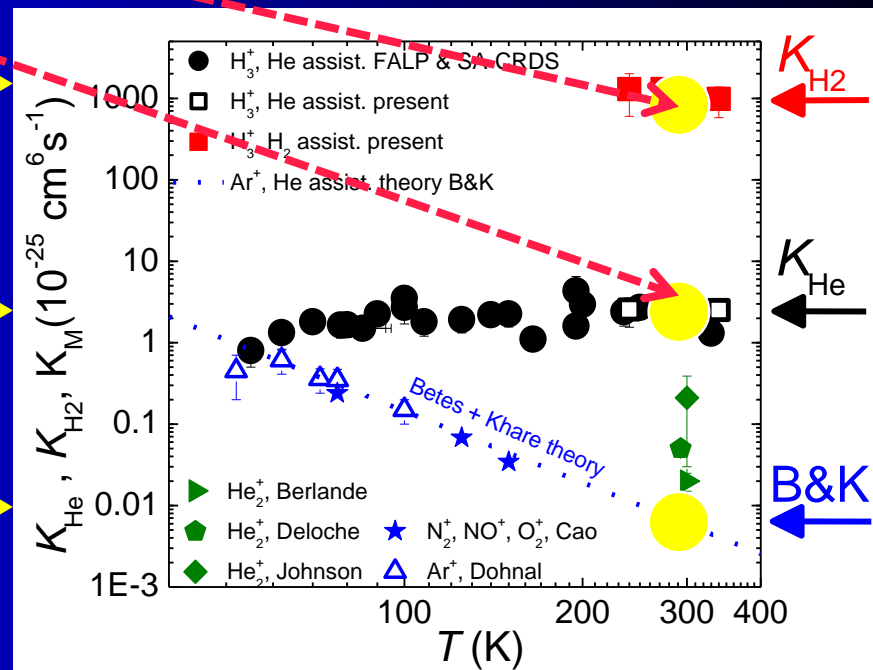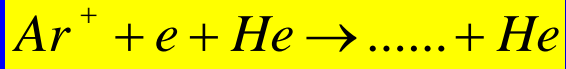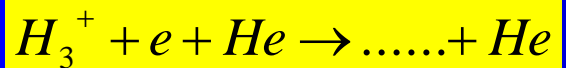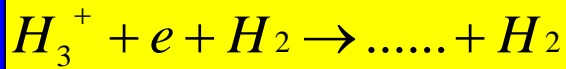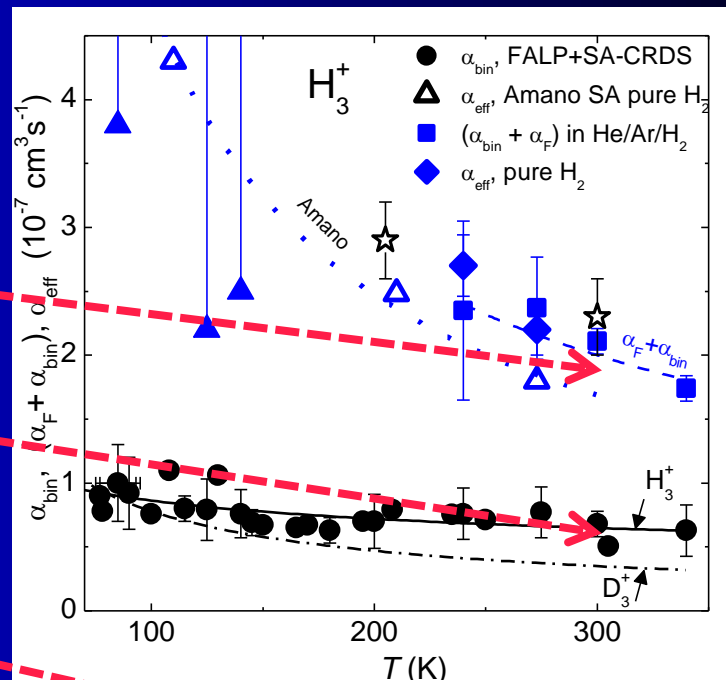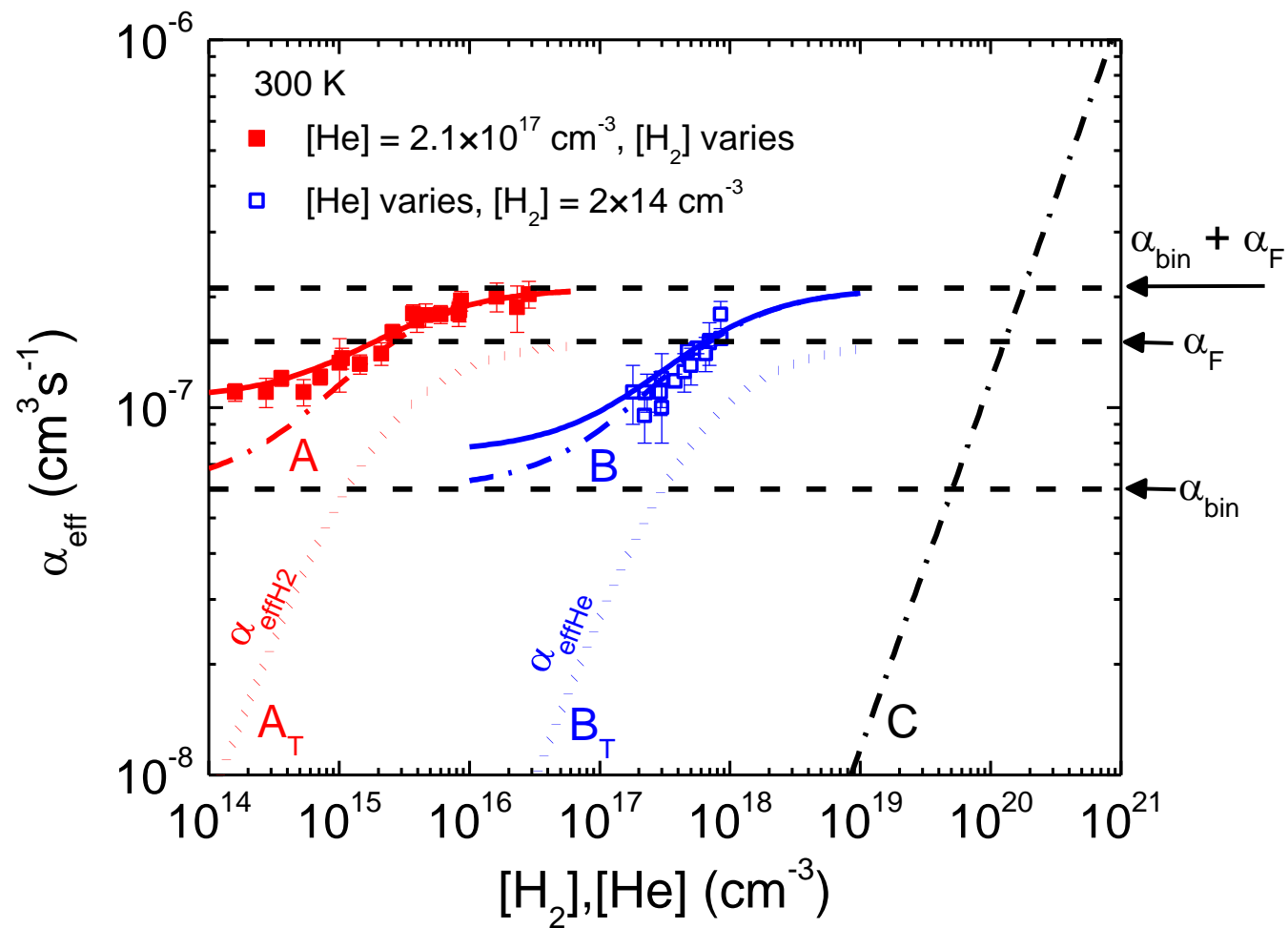
H_3^+ and its interaction of with e^- is FUNDAMENTAL

$H_3^+ + e^-$

If you understand hydrogen,
you understand all
that can be understood.
(*V. Weisskopf & G. Herzberg*).

H_3^+

DR   HeH$^+$ H$_2^+$ HD$^+$ H$_3^+$ D$_3^+$ H$_2$D$^+$ H$_2$D$^+$
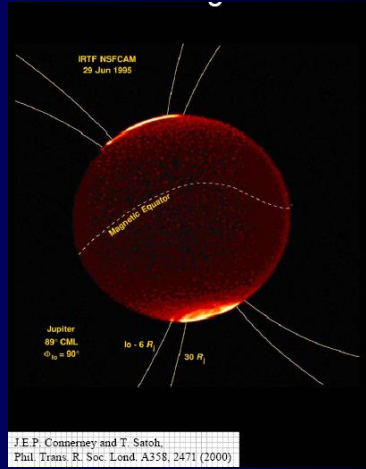
ψ

α

σ

τ

Evergreens and Bestsellers
H$_3^+$ & D$_3^+$

I JAKD KOMIKS.

J.E.P. Connerney and T. Satoh,
Phil. Trans. R. Soc. Lond. A358, 2471 (2000)

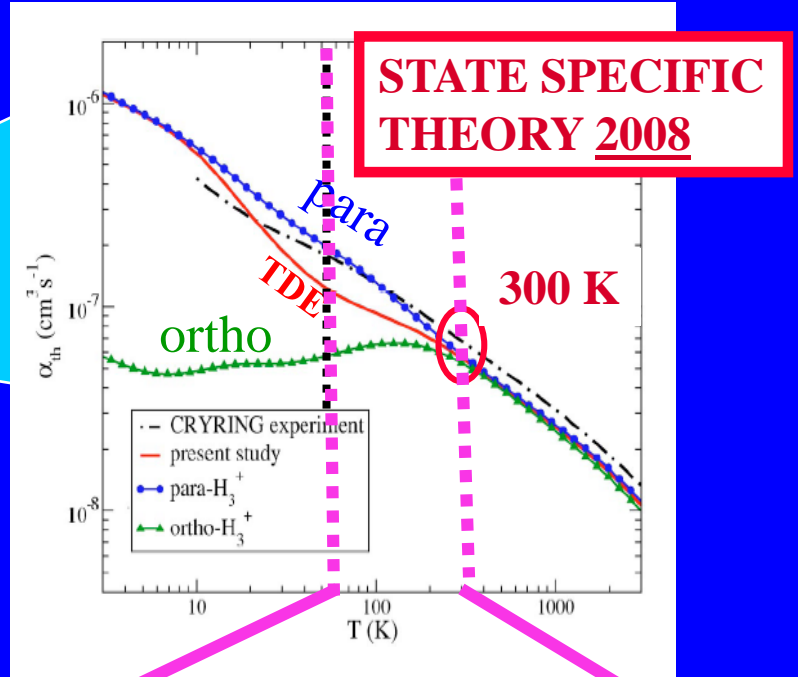# Ion storage rings

AISA

FALP

Quo vadis??

300 K

$\alpha=2.5(-6)$ 1949

1955

THEORY 2003

	D_3^+	H_3^+	
		▲	SA
	○	●	FALP
	◇	◆	MB
	⬠	⬠	Stor. Ring
		■	Other methods

A – M.A. Biondi
B – K.B. Persson
C – J.A. Mac Donald
D – N.G. Adams
E,F – A. ...
H,G,I
J
M – M. Larson
N – D. Mathur
O – T. Amano
P – P. Van der Donk
(1) – $\nu=0$
(2) – $\nu>0$

STATE SPECIFIC THEORY 2008

para
TDE
ortho
300 K
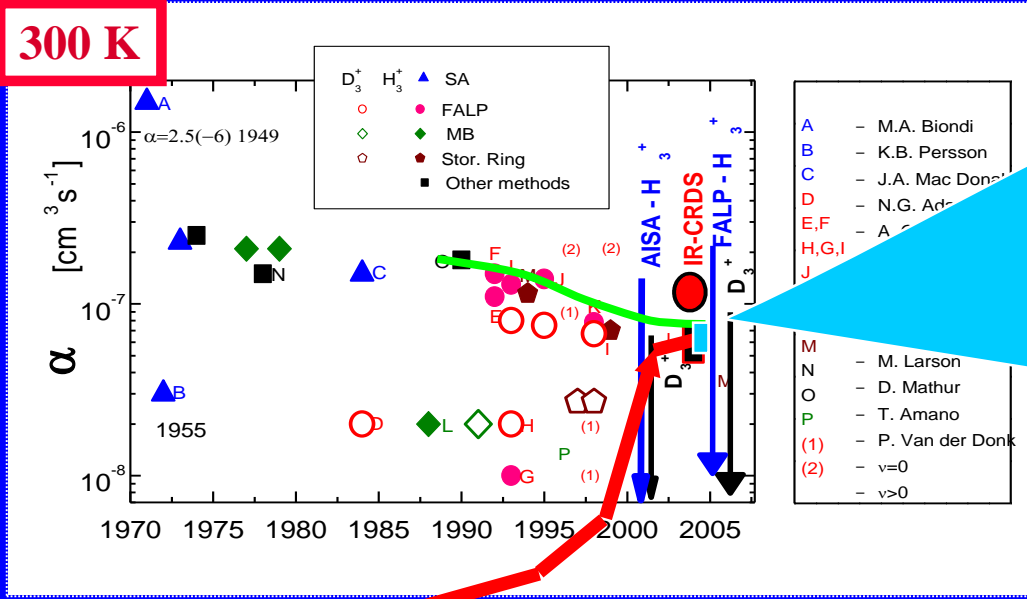
FIG. 5. (Color online) The present theoretical thermal rate coefficient ...

b) DIFFUSE CLOUDS: DESTRUCTION: $H_3^+ + e^-$

$\underline{d[H_3^+]/dt \quad \sim - \alpha_{DR} [H_3^+][e^-]}$

$[e^-] \sim [C]$

$\alpha_{DR} = 2 \times 10^{-7} cm^3 s^{-1} \times (T/300)^{-0.65}$?

$[H_3^+] = \gamma / \alpha_{DR} \cdot [H_2]/[C] = \sim \underline{1 \times 10^{-7} cm^{-3}}$

~ NO with observation

?

$^p\alpha_{bin} = {}^p\alpha_{bin}(T)$ $^o\alpha_{bin} = {}^o\alpha_{bin}(T)$

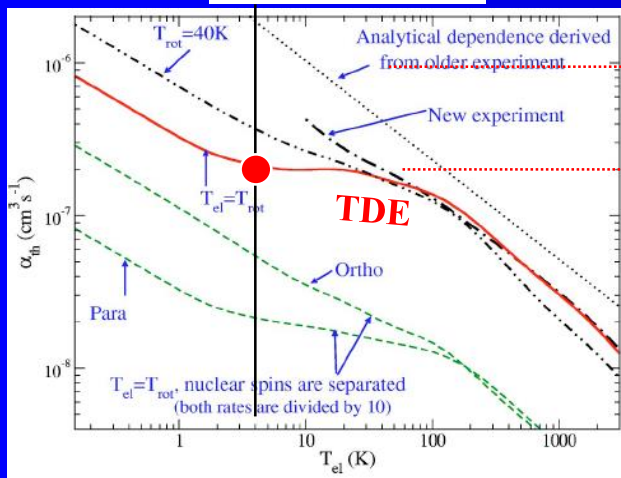**State of the art – 1st December 2014**
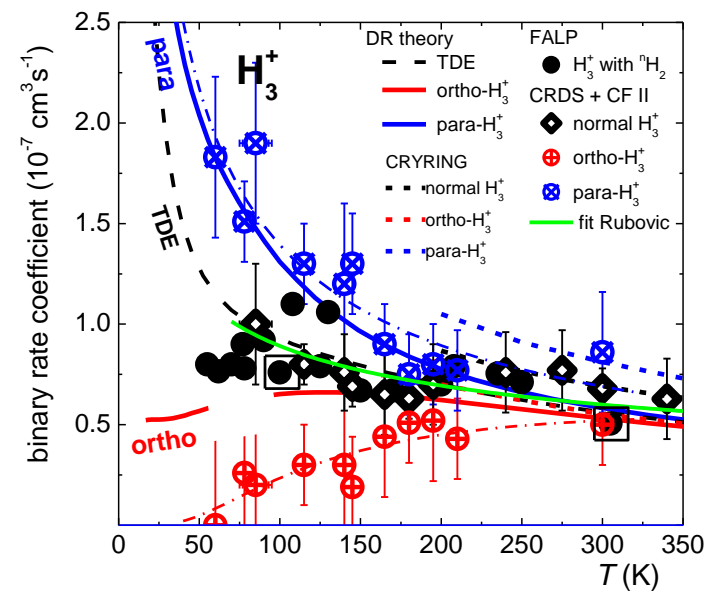
New "state selective" study with "cold ion source" observed faster recombination of para H_3^+ in comparison with ortho H_3^+ …...

B. J. McCall, et al. *Physical Review A* (2004)   H. Kreckel, et al. Phys. Rev. Lett. 2005,

Before 2007
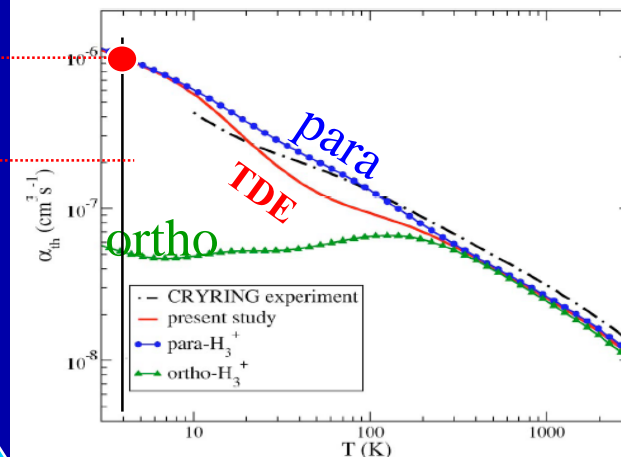

2008, new improved calculations

FIG. 5. (Color online) The present theoretical thermal rate coefficient for dissociative recombination of H_3^+ is compared with the experimental rate coefficient deduced from the storage ring experiment of McCall and co-workers (Refs. 9 and 10).

In the middle of 2008 M. Larsson et al wrote the Frontier article to Chem. Phys. Let., [Larsson 2008].

This was written in the abstract:
"…. *Two independent ion storage ring experiments with rovibrationally cold H3+ ions are in excellent agreement*, and quantum mechanical calculations agree with the storage ring results quantitatively for the thermal rate constant, *if not in all details* concerning the cross section. *The recombination mechanism is understood.* A direct consequence of this progress is that the cosmic-ray ionization rate in diffuse clouds must be shifted upwards to a value larger than $10^{-16} s^{-1}$. … "

In the abstract of [Petrignani 2010] it is written:
"… A systematic experimental assessment of *heating effects* is performed which, together with a survey of other *recent storage-ring data, suggests that the present rotationally cool rate-coefficient measurement was performed at 380 (+50 -130) K and that this is the lowest rotational temperature so far realized in storage-ring rate-coefficient measurements on H3+….*

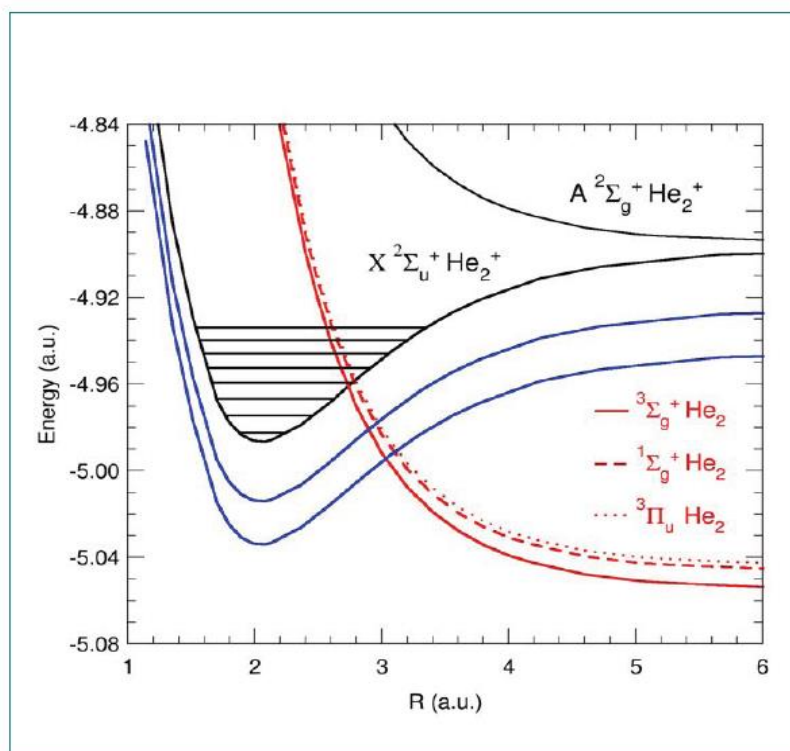…. Unfortunately the experiments on storage rings were stopped …. ☹ ... ☹…
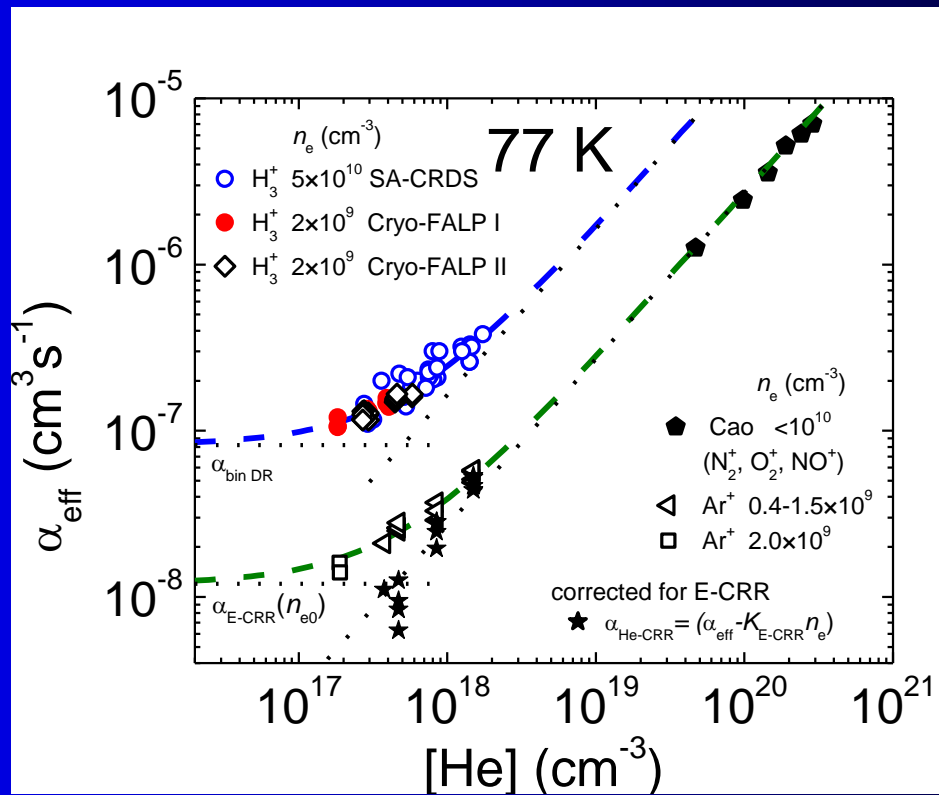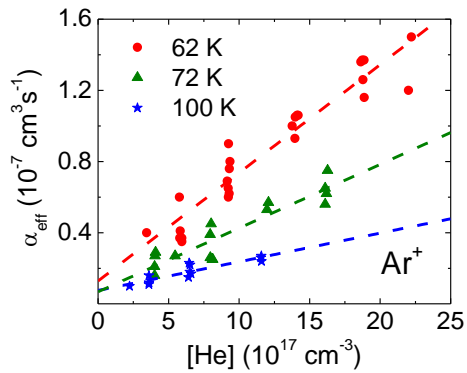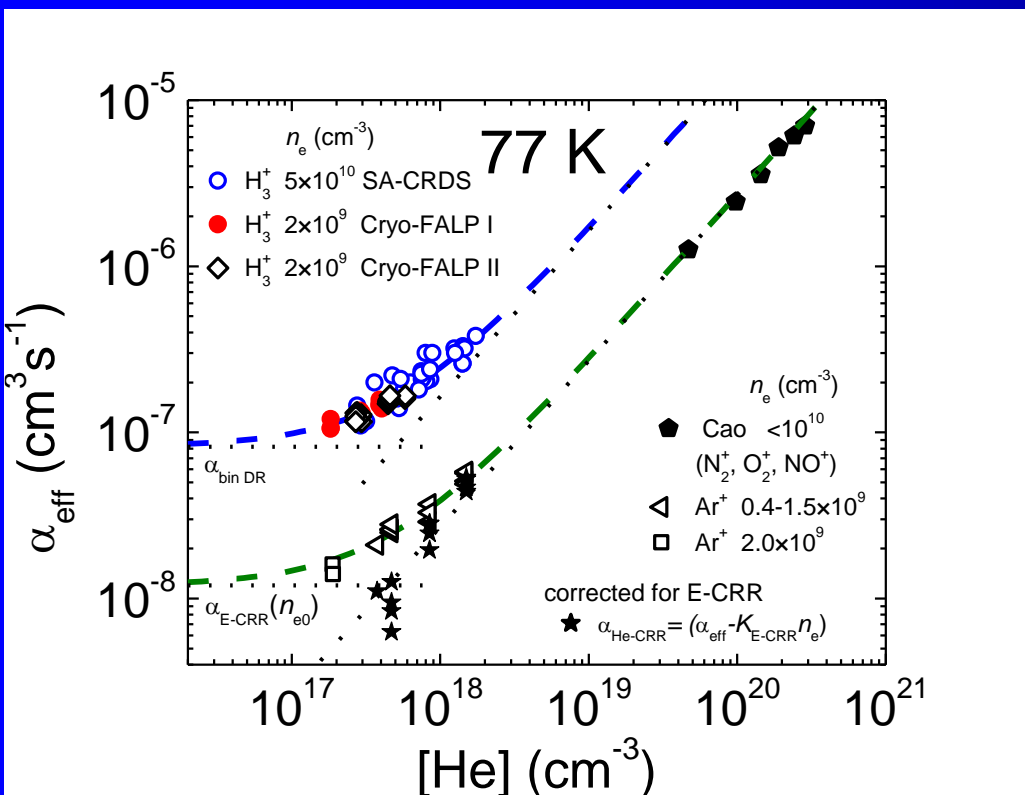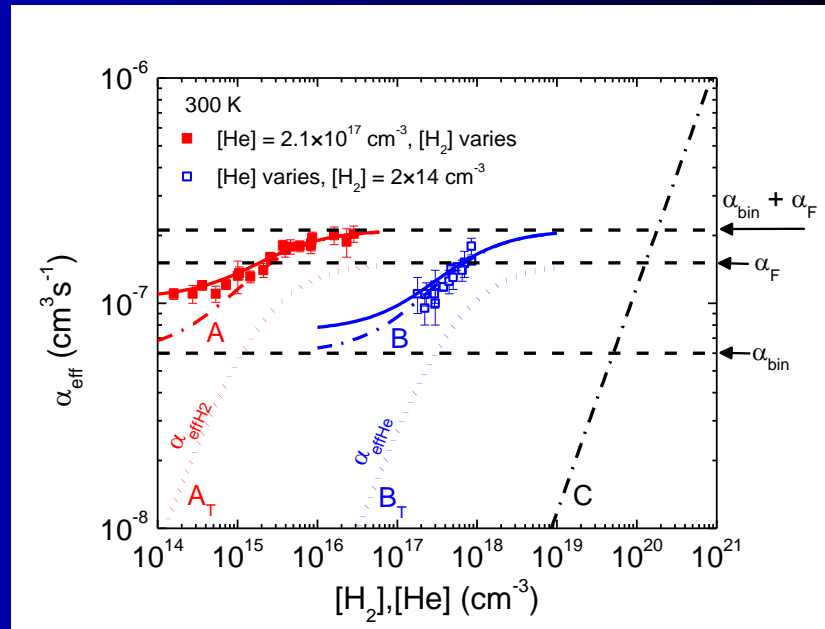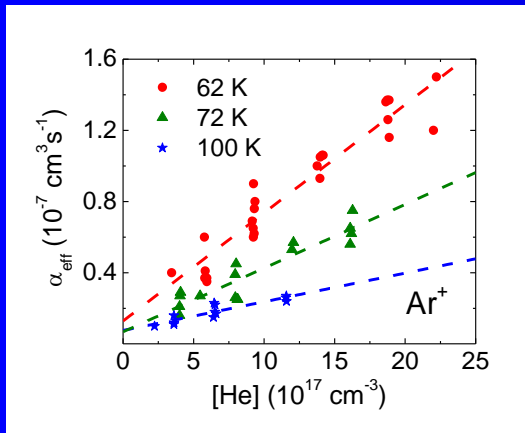
He_2^+

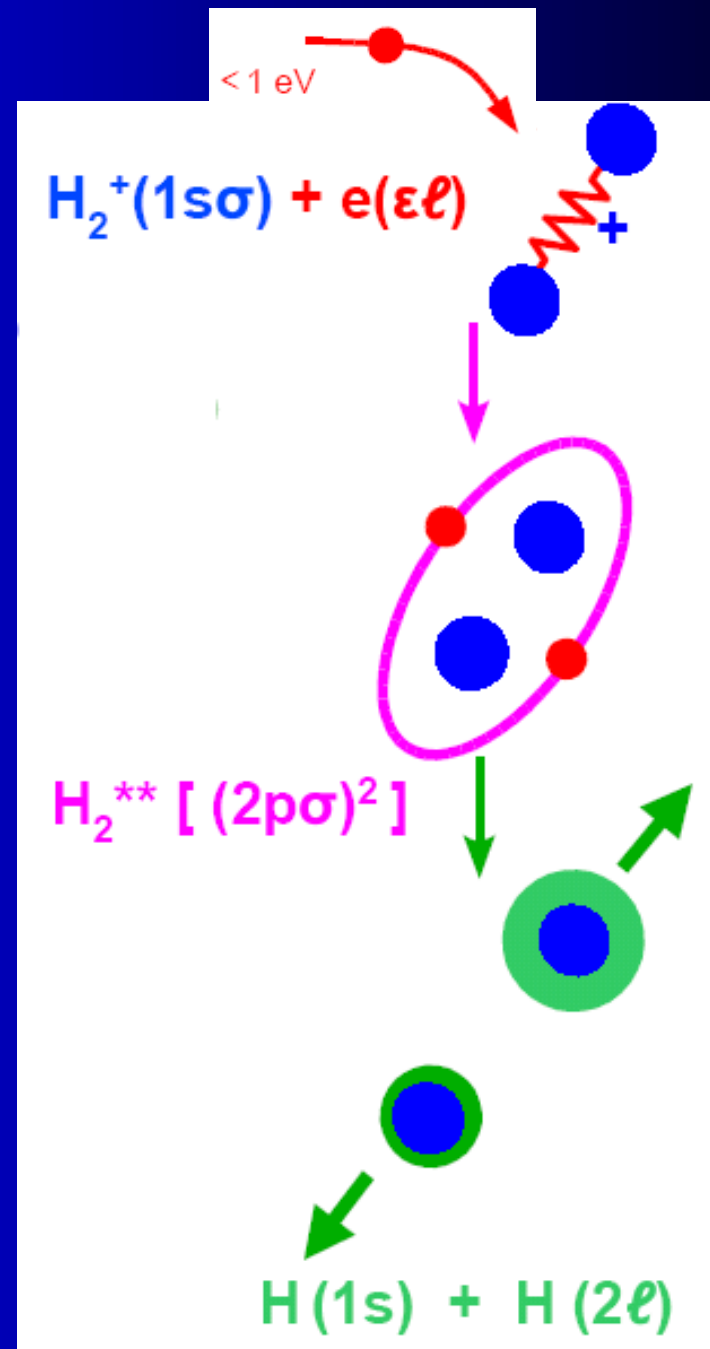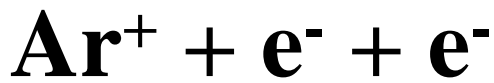**The states involved: exemple for He_2^+/He_2 system**

2004 DR6 Mosbach

I. Schneider, et al., DR2004 Mosbach

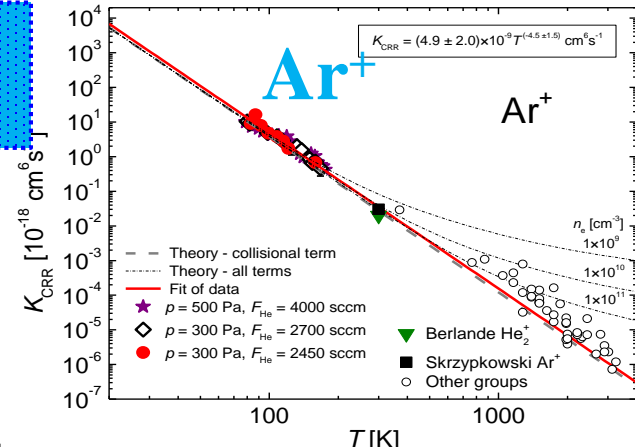# Electron - Ion Collision

Electron collisions with H_2^+

$< 1\ eV$

$H_2^+(1s\sigma) + e(\varepsilon\ell)$

$H_2^{**}\ [\ (2p\sigma)^2\ ]$

$H\ (1s)\ +\ H\ (2\ell)$